ISOTOPIC STUDY OF GROUNDWATERS AND THEIR HOST ROCKS

ISOTOPIC STUDIES OF THE GROUNDWATERS AND THEIR HOST ROCKS AND MINERALS FROM THE UNDERGROUND RESEARCH LABORATORY (URL), PINAWA, MANITOBA, CANADA

ISOTOPIC STUDIES OF THE GROUNDWATERS AND THEIR HOST ROCKS

AND MINERALS FROM THE UNDERGROUND RESEARCH LABORATORY (URL),

PINAWA, MANITOBA, CANADA

by

WANGXING LI, B.Sc. (Hon.)

A Thesis

Submitted to the School of Graduate Studies

in Partial Fulfilment of the Requirements

for the Degree of

Master of Science

McMaster University

May, 1989

MASTER OF SCIENCE (1989)   McMASTER UNIVERSITY
(Geology)   Hamilton,
Ontario

TITLE: Isotopic Studies of the Groundwaters and

Their Host Rocks and Minerals from the

Underground Research Laboratory (URL),

Pinawa, Manitoba, Canada.

AUTHOR: WANGXING LI

B.Sc. Honours (Zhongshan University)

SUPERVISORS: Dr. R. H. McNutt

Dr. H. P. Schwarcz

NUMBER OF PAGES: xix
202

ABSTRACT

This is a study of the groundwaters and their associated rocks and minerals from the Lac du Bonnet batholith at the Underground Research Laboratory (URL), Pinawa, Manitoba, to assess the water-rock interaction in crystalline rocks by using Sr, O and U-series isotopes. Emphasis is also placed on the development of the analytical techniques.

A high precision analytical technique of U-series isotopes has been developed in this study by using solid-source mass spectrometry. A precision of better than 1% (2σ) is achieved in determining the $^{234}U/^{238}U$ and $^{230}Th/^{234}U$ ratios using 10^{-8} g of U and 10^{-11} g of ^{230}Th. The potential applications of this method is demonstrated by dating small speleothem samples and the results agree well with those of α-spectrometry. This method also applies well to precise determination of the $^{234}U/^{238}U$ ratios in groundwaters and igneous rocks and minerals using small quantities of samples. However, precise measurements of ^{230}Th in igneous rocks and minerals are limited by the large ^{232}Th tail in the Th mass spectrum. Even better precision is achievable if pure Th spike is used.

An ICP-MS isotope dilution method is also developed for fast and precise determination of Sr concentrations in groundwater samples. A precision of 1% is routinely achieved by taking into account the dead-time effect of the

Channel Electron Multiplier (CEM) and the sample-to-spike ratios.

The isotope results of both the groundwaters and the host rocks and minerals have revealed the processes of water-rock interaction and water mixing through the history of the batholith. Strontium isotope systematics of the rocks and their constituent minerals have shown that Sr loss occurred on whole-rock scale during both the high-temperature alteration (about 2300 Ma ago) and the low-temperature alteration which lasted at least 450 Ma. The Sr loss is most pronounced in plagioclase of altered samples. Uranium-series results indicate the disequilibrium of both whole-rock samples and minerals, and migration of U on whole-rock scale in, at least, the last million years.

The Sr and O isotopic results have shown that the groundwaters from the three sub-horizontal, successively deeper fracture zones (FZ) have distinct isotopic signature: $^{87}Sr/^{86}Sr=$ 0.715 to 0.719 and $\delta^{18}O=-13‰$ for FZ-3; $^{87}Sr/^{86}Sr=$ 0.720 to 0.729 and $\delta^{18}O=-13$ to $-20‰$ for FZ-2; $^{87}Sr/^{86}Sr=$ 0.730 to 0.738 and $\delta^{18}O=-13$ to $-17‰$ for FZ-1. Uranium-series results show that all the groundwaters are highly enriched in ^{234}U and the $^{234}U/^{238}U$ activity ratios range from 2.6 to 7.7. Mixing of three groundwaters is indicated by the Sr and O isotopes and the elemental chemistry. The three end-members are fresh surface water, the deep fresh (possibly glacial melt) groundwater and the

deep saline groundwater.

Comparison between the rocks and associated groundwaters shows that Sr isotopic equilibrium exists between plagioclase of altered samples and the groundwaters. This similarity indicates the vulnerable mineral phase control, such as plagioclase in this case, of the isotopic signatures, hence, chemistry of the groundwaters.

Franklyn for his help in mineral separation and valuable discussions, to Jean Richardson for her help and comments, to Joyce Lundberg for her interest and discussions.

Financial support from the People's Republic of China in the form of a scholarship is appreciated.

I would like also thank all my colleagues in geology who made my stay at McMaster unforgettable. Among them, especially are Franco, Steve, Fereydoun, Marcus, Cathy, and Catharina, who gave me much needed emotional support and friendship, especially during those frustrating days. Particular gratitude is owed to Mr. and Mrs. Malon for their friendship, encouragement and support.

Last, but not least, I thank Youjuan for her understanding, patience, encouragement and support.

TABLE OF CONTENTS

CONTENT

SPECTROMETRY

LIST OF FIGURES

LIST OF TABLES

CHAPTER ONE

INTRODUCTION

1.1 PURPOSES OF THIS STUDY

The widespread use of nuclear energy all over the world since the "energy crises" of the 1970's has produced tonnes of radioactive waste (radwaste) from nuclear reactors. This waste is known to have long-term (up to 10^6 years) effects on the ecological system of the earth. Increasing concern about the hazard of the waste has resulted in planning for permanent isolation of the already accumulated radwaste worldwide. Among the proposed methods of waste disposal (Donath, 1982; Pohl, 1982), compromise between present technology and present government policy has eliminated all proposed methods but one: burying the waste in excavated cavities in deep geological units, such as salt beds, granites, or volcanic tuff.

Thorough studies of the possible geological units where the radioactive waste could be stored are essential to the safety of the waste disposal. The nature and the extent, in time and space, of the migration of these nuclides in the geological units via groundwater is an important consideration in this problem. The most recent events have geochemically disturbed the host rocks are most pertinent to

this study. Isotopic geochemistry studies of the rocks and associated water are very good indicators of the nature and extent of water/rock interactions and nuclide migration. Such studies, therefore, provide very important assessments of the feasibility of using certain geological units as potential repositories for high level radioactive waste (Karlsson and Wikberg, 1987; Vandergraaf, 1987). Those isotopes currently used include uranium-series (Schwarcz et al., 1982; Gascoyne and Schwarcz, 1986; Airey, 1986; Gascoyne and Cramer, 1987; Latham and Schwarcz, 1987a and 1987b), U-Th-Pb system (Stuckless, 1986), strontium isotopes (McNutt, 1987; McNutt et al., 1986), oxygen and hydrogen isotopes (Frape et al., 1984; Kerrich and Kamineni, 1985; Gascoyne et al., 1987).

Uranium-series has specific features in that it can give direct time signatures. Uranium-series isotopes in any geological system which has been chemically closed for more than one million years will reach secular radioactive equilibrium, that is, $(^{230}Th/^{234}U)$ and $(^{234}U/^{238}U)$ activity ratios equal to one. If the secular equilibrium system is disturbed, so called disequilibrium, $(^{230}Th/^{234}U)$ and $(^{234}U/^{238}U)$ will return to unity on the time scale of several half lives of the daughter isotopes. In this case, $(^{230}Th/^{234}U)$ will return to unity within about five half lives of ^{230}Th, 350 ky, and $(^{234}U/^{238}U)$ within five half

lives of ^{234}U, one million year. Therefore, U-series disequilibrium study will provide time information of any geological processes disturbing the U-series system. Its applications to assess the stability of plutonic rocks for the last million years have be made by Schwarcz et al.(1982), Gascoyne and Schwarcz (1986).

The Lac du Bonnet granitic pluton in eastern Manitoba, is currently being studied by the Canadian Nuclear Fuel Waste Management Programm (CNFWMP) of Atomic Energy of Canada Limited (AECL) to assess the possibility of using granitic plutons as containments of radioactive waste. An underground shaft and drifts--Underground Research Laboratory (URL) was excavated to the depth of about 250 meters below the surface within this batholith for this purpose. Uranium-series disequilibria, strontium isotopes, and oxygen isotopes are employed in this thesis to investigate water/rock interaction and nuclide migration by observing both the host rocks, minerals, and their associated groundwaters sampled from the boreholes, surface, and the underground shaft.

This thesis involves the development of new analytical techniques to help monition uranium-series and strontium isotopes. Particularly, a uranium-series analytical method utilizing a solid-source mass spectrometer has been developed to overcome previous limitations on sample sizes

and analytical precision inherent in conventional α spectrometry. An isotope dilution method using an Inductively Coupled Plasma Mass Spectrometry (ICP/MS) is employed to determine the Sr concentrations of the water samples.

1.2. GENERAL GEOLOGY

The Lac du Bonnet granite batholith is located in the southeastern part of Manitoba, in the English River Structural Subprovince of the Superior Province of the Canadian Shield. It intrudes and has a sharp contact with metavolcanic and metasedimentary rocks of the Bird River greenstone belt to the north and is in gradational contact with foliated tonalite-granodiorite gneiss and migmatites to the south. It is overlain to the west by Upper Ordovician sedimentary rocks. The rocks range in composition from a biotite granodiorite to a biotite granite, with xenoliths in the margins and the roof zone of the batholith (McCrank, 1985).

CHAPTER TWO

METHODOLOGY

2.1. SAMPLE PREPARATION

Rock and water samples were sent by Dr. Gascoyne of AECL at Pinawa. The rock samples were collected in the Underground Research Laboratory (URL). Fresh samples were collected from the excavation shaft above 100m below surface, while all the altered samples were from the fracture zone two (FZ-2) in the shaft excavation area (see Fig.5.2). Sample descriptions are found in Appendix 2.1. The water samples were collected from the boreholes drilled at various locations in the Lac du Bonnet granite (Fig.6.2). Water samples were acidified to a pH of 2 and stored in precleaned, 125 ml high density polyethylene (HDPE) Nalgene bottles.

Rock sample preparation followed the procedure of Franklyn (1988) with a few modifications in mineral separation. Rock powders with grain size of +50 to -150 mesh (0.3 -0.149 mm) (instead of +60 to -100, Franklyn, 1988) were used for mineral separation. Magnetite was initially removed using a Carpco magnetic separator prior to the Franz Isodynamic Magnetic Separator and density separation. The purity of both potassium feldspar and

5

plagioclase after each heavy liquid separation were checked under a binocular by staining a small portion of the separates using HF-sodium colbatinitrite method. The final purity was better than 95%.

2.2. CHEMICAL AND ISOTOPIC ANALYSIS
2.2.1. STRONTIUM AND Rb ANALYSIS

Strontium and Rb concentrations of the whole rock samples were determined by the Mo-compton peak XRF method using powder pellets. Rock standards were analyzed along with the samples. Detail of this analytical procedure is found in Franklyn (1988). The results of BCR-1, AGV-1 and G-2 rock standards agree with the recommended values within 1%.

The Sr and Rb concentrations in the mineral separates were determined by the isotope dilution method using a VG-354 solid source mass spectrometer and an Elan ICP-MS, respectively. A ^{84}Sr spike (97.46%) was used for Sr concentration analysis. Its concentration was recalibrated to be 5.66 ± 0.091 ug/g (2σ) by Franklyn (1988). The ^{87}Rb spike (99.2%) was recalibrated to be 18.033 ± 0.26 ug/g (2σ) by Marcantonio (1988). Details of these procedures were discussed by Franklyn (1988).

Strontium concentrations of the water samples were measured by isotope dilution on the ICP-MS using a ^{86}Sr spike (97.6%) with a concentration of 1.39 ug/g. This analytical method is discussed in detail in chapter four of this thesis.

2.2.2. STRONTIUM ISOTOPIC ANALYSIS

^{87}Sr/^{86}Sr isotopic ratios of both rock and water samples were determined using the VG-354 mass spectrometer with a dynamic multicollection SrST program. Procedures including sample dissolution, column chemistry and mass spectrometry were discussed by Franklyn (1988). The precision for each sample run was better than 0.0002% (2 standard error). Accuracy of the measurements was shown by running the NBS 987 Sr standard along with the samples. The results of the standard run over the period of this study are shown in Table 2.1.

2.2.3. OXYGEN ISOTOPIC ANALYSIS OF WATER SAMPLES

Oxygen isotopic compositions of the water samples were determined using conventional water-CO_2 equilibrium method (Epstein and Mayeda, 1953). About 2 ml of water was equilibrated with pure CO_2 in a sealed 35 ml flask at a temperature of 25 $^{\circ}$C for forty eight hours. The CO_2 was

Table 2.1.   Results of the NBS 987 Standard.

Date	$^{87}Sr/^{86}Sr$
16/06/87	0.710183 ± 0.000011
16/06/87	0.710207 ± 0.000011
12/08/87	0.710202 ± 0.000014
17/08/87	0.710181 ± 0.000013
22/08/87	0.710219 ± 0.000013
05/09/87	0.710184 ± 0.000013
17/09/87	0.710212 ± 0.000013
29/09/87	0.710229 ± 0.000013
19/10/87	0.710185 ± 0.000017
01/11/87	0.710211 ± 0.000013
07/06/88	0.710203 ± 0.000018
Mean	0.710203 ± 0.000031

The precision is presented in two standard error
calculated using the following equation:

$$\text{Std Error} = \sqrt{\frac{\Sigma(X-X_i)^2}{n(n-1)}}$$

while n is normally 150.

isolated from the water and analyzed for its oxygen isotopic composition using a VG MICROMASS 602D mass spectrometer at McMaster. The δO^{18} values, in respect to SMOW, of the water samples were then obtained using a fractionation factor of 1.0412 between CO_2 and water at 25 °C. Typical precision of the analysis is 0.2‰ (1σ).

2.2.4. URANIUM-SERIES ANALYSIS

Uranium-series analysis was performed for both water and rock samples using the VG-354 solid-source mass spectrometer at McMaster. This analytical method was developed during this study and is fully discussed in chapter three.

CHAPTER THREE

URANIUM-SERIES ANALYSES BY MASS SPECTROMETRY

3.1. INTRODUCTION

The spontaneous decay of the long-lived radioactive isotope ^{238}U produces a series of radioactive daughter isotopes of many different elements that have a wide range of half lives -- a so called "decay chain" (Fig. 3.1). ^{235}U and ^{232}Th also have decay chains, but except for ^{232}Th the isotopes in those two decay chains are not studied in this thesis. Each of the daughter isotopes in the decay chain will reach radioactive equilibrium with its parent if it remains chemically undisturbed for a time span of more than ten times its half life. For example, ^{234}U will be in radioactive equilibrium with its parent, ^{238}U, in less than two million years.

Radioactive equilibria can be destroyed by the separation or fractionation of these isotopes in the decay chain during some geochemical processes. This is because of the differences in chemical properties between the parent and daughter isotopes. Typical processes could include chemical weathering, precipitation of minerals from aqueous solution, absorption on suspended particles, and partial melting during magma generation or crystallization.

Figure 3.1.   Uranium and Th decay series showing the
    isotopes in each decay chain and their half lives (after
    Harmon, 1977).

<u>^{238}U SERIES</u>

^{238}U
(4.51 x 10^{9}y)

α ↓

^{234}Th
(24.1 d)

ß ↓

^{234}Pa
(1.18 m)

ß ↓

^{234}U
(2.47 x 10^{5}y)

α ↓

^{230}Th
(7.52 x 10^{4}y)

α ↓

^{226}Ra
(1602 y)

┆
↓

^{206}Pb
(stable)

<u>^{232}Th SERIES</u>

^{232}Th
(1.4 x 10^{10}y)

α ↓

^{228}Ra
(6.7y)

ß ↓

^{228}Ac
(6.13h)

^{232}U
(72y)

α ↓

^{228}Th
(1.910y)

α ↓

^{224}Ra
(3.64d)

α ↓

^{220}Rn
(54.4s)

α ↓

^{216}Po
(0.16s)

┆
↓

^{208}Pb
(stable)

<u>^{235}U SERIES</u>

^{235}U
(7.13 x 10^{8}y)

α ↓

^{231}Th
(25.6h)

ß ↓

^{231}Pa
(3.25 x 10^{4}y)

α ↓

^{227}Ac
(21.6y)

ß ↓

^{227}Th
(18.2d)

α ↓

^{223}Ra
(11.43d)

┆
↓

^{207}Pb
(stable)

β (arrow from ^{228}Ac to ^{228}Th)
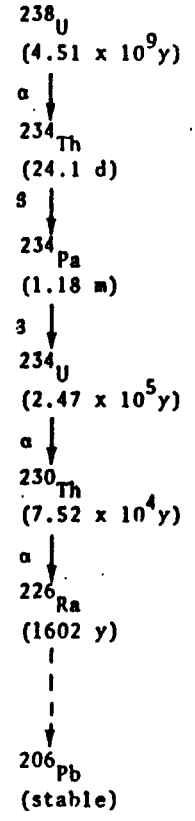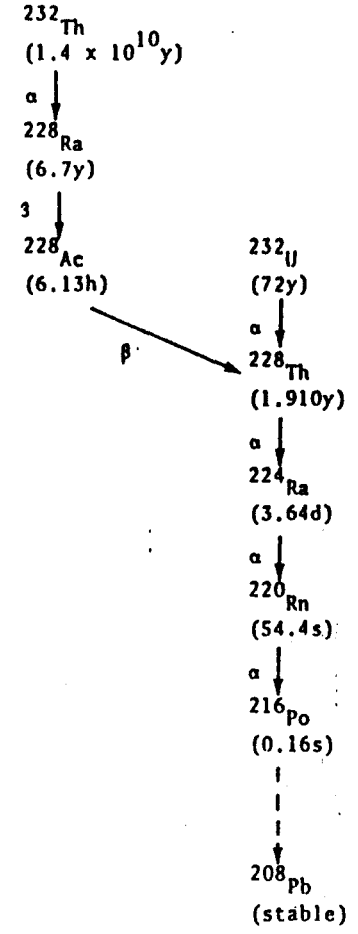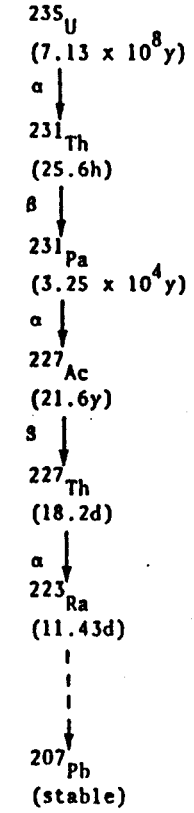
Therefore, such radioactive disequilibrium can be used as a tracer and chronometer of those geological processes that cause disequilibria. The wide range of the half-lives of the isotopes, from millions of years to millionths of seconds, in the decay chain makes the U-Th method uniquely well suited for this purpose, on the time scale of less than one million years.

Previous applications of U-series isotopes, including those in ^{235}U and ^{232}Th decay chains, as both chronometers and tracers have been very successful in the study of Pleistocene geology, volcanology, and chemical oceanography (Ivanovich and Harmon, 1982). Study of U-series disequilibrium has focused on absolute age determination of Pleistocene geological events which date to about one million years (Ku, 1976; Schwarcz and Gascoyne, 1983).

Uranium-series disequilibria (including ^{232}Th) have been used as both geochronometers and geochemical tracers in the study of young volcanic rocks (<250 ky). Applications have included dating the eruption events, study of the characteristics of magma sources and the fractionation of elements during partial melting and subsequent crystallization, and investigating magma evolution in deep magma chambers, during magma mixing, and subsequent crustal contamination of mantle-derived magma (Newman et al., 1986,

1984; Krishnaswami et al., 1984; Condomines et al., 1981, 1976; Condomines and Allegre, 1980; Allegre and Condomines, 1976, 1981; Oversby and Gast, 1968).

Uranium-series isotopes, as well as ^{232}Th, are used to study the physical, chemical, and biogeochemical cycling of elements in the ocean (Broecker and Peng, 1981). These isotopes are particularly usefully monitors of the chemical and physical interactions and transformations of elements between dissolved substances and various forms of particulate matter. Th isotopes, especially ^{230}Th, have been found very useful in the study of kinetics of adsorption and desorption reactions between particulates and dissolved substances. These isotopes also help clarify the relationship among chemical scavenging processes in the deep ocean and temporal variability in the fluxes and composition of particulate matter (Jannasch et al., 1988; Huh and Beasley, 1987; Nozaki et al., 1987, 1981; Anderson et al., 1983; Bacon and Anderson, 1982).

Up to now, all applications of U-series disequilibrium have involved the determination of the activity ratios (given here in brackets, otherwise atomic ratios are intended) of the isotopes of interest, particularly (^{234}U/^{238}U), (^{230}Th/^{234}U), and (^{230}Th/^{232}Th). Those ratios are typically measured by α-spectrometry because many of the

daughter isotopes are α emitters. The analytical procedures generally involve the chemical separation of U from Th and counting of α particles for time periods of up to several weeks.

Full exploitation of U series disequilibrium in the studies mentioned above has been limited by this conventional α-spectrometric measurement of ^{234}U and ^{230}Th, both in the statistical uncertainty in α counting and by the large sample size needed for each analysis. For a 120 ky old coral sample, more than 10 μg of U, equivalent to about 10 g coral, is required to give the typical precision of >10% (2σ) (Harmon et al., 1979). This precision level has limited the precision of the study of Pleistocene climatic changes between 70 ky and 150 ky. These climatic changes were thought to be the results of astronomical events periodicities as short as 20 ky, correlated with the so-called Milankovitch cycles. The typical α counting analytical techniques can barely resolve these events at 2σ level of 10 ky (Edwards et al., 1987a, 1987b), and therefore, some aspects of the Milankovitch theory cannot be tested.

The study of magmatic fractionation of elements using U-series isotopes and ^{232}Th, depends critically on the ability to measure activity ratios that differ only slightly

from unity. Although the study has been carried on for more than two decades, it is still uncertain if U is fractionated from Th during partial melting since both are magmatophile elements. Disequilibria between ^{230}Th and ^{238}U found in historical age volcanic rocks have been interpreted to be the result of either fractionation during partial melting (Oversby and Gast, 1968; Allegre and Condomines, 1982; Newman et al., 1983, 1984) or post-emplacement processes, especially for submarine basalts (Bennett et al., 1982, Krishnaswami et al., 1984). This controversy can only be resolved by improvement in analytical precision and by substantial reduction of the sample size. Reduction in sample size is essential to avoid contamination due to the difficulty of hand-picking up to 15 g of fresh rocks from altered submarine basalts. Analytical techniques capable of precisely measuring subnanogram quantities of U and Th will extend U-series geochemistry and geochronology to low-U and -Th content mineral separates, such as feldspars.

Study of chemical oceanography has been limited by the lack of Th isotope data due to the extremely low Th contents of seawater (as low as sub-ppt level). In the past, hundreds of liters of seawater have been collected to do α counting (Bacon and Anderson, 1982). The ability to measure nanograms of Th is a prerequisite for further study of Th isotopes in the ocean.

Isotope dilution mass spectrometry is known to be a very precise analytical technique for trace and isotopic analyses. With the state-of-the-art mass spectrometry in geochronology, isotopic ratios, such as $^{87}Sr/^{86}Sr$ and $^{143}Nd/^{144}Nd$ ratios, can be measured routinely to a precision of better than 5×10^{-5} (2σ) using only a few nanograms of samples. Each analysis can be performed in less than three hours. Therefore, U-series analyses by mass spectrometry are expected to have the advantages of higher precision, smaller sample sizes, and less analyzing time and labour compared with α counting.

However, precise measurement of $^{234}U/^{238}U$ and $^{230}Th/^{232}Th$ ratios is limited by the extreme low values of these ratios in nature (10^{-5} and 10^{-6} respectively for igneous rocks) and by the present abundance sensitivity of instruments. The measurement of ^{234}U and ^{230}Th at the level of nanogram U and Th in coral samples, to a precision better than 0.5% (2σ) by mass spectrometry has been achieved (Edwards et al, 1988; 1987; Chen et al., 1986). However, this method has not been adopted and has not been tried on igneous rocks. Therefore, this thesis was centered around developing a routine procedure that is capable of precisely measuring isotopic ratios (hence activity ratios) at the nanogram level for U and Th by thermal ionization mass

spectrometry (TIMS). This analytical method encompasses two steps. Trace amounts of U and Th are chemically extracted, separated, and purified. The isotopic ratios are then measured by TIMS. A schematic flow diagram outlining the whole analytical procedure is shown in Fig.3.2.

3.2. SAMPLE PREPARATION
3.2.1. REAGENTS

The reagents used in the chemical procedures are 16 M, 7.5 M, and 2 M HNO_3, 6 M and 0.5 M HCl, 1 M HBr and Concentrated HF (48%). All these solutions were made from reagents that have been distilled in either Teflon or pure quartz containers using sub-boiling method from concentrated analytical level reagents (ACS Grade).

NH_4OH (28-35%) and $FeCl_3$ (0.4 g/ml) were made from analytical level (ACS Grade) reagents that have not been further purified.

The water used was 18 megohm deionized from distilled water, so called MILLIQ.

Bio-Rad AG 1-X8 100-200 mesh and 200-400 mesh anion-exchange resin was used in this study. The ion-exchange resin was washed and sized with MILLIQ several times in a

Figure 3.2. Schematic flow diagram for the chemical

procedure of U and Th analysis by TIMS

| SILICATES | CARBONATES | WATERS |

DISSOLUTION — Concentrated HF | 7 M HNO$_3$ | Acidified 7 M HNO$_3$

PRIMARY EXTRACTION OF U+Th — Set "L" (12 ml) columns | FeCl$_3$ coprecipitation

Set "M" (2.8 ml) columns

PURIFICATION AND SEPARATION OF U FROM Th — Set "S" (0.28 ml) Columns

MASS SPECTROMETRY — Uranium | Thorium
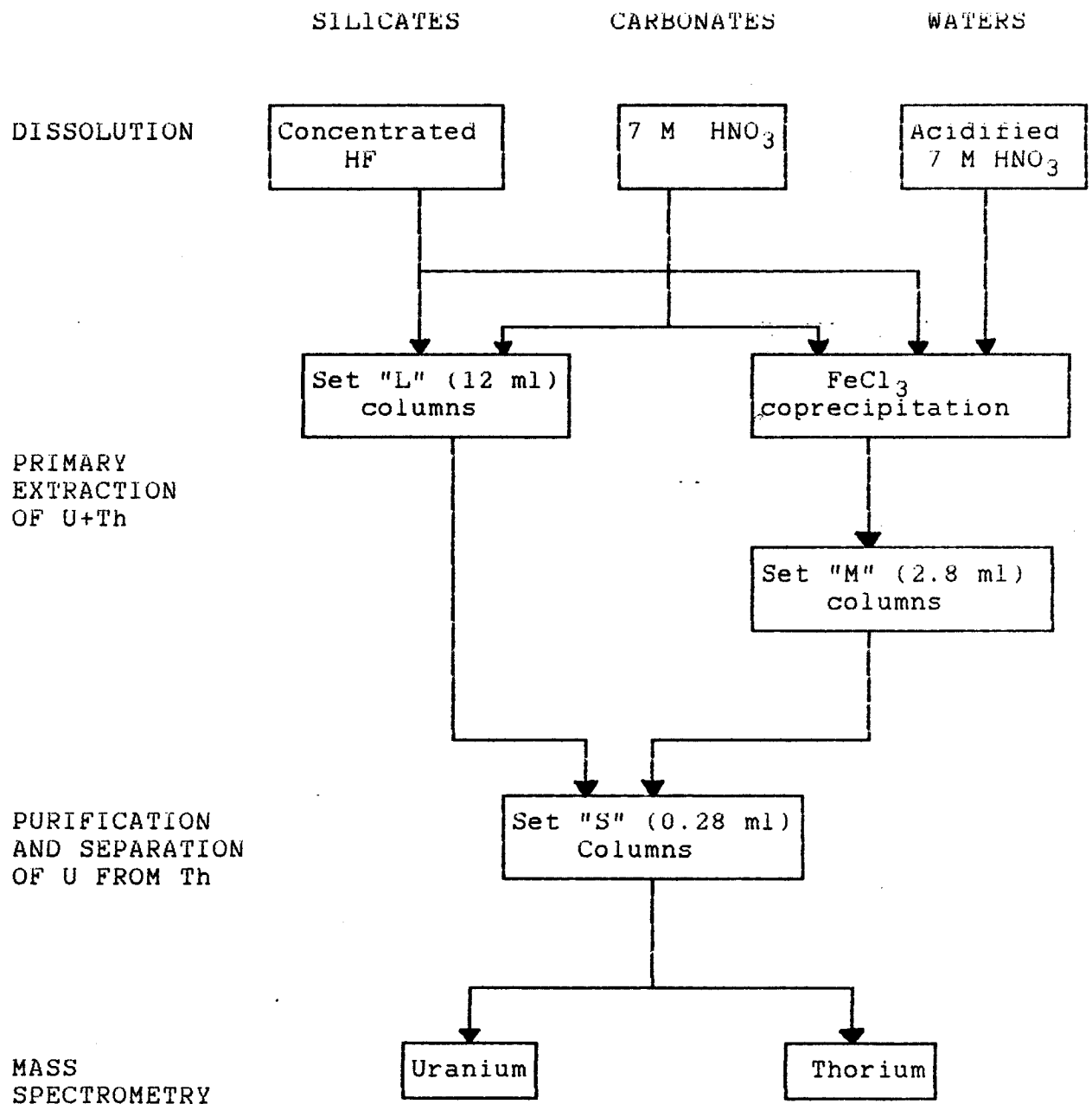
precleaned beaker and the fines decanted until the water was clear. Then the resin was stored in MILLIQ in a teflon bottle for use.

3.2.2. SAMPLE DISSOLUTION

Three different kinds of samples, silicates, carbonates, and waters were analyzed during this study. For whole-rock and mineral silicates, samples were crushed to-200 mesh. About 150 mg of whole-rock powder and up to 1.5 g (depending on their U and Th contents) of mineral separates were weighed into 50 ml Teflon bombs and 10 ml HF added. The bomb was sealed and the sample was digested in an oven at about 120°C for three days (seventy-two hours). Then the bombs were removed from the oven, placed on hot plates, and evaporated. About 5 ml of 16 M HNO_3 was added before the solution was completely dried. Finally, the samples were redissolved in 7.5 M HNO_3. If there was any undissolved residue in the bomb, the solution was dried and the entire procedure was repeated until the sample was completely dissolved.

Completely dissolved samples were then spiked with a $^{236}U-^{229}Th$ mixed spike so that the $^{235}U/^{236}U$ ratio should lie between 0.2 to 5.0. The spiked solution was shaken vigorously to ensure homogenization and then evaporated to

dryness on the hot plates and redissolved in less than 1 ml 7.5 M HNO_3. Large samples (more than 1 g) which could not be dissolved in 1 ml 7.5 M HNO_3 were dissolved with about 10 ml 2 M HNO_3 and were ready for coprecipitation (see below).

Carbonate samples, either powder or coarsely crushed grains (-2 mm) were weighed into 50 ml Teflon bombs. 7.5 M HNO_3 was added slowly (over 15 minutes) until the solution turned clear. Any organics were oxidized by refluxing the solution in the bombs with lids on under the heat lamps for about two hours. Then the samples were spiked and shaken vigorously before coprecipitation.

The water samples were weighed (they varied from 10 to 40 grams) and placed in Teflon bombs and spiked prior to coprecipitation. All sample solutions, including carbonates and silicates, were acidified, using HNO_3, to a pH less than 2 before coprecipitation.

3.2.3. COPRECIPITATION OF U AND Th WITH Fe(OH)$_3$

Large quantities of material passing through even 12.5 ml columns can block the columns and leave unwanted material (probably calcium) in the eluate. This unwanted material cannot be washed away even when put through the columns repeatedly. In the case of large low-U and -Th content

samples, such as feldspar, carbonates, and water samples, preconcentration of U and Th is necessary and $Fe(OH)_3$ was used to coprecipitate U and Th so that the volume of sample solution could be reduced to less than 0.5 ml, which is easily handled by small columns.

About 12 mg $FeCl_3$ (one drop using a 1 ml pipette) was added to the spiked sample HNO_3 solution, pH less than 2, and heated either under heat lamps or on a hot plate for about 30 minutes. HNO_3 was preferred over HCl because HNO_3 will convert U to the U^{6+} which allows U to coprecipitate with $Fe(OH)_3$ and because only U^{6+} is taken up on the ion exchange resin under the conditions used here. Heating was necessary to degas dissolved CO_2 because CO_2 forms a soluble U complex that would not coprecipitate (Gascoyne, 1977).

Concentrated ammonia was added very slowly to the warm solution using a pipette until dark-orange flocculates formed and the solution turned from brownish to clear. Uranium and Th (and some other trace elements such as the REE and Ba) were coprecipitated with the $Fe(OH)_3$, but little Ca or Mg. During this procedure, the pH of the solution changed from less than 2 to about 8. The $Fe(OH)_3$ began to precipitate at pH around 3.5.

The precipitate was then left for 3 hours to cool and

settle. The supernate was decanted carefully with a pipette and precipitate transferred to a 15 ml test tube or a 12 ml Teflon container and centrifuged for 10 minutes. Any remaining solution was again decanted and the precipitate washed three times with MILLIQ and redissolved in 2 ml of 7.5 M HNO_3, and evaporated to dryness to remove any residual ammonia. The precipitate was finally redissolved in less than 1 ml 7.5 M HNO_3 and was then ready for the ion-exchange columns.

3.3. COLUMN CHEMISTRY
3.3.1. INTRODUCTION

Ion-exchange chromatographic separation of trace amount U and Th from matrix and the later separation of U from Th is not trivial. Anion exchange resin in HNO_3 medium is popularly used since almost all common matrix elements in geological samples are absorbed from solutions ranging from 0.1 to 14 M HNO_3 (Faris and Buchanan, 1964). However, U can be partly or completely lost after uptake by the ion exchange resin due to its low distribution coefficient (Arden and Gale, 1974). This problem is easily controlled by using only small volumes of HNO_3 to wash the columns.

3.3.2. COLUMN PREPARATION
Three sets of columns of different volume were used in

this study (Table 3.1). The "L" columns (large column volume) were designed for the primary separation of U and Th from the matrix in large samples (>1.0 g). They were made of quartz tubing and were precleaned using 7.5 M HNO_3 and MILLIQ water before the resin was loaded. Precleaned quartz wool was placed at the bottom of each column to retain the resin. Originally, 200-400 mesh anion resin was used, but was later replaced by 100-200 mesh resin. The finer resin is more easily blocked when the columns are washed with 7.5 M HNO_3 because it is less porous.

Set "M" (=medium) and "S" (=small) columns were used for small samples (<1.0 g) and for purifying and separating U from Th after the primary extraction of both elements by the "L" columns or after coprecipitation. "M" and "S" columns were made of polyethylene tubing with clean cotton placed at the bottom of the columns to retain the 200-400 mesh resin.

All columns were washed with 40 ml, 4 ml, and 3 ml of solutions for "L", "M", and "S" columns respectively in the following order: H_2O - 2 M HNO_3 - 0.5 M HCl - H_2O and preconditioned with 30 ml, 4 ml, and 3 ml of 7.5 M HNO_3 respectively. The washing and conditioning procedure was repeated before and between uses.

Table 3.1. Ion Exchange Columns and Operating Procedure

	Set L	Set M	Set S
Length	15cm	5.5cm	2.2cm
Diameter	1.0cm	0.8cm	0.4cm
Column Volume	12ml	2.8ml	0.28ml
Reservoir Volume	90ml	4ml	4ml
Resin Mesh Size	100 -200	200-400	200-400

Clean:

	Set L	Set M	Set S
H_2O	40ml	4ml	3ml
2M HNO_3	40ml	4ml	3ml
0.5M HCl	40ml	4ml	3ml
H_2O	40ml	4ml	3ml

Precondition:

| 7.5M HNO_3 | 30ml | 4ml | 3ml |

Load: 7.5M HNO_3

| | 5ml | 1.0ml | 0.2ml |

Wash: 7.5M HNO_3

| | 10ml | 1.0ml | 0.3ml |
| 7.5M HNO_3 | 20ml | 2.0ml | 0.3ml |

Elute:(U+Th) H_2O

| | 10ml | 2ml | (1ml) |
| 1M HBr | 40ml | 6ml | (4ml) |

Or:
Elute: Th:6M HCl

| | | | 4ml |

U: 1M HBr

| | | | 4ml |

The resin in the "S" columns was discarded after each use and that in the "M" columns was discarded after using twice because they were critical in controlling contamination. The empty columns were cleaned via a multi-acid process. They were placed in successive warm baths of 2 M HNO_3 – 2.5 M HNO_3 – H_2O – H_2O for about two hours each. The resin in "L" columns was not replaced for the reason that they were used only for the primary U and Th separation from large samples, and also due to the cost of the large quantity of resin involved. They were cleaned using the cleaning procedure in Table 3.1.

3.3.3. COLUMN CALIBRATION

All columns were carefully calibrated as follows (Table 3.1). Preconditioned columns were loaded with about 1 μg U and Th dissolved in 7.5 M HNO_3 and then washed with an appropriate volume of 7.5 M HNO_3, and eluted with H_2O and 1 M HBr. Fractions, ranging from 0.2 ml to 5 ml increments depending on sizes of the columns, of all the solutions passing through the columns were collected and each fraction was then analyzed by ICP-MS for U and Th. The counts of U and Th (in counts/second) for each fraction from each set of columns were plotted against the accumulated volume of solution (Fig. 3.3, 3.4, 3.5, 3.6). Uranium was washed out partly or completely when more than 4 column volumes of

Figure 3.3.   Column calibration of Set S columns for U and Th
after primary separation on Set L or Set M columns.   The
columns are washed with 1 ml   7.5 N HNO_3, and U and Th
are eluted with 4 ml 1 N HBr.   Note the Th "tail".
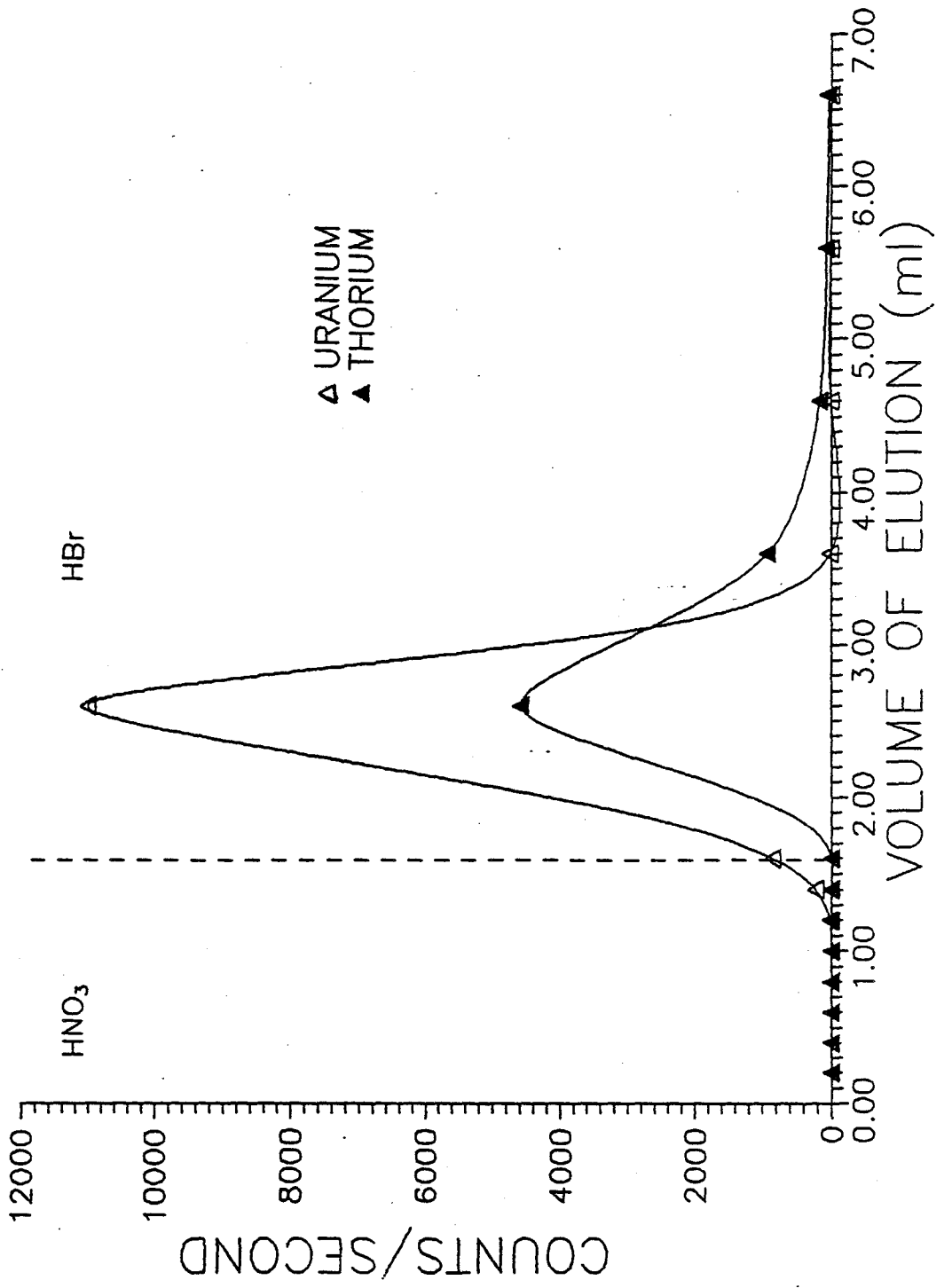
Figure 3.4. Column calibration of Set M columns for primary
      separation of U and Th from matrix. Samples are washed
      with 4 ml 7.5 N HNO_3, and U and Th are eluted with 6 ml
      1 N HBr. It also shows the Th "tail".
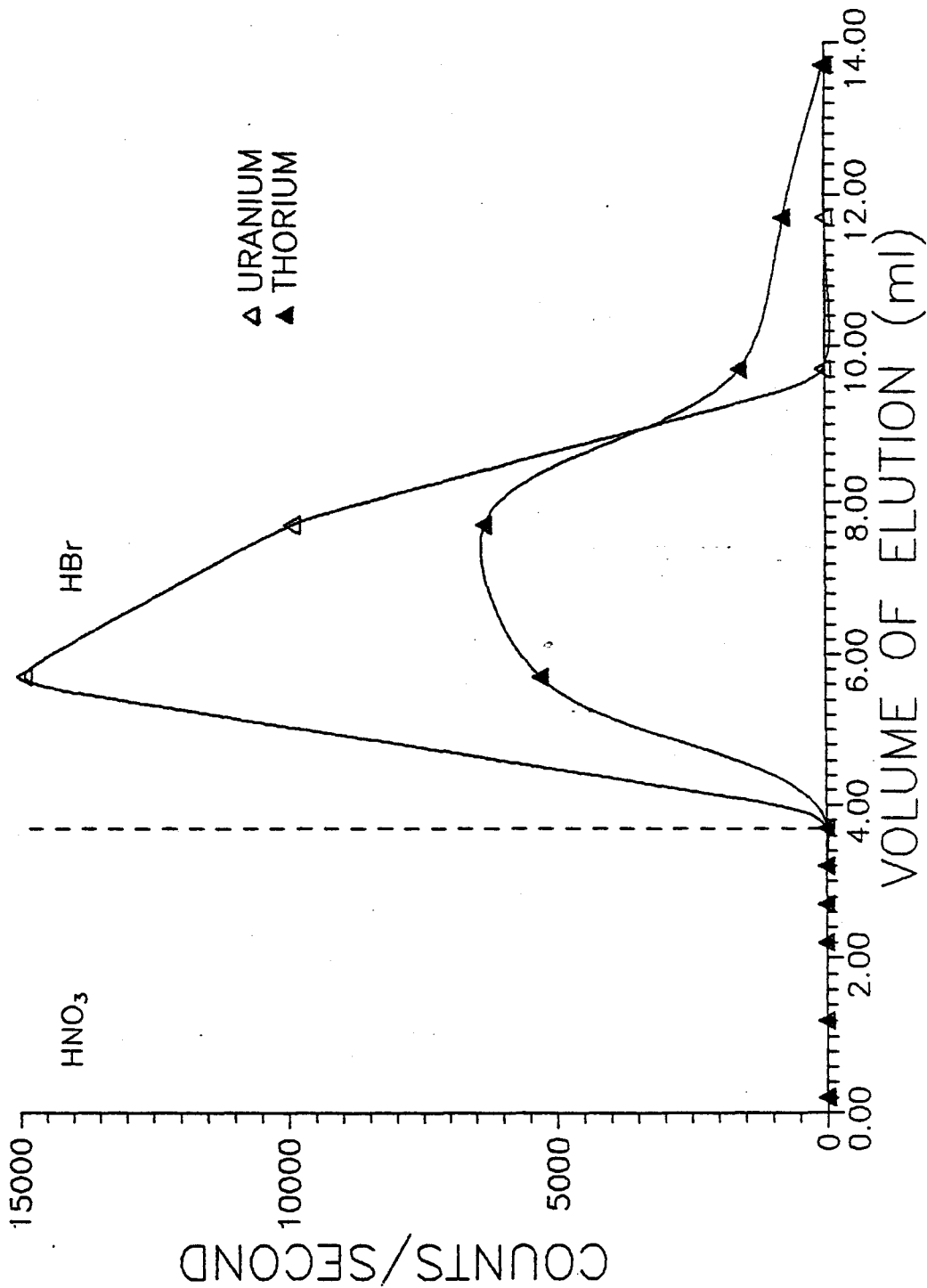
Figure 3.5. Column calibration of Set L columns (200-400 mesh) for primary separation of U and Th from large samples. Samples are washed with 50 ml 7.5 M HNO_3, and U and Th are collected with 10 ml of water followed 40 ml of 1 M HBr.
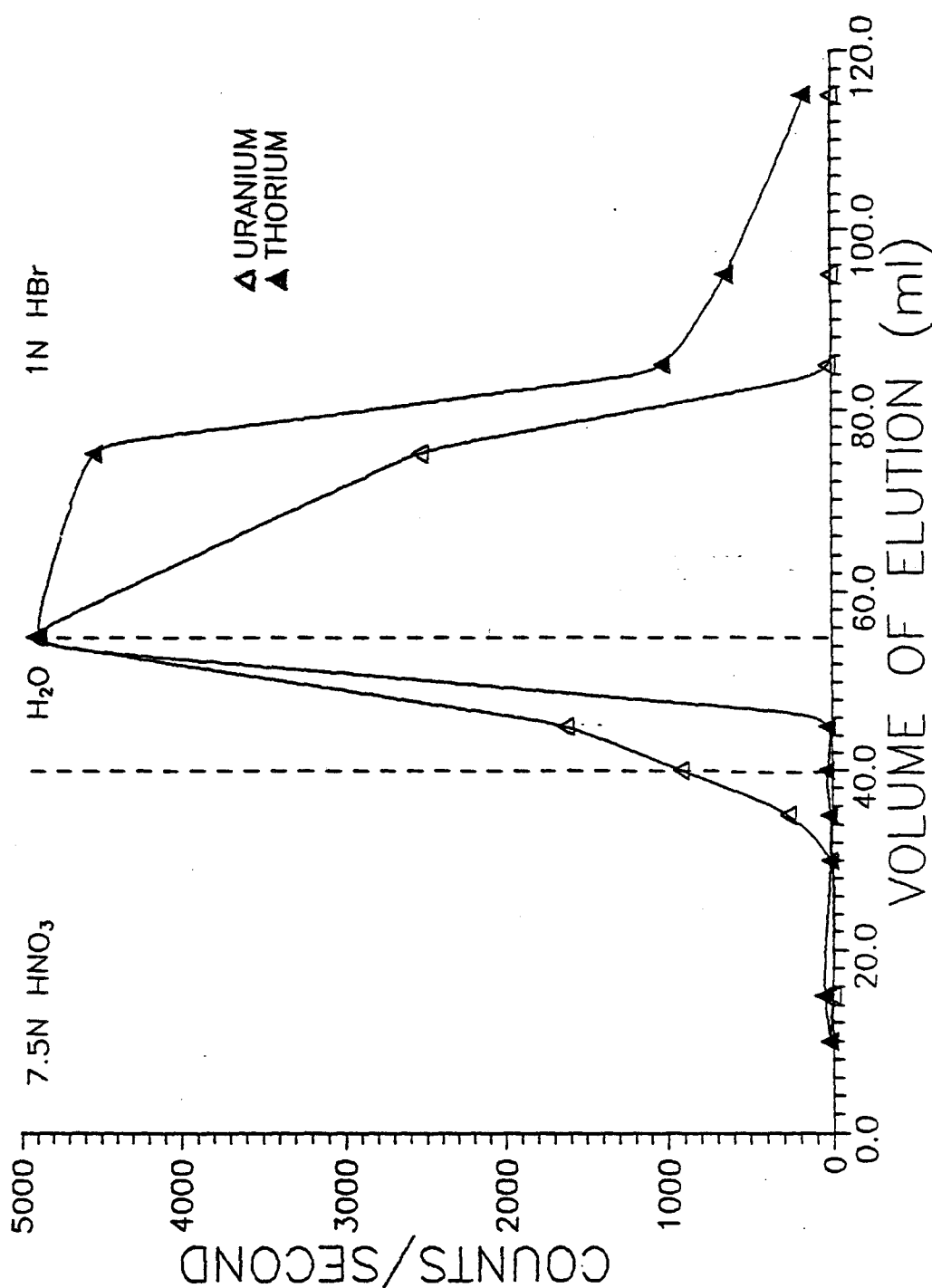
Figure 3.6. Column calibration of Set L columns (100-200 mesh) for primary separation of U and Th from large samples. Samples can be washed with only 35 ml 7.5 M HNO_3 compared with 50 ml for 200-400 mesh resin. Uranium and Th are eluted with water and 1 M HBr as usual.

HNO₃ H₂O HBr

△ URANIUM
▲ THORIUM

VOLUME OF ELUTION (ml)

COUNTS/SECOND
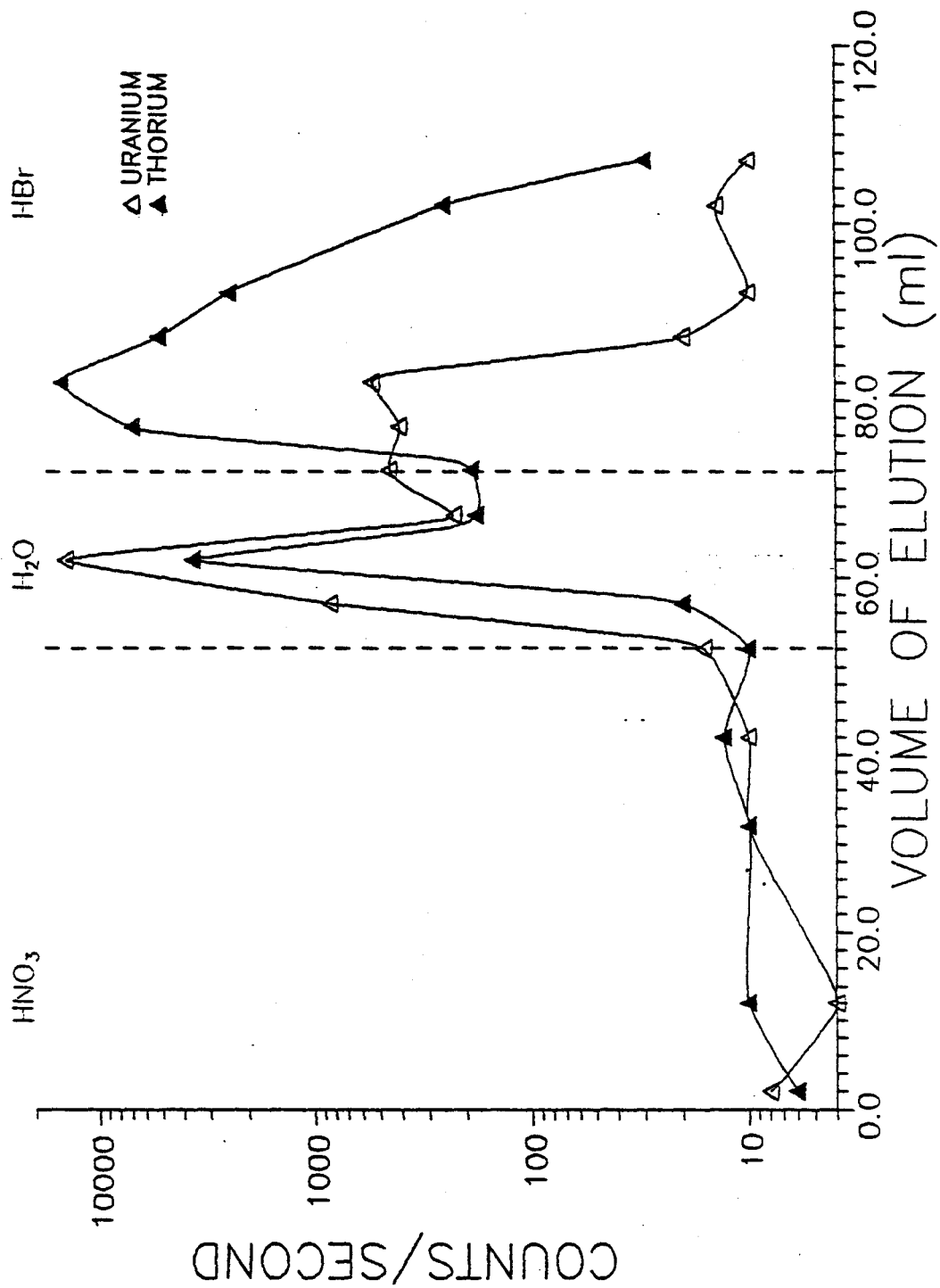
total 7.5 M HNO_3 was used (including loading and washing in Table 3.1). For instance, more than 1 ml of HNO_3 for set "S", 4 ml for set "M", and 40 ml for set "L" columns, resulted in significant U loss when washing columns packed with 200-400 mesh resin. In the case of set L columns when 100-200 mesh resin was used, the total volume of 7.5 M HNO_3 necessary to wash the columns was reduced to about 35 ml, slightly less than the 40 ml required for the finer resin of the same column volume.

Uranium has a sharp or well-defined elution curve, while the Th always has a tail. This is due to the difference in distribution coefficient in HNO_3 between U (<10) and Th (>100). However, almost all the U and Th was eluted using 10 ml H_2O and 40 ml 1 M HBr for set "L" columns, 2 ml H_2O and 6 ml 1 M HBr for set "M" columns, and 1 ml H_2O and 4 ml 1 M HBr for set "S" columns. The H_2O elution was used to remove any residual HNO_3 in the columns before elution with HBr. This is very important because HBr could be oxidized by HNO_3 to form dark orange Br_2 which interferes with elution. The result of column calibration as summarized in Table 3.1 and was used as a routine column operation procedure.

The "S" columns, for separating U from Th, were calibrated the same way except that 6 M HCl was used to

precondition, to load and to wash (Fig. 3.7). Thorium is not absorbed and flows through the columns directly. Uranium is strongly retained in the columns and is easily eluted with 1 M HBr. This separation procedure was later modified so that separation of U from Th was done immediately after purification in the same set "S" column. That is, the columns were preconditioned, loaded and washed with 7.5 M HNO_3, after which Th was eluted with 4 ml 6N HCl. Uranium was then eluted using 1 M HBr.

3.3.4. PRIMARY EXTRACTION U AND Th FROM MATRIX

The primary extraction of U and Th from the other elements was accomplished using either the "L" for large samples (>1 g), or the "M" columns for small samples (<1 g) or for large samples after coprecipitation. Although set "L" columns were replaced at the later stage in the study by adoption of $Fe(OH)_3$ coprecipitation, most samples were done using set "L" columns. The samples were dissolved in about 5 ml 7.5 M HNO_3 and loaded onto the columns. The column was washed with a total of 30 ml (35 ml for 200-400 mesh resin) 7.5 M HNO_3. Most matrix elements including Ca, Mg, K, Fe, etc., were removed while U and Th were retained in the columns. They were eluted using 10 ml H_2O and 40 ml 1 M HBr. The collected sample was dried and redissolved in 2 ml 2 M HNO_3, and redried. This procedure could remove any HBr

Figure 3.7.   Column calibration of Set S columns for
    separation of U from Th.   Samples are loaded in 6 M HCl.
    Thorium goes through the column whil U retains in the
    column.
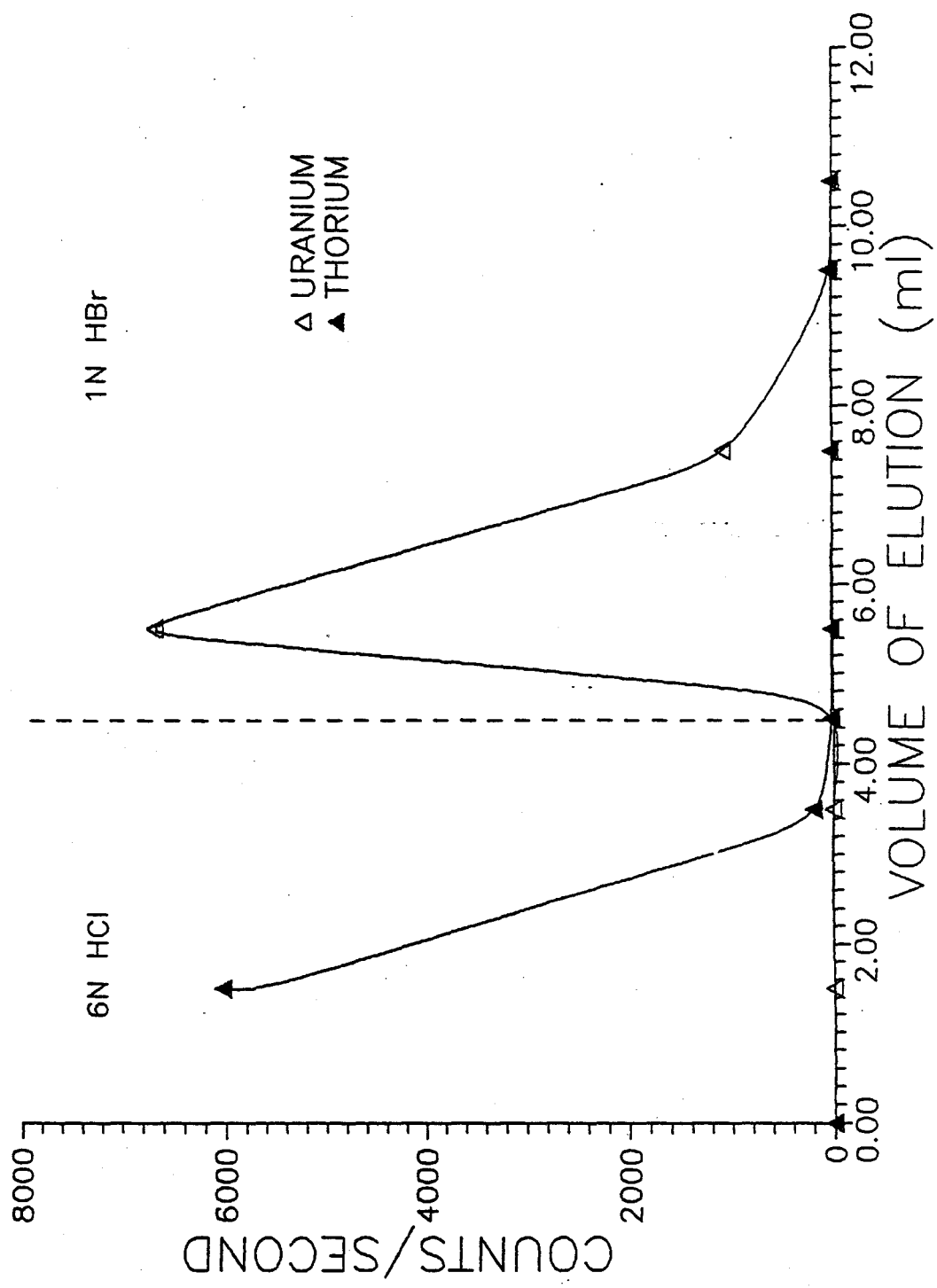
collected. The samples were then dissolved in about 0.2 ml 7.5 M HNO_3 for purification.

The primary separation using the "M" columns was similar to the "L" columns (Table 3.1). Samples dissolved in about 1 ml 7.5 M HNO_3 were loaded on the columns followed by washing with 3 ml of the same acid. U and Th were then collected using 2 ml H_2O and 6 ml 1 M HBr. The collected eludes were dried and dissolved in about 1 ml 2 M HNO_3 and then redried. The samples were redissolved in 0.2 ml 7.5 M HNO_3 for purification.

3.3.5. PURIFICATION AND SEPARATION OF U FROM Th

After the primary separation, the samples were purified using the "S" columns. Uranium was separated from Th to enhance mass spectrometry success. After the primary extraction, samples dissolved in 0.2 ml 7.5 M HNO_3 were loaded into the "S" columns which were then washed with a total of 0.8 ml of 7.5 M HNO_3 (Table 3.1). This will help wash any unwanted elements such as Fe. Thorium was eluted with 4 ml 6 M HCl. Uranium was then collected using 4 ml 1 M HBr. The U and Th fractions were dried and dissolved in a few drops 2 M HNO_3, dried again, redissolved in one drop of 0.04 M H_3PO_4 and 3 M HNO_3 mixed solution. The samples were then finally dried in clear dots in the beaker prior to mass

spectrometric analyses.

3.4. MASS SPECTROMETRY

3.4.1. INTRODUCTION

Precise thermal ionization mass spectrometric analyses of U and Th has been a well-known challenge for a long time due to the following problems: 1). molecular ion interference due to the high masses of U and Th; 2). sporadic instrumental isotope fractionation; 3). control of the ion species (metal vs. oxide); and 4). the extreme isotopic ratios characteristic of natural samples (P.de Bievre, 1978). The first problem is now less pronounced due to the improvement in ultra-high vacuum technology, instrument resolution, and sample separation and purification techniques. Instrumental isotopic fractionation can be corrected by using a double-spike technique (Chen and Wasserburg, 1981). Several loading techniques were reported to enhance the emission of U metal ions, but none are both successful and straight forward. Although indirect measurement of $^{234}U/^{238}U$ ratios, i.e., measuring this ratio through an intermediate isotope such as ^{235}U, was achieved by mass spectrometry recently (Chen et al., 1986; Edwards et al., 1987a), the direct routine measurement of this ratio requires mass spectrometers of ultra-high abundance sensitivity, that is, the double-

focusing machine.

Less effort has been made to precisely measure the Th isotopes in natural samples because Th has no long lived isotopes except ^{232}Th. ^{230}Th has only been measured precisely by mass spectrometry in natural samples which contain almost no ^{232}Th (Edwards et al., 1987a, 1987b, 1988).

3.4.2. THE MASS SPECTROMETER

The mass spectrometer used in this study is a VG-354 with a 27 cm radius and 90° magnet sector. It has one Daly multiplier detector and one fixed and four externally adjustable Faraday collectors. Measurement of ion currents can be accomplished by either static multicollection mode or dynamic multicollection mode (combination of peak-jumping and static multicollection) in addition to the conventional peak-jumping mode. In peak-jumping mode, ions of all the isotopes of interest are measured sequently by the same collector. In static multicollection mode, on the other hand, ions of all the isotopes are measured simultaneously by their assigned individual collectors. This machine has a resolution of 370 and an abundance sensitivity of 2 ppm at mass 238.

The superior advantages of the Daly multiplier detector (Daly, 1960) have been taken of in this study. In contrast to an electron multiplier, the Daly detector has higher efficiency in measuring ions of low and high mass range, higher gain stability, and less mass discrimination. The Daly detector is run in the analogue mode with a feed-back resistor of 1011 Ω, and can measure an ion signal ranging from less than 10^{-16} A up to 5×10^{-13} A (corresponding to 100 to 500,000 ions/second). The detector is linear within 0.25% when the signal is less than 5×10^{-13} A (VG 354 Manual). The high voltage on the Cathode of the Daly knob and the multiplier voltage for the Photomultiplier were checked and adjusted regularly to maintain a peak flatness for ^{238}U of about 2×10^{-3} for an accelerating voltage of 6 kV. These voltages were about -13.8 kV for the cathode and 1030 V for the photomultiplier.

3.4.3. FILAMENT BEADS AND BLANK

Cathodeon eight-pin filament beads (Cathodeon Ltd.) were used. They were cleaned in boiling deionized water for about 5 minutes prior to use. Different filament configurations were employed for U and Th analyses (Fig. 3.8). Uranium was loaded on the side of a double filament assembly. Re ribbon was used as the center and Ta ribbon as the side filament. Triple filaments composed of Re ribbon

Figure 3.8.   Double and triple filaments configuration.
    Uranium is loaded on to the center of the Ta side of the
    double filament.   Thorium is loaded on to the crimped Re
    side of the triple filament.
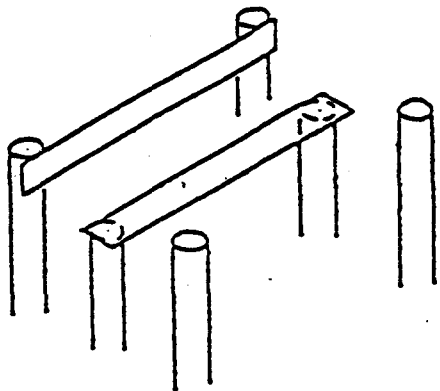
Double Filament (Ta-Re)
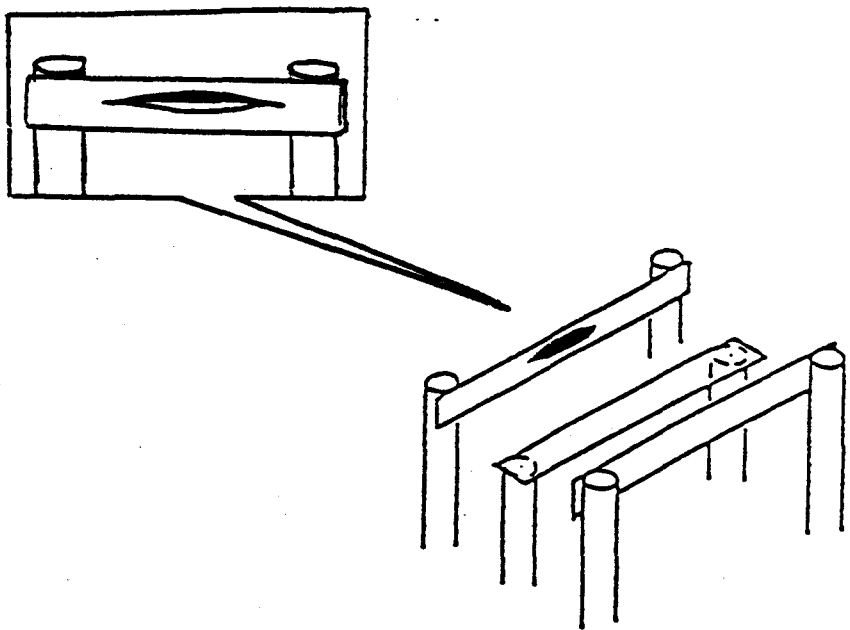
Triple Filament (Re-Re-Re)

as the center and both sides were used for Th analyses. Thorium samples were loaded on the side filament which was crimped into a V-shape using pliers to enhance the ionization efficiency. Filaments were outgassed for 15 minutes at 2.5 A under vacuum before samples were loaded.

All filament ribbon (H. Cross Company) was 25 μm thick and 760 μm wide. Filament blanks for four kinds of ribbon (standard purity Re, high purity Re, and standard purity Ta, and high purity Ta) were assessed by analyzing both pre-outgassed and non-outgassed filament beads with no samples. One batch of standard purity (99.95%) Re ribbon was found to generate U and Th signals at a filament current of about 4 A. When filaments were heated to the typical running current of 5 A, the $^{238}U^+$ current was found to be between 200 and 10,000 ions/second, while $^{232}Th^+$ ranged from 200 to 50,000 ions/second.

Zone-refined high purity Re ribbon from four different batches (supplied to McMaster, Royal Ontario Museum, and Lamont-Doherty Geological Observatory) was tested. When filaments were heated to 5 A, $^{238}U^+$ was between 5 and 150 ions/second with the majority gave less than 20 ions/second. The $^{232}Th^+$ was about 10 to 250 ions/second, with the majority less than 30 ions/second. A new batch of Zone-refined Re ribbon obtained in July, 1988, (H. Cross Company)

shows U and Th signals of less than 20 counts/second at a current of 5.4 A. The U and Th blanks were consistent for all the four batches. No $^{234}U^+$ and $^{230}Th^+$ signals were seen for any of the ribbon tested.

Standard purity Ta ribbon used at McMaster was found to produce $^{238}U^+$ (or $^{254}UO^+$) and $^{232}Th^+$ (or $^{248}ThO^+$) signals only when heated above 3.3 A. It has a much higher Th blank than standard purity Re ribbon. A recently purchased high purity Ta ribbon has U and Th blanks of less than 30 counts/second at 5.4 A. The Ta filament blank was not a problem even using standard purity Ta ribbon since all samples were run at side filament currents less than 2.8 A.

Outgassing of the filaments for a longer time before loading into the mass spectrometer did not reduce the blanks. However, during the first two minutes of the run, when the filament current was brought up to about 5 A, abnormally large U and Th signals were always found. They both quickly died away in about 5 minutes. These abnormal signals could be the result of molecular hydrocarbon ions because the high U and Th signals were coupled with an increase in vacuum pressure (above 5×10^{-7} mbar) during the initial outgassing of the filaments. The samples were normally run at the vacuum of below 5.0×10^{-7} mbar.

3.4.4. LOADING TECHNIQUE, ION SPECIES, AND IONIZATION EFFICIENCY

Metals like U and Th, with high ionization potentials, tend to emit as oxide ions rather than metal ions from thermal ionization sources at low filament temperature. Control of ionic species is very important especially in trace analyses because single ion species emission will lengthen the sample life. Measuring U and Th through oxide ions by TIMS also encounters problems as such as magnet shift due to their higher masses, and corrections for oxygen isotope composition.

Several methods had been tried to enhance U and Th metal ion emission, and some were successful in determining U as low as 10^{-14} g/ml. A thermal ionization-diffusion method involving coating the sample on the filament with a high work function material such as Pt, had been successful in allowing trace U analyses in water samples (Rec et al., 1974). However, this is very time consuming and it is very difficult to control the thickness of the coating. This method was later modified by using electrodeposition as a loading technique so that U^+ ions could emit at a low filament current and therefore significantly reduce the filament blank (Rokop et al., 1982). However, in electrodeposition there is inevitably some loss of U during

electrodeposition.

The in-situ reduction of oxide to metal by either coating the outgassed ribbon with or loading the sample with graphite was used by Chen and Wasserburg (1981) and Arden and Gale (1974). However, when this method was tried here, it was found to have two problems: increase in U and Th blanks due to the impure graphite and loss of the samples because they were easily shaken off the filaments, i.e., the samples did not adhere well to the filament.

Uranium and Th metal ions are emitted at high temperatures. Triple and double filaments first designed by Inghram and Chupka (1953) are used because the sample evaporation rate can be controlled by adjusting the side filament current, and the ionization efficiency is enhanced by adjusting the center filament current.

Uranium was loaded on the center of the Ta side filaments with approximate 1 μl of 0.3 M H_3PO_4 and dried by slowly increasing the current to 2.0 A. Thorium was loaded onto the center of the V-shaped side filament with approximate 1 μl of 0.3 M H_3PO_4 and dried by slowly increasing the current to 2.0 A.

Samples were preheated under the in the mass

spectrometer for 5 minutes at a center filament current of 3.5 A and a side filament current of 1.5 A for U and 1.8 A for Th. Uranium samples were run at a Re^+ ion current of 2.0×10^{-12} A (corresponding to a center filament current of about 4.7 A) and the side filament currents between 1.9 and 2.4 A. Thorium samples were run at a Re^+ ion current of 2.0×10^{-11} A (corresponding to a center filament current of about 5.0 A) and at side filament currents of 2.3 to 2.7 A.

Both U^+ and Th^+ metal ion signals increase rapidly with increasing center filament current (Table 3.2, Fig.3.9, 3.10, 3.11, 3.12). For U analyses, Ta ribbon was preferred to Re as the side filament because it produced a more stable signal and a higher U^+/UO^+ ($>10^4$). At the typical running center filament current, the Th^+/ThO^+ ratio was about two to three.

A filament loaded with about 50 ng pure Th standard produced an ion beam of 5×10^{-13} A that lasted for 3.5 hours. A 50 ng pure natural U standard gave a $^{235}U^+$ ion beam of 3.0×10^{-14} A that lasted for about 4 hours. The overall efficiency, including ionization and transmission, of U emitted as metal ions was about 4×10^{-3}, while that of Th as metal ions was about 5×10^{-5}.

Due to the difference in evaporation and ionization

Table 3.2. Temperature Effect on Ion Intensities and Ion Species.

TRIPLE Re FILAMENT WITH 100 ng Th

CURRENTS (A)		C232	C248	TOTAL	R248/232
CENTER	SIDE	(IONS/S)	(IONS/S)	(IONS/S)	
4.70	2.6	21000	72000	93000	3.42
4.78	2.6	68500	76200	145000	1.12
4.95	2.6	110000	76000	186000	0.69
5.00	2.6	116000	74000	190000	0.63
5.10	2.6	158000	72000	230000	0.45
5.25	2.6	205000	68000	273000	0.33
4.72	2.6	7300	7700	15000	1.06
4.80	2.6	38600	33100	71700	0.86
4.98	2.6	42100	24800	66900	0.59
5.02	2.6	51500	18500	70000	0.36
5.05	2.6	57500	14300	71800	0.25
5.15	2.6	67500	11400	79000	0.17

DOUBLE Re FILAMENT WITH 100ng U

CENTER	SIDE	C238	R254/238
		(IONS/S)	
4.22	1.98	76300	0.325
4.30	1.98	140000	0.152
4.55	1.98	345000	0.051
4.95	1.98	425000	0.024
5.05	1.98	470000	0.016
5.10	1.98	530000	0.011

DOUBLE Re/Ta FILAMENT WITH 100ng U

CENTER	SIDE	C238	R254/238
		(IONS/S)	
4.40	2.0	138000	0.00007
4.60	2.0	142000	0.00004
4.72	2.0	300000	0.00008
4.82	2.0	540000	0.00007

1: C232 and C248 are the count rates measured at mass
   positions of 232 and 248, C238 and C254 the count
   rates at 238 and 254 repectively.
2: R248/232 and R254/238 are the ratios of oxide ions
   to metal ions.

Figure 3.9. $^{238}U^+$ intensity (in ions per second) increases rapidly with the center filament current that corresponds to temperature. About 100 ng U was loaded on to a double Re-Re filament which was run at a side filament current of 1.98 A.
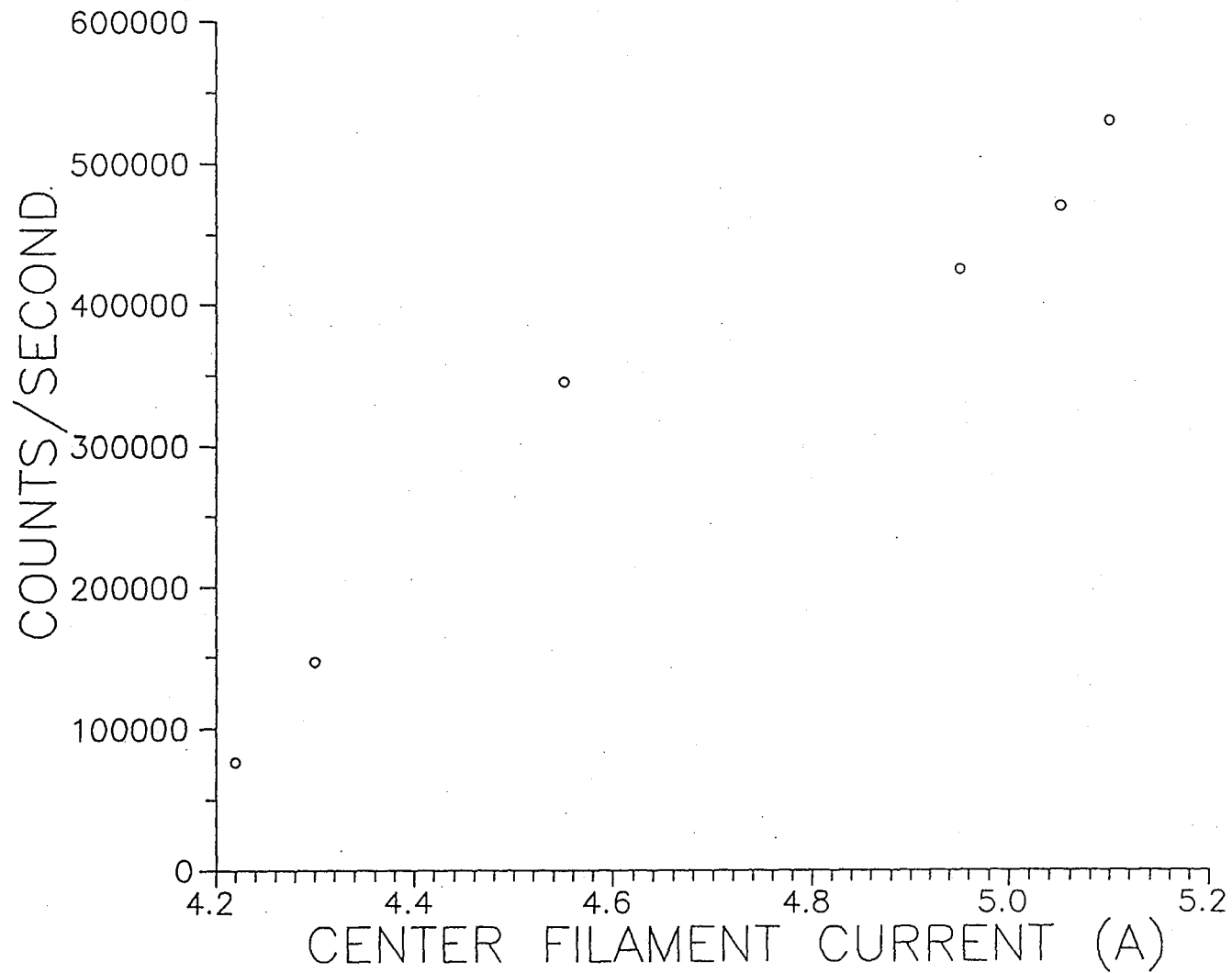
Figure 3.10. Variation of Th ion intensities with the center filament current. ^{232}Th$^+$ increases rapidly with center filament current, while ^{248}ThO$^+$ stays the same. About 100 ng Th was loaded on to a triple Re-Re-Re filament bead which was run at a side filament current of 2.6 A.
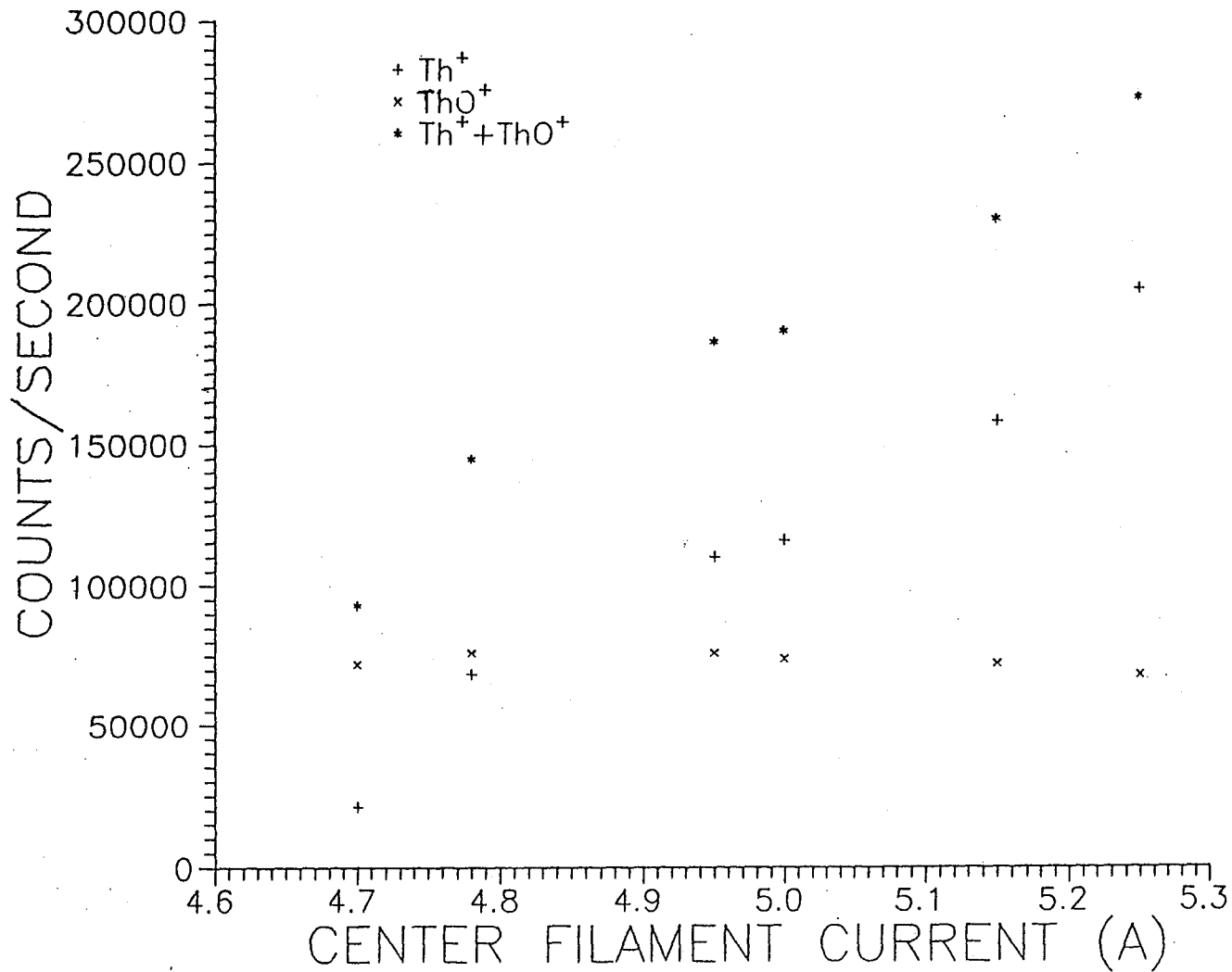
Figure 3.11. Variation of $^{254}UO^+/^{238}U^+$ with the center filament current. Uranium metal ion is more than 95% of the total ions at the typical center filament current of 4.6 A. This was a double Re-Re filament bead loaded with about 100 ng U and run at a side filament current of 1.98 A.
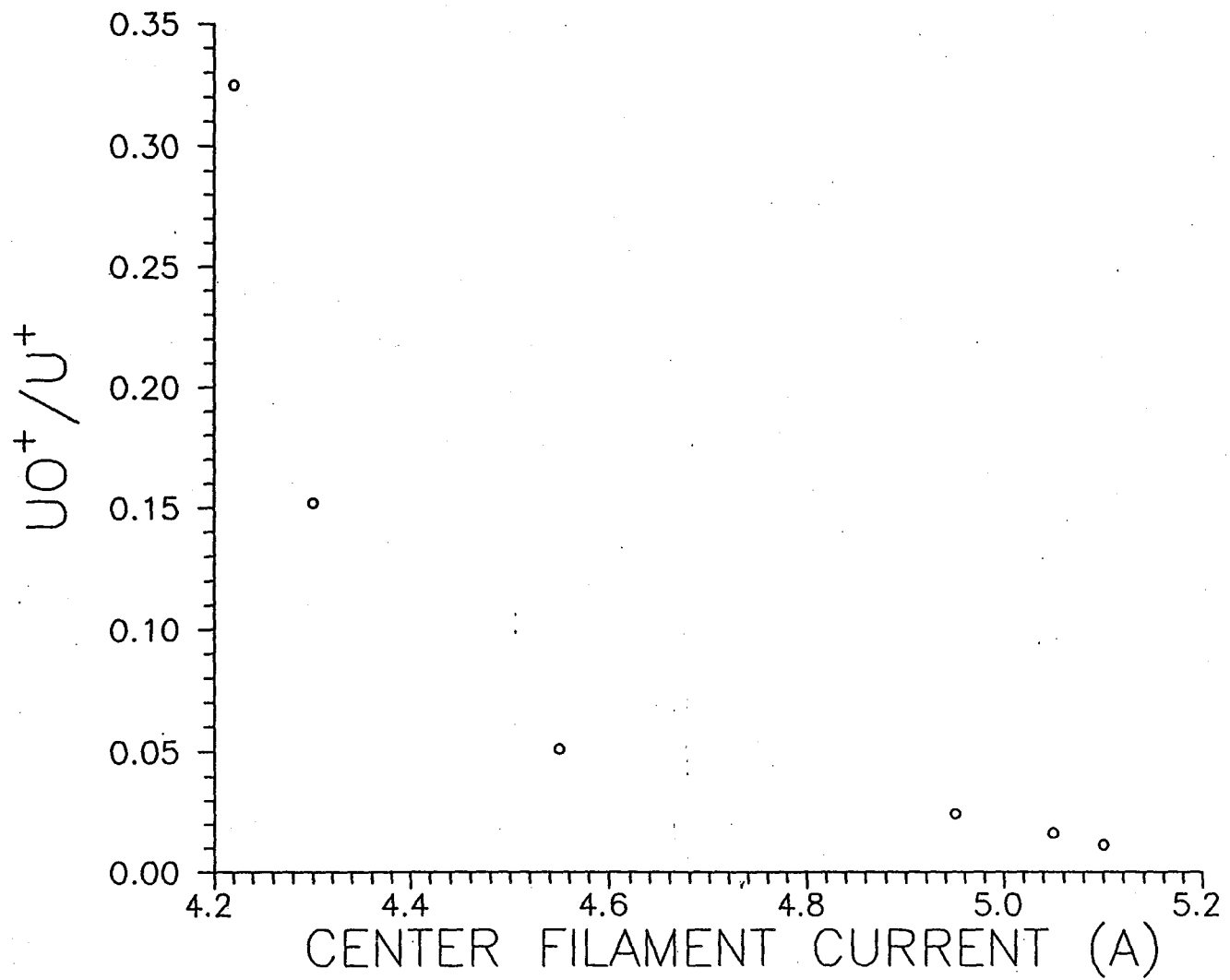
Figure 3.12. Variation of ^{248}ThO$^+$/^{232}Th$^+$ ratios with the center filament current. Thorium metal ions is more than 70% of the total at the typical center filament current of 5.0 A. These two beads were triple Re filaments loaded with 100 ng Th and were run at a side filament current of 2.6 A.
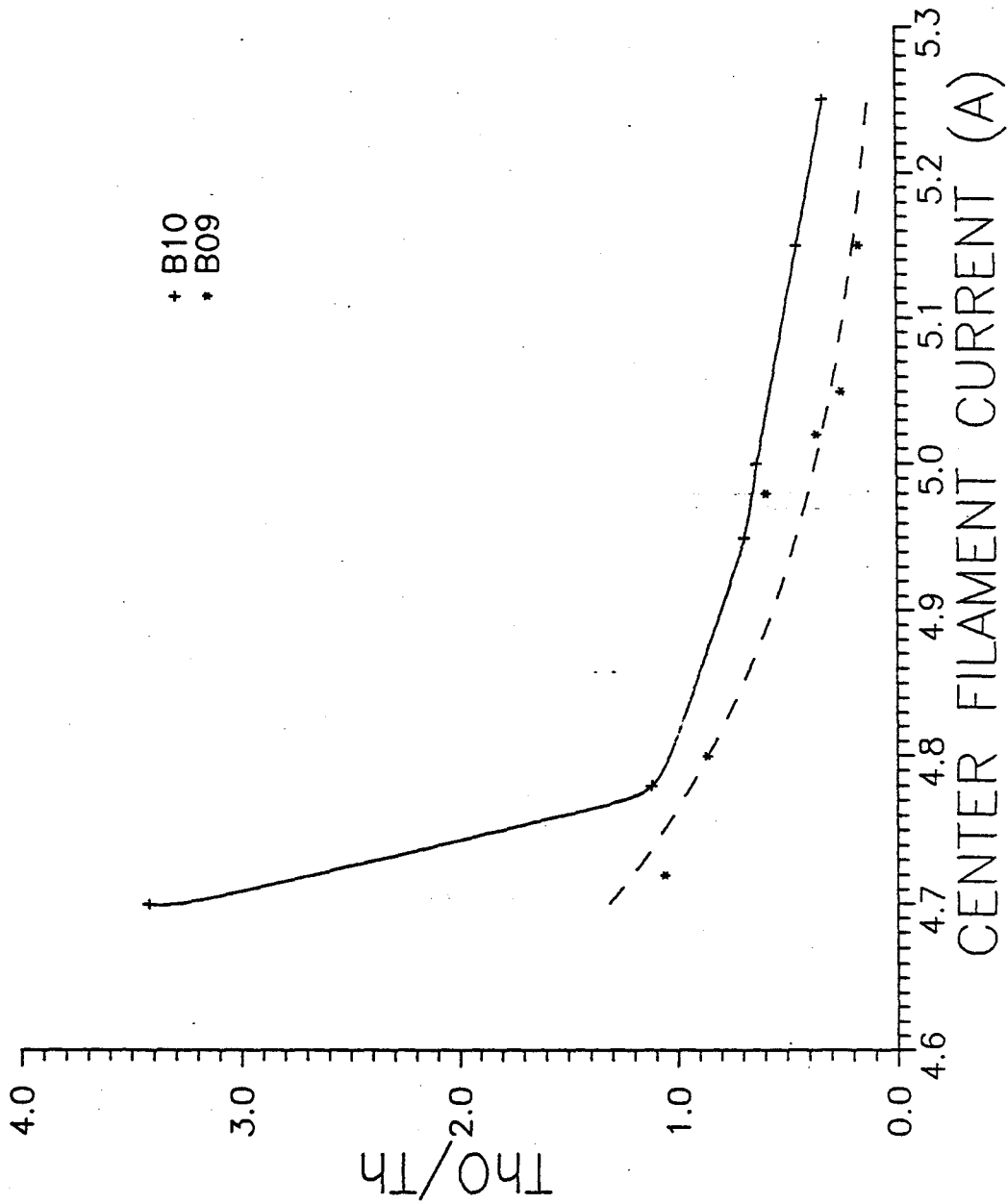
temperatures between U and Th, U and Th can be loaded on to the same filament bead. Uranium can be run at a low temperature (at the center filament current of 4.6 A and side around 2.1 A) without any loss of Th. Thorium can be run later at a higher temperature (at a center filament current of 5.0 A and side around 2.6 A). This method was used at the beginning of the study. However, frequent center filament failure occurred after U runs due to the high center filament current necessary for U and Th analyses. In addition, the presence of U in Th samples or the presence of Th in U samples will reduce the ionization efficiency of Th or U (Edwards et al., 1987a). Therefore, U and Th were run on separate filament beads in this study.

3.4.5. DATA ACQUISITION AND BACKGROUND

All the isotopic analyses were computer controlled using a HP9121 computer programmed in HP basic. The running parameters, such as the filament currents, ion beam sizes, ratios to be measured, integration time for each mass, and number of data to be collected, etc., were also programmed. Those programs (so-called overlays) used for U and Th analyses were listed in Appendix 3.1. The Daly detector was used for all the ion current measurements through this study.

Uranium analyses were done using a two-stage program because the extreme $^{234}U/^{238}U$ ratio and the dynamic range of the Daly detector (maximum of 500,000 ions/second) limits the direct, precise measurement of $^{234}U/^{238}U$ ratios in natural samples. In the first stage, $^{235}U/^{238}U$ and $^{236}U/^{238}U$ ratios were measured in the scanning sequence of $^{235}U-^{236}U-^{238}U$. Backgrounds were measured at 0.5 mass units above and below each mass. ^{235}U was measured for 4 seconds, ^{236}U for 6 seconds, and ^{238}U for 1 second. Integration time for backgrounds was 2 seconds. Each cycle started by measuring mass 233.5 for 4 seconds to eliminate any ^{238}U memory effect on the detector. No ^{238}U tails on mass positions of 235 and 236 were found with ^{238}U intensities up to 500,000 ions/second since the backgrounds measured at 0.5 mass units of each peak are the same as that measured at 227 mass position. The U beam was slowly brought up to 400,000 ions/second for ^{238}U within 30 minutes. Then forty ratios were collected within about 40 minutes.

In the second stage, $^{234}U/^{236}U$ and $^{235}U/^{236}U$ ratios were measured in the sequence: $^{234}U-^{235}U-^{236}U$. ^{234}U was counted for 6 seconds, while ^{235}U and ^{236}U were counted for 4 seconds. Backgrounds were measured for 2 seconds at 0.5 mass units above and below each mass. One hundred ratios were collected over about 90 minutes with the ^{234}U

intensities ranging from 80 up to 1000 counts/second, depending on individual samples. Aiming current was optimised through the run to maintain a stable and a maximum ^{234}U ion beam and so that samples were not consumed too quickly. The background in the vicinities of ^{234}U peak was usually less than 1% of ^{234}U. A small ^{238}U tail was found on the high mass range side of 235 because the ^{238}U signal was normally larger than 3.0×10^{-12} A. For example, with a ^{238}U of 4.5×10^{-12} A, 14, 8, 3, 2, and 2 counts/second were found at the half mass positions 236.5, 235.5, 234.5, 233.5, and 232.5 respectively. Using a linear background correction (i.e., I(236)c = I(236) -[0.5xI(235.5) + 0.5xI(236.5)]) instead of the more correct hyperbolic background correction did not introduce a systematic error on ^{234}U and ^{235}U. This is because the ^{238}U tail was essentially linear over the mass 234 and 235 positions. This linear background correction would introduce a systematic error of no larger than 0.2% on ^{236}U since ^{236}U was normally larger than 8,000 counts/second. In practice, the ^{234}U was not affected at all by the ^{238}U tail. A typical U mass spectrum from a spiked sample is shown in Fig. 3.13.

Thorium was analyzed using different overlays for carbonate samples and for granitic rock samples respectively due to the difference in ^{232}Th content. Carbonate samples

Figure 3.13.   Mass   spectra of a spiked sample.   Note the
     change in scale of the peaks.   No interferences or tails
     of the major isotopes on minor isotopes are observed.

234U
1.5×10⁻¹⁶ A

235U
1.7×10⁻¹⁴ A

236U
6.8 × 10⁻¹⁵ A

235U
3.6×10⁻¹⁵ A

236U
1.5×10⁻¹⁵A

238U
5.0×10⁻¹³ A
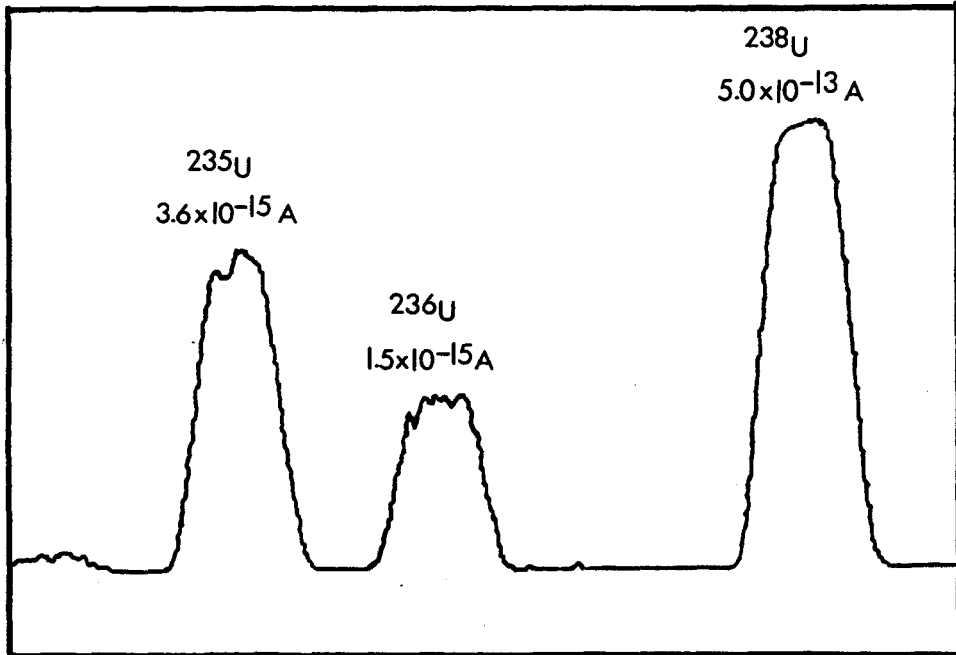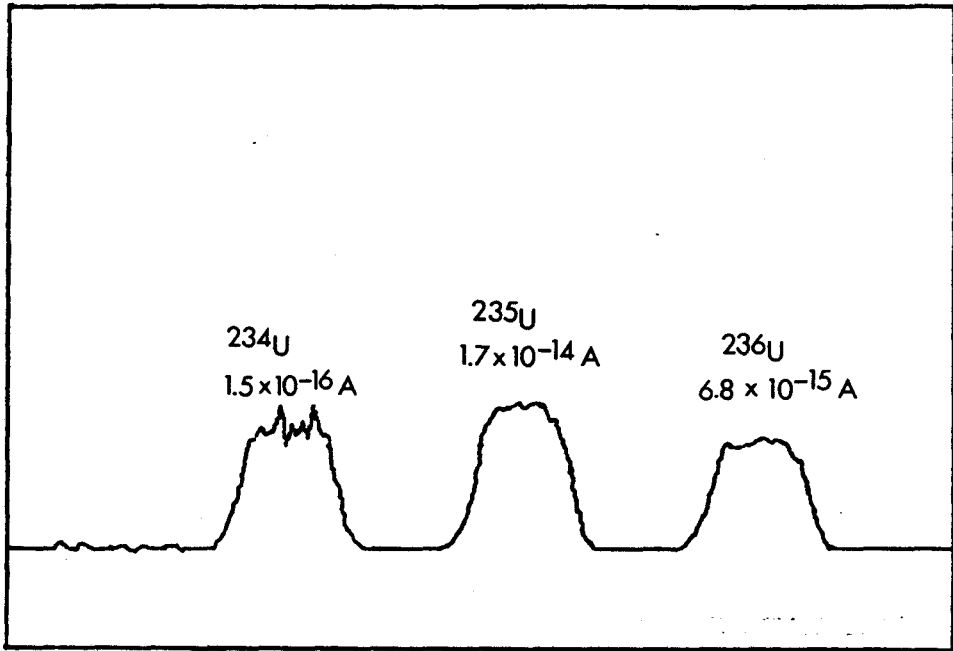
were analyzed using a one-stage program. The Th ion beam was optimised and stabilized within about 40 minutes, by adjusting the aiming current. The data were then collected. One hundred ratios were collected in eighty minutes in the scanning sequence ^{229}Th-^{230}Th-^{232}Th. ^{229}Th and ^{230}Th were measured for 6 seconds and ^{232}Th for 2 seconds. Backgrounds were measured for 3 seconds at 0.5 mass units below and above each mass. ^{230}Th ranged from 60 to 700 counts/second. Background on both sides of the ^{230}Th was less than 1% of the ^{230}Th peak when ^{230}Th was larger than 150 counts/second. No tail effect was found on ^{230}Th from either ^{229}Th or ^{232}Th since ^{232}Th was normally less than 100,000 counts/second and ^{229}Th was even smaller.

Thorium from granitic samples was analyzed using a two-stage program since the $^{230}Th/^{232}Th$ ratio was normally less than 10^{-6} and this ratio could not be measured directly. In the first stage the $^{229}Th/^{232}Th$ ratio was measured with a ^{232}Th current of 450,000 counts/second. ^{229}Th was counted for 6 seconds and ^{232}Th for 1 second. Backgrounds were measured for 2 seconds at 0.5 mass units below and above 229. Background on the two sides of ^{229}Th was normally 1 to 2%. Memory effects of the large ^{232}Th peak on the Daly detector were eliminated by counting the 227.5 mass position for 4 seconds. The $^{229}Th/^{232}Th$ ratio was usually very small (around 10^{-3}) and could not normally be measured to a

precision of better than 1% (2σ). For better results, a sample aliquot should be spiked separately from the aliquot for ^{230}Th analysis so that a higher ^{229}Th/^{232}Th ratios would give a better determination of the ^{232}Th content.

In the second stage of the program, the ^{230}Th/^{229}Th ratio was determined by counting only ^{229}Th and ^{230}Th for 4 and 6 seconds respectively. Backgrounds for ^{229}Th were measured for 2 seconds at 0.5 mass units below and above mass 229. Backgrounds for ^{230}Th were measured at 230.3, 230.5, 230.7, 231.0, and 231.3 mass positions to correct for ^{232}Th tail. This defined a hyperbolic background curve extending from mass position of 229.5 and up. When ^{232}Th was about 2.0×10^{-11} A, the background at 230.3 was as high as 31 counts/s. However, normal background at 230.3 was between 5 and 25 counts/s. The background correction for ^{230}Th assuming a linear background between 229.5 and 230.3 ($B(230) = 0.5 \times I(229.5) + 0.5 \times I(230.3)$) was as good as the background correction using the best-fit hyperbolic background correction within the counting error (Table 3.3, Fig.3.14). Background for ^{230}Th for most samples was corrected assuming it was linear between mass 229.5 and 230.3. The ^{230}Th signal ranged from 35 to 150 counts/s and was typically 80 counts/s.

Table 3.3.   Backgound Correction of Th-230 Mass Spectrum.

MASS POSITION	A	B	C	D	E
228.5	0	0	2	7	26
229.5	0	2	8	11	38
230.3	1	10	18	23	63
230.5	3	14	24	31	66
230.7	6	18	31	42	76
231.0	12	35	51	61	109
231.3	30	66	101	124	178
CALCULATED BKG	0.5	6	13	17	50.5
CURVE FIT BKG	0.5	6	12.85	16.71	

1: A, B, C, D and E are the background in ions/second for
    different tail sizes of Th-232.   C is the typical tail size.

2: CALCULATED BKG is obtained assuming linear background
    between mass 229.5 and mass 230.3

3: CURVE FIT BKG is obtained from the fitted curved backgound
    as in Figure 2.13.

Figure 3.14. The curved background of ^{230}Th in granitic samples due to the ^{232}Th tail. The background was measured at mass positions 228.5, 229.5, 230.3, 230.5, 230.7, 231.0, and 231.3. Curves A, B, C, and D corresponds to the increase in ^{232}Th tail. The background obtained by fitting a curve doesnot differ from the one calculated assuming linear background between mass 229.5 and mass 230.3 (Table 2.3).
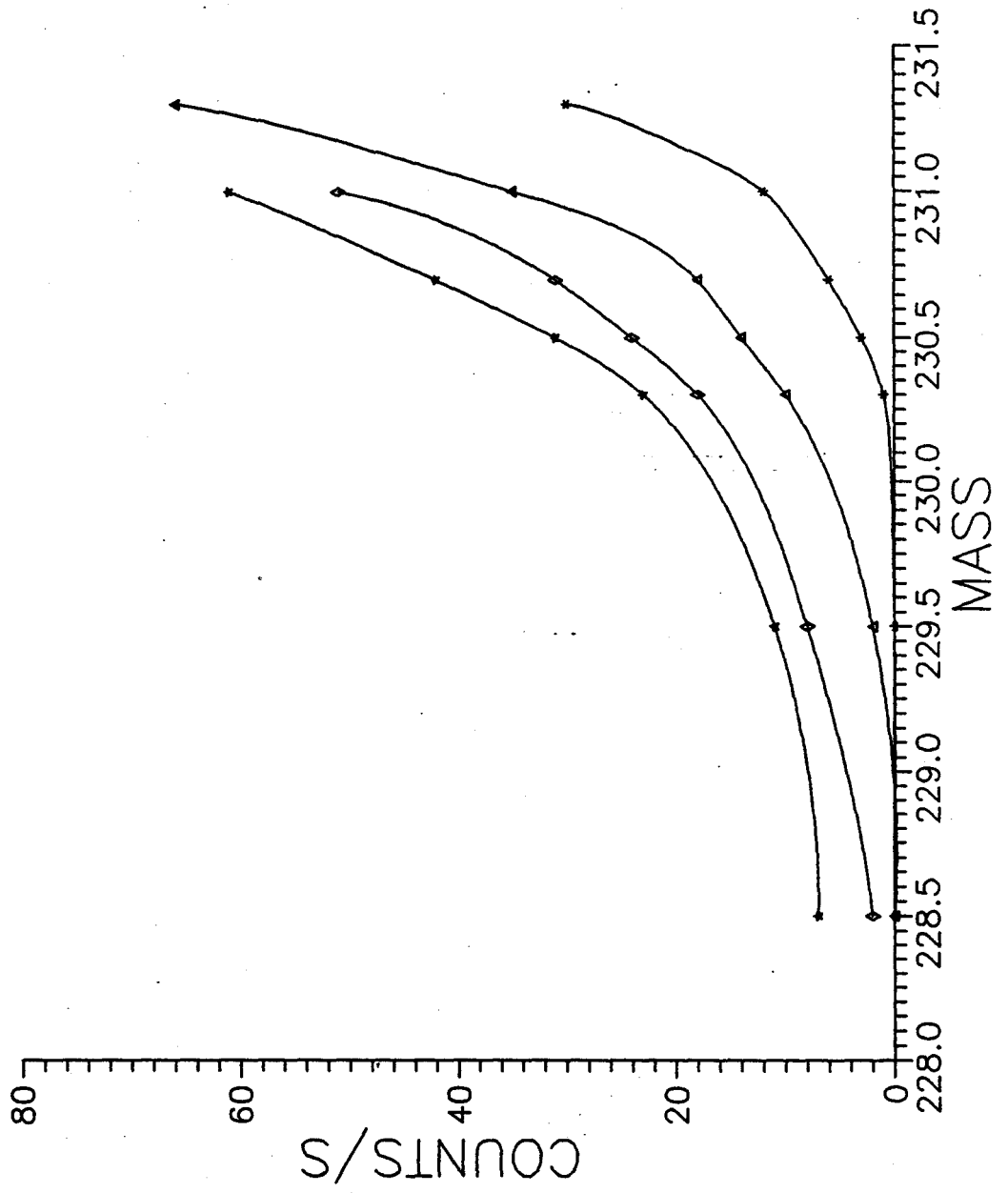
3.4.6. INSTRUMENTAL MASS FRACTIONATION AND DISCRIMINATION

Instrumental mass fractionation is a fundamental limitation to the accuracy and precision of isotopic ratio measurements in mass spectrometry. Deviations of the measured isotopic ratios from their true values are normally attributed to two major sources when Daly multiplier detectors or electron multipliers are used. They are the mass fractionation in the ion source of the mass spectrometer when the atoms are ionized and mass discrimination at the detectors where the charged ions are measured. Mass discrimination is normally constant with constant ion kinetic energy. However, mass fractionation is dependent on various factors, such as temperatures at which the samples are evaporated and ionized, sizes of samples, loading techniques, sample purity and chemical forms, etc.. Uranium is a well-known example (P de Bievre, 1978).

Both mass fractionation and discrimination are mass dependent and enhance the signals of the lighter isotopes by the same first order approximate factor of $(m/n)^{0.5}$, where m and n are the mass numbers of the heavy and light isotopes respectively. Unfortunately, these two sources cannot be assessed separately if the Daly detector is used. However, the mass fractionation was shown to be very small by the measurements of the NBS 500 U standard using the Faraday

collector. The latter does not introduce any significant mass discrimination effects (Table 3.4). The mean fractionation factor obtained from the mean of six measured $^{235}U/^{238}U$ ratios of the NBS 500 U standard was only -0.07‰ per mass unit. In contrast, the overall deviation of the mean measured $^{235}U/^{238}U$ ratio of twelve analyses using the Daly was as large as 5.00‰ per mass unit (Table 3.5), confirming that the mass discrimination on the Daly detector was the major source of the large deviation of the measured isotopic ratios. Fortunately, the overall deviations in permil per mass unit calculated from the measured $^{234}U/^{238}U$, $^{235}U/^{238}U$, and $^{236}U/^{238}U$ ratios of the NBS 500 U standard were very similar (Table 3.5), which indicates that the overall deviation is still mass dependent and can be corrected as if only mass fractionation happens when the Daly detector is used. This observation is consistent with the fact that the discrimination factor $(m/n)^{0.5}$ is equivalent to a fractionation law at the first order. Note that the mean fractionation factors in permil per mass unit calculated from the measured $^{236}U/^{238}U$ ratio in both Table 3.4 and 3.5 are slightly larger than those from the measured $^{234}U/^{238}U$ and $^{235}U/^{238}U$. This can be attributed to the error in measuring the small ^{236}U peak. Therefore, mass discrimination is corrected along with mass fractionation correction, hence, both of them were discussed under the instrumental mass fractionation thereafter.

Table 3.4. NBS 500 U Standard Analyses Using the Faraday Collector.

SPM. #	Rm48	2 SIGMA	Rm58	2 SIGMA	Rm68	2 SIGMA	Rc48	Rc68	Fract	FRACT48	FRACT58	FRACT68
1	0.0104169	0.0000073	0.99926	0.00010	0.0015129	0.0000062	0.0104231	0.0015133	1.00015	-0.12	-0.15	-1.95
2	0.0104223	0.0000086	0.99992	0.00022	0.0015200	0.0000099	0.0104192	0.0015198	0.99993	0.01	0.07	0.33
3	0.0104214	0.0000098	0.99904	0.00002	0.0015151	0.0000100	0.0104306	0.0015158	1.00022	-0.01	-0.22	-1.22
4	0.0104158	0.0000083	0.99908	0.00005	0.0015124	0.0000059	0.0104244	0.0015130	1.00021	-0.15	-0.21	-2.11
5	0.0104359	0.0000123	1.00036	0.00010	0.0015133	0.0000108	0.0104267	0.0015126	0.99978	0.33	0.22	-1.82
6	0.0104100	0.0000106	0.99929	0.00005	0.0015074	0.0000105	0.0104157	0.0015078	1.00014	-0.29	-0.14	-3.77
TRUE VALUE	0.0104220 +/-0.000018		0.99970		0.001519 +/-0.000006		0.0104220	0.001519				
MEAN(S)	0.0104204		0.99949		0.0015135		0.0104233	0.0015137	1.00007	-0.04	-0.07	-1.75
2 SIGMA	0.0000161		0.00097		0.0000075		0.0000097	0.0000072				

1. Samples were run using the accelerating votage of 6 kv.
2. Rm donates the measured ratio, while Rc48 and Rc68 are the fractionation corrected ratios using 235U/238U ratio of 0.99970.
3. Fract is the fractionation factor in per mass unit obtained through Rm58 ratios. FRACT48, FRACT58 and FRACT68 are fractionation factors in permil per mass unit obtained through Rm48, Rm658, and Rm68 respectively.

Table 3.5 NBS 500 U Standard Analyses Using the Daly Detector

SAMP. #	Rm48	2 SIGMA	Rm58	2 SIGMA	Rm68	2 SIGMA	Rc48	Rc68	Fract	FRACT48	FRACT58	FRACT68
1	0.0106254	0.0000085	1.01329	0.00097	0.0015316	0.0000022	0.0104358	0.0015179	0.99551	4.82	4.49	4.19
2	0.0106455	0.0000066	1.01472	0.00046	0.0015345	0.0000021	0.0104359	0.0015193	0.99504	5.29	4.96	5.13
3	0.0106852	0.0000053	1.01815	0.00024	0.0015546	0.0000022	0.0104278	0.0015358	0.99392	6.22	6.08	11.58
4	0.0106657	0.0000077	1.01698	0.00020	0.0015391	0.0000022	0.0104248	0.0015216	0.99430	5.76	5.70	6.62
5	0.0106557	0.0000064	1.01608	0.00016	0.0015395	0.0000020	0.0104273	0.0015229	0.99460	5.53	5.40	6.75
6	0.0106600	0.0000049	1.01682	0.00014	0.0015475	0.0000018	0.0104214	0.0015301	0.99436	5.63	5.64	9.32
7	0.0106651	0.0000058	1.01671	0.00024	0.0015368	0.0000014	0.0104279	0.0015196	0.99439	5.75	5.61	5.87
8	0.0106221	0.0000076	1.01425	0.00039	0.0015389	0.0000026	0.0104194	0.0015241	0.99520	4.74	4.80	6.55
9	0.0106321	0.0000098	1.01225	0.00051	0.0015271	0.0000036	0.0104567	0.0015145	0.99585	4.98	4.15	2.72
10*	0.0105901	0.0000070	1.01090	0.00032	0.0015336	0.0000021	0.0104339	0.0015223	0.99629	3.99	3.71	4.84
11*	0.0106222	0.0000068	1.01361	0.00016	0.0015342	0.0000018	0.0104283	0.0015201	0.99540	4.75	4.60	5.03
12*	0.0106380	0.0000061	1.01453	0.00024	0.0015338	0.0000020	0.0104312	0.0015188	0.99510	5.12	4.90	4.90
TRUE VALUE	0.0104220 +/-0.000018		0.99970		0.001519 +/-0.000006		0.0104220	0.001519				
MEAN(12)	0.0106423		1.0149		0.001538		0.0104309	0.001522	0.99500	5.21	5.00	6.13
2 SIGMA	0.0000495		0.0041		0.000014		0.0000184	0.000011				

1: Those marked with * were measured using the accelerating votage of 8 kv, others 6 kv.
2: Rm is the measured ratio, while Rc48 and Rc68 are the fractionation corrected ratios using
   235/238 ratio of 0.99970.
3: Fract is the fractionation factor in per mass unit obtained through Rm58 ratios. FRACT48, FRACT58 and FRACT68
   are fractionation factors in permil per mass unit obtained through Rm48, Rm58, and Rm68 respectively.

Despite the fact that mass fractionation accounts for a small portion of the large instrumental mass fractionation observed on NBS 500 U standard, variation in overall U instrumental mass fractionation using the Daly detector was still found to be sporadic and relatively large. The fractionation factor obtained from the individually measured $^{235}U/^{238}U$ ratios of the Natural U standard of McMaster ranged from 7.3‰ to 2.8‰ per mass unit, corresponding to a difference of more than 1% between measured $^{235}U/^{238}U$ ratios (Table 3.6). However, the fractionation factors for most individual measurements were consistent and had an average of 4.7‰ per mass unit, similar to what was observed on the 12 analyses of the NBS 500 U standard (Table 3.5). Changing the accelerating voltage from 6 kV to 8 kV did not affect the fractionation factor very much (Table 3.5).

Since instrumental fractionation can be sporadic as shown in Table 3.5 and 3.6, correction for instrumental fractionation using an average fractionation factor can introduce quite a large uncertainty, on the order of 1%. Therefore, accurate mass fractionation correction is a prerequisite for any precise and accurate isotopic ratio measurements. This can only be done by internal normalization. That is, the measured ratios of interest are corrected for fractionation using the fractionation factor

Table 3.6. Analyses of the Natural Uranium Standard.

DATE	Rm58	2 SIGMA	Frct.(permil)
10/04/88	0.007380	0.000001	5.79
10/04/88	0.007415	0.000040	7.34
10/04/88	0.007409	0.000017	7.09
10/04/88	0.007394	0.000036	6.43
22/04/88	0.007380	0.000020	5.81
22/04/88	0.007355	0.000023	4.68
31/12/87	0.007357	0.000026	4.75
09/06/88	0.007368	0.000028	5.25
09/06/88	0.007382	0.000026	5.88
12/12/87	0.007348	0.000008	4.35
12/12/87	0.007355	0.000003	4.66
31/12/87	0.007357	0.000026	4.75
31/12/87	0.007340	0.000005	3.98
23/01/88	0.007330	0.000004	3.53
23/01/88	0.007327	0.000004	3.40
23/01/88	0.007314	0.000007	2.81
23/01/88	0.007319	0.000007	3.03
23/01/88	0.007314	0.000005	2.81
23/01/88	0.007334	0.000005	3.71
TRUE	0.007253		
MEAN(19)	0.007357	0.000030	4.74 +/-2.69

1: Rm58 is the measured 235/238 ratio.
2: Fractionation in permil per mass unit is calculated
   using the recommeded value of 0.0072526.

acquired by normalizing a measured isotopic ratio to its
known constant value (the so-called internal standard).
This is possible only for those elements which have at least
three isotopes, among which there is at least one constant
and accurately known isotopic ratio. For example, in Sr
isotopic analyses, a fractionation correction is applied to
the $^{87}Sr/^{86}Sr$ ratio by normalizing the measured $^{87}Sr/^{86}Sr$
ratio against the measured $^{86}Sr/^{88}Sr$ which has an assigned
value of 0.1194. Either a linear law or a power law can be
used for fractionation correction (Russell et al., 1978;
Wasserburg et al., 1981). A power law was used in this
study, in which the fractionation factor in permil per mass
unit is obtained through equation 3.1.

$$Fract = [1-(Rt/Rm)^{(1/\Delta m)}] \times 1000 \qquad (3.1)$$

Where Rt is the true value of the normalizing isotopic
ratio, Rm the measured value and Δm the mass difference
between the two measured isotopes.

Even though natural U has a constant, well-determined
$^{235}U/^{238}U$ ratio of 0.0072526, it cannot be used directly as
an internal standard for ^{234}U determination because the
extreme low $^{234}U/^{238}U$ ratio hinders the direct, precise
measurement of $^{234}U/^{238}U$ and $^{234}U/^{235}U$ ratios while
$^{235}U/^{238}U$ ratio is measured. Therefore, other researchers

have used a double spiking procedure where the sample was added a mixed ^{233}U-^{236}U spike to allow fractionation correction (Dietz et al, 1962; Chen and Wasserburg, 1981; Chen et al., 1986; Edwards et al., 1987a).

However, a ^{236}U single-spike, two-stage scanning method was used in this study. The ^{236}U spike used in this study contains 0.2237 ± 0.0010% ^{238}U, 0.0074 ±.0013% ^{235}U, and undetectible ^{234}U (Table 3.8). Samples were spiked so that $^{236}U \approx ^{235}U$. Therefore, the $^{235}U/^{238}U$ ratio in the spiked samples would not be changed by more than 0.002% due to the ^{238}U and ^{235}U in the spike. In the first stage of the program, the $^{236}U/^{238}U$ ratio was corrected for fractionation by normalizing the measured $^{235}U/^{238}U$ ratio to its accepted value of 0.0072526 (equation 3.2). Then a fractionation-corrected $^{235}U/^{236}U$ ratio was obtained by dividing 0.0072526 by the fractionation corrected $^{236}U/^{238}U$ ratio obtained in the first-stage (equation 3.3).

$$Rc_{68} = Rm_{68} \times [(0.0072526/Rm_{58})^{(1/3)}]^2 \qquad (3.2)$$

$$Rc_{56} = 0.0072526/Rc_{68} \qquad (3.3)$$

Where Rm_{68} denotes the measured $^{236}U/^{238}U$ ratio, Rm_{58} the measured $^{235}U/^{238}U$ ratio, Rc_{68} the corrected $^{236}U/^{238}U$ ratio, Rc_{56} the corrected $^{235}U/^{236}U$ ratio and the 2 in the

superscript the mass difference of ^{236}U and ^{238}U.

The fractionation corrected $^{235}U/^{236}U$ ratio was used as an internal standard for fractionation correction in the second stage of the program. The measured $^{234}U/^{236}U$ ratio was corrected for fractionation using the fractionation factor obtained by normalizing the measured $^{235}U/^{236}U$ ratio in the second stage against its corrected value obtained in the first stage of the program (equation 3.4). The value of the fractionation factor of the second stage is different from that of the first stage by often more than 1%, confirming the necessity of using a internal standard for fractionation correction. Therefore, the fractionation corrected $^{234}U/^{238}U$ ratio was obtained by dividing the fractionation corrected $^{234}U/^{236}U$ ratio acquired in the second stage by 0.0072526 (equation 3.5).

$$Rc_{46} = Rm_{46} \times [(Rc_{56}/Rm_{56})]^2 \qquad (3.4)$$

$$Rc_{48} = Rc_{46} \times Rc_{68} \qquad (3.5)$$

Where Rm_{46} denotes the measured $^{234}U/^{236}U$ ratio, Rc_{46} its corrected ratio, Rc_{48} the corrected $^{234}U/^{238}U$ ratio.

The instrumental mass fractionation in Th analyses cannot be corrected by an internal standard method due to

the lack of a suitable long-lived isotope of Th to be used as an internal standard. Fortunately, Th mass fractionation was found to be relatively small. Fig.3.15 shows deviations (permil) of the means of ten successive measured ^{232}Th/^{229}Th ratios from the grand mean of the run (90 ratios) in a spike calibration run with about 10 ng total Th loaded on the filament. The fractionation D is calculated using equation 3.6 and is equivalent to the mass fractionation factor in permil per mass unit.

$$D=\{[(^{232}Th/^{229}Th)_t/(^{232}Th/^{229}Th)_g]^{(1/3)}-1\}\times1000 \quad (3.6)$$

where $(^{232}Th/^{229}Th)_t$ denotes the mean of any ten measured ratios, $(^{232}Th/^{229}Th)_g$ the mean of the run. The means of the ten measured ^{232}Th/^{229}Th ratio slightly increased throughout the run. The total variation caused by fractionation was less than 2.0‰ per mass unit over the run (Fig. 3.15). Smaller fractionation is expected when a larger sample size was used. In addition, the mass fractionation for Th was, unlike the sparadic variations in that of U, quite reproducible even for extreme values of the ^{230}Th/^{232}Th ratio (5.6x10^{-5}), (Table 3.7). Twelve of seventeen analyses of ^{230}Th/^{232}Th for the natural Th standard of McMaster, analyzed as Th metal ions, yielded a mean ratio of 0.0000756 ± 0.0000006 (2σ) without fractionation correction (the other five ratios with 2σ

Figure 3.15. Deviation of ten measured $^{232}Th/^{229}Th$ ratios from the grand mean of a spike run in parts per thousand. D is equivilent to mass fractionation factor. The X axis represnts the running time which is represented in number of cumulated ratios. The sample size is around 10 ng Th and the measured $^{232}Th/^{229}Th$ ratio is 1.308. This shows the mass fractionation of the run is very small and is within ± 2%..

$$D = \left(\left(\frac{\left(\frac{^{232}Th/^{229}Th}{}\right)_{tm}}{\left(^{232}Th/^{229}Th\right)_{gm}}\right)^{\frac{1}{3}} - 1\right) \times 10^{3}$$

~8 ng Th

NUMBER OF CUMULATED RATIOS

D (PERMIL)
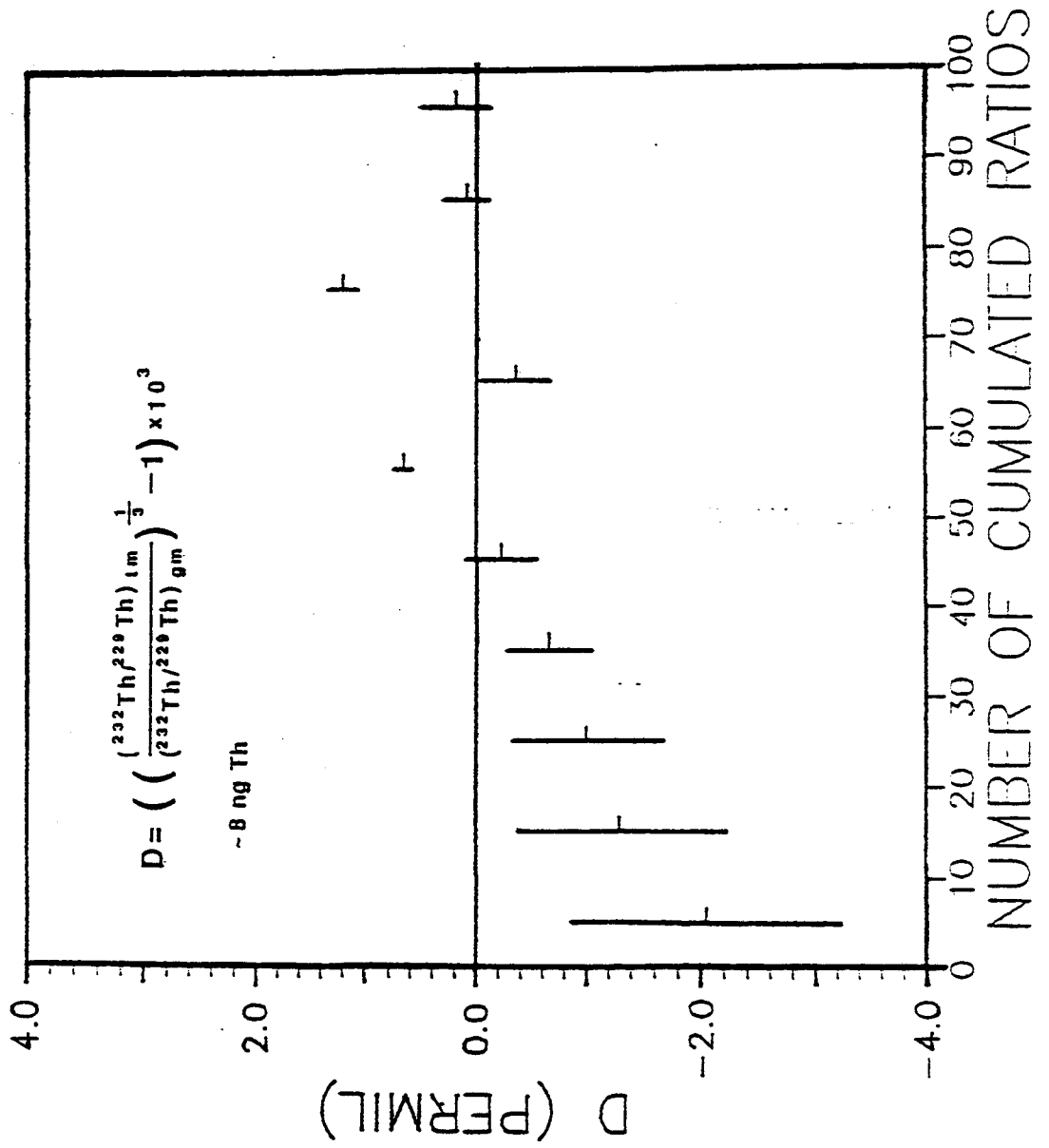
Table 3.7.   Analyses of the Natural Thorium Standard.

SAMP. #	DATE	RmO2	2 SIGMA	Rm68 !	2 SIGMA
1	17/09/87			0.0000757	0.0000004
2	19/10/87			0.0000747	0.0000007
3	31/12/87			0.0000745	0.0000004
4*	22/01/88	0.0000768	0.0000014		
5*	22/01/88	0.0000759	0.0000010		
6*	22/01/88	0.0000764	0.0000010		
7	07/03/88	0.0000754	0.0000007		
8	10/04/88	0.0000757	0.0000004		
9	10/04/88	0.0000754	0.0000005		
10	10/04/88	0.0000754	0.0000004		
11	10/04/88	0.0000752	0.0000006		
12	22/04/88	0.0000761	0.0000006		
13	22/04/88	0.0000754	0.0000004		
14	22/04/88	0.0000760	0.0000005		
15	22/04/88	0.0000755	0.0000004		
16	12/05/88	0.0000753	0.0000003		
17*	12/05/88	0.0000765	0.0000009		
18	12/05/88	0.0000760	0.0000005		
19	09/06/88	0.0000759	0.0000004		
20*	09/06/88	0.0000770	0.0000009		
MEAN OF 12		0.0000756	0.0000006		
MEAN OF 20		0.0000759	0.0000011		
MEAN OF 3				0.0000750	0.0000010

1: RmO2 is the measured 230/232 ratio, while Rm68 is the
   measured 246/248 ratio.
2: Those marked with "*" are not included in the mean of 12.
3: Those marked with "!" were measured as oxide ion.

larger than 1% were discarded). Therefore, the mass fractionation was not taken account in the correction of the total instrumental mass fractionation of Th measurements, and only the mass discrimination in the Daly detector was assumed and it could presumably be corrected by multiplying the measured ratio $^{n}Th/^{m}Th$ by $(n/m)^{0.5}$, where n and m are mass numbers. This approach would yield an unaccounted fractionation of less than 2.0‰ per mass unit. Fractionation corrected $^{230}Th/^{229}Th$ ratios for carbonate samples were obtained from corrected $^{230}Th/^{232}Th$ and $^{229}Th/^{232}Th$ ratios.

3.4.7. SPIKES AND STANDARDS

A $^{236}U-^{229}Th$ mixed spike was used in this study. The ^{236}U spike used for U series disequilibrium α spectrometry at McMaster was mixed with a ^{229}Th spike supplied from Dr. J. Harvey of the McMaster Nuclear Reactor (MNR). The ^{229}Th spike was scanned by ICP-MS. None of the U isotopes were found to be present.

The mixed spiked was diluted and stored in 2 M HNO_3 in a sealed 500 ml Teflon bottle. Isotopic compositions of U and Th in this mixed spike were determined by the mass spectrometer using 2 to 3 ml of the spike solution. Mass fractionation for U was corrected using the average

fractionation factor of 5.0‰ per mass unit, while for Th the fractionation was corrected using the method discussed in 3.4.6. Four Th runs and one U run gave the isotopic compositions of the mixed spike in Table 3.8. The ^{229}Th spike has very high ^{230}Th and ^{232}Th contents and this hinders the precise determinations of ^{230}Th and ^{232}Th contents in the samples, while the ^{236}U spike has very little ^{238}U and ^{235}U, and nondetectible ^{234}U with ^{236}U up to 4×10^5 counts/second.

To calibrate the spike concentrations, U and Th standards in HNO_3 were obtained from SPEX Industries Inc.. Uranium and Th concentrations are 1000 ppm ± 0.5% for both U and Th. These solutions were first diluted to about 100 ppm then to approximately 1 ppm. These diluted solutions (around 1 ppm) were stored in sealed 200 ml Teflon bottles in 2 M HNO_3 (Table 3.11). The isotopic compositions of the U standard was determined by mass spectrometer and the results were listed in Table 3.9. Six mass spectrometry runs of the Th standard show the ^{230}Th/^{232}Th and ^{229}Th/^{232}Th ratios were both less than 2×10^{-6}.

Five spike calibration runs for U yielded a mean total U concentration of 4.4710 ppm with a 2σ of the mean of 0.0036. All individual runs agreed with each other within 2σ error of less than 0.5% (Table 3.10). Five runs gave a

Table 3.8. Isotopic Compositions of the Spike.

Bead #	Rm09	2 Sigma	Rm29	2 Sigma	Rm56	Rm86
1	0.009041	0.000030	1.2890	0.0011		
2	0.009012	0.000056	1.3013	0.0010		
3	0.009072	0.000026	1.3034	0.0008		
4	0.009011	0.000065	1.3039	0.0018	0.000075 +/-13	0.002220 +/-10
Mean	0.009034	0.000058	1.2994	+/-0.0121		
Corrected	0.009054	0.000058	1.308	+/-0.012	0.000074 +/-13	0.002242 +/-10

Atomic percent:

U-234	<0.0002%		Th-229	43.158%
U-235	0.007%		Th-230	0.391%
U-236	99.769%		Th-232	56.451%
U-238	0.224%			

Table 3.9. Analyses of the Isotopic Compositions of U Standard (SPEX)

Date	Rm48 (x E-5)	Rc48 (x E-5)	2 Sigma (x E-7)	Rm58	Rc58	2 Sigma (x E-6)	Rm68 (x E-4)	Rc68 (x E-4)	2 Sigma (x E-5)
12/11/87	2.32	2.27	4	0.003249	0.003200	2			
12/11/87	2.09	2.05		0.003256	0.003206		1.520	1.505	
12/11/87	2.31	2.26	5	0.003255	0.003205	2			
12/11/87	2.42	2.37		0.003259	0.003209	9			
12/11/87	2.47	2.42	4	0.003245	0.003196	3			
12/11/87	2.33	2.28	6	0.003256	0.003206	3			
20/11/87				0.003265	0.003215	6	1.546	1.530	31
20/11/87	2.19	2.15		0.003246	0.003197	2			
20/11/87	2.67	2.62		0.003253	0.003203	3			
20/11/87	2.13	2.09		0.003261	0.003211	8			
20/11/87	2.56	2.51		0.003243	0.003194				
20/11/87	2.42	2.37	8	0.003248	0.003199	3	1.497	1.482	9
20/11/87	2.25	2.20	6	0.003239	0.003190	4	1.490	1.475	9
20/11/87				0.003237	0.003188		1.545	1.529	
20/11/87				0.003235	0.003186	3	1.556	1.540	10
15/12/87	2.32	2.27		0.003243	0.003194	4			
15/12/87	2.43	2.38		0.003256	0.003206				
15/12/87				0.003256	0.003206	7			
15/12/87	2.20	2.16		0.003255	0.003205	4			
15/12/87	2.18	2.14		0.003253	0.003203	4			
Mean		2.28			0.003201			1.510	
2 Sigma		+/-30			+/-15			+/-54	
Number of Data		16			23			6	

1. Fractionation is corrected using average fractionation factor of 5.0%o per mass unit.
2. Symbols are the same as in Table 3.4.

Table 3.10.   U/Th Spike Calibration

Sample #	Ustd(g)	Thstd(g)	SpkWt(g)	Rc68	2 Sigma	Rc92	2 Sigma	U(ppb)	Th(ppb)
1	0.38350	0.42545	3.29790	0.039234	0.000021	0.015077	0.000007	4.4715	4.8554
2	0.32602	0.36850	4.11008	0.057461	0.000024	0.021432	0.000007	4.4728	4.8378
3	0.22163	0.31303	3.62023	0.074350	0.000045	0.022285	0.000018	4.4695	4.8569
4	0.31398	0.31293	3.76964	0.054676	0.000023	0.023124	0.000014	4.4683	4.8439
5	0.30410	0.34451	3.81548	0.057191	0.000032	0.021334	0.000012	4.4730	4.8491
Mean of the Five								4.4710	4.8486
2 Sigma of the Mean								+/- 36	+/-143

Table 3.11.

Isotopic Compositions and Concentrations of Spike and Standard
----

U standard (SPEX)

$^{234}U/^{238}U$	$^{235}U/^{238}U$	$^{236}U/^{238}U$
0.0000228	0.003201	0.0001510
±30	±15	±54

Atomic Mass   238.0408

U concentration   0.99312 ppm

Th standard (SPEX)

$^{229}Th/^{232}Th$	$^{230}Th/^{232}Th$
$< 2 \times 10^{-6}$	$< 2 \times 10^{-6}$

Atomic Mass   232.038

Th concentration   1.06209 ppm

Spike

$^{234}U/^{236}U$	$^{235}U/^{236}U$	$^{238}U/^{236}U$	$^{230}Th/^{229}Th$	$^{232}Th/^{229}Th$
$<2.5*10^{-6}$	0.000074	0.002242	0.009054	1.308
	±13	±10	±58	±12

U   Atomic Mass: 236.050

Th Atomic Mass: 230.733

U   Concentration: 4.4710 ± 0.0036 ppb   (mean of 5)

Th Concentration: 4.8486 ± 0.0143 ppb   (mean of 5)

$^{229}Th/^{236}U$ (atomic ratio): 0.47993 ± 0.00147   (mean of 5)

mean of total Th concentration of 4.8486 ppm with a 2σ of the four of 0.0143. The relative large uncertainty in Th concentration could be the result of the high ^{232}Th content of the spike itself. Then the ^{229}Th/^{236}U atomic ratio in the mixed spike was calculated to be 0.47993 ± 0.00147 from the determined ^{229}Th and ^{236}U concentrations in the spike. The isotopic compositions and concentrations of the mixed spike and the SPEX U and Th standards are summarized in Table 3.11.

Standards for isotopic ratio measurement in this study were list in Table 3.12. The natural U and Th standards were used for all the experimental tests. Uraninite standard was obtained from J. Rosholt, U. S. Geological Survey, Denver, Colorado. This uraninite was provided in the form of a solution in 2 M HNO$_3$ stored in a polyethylene bottle. The uraninite itself is about 150 Ma old and was assumed to be in secular radioactive equilibrium (^{238}U=^{234}U=^{230}Th). It was originally used to calibrate spikes for U-series geochronology in McMaster U-series Geochronology Lab (Gascoyne, 1979). The 76001 standard is a homogenized sample of speleothem described by Gascoyne (1977) and was used as a standard for U-series dating. The JC1 standard is also a homogenized sample of speleothem from a cave in North Dakota, whose age is shown by α-spectrometry to be more than 350 ky old.

Table 3.12. List of Standards for the U-series Analysis

	RCOMMENDED VALUE				SOURCES
	230/232	234/238	235/238	236/238	
Natural Th	0.0000756 +/-11				this study
Natural U		0.00005365 +/-23	0.0072526		this study
NBS 500 U		0.010422 +/-18	0.99970	0.001519 +/-6	NBS
NBS 005A U		0.00003417 +/-70	0.005090	0.0000119 +/-1	NBS

	(230/234)	(234/238)	U (ppm)	(234/238)i	Age (ky)	
JC1	1.050 +/-25	1.010 +/-11	0.762 +/-24		>400	this study
76001	0.379 +/-27	1.88 +/-20	0.89 +/-22	2.01 +/-23	49.7 +/-4.2	Gascoyne, 1977.
Uraninite	1.00 +/-5	1.00 +/-5	N.A.		ca.150 Ma	Gascoyne, 1977.

1. Ratios in the brackets are activity ratios.

3.5. CONTAMINATION AND PROCEDURAL BLANK

Accurate and precise trace analyses of U and Th depend critically on the control of contamination and analytical blanks since less than several hundreds and in some cases even few tens of nanograms U and Th were analyzed. Efforts were made to avoid contamination at every step of the analyses by the strict cleaning procedures as described previously.

All reagents except $FeCl_3$ and NH_4OH used in this study were purified by the subboiling distillation method. Concentrations of U and Th, and other trace elements in those purified reagents were not separately determined, nor was the chemistry blank and the filament blank. Instead, an integrated procedural blank was determined. Two Th procedural blanks, without $Fe(OH)_3$ coprecipitation, yielded 44 pg ^{232}Th for the method using set "M" and "S" columns, 105 pg using set "L" and "S" columns. One U blank yielded 100 pg ^{238}U for set "L" and "S" columns. Use of non-pre-purified $FeCl_3$ solution for coprecipitation gave a high blank of 500 pg ^{232}Th and 230 pg ^{238}U using set "M" and "S" columns. This can greatly hinder the precise and accurate determination if trace amounts of Th and U in carbonates, is analyzed, as has been shown by the scatter of ^{232}Th

concentration data from the analyses of JC1 and 76001 standards (Table 3.15, 3.16). No corrections were made for the blanks in this study since the U and Th in the samples are normally more than 1000 times larger than the blanks.

3.6. U-SERIES DISEQUILIBRIUM DATING OF CARBONATES

A Quick Basic computer program was written for calculating activity ratios, U and Th concentrations and ^{230}Th ages of the samples (Appendix 3.2). The fractionation corrected measured isotopic ratios of $^{234}U/^{238}U$, $^{234}U/^{236}U$ and $^{230}Th/^{229}Th$ were corrected for ^{238}U and ^{230}Th in the spike. These ratios were then used to calculate the activity ratios of $(^{234}U/^{238}U)$, $(^{230}Th/^{234}U)$, and $(^{230}Th/^{238}U)$ using the $^{229}Th/^{236}U$ ratio of the spike. $^{230}Th/^{234}U$ ages were calculated using equation 3.7 (Kaufman and Broecker, 1965) by an iteration method on the computer:

$$(^{230}Th/^{234}U) = (^{238}U/^{234}U)[1-\exp(-\lambda_{230}T)] +$$
$$[1-(^{238}U/^{234}U)][\lambda_{230}/(\lambda_{230}-\lambda_{234})] \times$$
$$[1-\exp(-(\lambda_{230}-\lambda_{234})T)] \qquad (3.7)$$

The initial $(^{234}U/^{238}U)$ ratios were calculated from equation 3.8 using the age T obtained from equation 3.7:

$$(^{234}U/^{238}U)_o = 1 + [(^{234}U/^{238}U)-1]\exp(\lambda_{234}T) \qquad (3.8)$$

where the ratios in parentheses denote the activity ratios, λ's denote decay constants and T is the age. Decay constants and other constants are listed in Table 3.13. Initial ^{230}Th contents of the samples were checked by calculating $(^{232}$Th$/^{238}$U$)$ ratios and were corrected assuming that the initial activity ratio of $(^{230}$Th$/^{232}$Th$)$ was equal to 1.7 (Harmon, 1975). This correction is necessary when the $(^{232}$Th$/^{238}$U$)$ is larger than 0.005. Errors were calculated according to error propagation in the equations and the errors of the spike calibration were included. All errors were presented at 2σ. An sample printout is shown in Appendix 3.2.

3.7. ACCURACY AND REPRODUCIBILITY

The accuracy and precision of measuring small isotopic ratios using the Daly detector has been determined by analyzing the U standards for which the fractionation has been corrected using the internal standard method (Table 3.5). Even though the fractionation was as high as 5.0‰ per mass unit obtained from the measured ^{235}U$/^{238}$U ratios, when corrected by normalizing the measured ^{235}U$/^{238}$U ratio to its certified value of 0.9997, twelve analyses of the NBS 500 U standard yielded a mean ratio of 0.010431 ± 0.000019 (2σ) for ^{234}U$/^{238}$U and 0.001522 ± 0.000011 (2σ) for ^{236}U$/^{238}$U, all which are within the errors of their

Table 3.13. Constants Used in U-series Geochronology

	Mass	Decay Const		Half Life	Nat. Abund.	
NAT. Th	232.0382					
229Th	229.0316	9.443E-5		7340		
230Th	230.0331	9.195E-6	[4]	75383		
232Th	232.0382	4.9475E-11	[1]	14.010E+9	100	
NAT. U	238.03					
234U	234.0409	2.835E-6	[2,3]	2.445E+5	0.00543	[*]
235U	235.0439	9.8485E-10	[1]	0.7038E+9	0.72000	[*]
236U	236.0457	2.900E-8		2.39E+7		
238U	238.0508	1.55125E-10	[1]	4.468E+9	99.27456	[*]

ISOTOPIC RATIOS OF NATURAL U AND U-SERIES IN SECULAR EQUILIBRIUM

234/235	7.5448E-3	[*]	230/234	0.30832	[*]
238/235	137.8809	[1]	230/238	1.6871E-5	[*]
234/238	5.472E-5	[*]			
235/238	7.2526E-3	[*]			

*: Calculated from the new decay constants using 238/235=137.8809.

1. Steiger, RH and Jager, E., 1977, Subcommission on geochronology: Convention on the use of decay constants in geo- and cosmochronology, Earth Planet. Sci. Lett., 36, 359-362.

2. Lounsbury, M. and Durham, RW., 1971, The alpha half-life of 234-U, in: Proc. Int. Conf. Chem. Nucl. Data, Measurement and Applications, Canterbury, Hurrell, ML., ed., p215, Inst. Civil Engineer, London.

3. Bievre, P.de., Lauer, KF., Le Duigou, Y., Moret, H., Muschenborn, G., Spaepen, J., Spernol, A., Vainbrouks, R. and Verdingh, Y., 1971, The half life of 234U, in: Proc. Int. Conf. Chem. Nucl. Data, Measurement and Applications, Canterbury, Hurrel, M.L., ed., p21, Inst. Civil Engineer, London.

4. Meadows, JW., Armani,RJ., Callis, EL. and Essling, AM., 1980, Half life of 230-Th, Phys, Rev., C22, 750.

certified ratios of 0.010422 ± 0.000018 and 0.001519 ± 0.000006 respectively. This is a further check on the linearity of the Daly detector. It was shown to be linear for signals ranging up to 500,000 counts/second.

The internal precision (2σ) of all U isotopic ratios measured was better than 1‰. Typical run precision was 0.1% for $^{236}U/^{238}U$ ratios, and 0.3% for $^{234}U/^{236}U$ ratios, to give a typical precision of better than 0.5% for corrected ($^{234}U/^{238}U$) activity ratios.

Typical run precision for Th isotopic ratios of carbonate samples was about 0.1% for $^{229}Th/^{232}Th$ ratios, and better than 0.5% for $^{230}Th/^{232}Th$ ratios. However, a large uncertainty of more than 1.0% was introduced when $^{230}Th/^{232}Th$ ratios were corrected for ^{230}Th in the spike. This is because the spike has a high ^{230}Th content of 0.39% and typical carbonate samples contain less than 0.5% ^{230}Th. Half or more of the measured ^{230}Th in a spiked carbonate sample came from the spike since the spike has a $^{230}Th/^{229}Th$ ratio of 0.00905 (0.00690 for $^{230}Th/^{232}Th$ ratio) and the typical measured value for $^{230}Th/^{229}Th$ of a spiked sample was less than 0.02. These corrections for spike impurities and spike uncertainties resulted in more than 1.0% uncertainty in the consequent activity ratios of ($^{230}Th/^{234}U$) and ($^{230}Th/^{238}U$). The consequent calculated

ages have large uncertainties, more than 10% in 2σ, for ages of more than 300 ky old. The uncertainty is expected to be much smaller, about 2%, for ages less than 150 ky old (Table 3.16). Using less amount of spike to increase the sample to spike ratio could improve the precision. This will inevitably lead to an increase in the sample sizes. Therefore, high purity spike is essential for precise isotopic ratio measurements. This has now been obtained from ORNL but was not available in the course of this research.

^{230}Th determinations in granitic samples were hindered by the extremely low ^{230}Th/^{232}Th ratios because of the big ^{232}Th tail over ^{230}Th. The precisions of the measured ^{229}Th/^{232}Th and ^{230}Th/^{229}Th ratios, are normally worse than 2% depending on the magnitude of their values. The ^{232}Th tail was difficult to correct to the accuracy of better than 1% even using a fitted-background curve method.

The internal precision of one run is sometime better than external precision of the mean of several runs. This was shown by the analyses of the NBS 500 U standard (Table 3.5). This was also shown by the eleven analyses of the activity ratios of (^{234}U/^{238}U) of JC1 standard (Table 3.15) which had a 2σ of the mean of 1% contrasting with the normal 2σ of 0.5% for individual runs. However, this could be the

result of improper control of the analytical blank since the
first five, which did not utilize ferric iron
coprecipitation method, yielded a mean of 1.0055 ± 0.0059.
The second six, done using ferric iron coprecipitation
method, yielded a mean of 1.0123 ± 0.0086. Similar results
were shown for the analyses of 76001 standard (Table 3.16).

The accuracy and precision of the single-spike, two-
stage method for U analyses is shown by the determinations
of isotopic ratios of several standards (Table 3.14, 3.15,
3.16). Three measurements of $^{234}U/^{238}U$ ratio of the NBS
005a U standard gave a mean value of 3.416 ± 0.004 (x 10^{-5})
contrasting the certified value of 3.42 ± 0.02 (x 10^{-5})
(Table 3.14). Three analyses of an infinite-age uraninite
standard used at McMaster U-series Lab yielded a mean of the
($^{234}U/^{238}U$) activity ratio of 0.9996 ± 0.0032 (Table 3.14).
The measured ($^{230}Th/^{238}U$) ratios are slightly larger than
unity but they are the most precise values ever obtained on
this standard. Reproducibility of this method is better
than 0.5% for $^{234}U/^{238}U$ ratio measurements for the standards
to which the same chemical treatment, either columns only or
coprecipitation, was applied. Therefore, the relatively
larger variations in the determinations of the $^{234}U/^{238}U$
ratios of the JC1 and 76001 carbonate standard could be
attributed to the higher blanks introduced during the ferric
iron coprecipitation.

Table 3.14. Results of The Standards

	NBS 005A U $^{234}U/^{238}U$ (x 10^{-5})	Natural U $^{234}U/^{238}U$ (x 10^{-5})	Uraninite ($^{230}Th/^{234}U$)	($^{234}U/^{238}U$)
Recommended Value	3.42 ± 70		1.00 ± 5	1.00 ± 5
	3.414 ± 20	5.375 ± 22	1.027 ± 30	1.0001 ± 41
	3.418 ± 18	5.353 ± 19	1.039 ± 11	0.9978 ± 53
	3.416 ± 21	5.374 ± 17		1.0009 ± 31
		5.357 ± 16		
Mean Value	3.416 ± 2	5.365 ± 23	1.033 ± 17	0.9996 ± 32

1. Ratios in the brackets are activity ratios, others atomic ratios.
2. Recommended values of Uraninite are based on that it has an infinite age (ca 150 Ma) and α counting results show its radioactive equilibrium within an error more than 5% (2σ).
3. All the errors are presented in 2σ.

Table 3.15. Analyses of JC1 Speleothem

SAMPLE #	A04	2 SIGMA	A48	2 SIGMA	A08	2 SIGMA	U (ppm)	2 SIGMA	Th(ppb)	2 SIGMA
1	1.0527	0.0136	1.0089	0.0060	1.0624	0.0146	0.7597	0.0042	2.920	0.010
2	1.0479	0.0107	1.0001	0.0036	1.0484	0.0100	0.7589	0.0007	3.834	0.012
3	1.0757	0.0110	1.0051	0.0037	1.0314	0.0104	0.7617	0.0008	1.751	0.006
4	1.0409	0.0110	1.0069	0.0033	1.0483	0.0109	0.7587	0.0017	1.049	0.003
5	1.0262	0.0160	1.0067	0.0029	1.0334	0.0159	0.7430	0.0011	0.836	0.003
Mean of 5	1.0487	+/-0.0324	1.0055	+/-0.0059	1.0548	+/-0.0323	0.7564	+/-0.0136		
1*	1.0511	0.0108	1.0113	0.0018	1.0633	0.0108	0.7765	0.0008	0.991	0.003
2*	1.0537	0.0127	1.0107	0.0034	1.0653	0.0131	0.7789	0.0024	1.014	0.003
3*	1.0433	0.0072	1.0164	0.0027	1.0607	0.0069	0.7726	0.0010	0.866	0.003
4*	1.0521	0.0263	1.0186	0.0062	1.0721	0.0275	0.7679	0.0047	1.621	0.007
5*	1.0534	0.0232	1.0111	0.0029	1.0655	0.0234	0.7630	0.0016	0.829	0.004
6*			1.0054	0.0035			0.7410	0.0017		
Mean of 6	1.0507	+/-0.0077	1.0123	+/-0.0085	1.0654	+/-0.0076	0.7666	+/-0.0252	1.064	+/-0.574
Mean of All	1.0497	+/-0.0249	1.0092	+/-0.0105	1.0600	+/-0.0272	0.7620	+/-0.0242		

1. The A04, A48 and A08 are the activity ratios of Th-230/U-234, U-234/U-238 and Th-230/U-238, respectively.
2. The 2 SIGMA includes the error of the spike calibration.
3. The chemistry of those samples marked with × were done using coprecipitation, others done using columns only.

Table 3.16.   Uranium-series Results of 76001 Standard.

SAM.#	SAM.WT(g)	A04	2 SIGMA	A48	2 SIGMA	A08	2 SIGMA	U (ppm)	2 SIGMA	Th (ppb)	2 SIGMA	A48i	2 SIGMA	AGE(ky)	2 SIGMA
1	1.11362	0.3752	0.0094	1.3248	0.0050	0.7225	0.0130	0.7809	0.0013	8.174	0.025	2.064	0.010	49.44	1.50
2	1.25575	0.3532	0.0080	1.3214	0.0037	0.6739	0.0153	0.7829	0.0009	7.799	0.024	2.050	0.008	45.96	1.25
Mean of 2		0.3642 +/-0.0220		1.3231 +/-0.0034		0.7007 +/-0.043E		0.7819 +/-0.0020		7.987 +/-0.375		2.057 +/-0.014		47.70 +/-3.48	
3*	1.03421	0.3812	0.0103	1.3200	0.0043	0.7320	0.0209	0.7900	0.0012	9.576	0.030	2.061	0.010	50.46	1.75
4*	1.14656	0.3913	0.0095	1.3267	0.0073	0.7554	0.0138	0.7880	0.0026	8.383	0.027	2.074	0.013	52.15	1.54
5*	1.05306	0.3902	0.0093	1.3192	0.0089	0.7431	0.0131	0.7900	0.0034	9.092	0.028	2.065	0.015	51.66	1.54
6*	1.24548	0.3913	0.0081	1.3200	0.0069	0.7518	0.0158	0.7896	0.0027	8.360	0.029	2.067	0.012	52.08	1.32
7*	1.68301	0.3874	0.0095	1.3181	0.0315	0.7433	0.0220	0.7950	0.0130	9.065	0.028	2.062	0.041	51.42	1.54
8*	1.02569	0.3973	0.0151	1.3234	0.0122	0.7656	0.0234	0.7917	0.0049	8.935	0.028	2.073	0.022	53.10	2.43
9*	1.14378	0.3959	0.0065	1.3199	0.0084	0.7602	0.0128	0.7913	0.0027	9.109	0.003	2.068	0.013	52.61	1.10
Mean of 7		0.3903 +/-0.0102		1.3210 +/-0.0055		0.7510 +/-0.0208		0.7908 +/-0.0041		9.089 +/-0.431		2.071 +/-0.005		51.98 +/-1.62	

1. Age is 230-Th age calculated using equation 3.6.
2. A48i donetes the initial 234U/238U activity ratio as calculated using equation 3.7.
3. Other symbols are same as in Table 3.15.

Precise age determinations using this analytical method is demonstrated by the analyses of the 76001 standard (Table 3.16). Seven analyses using coprecipitation method yielded a mean age of 51.5 ± 1.6 (2σ) ky, compared to the mean of eight analyses of 49.7 ± 4.2 (2σ) ky by α counting (Gascoyne, 1977). Though the ages agree within error, the discrepancy of the ages is likely due to the differences in the spike calibration procedures. The mixed ^{232}U-^{228}Th spike used in α counting was calibrated against the Uraninite standard which was assumed to be in secular radioactive equilibrium, that is, both (^{230}Th/^{234}U) and (^{234}U/^{238}U) are equal to unity (Gascoyne, 1977). The equilibrium assumption was based on the fact that the uraninite was about 150 Ma old and analyses by α counting did show both (^{230}Th/^{234}U) and (^{234}U/^{238}U) were equal to unity within the analytical error of α counting which was not better than 5% at the 2σ level. However, three analyses of the uraninite in this study show that the (^{234}U/^{238}U) ratio is unity as expected, but the mean (^{230}Th/^{234}U) ratio of two analyses is 1.033 ± 0.017 (2σ), which is about 3% larger than unity (Table 3.14). This result indicates that the Uraninite is not in secular radioactive equilibrium as assumed. This finding is not surprising since uraninite is very vulnerable to leaching and loss of U relative to Th due to its self-radiation damage of its U and Th. The 3.3%

difference just accounts for the 1.7 ky age discrepancy between this work and the α counting results.

The two analyses of 76001 done without coprecipitation procedure gave relative small ages and a large scatter (Table 3.16). What caused the younger ages and the larger scatter is not clear. More data using only the column chemical treatment are needed to explain this problem.

Advantages of the mass spectrometry method over conventional α counting are easily seen. Compared with the α counting method, much smaller sample sizes, as low as 50 ng U for ^{234}U analyses of waters, is used in the mass spectrometry method. Precision and accuracy of better than 1% at 2α level can be easily achieved for the activity ratio measurements even though the spike used in this research has a high ^{230}Th content. Much labour and machine time is saved in each analysis. The sample preparation can be finished within two days, and each sample is measured on the mass spectrometer in only a few hours. Even more precise and accurate results are expected if higher purity spike is used and lower procedure blank is achieved.

CHAPTER FOUR

STRONTIUM ANALYSIS BY ICP-MS

4.1. INTRODUCTION

The Inductively Coupled Plasma-Mass Spectrometry (ICP-MS) has been shown in the past few years to be a versatile method for sensitive elemental and isotopic analyses. The intrinsic characteristics of the ICP and the Quadruple mass filter provides this ICP-MS technique unique advantages of low detection limits (sub ppb) especially for heavy metals, high sensitivities, short analysis time, multi-elemental analyses, and less interferences and simple mass spectra. It is especially suitable for trace element analyses in water samples (Gray, 1988; Houk and Thompson, 1988; Riddle et al., 1988).

Elemental analyses by ICP-MS are performed either by the isotope dilution or by the external standard calibration curve, including rhodium (Rh) as an internal standard. The external standard calibration curve method suffers the large uncertainties caused by the medium- and long-term drift of the ICP-MS. These include various factors, such as nebulizer instability, changes in ion optical voltages, and changes in mass calibration (Houk and Thompson, 1988). For example, continuous decrease in the sensitivity of the

machine was observed due to the deposition of material on the sampler and skimmer (McLaren et al., 1987; Garbarino and Taylor, 1987). This drift was also observed on the present instrument (Fig.4.1). Fluctuations of the count rates of the isotopes were observed with Sr concentrations ranging from 50 ppb to about 2.2 ppm. However, these fluctuations have less effect on the measured isotopic ratios. In addition, frequent running of standards, which is necessary, wastes machine time. Using Rh as an internal standard is a quicker semi-quantitative method of looking at samples. This method did not yield consistent results even for standards. This could be the results of the instability of the machine which affected the ionization of Rh differently from Sr.

On the other hand, ICP-MS has the capability of measuring isotopic ratios to a precision of better than 1.0% (Price and Bazan, 1987; Dickin et al, 1988). The isotope dilution method introduces an internal standard - an isotope of the element of interest. The scanning of the mass range of isotopes of interest takes only a few seconds. As a result, the changes in the rate at which ions arrive at the detector do not affect significantly the isotopic ratio measurements. Therefore, an isotope dilution method by ICP-MS was attempted to determine the Sr concentrations of the groundwater samples.

Figure 4.1.   Stability of the ICP-MS.   The count rates of ^{88}Sr and ^{86}Sr are plotted against the Sr concentrations for over six hour instrument running time.   Fluctuations are observed on the count rates of both isotopes with the Sr concentrations ranging from 50 ppb to 2.2 ppm. The fluctuations   indicate   the   unstability of the instrument, which affects the precise measurements of isotopic ratios.
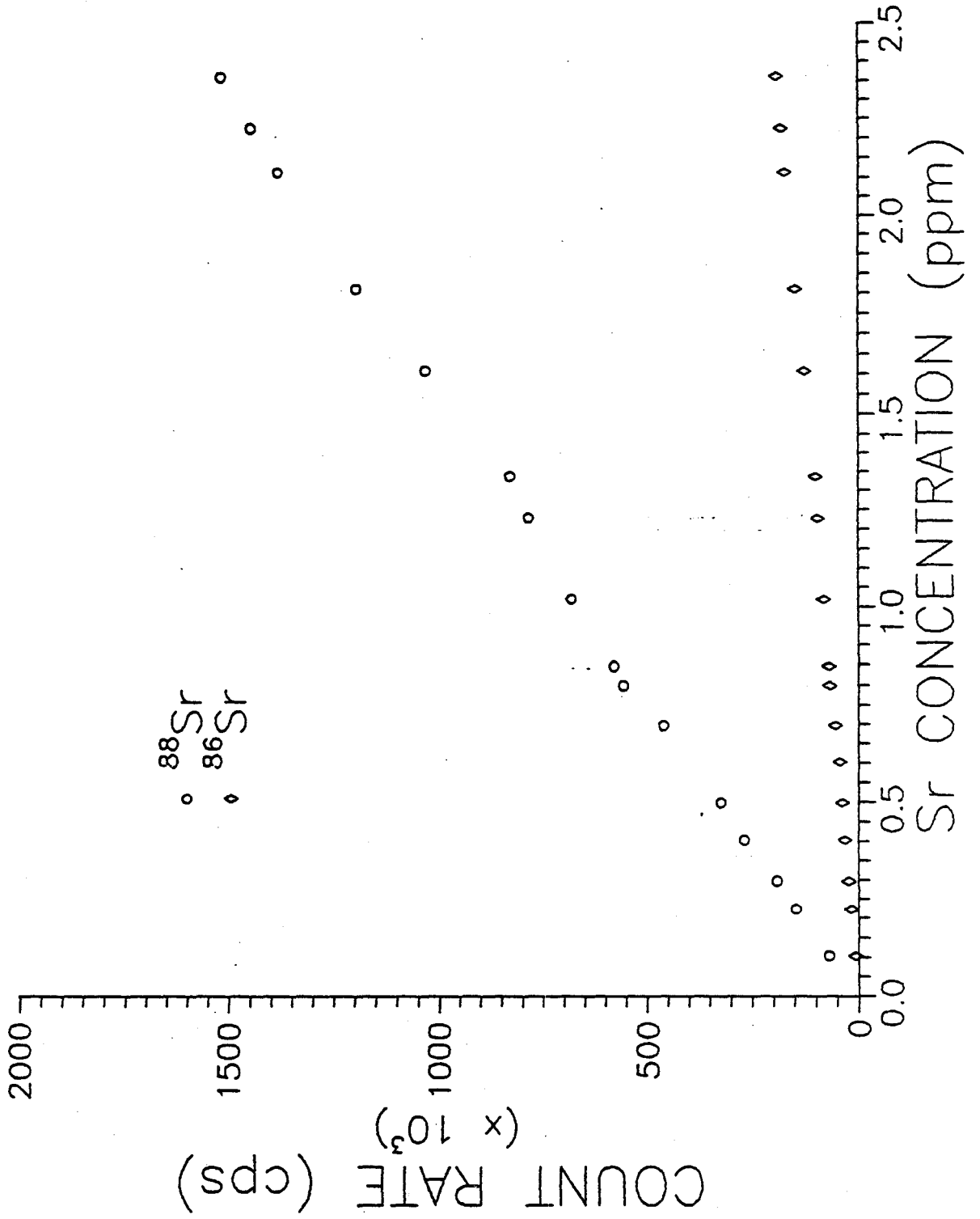
4.2. INSTRUMENTATION

The ICP-MS at McMaster is one of the first commercial ELAN 250 machines from SCIEX of Canada. It is composed of a plasma generator with a quartz torch, a quadrupole mass filter, the ion detection system with a Galileo channel electron multiplier (CEM), the data processing system, and the vacuum system including a cryogenic pump and a rotary pump. Argon gas flows to the nebulizer and the plasma torch are controlled by a LINDE mass-flow controller. The instrument is controlled by a computer with software supplied by the manufacturer. The sample solution is introduced to the nebulizer using a peristaltic MINIPULS pump at a rate of 0.6 ml/minute. The sample ions from the plasma are introduced to the mass filter in the vacuum chamber through a interface system which consists of a sampler and a cobalt skimmer. The sampler is made of copper or nickel with an orifice diameter of 1.14 mm. It was cleaned frequently with purified acids and was changed regularly.

The machine is operated through a computer. Operating parameters, such as mass range, number of measurements per peak, dwell time, integration time, and ratios to be calculated, are programmed. Ion beams are optimised by adjusting the ion optics and the position of the torch

relative to the sampler. Data are acquired in a peak-hopping mode, in which isotopes of interest, hence peaks, are measured sequentially in a pre-determined number of cycles. Ten measurements in intervals of 0.1 mass unit are made over each peak. Each measurement is counted for 20 ms (dwell time). The intensity of each peak is obtained by integration of the ten measurements. Ten cycles or scans are taken to give the mean intensity of each peak. A typical spectrum of the spiked sample is shown in Fig. 4.2. The asymmetric peak shape, in contrast to the symmetric peak shape with a flat top in magnetic sector mass spectrometry, is an intrinsic characteristics of the quadruple mass filter (Gray, 1988).

Backgrounds at the measured points of the isotopes of interest are obtained by analyzing a blank, MILLIQ water or distilled diluted 0.5 M HCl and the blank spectrum subtracted from the sample spectrum. A blank spectrum is shown in Fig. 4.3. The existence of these blank peaks is probably the result of the high sensitivity of the instrument. Backgrounds from either MILLIQ or dilute HCl did not differ from each other. Isotopic ratios are then acquired through the background corrected counts. Data processing was done either by using the supplied software or by transferring the raw data to a LOTUS file and then manipulating using an IBM computer.

Figure 4.2. A typical mass spectrum of the spiked sample. Note the asymmetric peak shape which is the intrinsic characteristics of the quadrupole mass filter.

Sr ISOTOPE DILUTION
SAMPLE #140
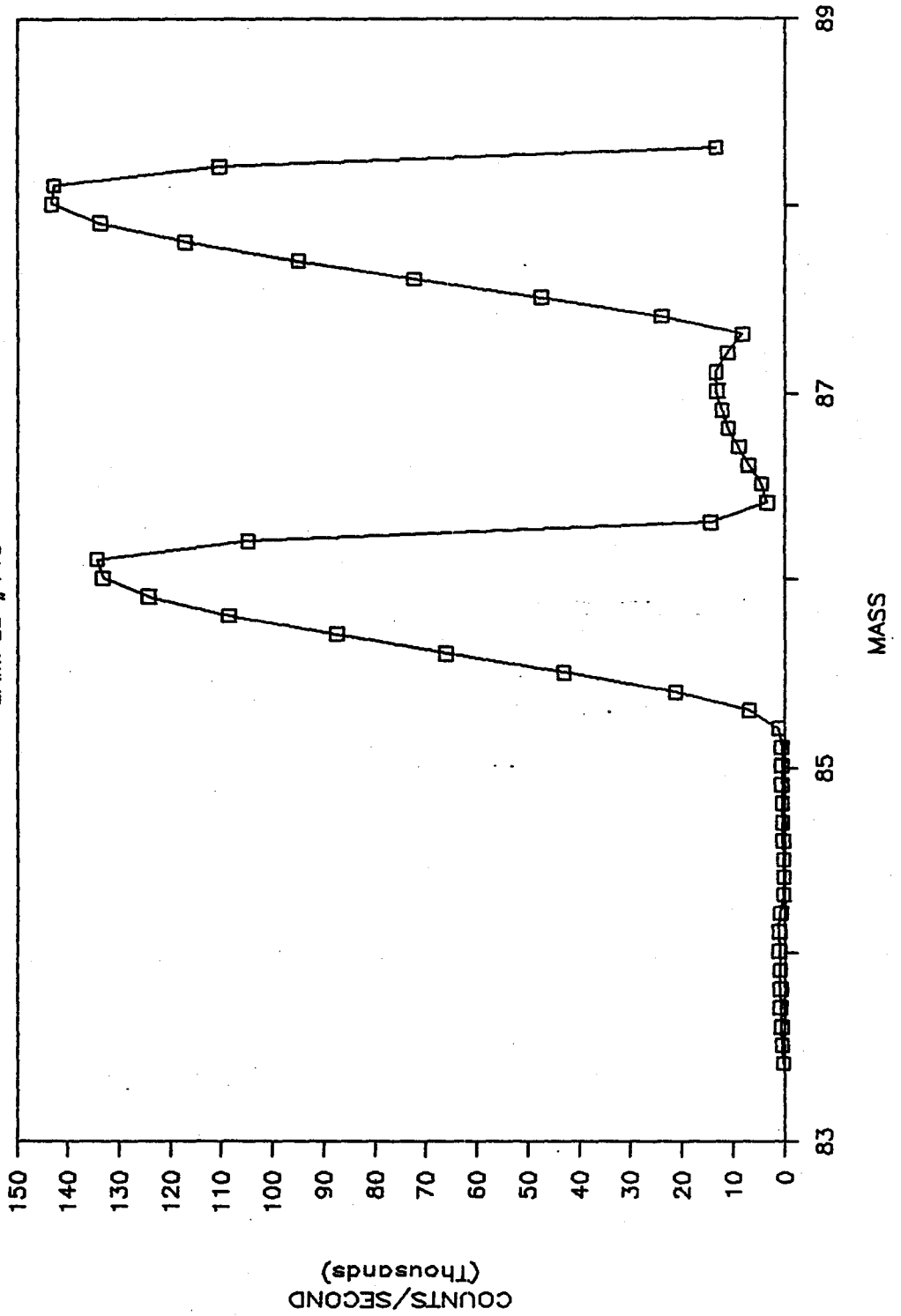
Figure 4.3. The mass spectrum of the Sr blank. The large
peak, relative to natural Sr, at mass 84 indicates the
isobaric interference of ^{84}Kr in the argon gas. The 88
peak shown is larger than it normally is. The normal
count rate at mass position 88.1 is around 130
counts/second.

Sr BLANK
(MILLI-Q)
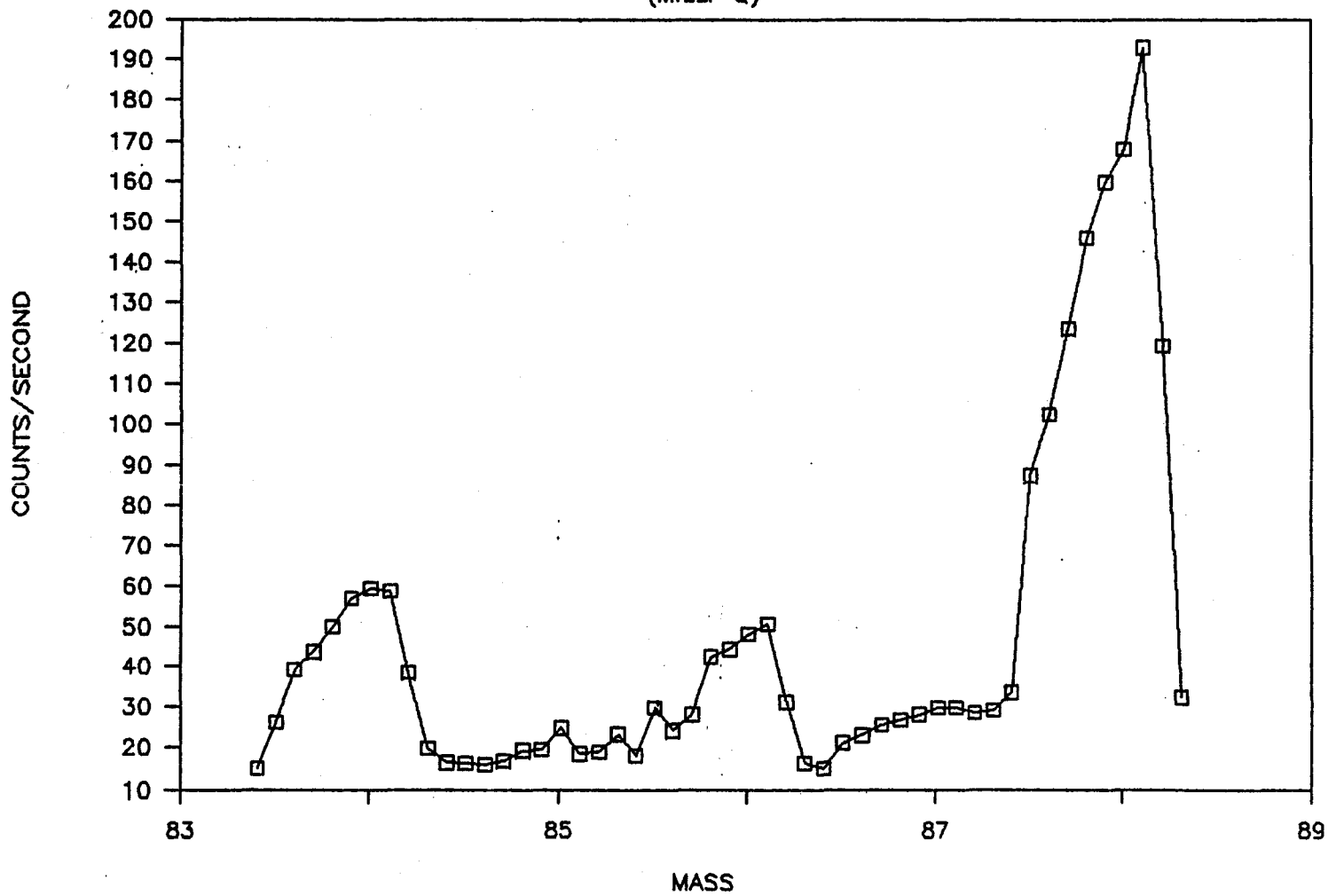
4.3. INSTRUMENT PERFORMANCE

Efforts were made to determine the biases of the machine in isotopic ratio measurements. The biases are shown to be the results of various facts, including settings of the ion optics, performance of the electron multiplier, concentration of the sample solution and sample flow rate, mass fractionation and interferences (Longerich et al, 1987; Russ and Bazan, 1987). These factors, except for the ion optics settings, were examined in this study. The ion optics settings were adjusted for best sensitivity.

4.3.1. PEAK INTEGRATION AND BACKGROUND

The intensity of each measured peak was obtained by summing the count rates of the selected measured points of each peak. The ten measurements/peak method was integrated with the software supplied by the manufacturer. In addition, summing two and five measurements/peak were also tried in a LOTUS file. The count rates of the corespondent measured points in the blank were subtracted. The result of the Sr standard shows that the ten-measurement summing method gave the best precision of 1 to 3% (1σ) and the two-measurement summing method the worst precision of larger than 3% (Table 4.1). This indicates the effect of the

Table 4.1. Integration Methods And Their Precision

| SAM. # | 2 points | | 5 points | | 10 points | |
	Rm86	STD	Rm86	STD	Rm86	STD
1	8.478	0.337	8.520	0.278	8.502	0.171
2	8.673	0.421	8.701	0.448	8.598	0.233
3	8.520	0.443	8.528	0.381	8.581	0.211
4	8.673	0.390	8.551	0.147	8.496	0.088
5	8.582	0.279	8.589	0.273	8.613	0.246
6	8.709	0.257	8.689	0.184	8.687	0.115
7	8.582	0.354	8.612	0.317	8.574	0.275
8	8.557	0.234	8.611	0.102	8.591	0.078
9	8.523	0.273	8.499	0.234	8.456	0.107
10	7.816	0.472	7.872	0.442	7.993	0.383
11	8.272	0.355	8.287	0.132	8.310	0.089

1. Rm86 denotes the measured 88Sr/86Sr ratio, while STD the standard deviation.
2. In "2 point" method, only two measured points of each peak, 86.0 and 86.1 for 86 peak, 88.0 and 88.1 for 88 peak, are integrated as the count rate of that peak.
3. In " 5 point" method, five measured points, at 85.8, 85.9, 86.0, 86.1 and 86.2 for 86 peak, are integrated.
4. In "10 point" method, all the ten measured points, e.g., from 85.4 to 86.3 for 86 peak, are integrated.

drift. When only two measured points were integrated they may be located in the top of the peak in one scan and may be located on the slope of the peak the next scan. This could cause larger uncertainty with fewer mass calibration shifts when the measured points are located to the right of the peak because of the asymmetric shape of the peak (Fig. 4.2). Therefore, the ten-measurement summing method was used.

The background at each measuring point of a peak is measured before each sample. Typical backgrounds at the mass positions 84, 86, 87, and 88 are 60, 50, 30, and 120 counts/second respectively. These normal backgrounds do not introduce more than 0.1% error on the 86 and 88 peak since they are normally more than 100,000 counts/second. The relatively high background at mass position of 84 is attributed to the isobaric interference of ^{84}Kr in the Argon gas. Therefore, measurements of ^{84}Sr are subject to larger uncertainties at a low count rate. Isobaric interferences from multiply charged elemental and molecular ions in sample runs were assumed to be negligible in water samples. Memory from previous samples was minimized by running diluted distilled HCl and MILLIQ after each sample. The backgrounds did not change by more than a few counts/second from one sample to another. No significant tail effect from the mass 87 peak was found on 86 and 88 mass positions.

4.3.2. SATURATION EFFECT OF THE CHANNEL ELECTRON MULTIPLIER (CEM) AND BIAS OF THE ISOTOPIC RATIO MEASUREMENTS

The bias study on the isotopic ratios was carried out using the Eimer & Amend $SrCO_3$ standard of varying concentrations. To avoid any isobaric interferences from ^{87}Rb, only the $^{88}Sr/^{86}Sr$ ratios were measured. When the machine was optimised for sensitivity, a correlation between the measured $^{88}Sr/^{86}Sr$ ratios and the count rate of ^{88}Sr was found (Table 4.2, Fig.4.4 and Fig.4.5). Notice that the precision of the mean of the five replicates is normally better than 0.5%, in contrast to that of 1 to 3% for single analysis (Table 4.1). This shows the reproducibility of the instrument. The measured $^{88}Sr/^{86}Sr$ ratio increased with a ^{88}Sr count rate up to about 150,000 counts/second, then stabilized at the value of 8.48, which is larger than its true value of 8.375, between a ^{88}Sr count rate of 150,000 and 500,000 counts/second. Thereafter, this measured ratio kept dropping with the increasing ^{88}Sr count rate up to the maximum count rate acceptable by the CEM. The curves in Fig.4.4 and 4.5 are likely the reflection of the performance of the CEM. The first part of the curve in which the measured ratios increase with the count rate could be nonlinearity of the CEM when the count rate is below 20,000 counts/second. When the ratios to be measured are too far

Table 4.2.   Isotopic Ratio Analyses of A+E Sr Standard

Sam. #	Sr Conc. (ppm)	88Sr Rate (cps)	Rm86	STD	Rc86	F
1	0.103	69918	8.377	0.020	8.377	1.000
2	0.224	145600	8.504	0.015	8.504	0.985
3	0.297	191100	8.490	0.014	8.490	0.986
4	0.404	268633	8.484	0.008	8.484	0.987
5	0.498	325575	8.484	0.014	8.484	0.987
6	0.603	376367	8.489	0.013	8.489	0.987
7	0.696	463500	8.468	0.014	8.496	0.986
8	0.798	557267	8.421	0.011	8.489	0.987
9	0.846	580350	8.414	0.029	8.492	0.986
10	1.019	683167	8.395	0.007	8.518	0.983
11	1.226	785200	8.318	0.023	8.485	0.987
12	1.335	830000	8.312	0.023	8.498	0.985
13	1.606	1031333	8.245	0.012	8.519	0.983
14	1.810	1195500	8.144	0.008	8.489	0.987
15	2.112	1383333	8.069	0.016	8.495	0.986
16	2.225	1447000	8.003	0.050	8.455	0.991
17	2.360	1517333	7.943	0.016	8.423	0.994
Mean					8.488	0.987
					+/-0.022	+/-0.003

1. Rm86 is the mean of five replicates of measured 88/86 ratios.
   Rc86 is the dead time corrected ratio using dead time of 50
   ns.   In comparison with Table 4.1, the standard deviation
   (STD), 0.1% to 0.5%, of the mean of the five is one order
   of magnitude better than that of a single run, 1 to 3%.
2. F is the bias factor calculated from the dead time
   corrected ratio Rc86 and its true value of 8.375.
3. The mean values do not include sample #.1 because
   its count rate is less than 100,000 cps.

Figure 4.4. Variations of the measured $^{88}Sr/^{86}Sr$ ratios with the ^{88}Sr count rates of the A+E Sr standard. These are the raw data of the means shown in Figure 4.5.
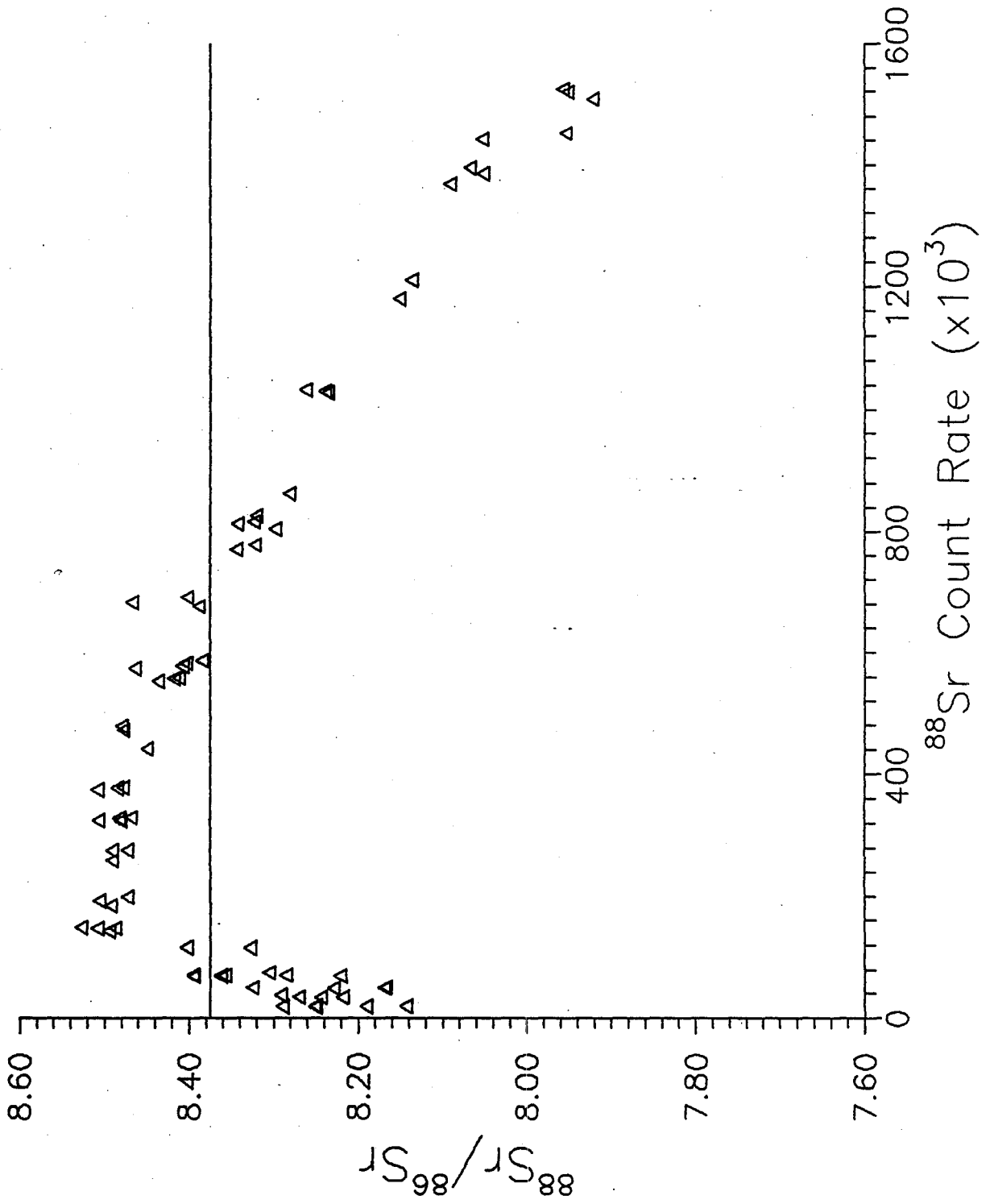
Figure 4.5.   Variations of the measured ratios with the ^{88}Sr

count rates of A+E Sr standard.   The error bars are the

1σ of the mean of five repeated measurements.   The

accepted value of 8.375 of the ^{87}Sr/^{86}Sr ratio is

indicated by the horizontal line.
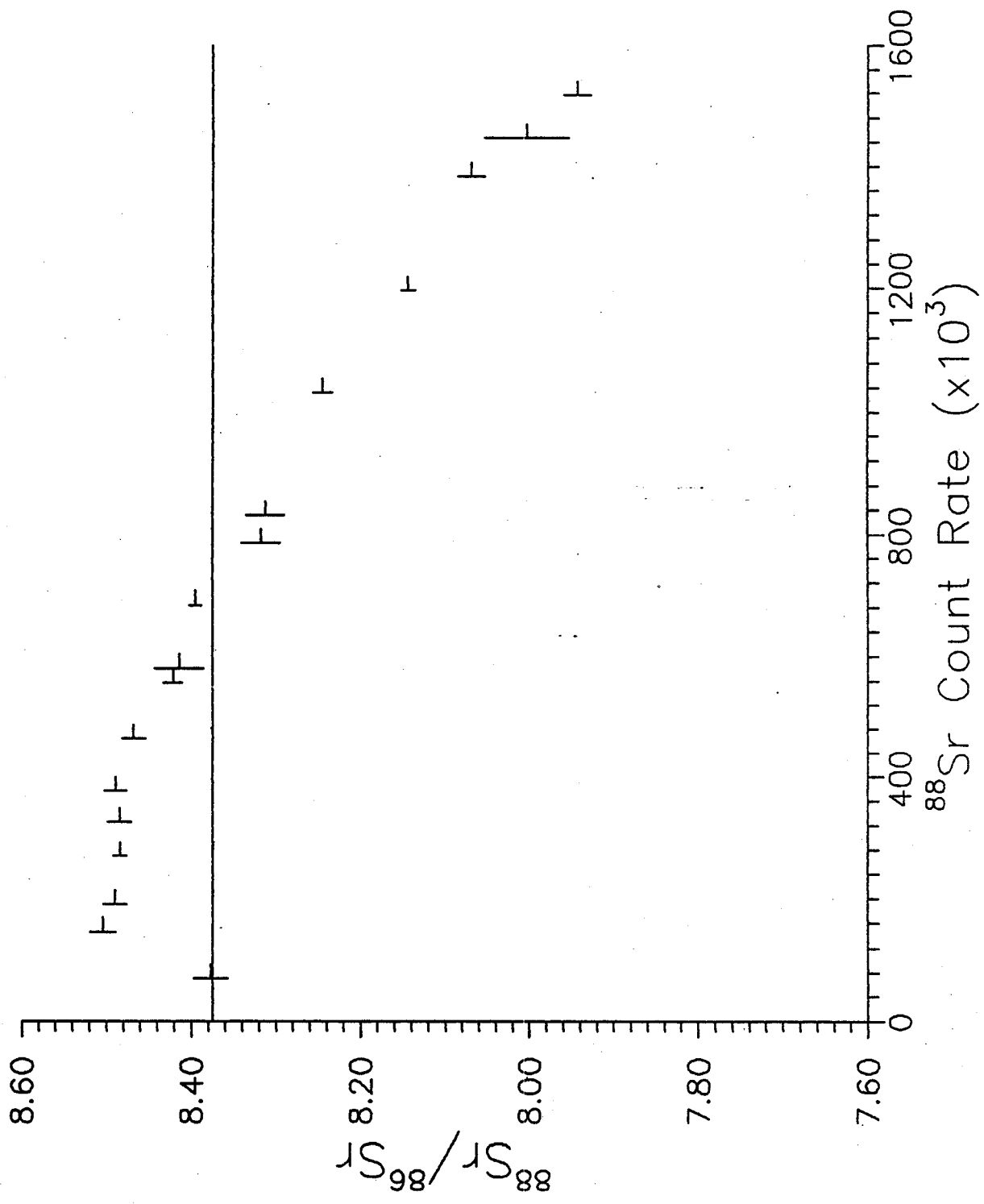
from unity and the count rates are less than 20,000 counts/second, large uncertainties are to be expected. Therefore, it is very important to spike the samples so that the measured ratios are close to unity because the accurate correction for the detector nonlinearity is extremely difficult.

A plateau on the curve was found (Fig.4.5). This plateau indicates that the CEM response is linear when the count rate on ^{86}Sr or ^{88}Sr is between 20,000 and 500,000 counts/second. This range should be used for isotope ratio measurements since the detector does not bias the isotopes differently in terms of their count rates. The deviation of the measured ^{88}Sr/^{86}Sr value, 8.48, from its recommended value of 8.375 is discussed below.

The third part of the curve in which the measured ratios decrease almost linearly with the count rate indicates the saturation effect, or the dead time of the CEM when the count rate exceeds 500,000 counts/second. During ion counting even with very fast detector circuitry, the detector tends to lose some counts because at a high count rate the ions arrive at the detector separated by times shorter than the detector resolving time. This effect is described in equation 4.1 (Knoll, 1979):

$$Ct = Cm/(1 - Cm \times \tau) \qquad (4.1)$$

where Ct and Cm are the true and measured count rate respectively, and τ the detector resolving or dead time.

This effect is more serious when the measured isotopic ratios are further away from unity. In this case, the true isotopic ratio Rt can be related approximately to its measured ratio Rm and the measured count rate of the major isotope by equation 4.2:

$$Rt = Rm/(1 - Cm \times \tau) \qquad (4.2)$$

Since the value of $^{88}Sr/^{86}Sr$ ratio in the standard, 8.375, is far away from unity, the saturation effect of the CEM can be thought to affect only ^{88}Sr. When those measured ratios with ^{88}Sr count rate above 500,000 counts/second are corrected for dead time effect using equation 4.2 with τ = 50 ns, all of them are in agreement with the $^{88}Sr/^{86}Sr$ value in the plateau in Fig. 4.5 within 1σ (Fig.4.6 and Table 4.2). This detector saturation effect indicates the limitation of the precise isotopic ratio measurements without correction for the dead time effect when the ratio is too far away from unity, hence, the importance of the closeness to unity of the ratio of the spike to the sample.

Figure 4.6. The saturation effect of the CEM on the measured isotopic ratios. When ratios with the ^{88}Sr count rates larger than 100,000 counts/second are corrected for the saturation effect of the detector using dead time of 50 ns, they show very good agreement with each other. This agreement also indicates the constancy of the bias of the instrument. The horizontal line and the vertical bar represent the mean value and its 1σ of the dead time corrected ratios.
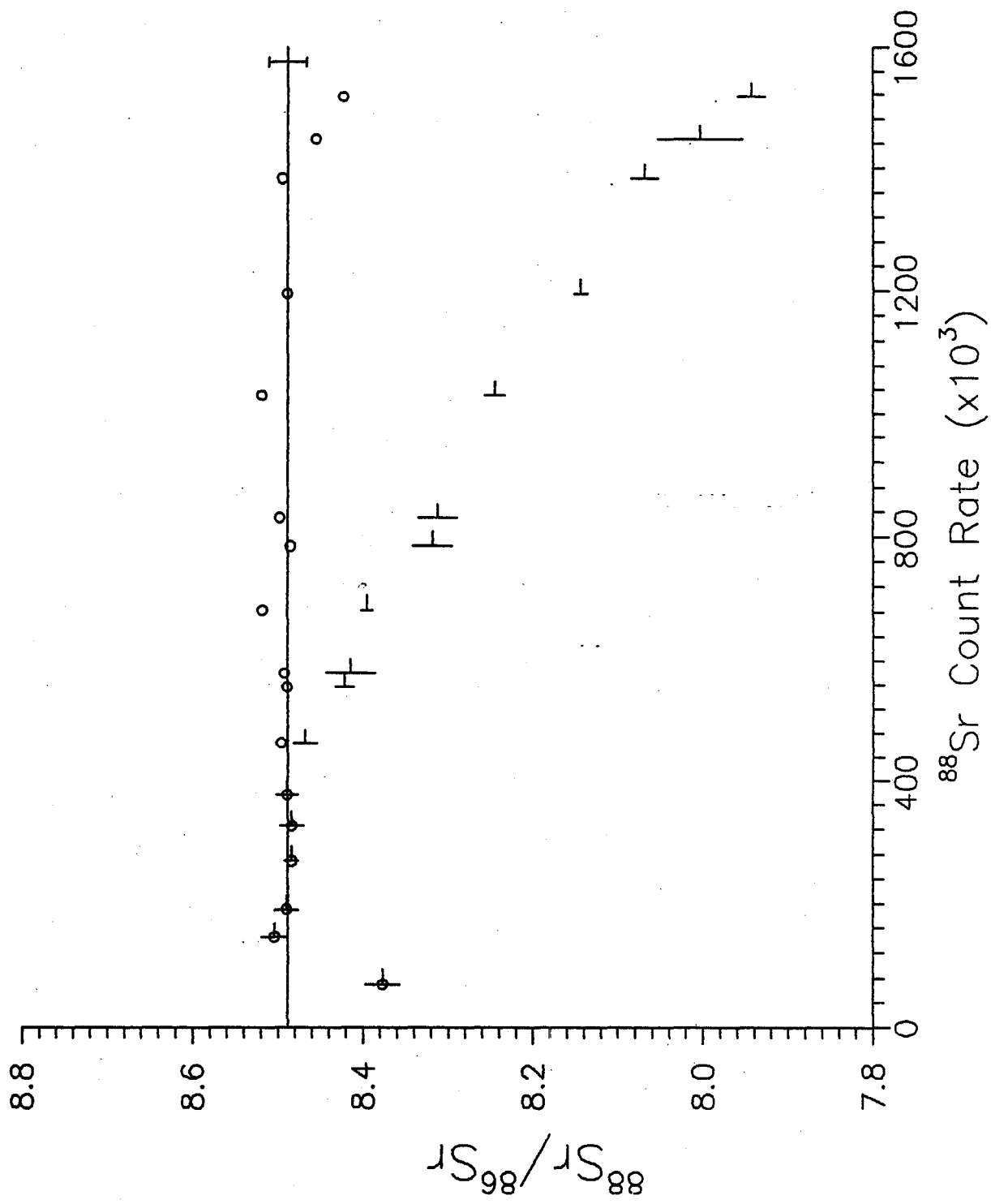
The value of the $^{88}Sr/^{86}Sr$ ratio, 8.48, in the plateau of Fig.4.5 is larger than its true value of 8.375. The deviation from its true value was attributed to mass fractionation and mass discrimination in the analyses. Even though mass fractionation and discrimination normally tend to enhance the lighter isotope, their integrated effect has been found in ICP-MS to bias the measured ratios either positively or negatively (Longerich et al., 1987; McLaren, et al., 1987; Russ and Bazan, 1987; Ting and Janghorbani, 1987). A mean bias factor of 0.987 was obtained from the dead time corrected measured $^{88}Sr/^{86}Sr$ ratios with ^{88}Sr count rate larger than 140,000 counts/second (Table 4.2). This bias factor was applied to all measured $^{88}Sr/^{86}Sr$ ratios of spiked samples.

4.4. SAMPLE PREPARATION AND DATA CALCULATION

Water samples were first run by ICP-MS to estimate their concentrations. They were concentrated simply by evaporation on the hot plates or diluted by the dilute distilled HCl depending on their estimated concentrations. Then approximate 1 ml samples were spiked using a ^{86}Sr spike so that the $^{88}Sr/^{86}Sr$ ratios of the spiked samples were close to unity from the reasons discussed already. No separation of the Sr from other elements such as Rb was needed. The Sr concentrations were then calculated using

equation 4.3 and the bias-corrected $^{88}Sr/^{86}Sr$ ratios, Rc86. The atomic mass of Sr was taken to be 87.589 amu, the ^{88}Sr abundance, 82.59% and the $^{88}Sr/^{86}Sr$ ratio of the unspiked samples, 8.375.

$$Csm=87.589(0.976Rc86-0.024)CspxWsp$$
$$/(0.8259x85.91Wsm(1-Rc86/8.375)) \qquad (4.3)$$

where Csm is the Sr concentration of the sample, Csp the Sr concentration of the spike. The ^{86}Sr spike is 97.6% enriched and other 2.4% is essentially ^{88}Sr. Wsp and Wsm are the sample weights of the spike and the sample respectively. The Sr concentration of the spike was 1.39 ug/g, obtained by simply diluted the concentrated ^{86}Sr spike with known concentration.

4.5. PRECISION AND ACCURACY

As discussed in 4.2, the precision and the accuracy of the measured isotopic ratios depends on the deviation of the ratio from unity and the bias correction. The normal precision of the measured $^{88}Sr/^{86}Sr$ ratios of individual runs for both the unspiked A+E standard and spiked samples is around 1% (1σ). However, the mean of this ratio for several replicate runs of the same sample solution yielded a precision better than 0.2% (1σ) for the A+E standard (Table

4.2). When ^{88}Sr count rate was above 100,000 counts/second and the ratios corrected for dead time effect of the CEM, 17 means of five replicates of measured ^{88}Sr/^{886}Sr ratios of A+E gave a mean of 8.488 with a 1σ of 0.022 (Table 4.2 and Fig.4.6). This indicates the constancy of the bias of the machine.

When samples were analyzed for Sr concentrations, they were not corrected for the dead time effect of the detector since the measured ^{88}Sr/^{86}Sr ratios were between 0.3 and 3 with the majority between 0.5 and 1.2, and the ^{88}Sr count rates were between 100,000 and 500,000 counts/second. The mean bias factor of 0.987 was applied to all the samples. The accuracy of this method was examined by analyzing water and rock standards. The results were shown in Table 4.3. The mean values of the Sr concentrations of four analyses of each standard are in good agreement with their recommended values within 2σ. A precision better than 1% (1σ) is easily obtained in individual runs. The Sr concentrations along with their 1σ of the water samples were shown in Table 4.4. Most of the samples have a precision better than 1%.

Table 4.3.   Strontium Analyses of the Standards

	NBS1643b		G-2		GSP-1		AGV-1		BCR-1	
	Sr Conc.	STD	Sr Conc.	STD	Sr Conc.	STD	Sr Conc.	STD	Sr Conc.	STD
	0.227	0.004	479	8	227	8	670	9	334	3
	0.223	0.002	483	9	225	3	671	10	334	5
	0.223	0.003	476	8	227	4	668	5	330	3
	0.223	0.002	479	8	227	3	663	6	331	6
Mean	0.224	0.002	479	2	227	1	668	3	332	2
Recommended	0.227		480		240		660		330	

1. The recommended values for rock standards are from Govindaraju, 1984.
2. The Sr concentrations are in ppm.

Table 4.4. Sr Concentrations of the Water Samples

Sam.Name	Sam.#	Sam.Wt. (g)	Spk.Wt. (g)	Rm86	Rc86	STD	Sr Conc. (ug/g)	STD
URL4-5-6	1141	3.58872	1.32989	0.4058	0.4005	0.0038	0.245	0.002
URL4-5-8	1148	3.72212	1.26425	0.4368	0.4311	0.0036	0.244	0.002
URL4-5-10	1156	3.77900	1.57417	0.3699	0.3651	0.0027	0.248	0.002
M6-2-4	1167	3.54142	1.07758	0.4442	0.4384	0.0042	0.223	0.002
M6-2-5	1174	3.64742	1.28280	0.3571	0.3525	0.0031	0.202	0.002
209-0C1-4	1240	1.60252	1.12336	0.8318	0.8210	0.0064	1.037	0.008
M13-2-4	1073	0.79524	0.59049	1.5280	1.5081	0.0098	2.250	0.015
M13-2-5	1079	0.72916	1.22694	0.7568	0.7470	0.0066	2.235	0.020
209-010-0C1	148	1.99438	1.32426	0.4786	0.4724	0.0041	0.528	0.005
209-0C1-2	1221	1.99868	1.02211	1.0890	1.0748	0.0064	1.032	0.006
209-0C1-3	1233	1.99500	1.07062	1.0540	1.0403	0.0063	1.042	0.006
206-007-HC7	1186	8.95704	1.29819	0.6610	0.6524	0.0052	0.165	0.001
201-010-HC7	198	8.95830	1.33433	0.7029	0.6938	0.0047	0.182	0.001
URL6-SW9	1265	9.54600	1.12167	1.0070	0.9939	0.0058	0.216	0.001
URL10-6-5	1089	2.98300	1.01308	0.7611	0.7512	0.0068	0.454	0.004
URL10-6-6	1094	2.99470	1.13542	0.6747	0.6659	0.0062	0.442	0.004
URL10-6-7	1100	2.98043	1.14550	0.6633	0.6547	0.0067	0.440	0.005
M2A-3-2	1005	5.97272	1.13385	0.5371	0.5301	0.0054	0.172	0.002
M2A-3-4	1011	5.97755	1.21240	0.4722	0.4661	0.0043	0.159	0.001
M2B-2-1	005	6.01492	1.22171	0.3909	0.3858	0.0045	0.129	0.002
M4A-4-4	1118	0.98908	1.36900	0.5993	0.5915	0.0053	1.414	0.013
M4A-4-6	1126	0.99252	1.20700	0.6735	0.6647	0.0049	1.416	0.010
M8-3-4	1046	10.96183	1.53769	0.6891	0.6801	0.0060	0.168	0.001
M8-3-7	1054	8.50004	1.18944	0.6160	0.6080	0.0046	0.147	0.001
M7-SW28	1210	1.99284	1.20836	0.7199	0.7105	0.0028	0.761	0.003
M7-4-4	1227	0.19728	1.20019	2.2560	2.2267	0.0235	30.562	0.323
M7-4-6	167	0.41974	1.16787	3.8150	3.7654	0.0143	31.670	0.120
M7-4-9	183	0.15414	0.98253	2.0850	2.0579	0.0097	28.777	0.136
M7-4-9	184	0.27908	1.05634	3.0530	3.0133	0.0211	29.593	0.207
M7-4-9	185	0.17678	1.11714	2.1960	2.1675	0.0132	30.597	0.186
M7-4-9	186	0.22057	1.18791	2.4620	2.4300	0.0186	30.564	0.234
M7-4-11	209	0.27544	1.22471	2.8210	2.7843	0.0264	30.785	0.292
M14-4-1	1021	0.18146	1.31792	1.4580	1.4390	0.0076	20.774	0.110
M14-4-4	1030	0.12599	1.32678	1.0570	1.0433	0.0057	20.522	0.112
URL12-11-7	161	3.99535	1.18587	0.6346	0.6264	0.0064	0.323	0.003
URL12-11-8	173	3.98241	1.16186	0.6110	0.6031	0.0056	0.305	0.003
URL12-11-13	225	3.98474	1.32419	0.5070	0.5004	0.0057	0.282	0.003
URL12-7-8	098	0.21029	1.25999	0.6912	0.6822	0.0047	7.184	0.049
URL12-7-10	104	0.24692	1.47121	0.8037	0.7933	0.0062	8.473	0.066
URL12-7-18	121	0.25408	1.57586	0.8263	0.8156	0.0051	9.102	0.057
URL12-7-21	140	0.25031	1.14129	1.0910	1.0768	0.0043	9.220	0.037
URL10-3-2	039	1.70495	1.15205	0.2274	0.2244	0.0032	0.232	0.003
M10-3-1	012	0.25775	1.32027	1.0540	1.0403	0.0051	9.949	0.049
M10-3-2	019	0.24689	1.27108	1.1550	1.1400	0.0047	11.132	0.046
M10-3-3	023.6	0.27157	1.27364	1.2960	1.2792	0.0088	11.630	0.080
WN8-4	056	5.78331	1.10776	0.6638	0.6552	0.0063	0.219	0.002
WN8-6	063	5.98456	1.00987	0.8865	0.8750	0.0061	0.268	0.002
WN8-7	070	6.45536	1.33594	0.8193	0.8086	0.0049	0.301	0.002
WN8-9	086	6.93513	0.94937	1.1320	1.1173	0.0043	0.289	0.001
WN11-19-15C	453	2.01770	1.57016	5.7610	5.6861	0.0370	22.982	0.150

CHAPTER FIVE

ISOTOPE GEOCHEMISTRY OF THE HOST ROCK

5.1. BACKGROUND

5.1.1. GEOCHRONOLOGY OF THE LAC DU BONNET BATHOLITH

The geochronology of the Lac du Bonnet batholith was recently summarized by Beakhouse et al (1988). Based on the analyses of five whole-rock biotite granite samples, Penner and Clark (1971) obtained a Rb-Sr isochron age (recalculated with $\lambda_{Rb}=1.42 \times 10^{-11}$ a^{-1}) of 2443 ± 136 Ma with an initial $^{87}Sr/^{86}Sr$ ratio of 0.7088 ± 0.0068. Farquharson (1975) analyzed an additional three samples and reported a revised age (omitting one sample analyzed by Penner and Clark) of 2621 ± 160 Ma and an initial ratio of 0.6999 ± 0.0067. Uranium -Pb zircon geochronology study by Krogh et al (1976) yielded an age of 2665 ± 20 Ma. This age is among the youngest U-Pb zircon ages reported for the Superior province. Based on the comparative Rb-Sr and U-Pb zircon geochronology study of the Winnipeg River Belt, Beakhouse et al (1988) suggested that the U-Pb zircon age represents the age of crystallization of the batholith while the relatively younger Rb-Sr whole-rock isochron date is the time of the subsolidus (deuteric or hydrothermal alteration) redistribution of Rb and Sr accompanying the slow cooling of the batholith.

5.1.2. GEOLOGY AND HYDROGEOLOGY

The URL leased area is located in the southeastern part of the Lac du Bonnet batholith, and is about 70 km to the northeast of Winnipeg (Fig. 5.1). In addition, Fig. 5.1 also shows the Whiteshell Nuclear Research Establishment (WNRE) that is located in the southwest margin of the batholith. Extensive geological and hydrogeological investigations have been carried out by the AECL and the results summarized by Brown and Davison (1986). A series of boreholes and the URL shaft within the leased area have revealed that the batholith at the URL location is dominated by two major phases: a lower grey (magnetite-bearing) granite - granodiorite and a upper pink (hematite-bearing) granite (Gascoyne and Cramer, 1987). This vertical petrological variation was interpreted as the result of the slow-cooling of the magma as revealed by the U-Pb zircon and Rb-Sr geochronology. Increase in $f(O_2)$ and $f(H_2O)$ in the cooling magma, probably due to both chemical differentiation and increasing involvement of surface meteoric water, has resulted in transgression of the magnetite/hematite boundary within the rock body. The grey granite, which is almost unaltered, represents the primary phase of granite, while the pink granite, which contains abundant secondary minerals, is overprinted by hydrothermal alteration. This

Figure 5.1.   Map   showing the   location of   the URL research
        area. The location of WNRE is also shown (after Gascoyne
        and Cramer, 1987).

POINTE DU BOIS

BIRD RIVER

WINNIPEG RIVER

LEE RIVER

LAC DU BONNET

URL

PINAWA

WNRE

LAC DU BONNET

CANADA

N

km

0   5   10

315

313

313

211

307

307

11

11

214
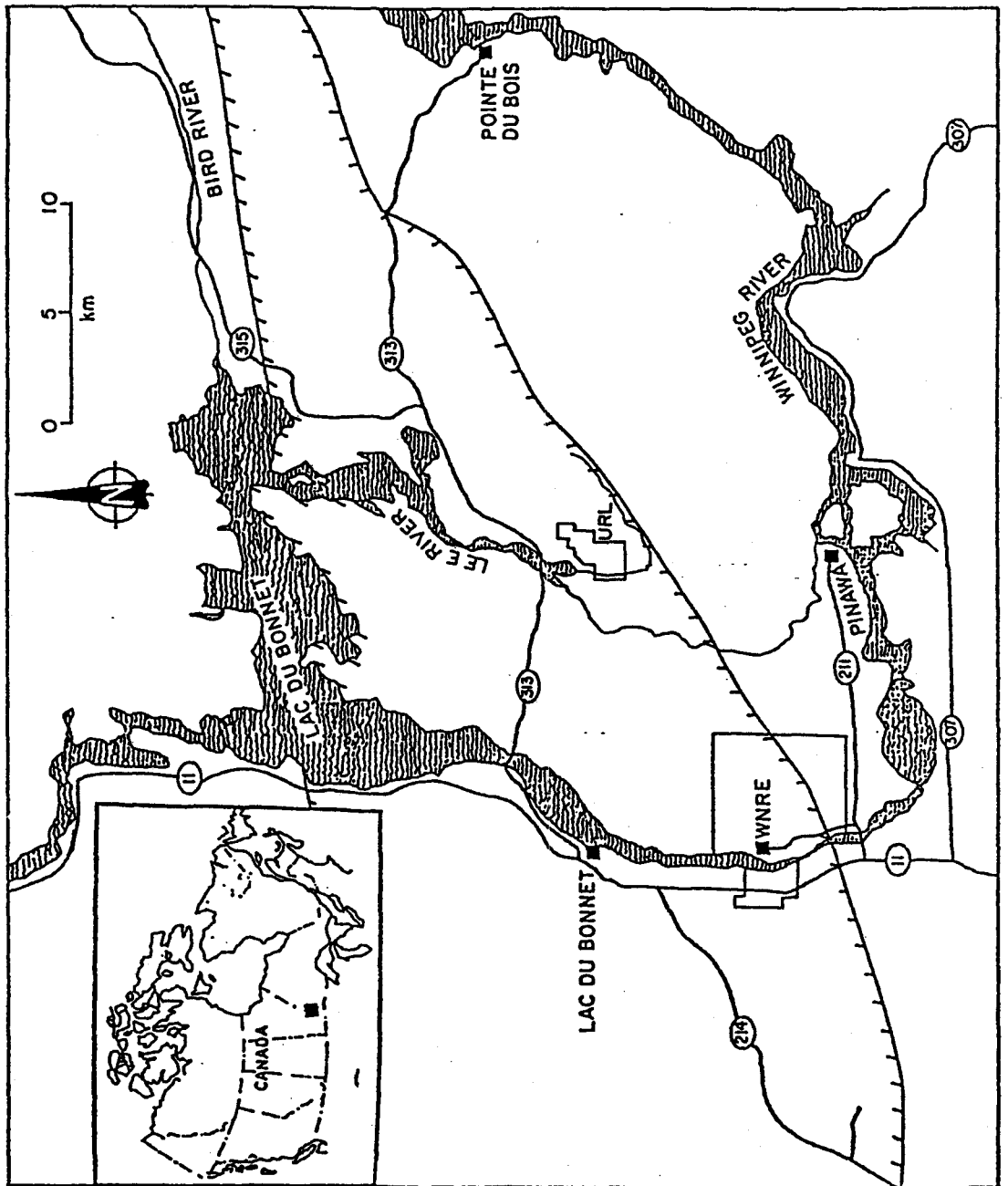
boundary between the lower grey granite-granodiorite and the upper pink granite at the URL location occurs at a depth between 200m and 250m (Gascoyne and Cramer, 1987).

The batholith as a whole is relatively unfractured. However, numerous near-vertical fractures and three sub-horizontal fracture zones were found from the boreholes and the shaft excavation (Fig. 5.2). The intensity of the sub-vertical fractures increases closer to the surface and to the fracture zones. These sub-vertical fractures are parallel to the pegmatitic dikes and quartz veins within the batholith. Some of the fractures are filled with high temperature minerals, such as epidote and chlorite. No evidence of post-crystallization tectonic events disturbing this batholith exists. Therefore these fractures are believed to be formed under the regional stress during the cooling of the magma and subsequent hydrothermal events.

The three fracture zones are complex in structure and vary in thickness. They dip slightly east-southeast and extend 15 km westward to the Whiteshell Research area as revealed by boreholes. Tests show that the hydrogeology is controlled by these sub-horizontal fracture zones (Davison, 1984). These zones are partially interconnected by vertical fractures, therefore allowing surface water to circulate to a depth of 400m.

Figure 5.2.   A schematic cross-section from NW   to SE through

the URL   research area showing the subvertical fractures

and the three subhorizontal fracture zones.   The surface

locations of the boreholes and the URL shaft are also

shown.   The relative permeability of the rocks is also

indicated (from Gascoyne and Cramer, 1987).
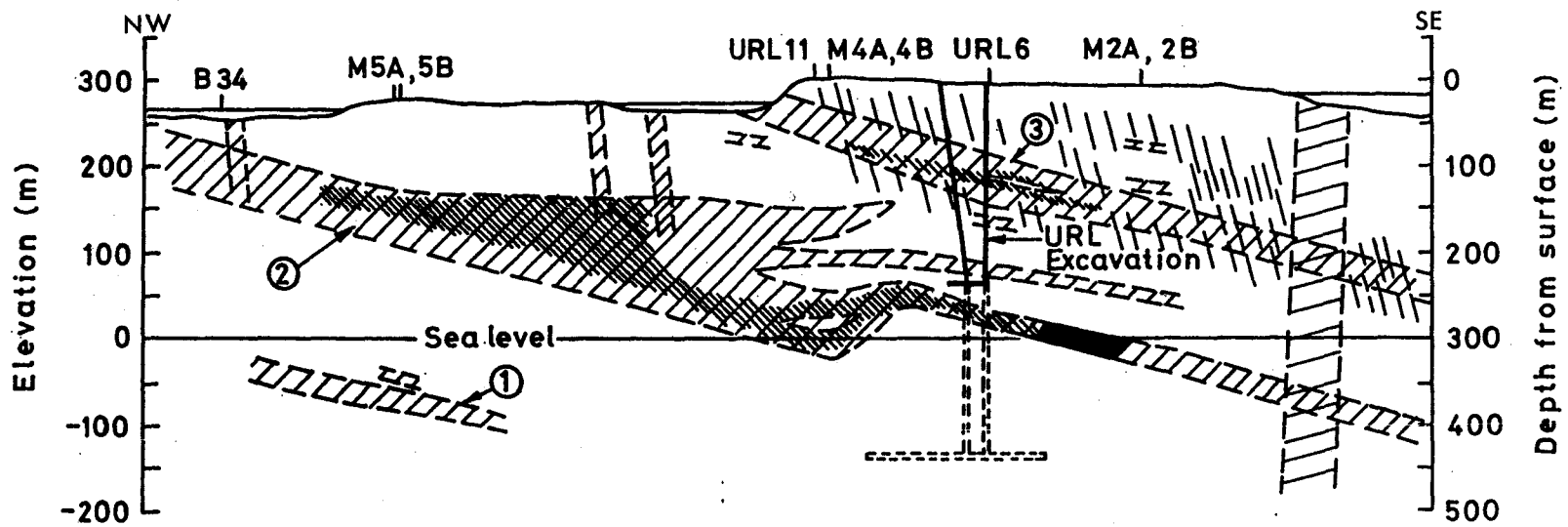
5.1.3. ALTERATION OF THE HOST ROCK

Petrological studies of samples from both borehole cores and the URL shaft indicate that the granite was subjected to a two-stage alteration -- first at high- and then at low-temperature (Kamineni et al, 1986 and Gascoyne and Cramer, 1987). During the cooling of the magma, circulation of the fluids derived from the magma and meteoric water supplied through the fractures within the batholith resulted in deuteric and hydrothermal alteration. This high temperature alteration is characterized by the pink coloration of the unaltered grey granite in the roof zone of the batholith, and by the presence of high-temperature fracture-filling secondary minerals, such as epidote, quartz, hematite, phengite, and chlorite. The pink coloration is the result of leaching Fe from Fe-bearing minerals such as biotite, and varies in intensity from reddish to deep-red towards fractures. This indicates the involvement of oxidizing fluids circulating in the fractures. The high-temperature hematization is observed only in the areas close to the fractures in the lower grey granite. It is believed, on the bases of U-Pb zircon, Rb-Sr and Ar-Ar geochronology, that the high-temperature alteration lasted about 2000 Ma until the cooling batholith reached ambient temperatures at the depth of emplacement

(Gascoyne and Cramer, 1987).

The low-temperature alteration is, on the other hand, characterized by the presence of abundant clay minerals such as illite, vermiculite, etc., in the Fe-bleached cream-coloured zones in the fractures. Oxygen isotope study of illite ($\delta^{18}O=17.1-20.9‰$) indicates the low temperature formation of the clays (Kerrich and Kamineni, 1985). This low-temperature alteration occurs mainly within and close to the fractures. It is estimated to have lasted for at least 450 Ma since the batholith is overlain in the west by Upper Ordovician sedimentary rocks (Gascoyne and Cramer, 1987).

Biotite and plagioclase are the two major minerals affected by both high- and low-temperature alteration. They are slightly or completely replaced by secondary minerals depending on the degree of alteration. Potassium feldspar is much less altered compared to plagioclase and most is fresh even in highly altered rocks. Quartz is normally not affected at all.

Kamineni et al (1986) divided the granite into four major groups in terms of the degree of alteration (in order of increasing alteration): 1). unaltered grey granite, 2). pink granite, 3). deep-red granite, 4). cream-coloured clay-rich granite. The grey granite occurs at the URL site

normally below 260m and contains plagioclase, microcline , quartz, and biotite as the major minerals. Slight alteration in plagioclase and biotite was observed.

The pink granite, while similar to the grey granite in its major mineralogy is different as the plagioclase is more altered and has epidote, carbonate, and phengite in it (Kamineni et al., 1986). Chlorite occurs, mainly in biotite, partly along the (100) cleavage and partly surrounding this mineral. Iron oxide is commonly present, concentrated in plagioclase and in microfractures.

The deep-red granite is limited to the vicinity of the fractures. It is distinguished from pink granite by its more abundant microfractures and secondary minerals. Biotite is highly altered to chlorite and muscovite, and plagioclase is highly altered to sericitic phengite. More abundant Fe-oxide in plagioclase, some microcline, and fractures imparts a brick-red colour to the rock samples.

The cream-coloured clay-rich altered granite is restricted to the fractures. It is characterized by the presence of abundant clays, mainly illite, in mineral grains and in fractures, and by the absence of Fe-oxide. Plagioclase and biotite are completely altered to clays and chlorite.

These four types of granites define an evolutionary sequence of alteration of a decrease in alteration temperature from the grey to cream-coloured granite. Their occurrence and mineral assemblages are summarized in Table 5.1.

5.1.4. GEOCHEMISTRY

Kamineni et al (1986), analyzed the U and Th concentrations of almost 400 core samples. Their results are summarized in Table 5.2 along with the major elements and other trace elements. Compared to the unaltered fresh grey granite, the altered granites have been subjected to significant Ca, Na, and Sr loss. Even though the U concentration values of the four rock types agree within error, the statistics of F-test and T-test show that the means of the grey and pink, the pink and deep-red, the pink and the cream-coloured granites are distinct. Therefore, Kamineni et al., concluded that the pink granite, which had been subjected to high temperature alteration, had lost significant U. While the more altered deep-red and cream-coloured granites had gained U. The high U concentration in the deep-red granite is associated with the high total Fe content and high Fe^{3+}/Fe^{2+} ratio. The U enrichment in the cream-coloured granite, associated with low Fe^{3+}/Fe^{2+}

Table 5.1. Alteration Mineral Assemblages of Host Rocks

----

1. Grey granite/granodiorite

    Fresh except slight alteration of plagioclase

2. Pink granite

    Occurrence: massive above 260m

    Alteration: plagioclase - epidote, phengite,
                     and carbonates.
              biotite - chlorite along cleavage.

    Fe-oxide: most in plagioclase.

    Fractures: epidote, chlorite, and Fe-oxide.

 3. Deep-red granite

    Occurrence: close to fractures

    Alteration: plagioclase - phengite and Fe-oxide.
              biotite - chlorite, vermiculite and
                    Fe-oxide.

    Fe-oxide: massive in plagioclase and biotite.

    Fractures: chlorite and Fe-oxide.

 4. Cream-coloured granite

    Occurrence: within the fractures and their vicinities.

    Alteration: plagioclase - massive clays (illite).
              biotite - completely chlorite.

    Fe-oxide: disappeared

    Fractures: clays, calcite and goethite.

Table 5.2.   Chemical Analyses of the Core Samples From URL

	Grey Granite		Pink Granite		Deep-red Granite		Cream-coloured Granite	
	Mean	Std	Mean	Std	Mean	Std	Mean	Std
Major Elements (%)								
SiO2	71.87	2.88	72.20	2.65	72.25	1.10	71.25	0.85
TiO2	0.22	0.14	0.21	0.13	0.22	0.05	0.20	0.04
Al2O3	14.95	0.96	14.22	1.58	13.72	0.90	14.79	0.60
Fe2O3	1.23	0.76	1.62	0.61	2.79	0.51	1.91	0.37
FeO	1.14	0.35	1.09	0.28	1.00	0.39	0.92	0.21
MgO	0.41	0.21	0.48	0.33	0.60	0.21	0.94	0.30
CaO	1.66	0.50	1.49	0.46	1.05	0.25	0.86	0.53
Na2O	4.07	0.96	3.95	0.83	3.66	0.75	1.85	0.40
K2O	4.85	1.15	4.90	1.01	5.00	0.88	7.30	0.55
Trace Elements (ppm)								
Ba	673	218	583	180	563	90	633	78
Rb	227	45	208	39	220	34	265	33
Sr	279	57	222	48	205	28	136	37
U	6.60	4.31	4.96	2.40	6.67	2.98	9.87	4.42
Th	37.01	13.85	45.63	36.77	42.25	18.62	42.50	17.50

Water (H_2O) and MnO are not listed.

Data from Kamineni et al., 1986.

ratios and with abundant clays, is interpreted by a model
that has a low Eh groundwater passing through the fractures
and Fe was bleached as Fe^{2+}. Uranium was less mobile in the
reducing environment and was probably absorbed in the clay
minerals. Little variation in Th concentration was found
among fresh and altered samples and was attributed to the
general immobility of Th in various environments.

A U-series profile study by Gascoyne and Cramer (1987)
of four boreholes gave similar conclusions. Compared with
the fresh unaltered grey granite at a depth of 730m, the
analyses show that the high-temperature alteration has
caused significant Ca, Na, REE, U and Th (Th result was not
discussed in their paper) loss and Fe enrichment in rocks
adjacent to the fractures in the upper part (pink granite)
of the batholith. Low-temperature alteration due to
reducing groundwater had resulted in Fe loss and U and
slight REE enrichment in the fracture surfaces in heavily
altered rock from fracture zones at intermediate depth.
Uranium-series isotopic results show that the near surface
rock has been subjected to recent U loss without U isotope
fractionation. On the other hand, U (probably Th as well)
migration in the heavily altered samples happened recently
(less than 1 Ma) and was controlled by the redox front of
the modern groundwater. Uranium-series results of deep
samples indicates that no loss or gain of U and Th happened

within the last 1 Ma.

5.2. ISOTOPE GEOCHEMISTRY OF THE HOST ROCKS
5.2.1. STRONTIUM ISOTOPES

Five relatively fresh (pink) and twelve altered (deep-red and cream-coloured) granite samples were analyzed for Sr isotopic ratios and Rb and Sr concentrations in both whole rocks and mineral separates. Results are presented in Table 5.3. The Rb concentrations of the altered whole-rock samples, plagioclase and biotite mineral separates tend to be similar to their fresh counterparts. However, the Rb concentrations of potassium feldspar separates of altered samples are lower than those of fresh potassium feldspars. Strontium concentrations of altered samples are lower than their fresh counterparts, especially the mineral separates. This indicates some Sr was lost in altered samples and even the whole rock was not a closed system with respect to Sr.

The Sr isotopic ratios in the whole-rock and mineral separates of altered samples are generally higher than those of fresh samples. When plotted in the Rb-Sr isochron diagram, all the data points, except for biotite, scatter around a 2100 Ma reference line (Fig. 5.3). A 2600 Ma reference isochron with initial $^{87}Sr/^{86}Sr$ ratio of 0.701 is

Table 5.3. Strontium Isotopic Analyses of the Host Rocks And Minerals

SAMPLE	Rb ppm	Sr ppm	87Rb/86Sr	87Sr/86Sr	2STDERROR	D-Sr
FRESH SAMPLE						
P1-WR	157.0	283.0	1.613	0.760309	0.000016	-17.8
P2-WR	202.1	250.7	2.350	0.783460	0.000016	-74.6
P3-WR	148.1	221.4	1.947	0.771241	0.000014	-38.5
JSS1	134.7	283.9	1.379	0.751067	0.000014	-23.5
JSS2	182.3	285.5	1.858	0.768391	0.000014	-32.2
P1-PL	20.3	446.6	0.132	0.710293	0.000012	61.6
P2-PL	22.5	277.4	0.235	0.714776	0.000014	69.7
P3-PL	15.4	331.3	0.135	0.711585	0.000012	78.3
JSS1-PL	13.0	212.7	0.177	0.711354	0.000012	52.3
JSS2-PL	14.7	194.9	0.218	0.713774	0.000012	64.4
P1-KF	436.4	272.0	4.695	0.824743	0.000014	-601.6
P2-KF	346.9	283.5	3.581	0.824858	0.000016	-129.0
P3-KF	385.3	233.7	4.844	0.865649	0.000018	-197.9
JSS1-KF	308.6	257.4	3.506	0.816305	0.000012	-198.2
JSS2-KF	348.3	338.6	3.006	0.808622	0.000014	-66.2
P1-BI	225.3	50.8	14.863	2.326023	0.000046	8462.7
P2-BI	255.2	45.1	20.062	3.011934	0.000066	10695.9
P3-BI	567.9	35.8	57.715	3.340124	0.000066	1633.7
JSS1-BI	683.8	44.9	51.695	2.478445	0.000044	-628.8
JSS2-BI	718.5	84.1	27.363	1.806992	0.000018	445.9
ALTERED SAMPLE						
HC01	179.7	187.1	2.804	0.800707	0.000012	-71.0
HC02	181.4	193.7	2.733	0.796629	0.000012	-88.8
HC19	153.7	123.2	3.644	0.806445	0.000012	-376.9
3D1-1	160.6	249.5	1.875	0.776999	0.000012	71.3
3D1-2	163.3	248.5	1.915	0.780359	0.000012	95.3
3D1-3	166.1	252.6	1.923	0.819464	0.000016	596.8
3D2	135.7	215.0	1.838	0.773510	0.000014	44.2
3D3	158.1	152.8	3.025	0.815351	0.000012	7.4
3D4-1	157.4	241.2	1.900	0.772024	0.000014	-5.3
3D4-2	148.2	229.6	1.879	0.772986	0.000012	17.1
3D5-1	143.1	257.9	1.614	0.764892	0.000012	41.9
3D5-2	186.5	256.9	2.117	0.788916	0.000010	106.5
HC01-PL	30.5	159.9	0.553	0.725964	0.000014	57.9
HC02-PL	23.8	175.1	0.394	0.721388	0.000010	78.0
HC19-PL	28.8	78.7	1.061	0.733956	0.000012	-93.9
HC01-KF	268.1	180.1	4.367	0.850363	0.000014	-171.5
HC02-KF	296.9	176.6	4.940	0.867835	0.000014	-213.4
HC19-KF	223.0	133.3	4.906	0.846901	0.000016	-435.6
HC01-BI				12.142015	0.000316	
HC02-BI	709.6	9.5	435.651	11.070344	0.000110	-3519.1
HC19-BI	626.7	13.3	220.112	6.927586	0.000070	-2283.1

1. D-Sr is calculated using equation 5.1.

Figure 5.3.   Rubidium-Sr isochron plot of all the rock
    samples and mineral separates from the URL area.   The
    diamonds, triangles, squares and circles stand for
    plagioclase, k-feldspars, biotite and whole-rock
    samples.   The open symbols are fresh samples and the
    solid are the altered samples.   The dashed line is a
    2600 Ma isochron with an initial Sr ratio of 0.701.
    This line represents the lowest limit of the age of the
    Lac du Bonnet Batholith.   The solid line is the
    regression line of all the data points except biotite.
    This regression line corresponds to a reference age of
    2100 Ma.   The insert shows the biotite points.

Ref. Isochron (2600 Ma)

$^{87}Rb/^{86}Sr$

$^{87}Sr/^{86}Sr$
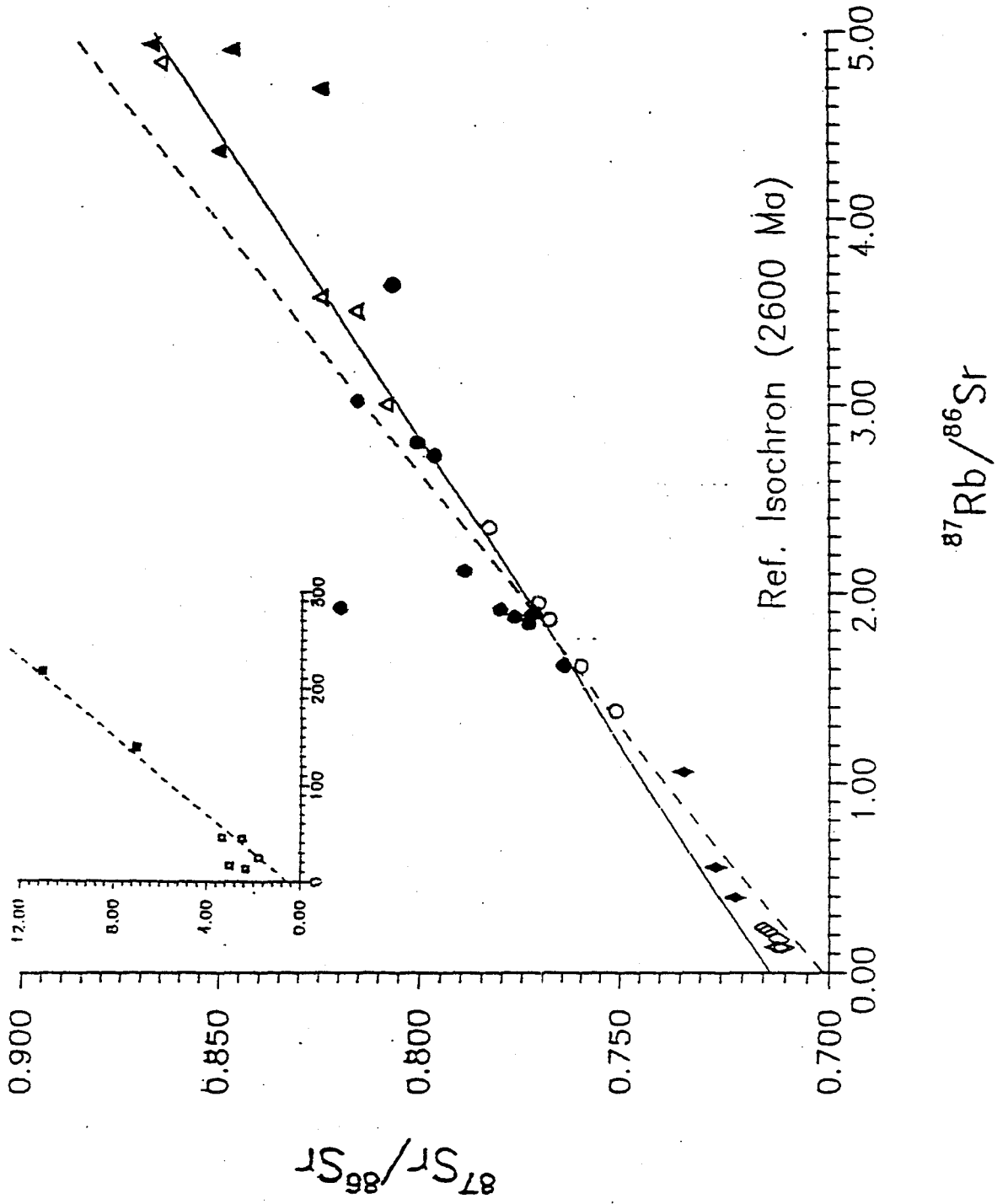
shown for comparison, and represents the lowest limit of the age of the Lac du Bonnet batholith in terms of previous Rb-Sr and U-Pb zircon geochronological studies (Beakhouse et al., 1988). If only fresh samples are plotted in the Rb-Sr diagram, a more constrained trend is shown in Fig. 5.4. This trend represents an age of 2302 ± 62 Ma (MSWD=56) with an initial value of 0.70637 ± .00003. This age may reflect the approximate time at which the high-temperature alteration (pink-coloration of the primary grey granite) following crystallization, that resulted in the redistribution of the Rb and Sr within the batholith. If the value of 0.701 is the lowest limit of the initial $^{87}Sr/^{86}Sr$ ratio of the Lac de Bonnet magma and 2600 Ma the upper limit of the age (Beakhouse et al., 1988), the $^{87}Sr/^{86}Sr$ ratio of the whole rock should approximately be 0.709 by 2300 Ma, as calculated using the average $^{87}Rb/^{86}Sr$ value of 1.83 for the five fresh whole-rock samples in Table 5.3. In contrast, the lower value of about 0.706 indicated in Fig.5.4 suggests open-system behavior during the alteration on a whole-rock scale. Either some radiogenic ^{87}Sr was lost to the circulating fluids in the fractures or the rock gained some Rb from other sources during the alteration. The former is more preferred since Rb has been found to be immobile in most geochemical processes (Nesbitt, 1979; Kamineni et al., 1986).

Figure 5.4. Rubidium-Sr isochron plot of the fresh rock
        samples and their mineral separates except sample P1-KF.
        The   data   points   slightly   scatter   around   a   2300 Ma
        reference line with an   initial   Sr   ratio of 0.706 (the
        solid line).   The   2600 Ma   isochron is· also shown (the
        dashed line).   Symbols are the same as Fig. 5.3.

Ref. Isochron (2600 Ma)

$^{87}Rb/^{86}Sr$

$^{87}Sr/^{86}Sr$
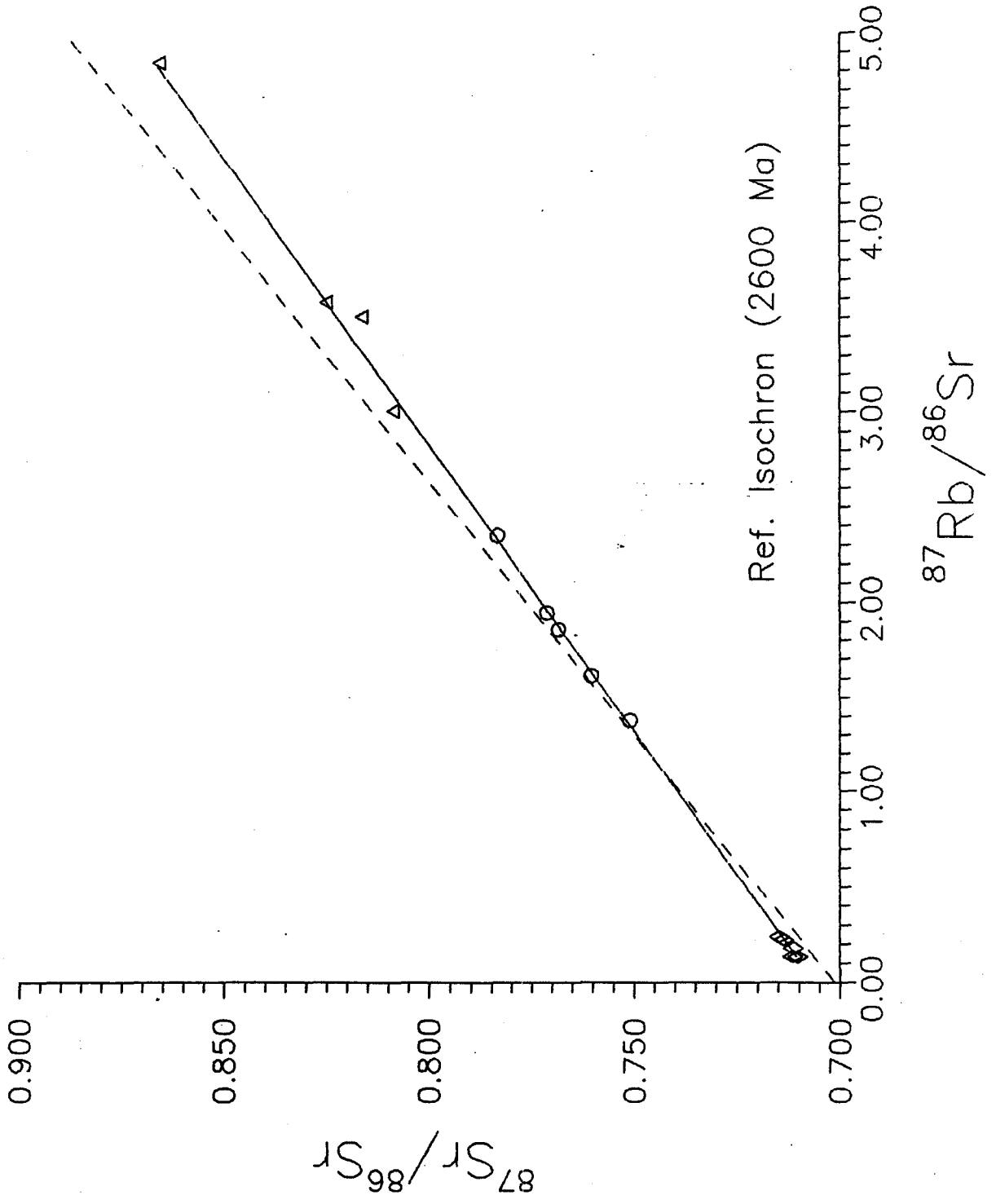
The scatter of the altered samples (Fig.5.3) indicates Rb and/or Sr was possibly redistributed due to possible low-temperature alteration. The scatter implies that this redistribution of Rb and Sr was local, otherwise, a tighter trend would be found.

In an attempt to assess the disturbance of the Rb-Sr system due to the two-alteration events of the batholith, deviations of the Sr isotopic ratios from the 2600 Ma isochron with the initial ratio of 0.701 are calculated assuming Rb is not mobile during alteration events. The deviation, D-Sr is calculated using the following equation:

$$D\text{-}Sr = \{[(^{87}Sr/^{86}Sr)_m - (^{87}Sr/^{86}Sr)_c]/(^{87}Sr/^{86}Sr)_c\}10^4 \qquad (5.1)$$

$$(^{87}Sr/^{86}Sr)_c = 0.701 + (^{87}Rb/^{86}Sr)_m(e^{\lambda T}-1) \qquad (5.2)$$

where $(^{87}Sr/^{86}Sr)_m$ and $(^{87}Rb/^{86}Sr)_m$ are measured ratios, T equals 2600 Ma, and λ is the decay constant of ^{87}Rb (1.42×10^{-11} y^{-1}). D-Sr data are listed in Table 5.3 and are shown in Fig.5.5. In this diagram, when D-Sr=0, the point plots on the 2600 Ma Rb-Sr isochron; when D-Sr>0, the point plots above the 2600 Ma isochron indicating either gain of Sr or loss of Rb; while for D-Sr<0, the point plots below the isochron indicating Sr loss or Rb gain.

Figure 5.5.   Plot   of ^{87}Rb/^{86}Sr against D-Sr of all the rock

samples and mineral separates from the URL area.   The D-

Sr, defined   by equation   5.1., is   the deviation of the

observed ^{87}Sr/^{86}Sr ratio from its   value   on   a · 2600 Ma

isochron   with   an   initial   Sr   isotopic ratio of 0.701.

The horizontal line with D-Sr value of 0   represents the

2600 Ma   isochron.   The   fresh   whole rock   samples   and

their   plagioclase   and   potassium   feldspar   separates,

except P1-KF,   have smaller   scatter compared with those

of the altered samples.   The biotite separates are shown

in the   insert.   See text   for discussion.   Symbols are

the same as in Fig. 5.5.
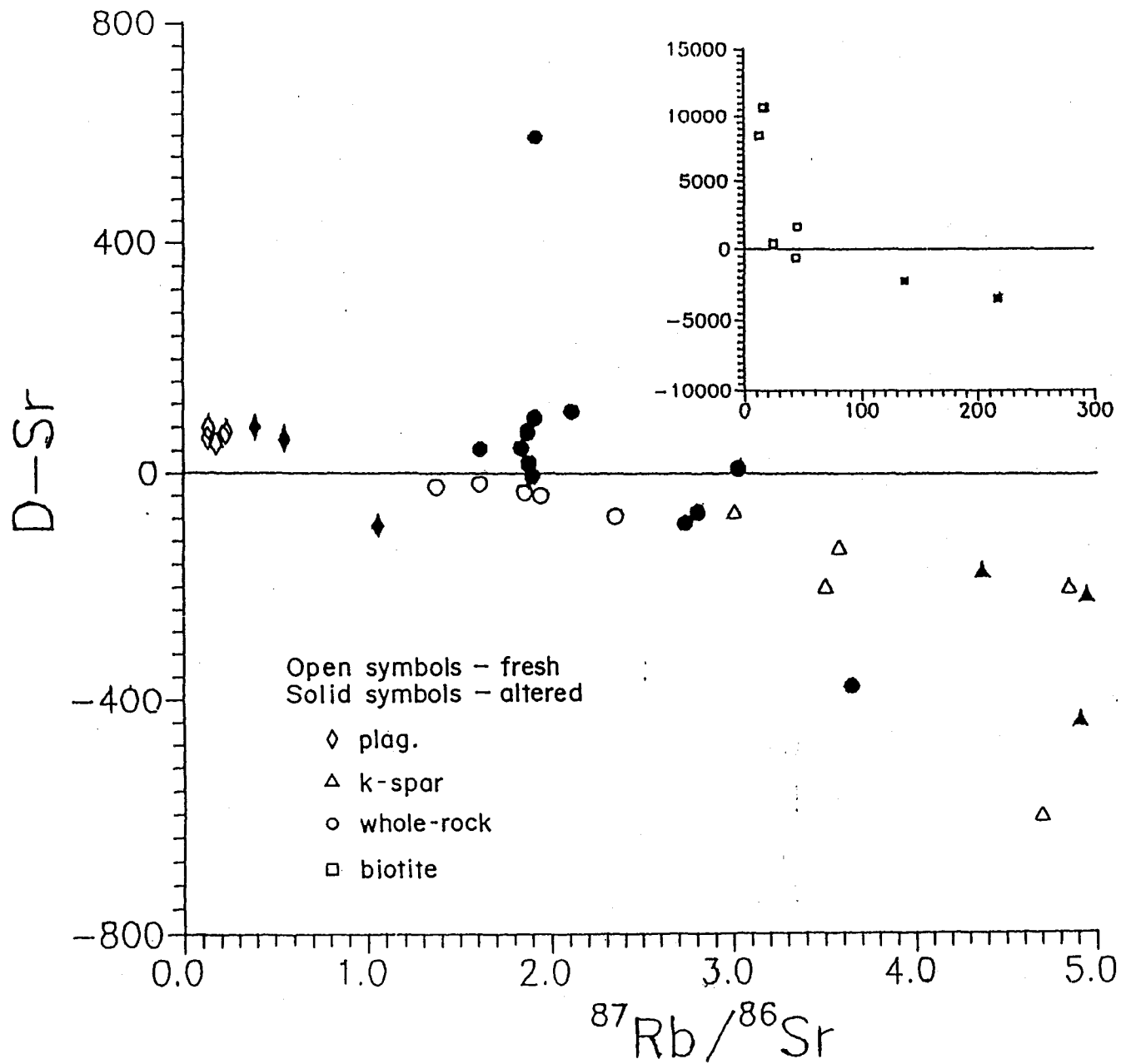
Most data points have negative D-Sr values and plot below the 2600 Ma isochron, the horizontal line with the D-Sr value of zero. The D-Sr values generally decrease with increasing $^{87}Rb/^{86}Sr$ ratios, i.e., the larger the Rb/Sr ratio, the further the data point is away from the 2600 Ma isochron. Biotite separates have the largest absolute D-Sr values, and therefore they are the most vulnerable phase in Rb-Sr geochronology. This is expected since biotite has most radiogenic ^{87}Sr which occupies the unstable sites and is easily subject to loss.

Except for one feldspar separate, P1-KF, all the fresh samples have relatively small variation of D-Sr values. All fresh whole-rock samples have small negative D-Sr values. This is interpreted as Sr (bulk Sr or ^{87}Sr, or a combination of the two) loss from the rocks during high-temperature alteration, and hence indicates an open-system behavior with respect to the whole-rock scale. The potassium feldspar of fresh samples has negative D-Sr values and falls below the isochron, which indicates loss of Sr (more likely with preferential ^{87}Sr loss). In contrast, all the plagioclase has small positive D-Sr values and plots above the isochron. That means plagioclase had gained radiogenic ^{87}Sr. This redistribution of Sr within mineral phases is believed to be the result of fluid-rock interaction during the high-temperature alteration (pink-coloration). Fluids of various

origins, possibly both magmatic fluids due to the cooling of the magma and meteoric water penetrating through fractures, reacted with the rocks and caused redistribution of Sr. Mineral phases like potassium feldspar with high $^{87}Sr/^{86}Sr$ ratios lost some radiogenic Sr and those like plagioclase with low $^{87}Sr/^{86}Sr$ ratios gained some radiogenic Sr. Part of the Sr was lost from the host rock to the fluids.

In contrast to potassium feldspar of the fresh samples, four of the five biotite separates of fresh samples have large positive D-Sr values. This might be result of either loss of Rb or gain of Sr from a more radiogenic sources during the alteration. It is unlikely that biotite will gain radiogenic Sr because it is not a receptor for Sr in addition to its high Rb/Sr ratios. Therefore, Rb probably was lost from biotite during the high-temperature alteration of biotite to chlorite around 2300 Ma ago. This is shown by the low Rb concentrations of some biotites, P1-BI, P2-BI and P3-Bi in Table 5.3. Strontium is expected to be lost as well during alteration but the Sr loss might be less severe than that of Rb, and the overall effect will show Rb loss relative to Sr. However, one biotite separate, JSS1-BI, which shows a negative D-Sr value, indicates more Sr than Rb was lost.

Compared to the fresh samples, altered samples have a

wider D-Sr variation. Potassium feldspars of the altered samples have more negative D-Sr values and indicates further loss of radiogenic Sr during low-temperature alteration. Biotite separates which have the highest Rb concentration os unaltered samples, show very large negative D-Sr values in contrast to those of fresh samples. The negative D-Sr values and high Rb concentrations in addition to the low Sr concentration suggests biotite was subjected to severe loss of Sr and, possibly, some gain of Rb. The lower Sr concentration in plagioclase of the altered samples indicates large quantity of Sr had been lost during the low-temperature water-rock interaction. This Sr loss must have occurred shortly after the high-temperature alteration because of the high $^{87}Sr/^{86}Sr$ ratios which is built up by decay of Rb. Two plagioclase separates which show positive D-Sr values presumably still preserved the high-temperature alteration signature.

In contrast to fresh whole-rock samples, altered whole-rock samples show a wider range and both negative and positive D-Sr values. Generally samples with positive D-Sr have higher Sr concentration than samples with negative D-Sr, and both have similar Rb concentration. This is interpreted to mean that Sr is more mobile than Rb during low-temperature alteration as believed by Nesbitt, 1979. Samples, such as 3D1, 3D4, and 3D5, sub-samples of one large

sample show different D-Sr, indicating they are subjected to various degrees of Sr loss or gain on a local scale. Therefore, both gain and loss of Sr occurred on the whole-rock scale during low-temperature water-rock interaction. What factors control the Sr loss or gain are not identifiable yet. It is most likely the microfractures and secondary minerals played an important role. More altered samples such as HC19, HCO1 and HCO2 show more severe Sr loss. Loss of Sr is most pronounced in plagioclase and biotite, correlating with the petrological observations.

5.2.2. URANIUM-SERIES DISEQUILIBRIUM

Samples analyzed for Sr isotopes in Table 5.3 were also attempted for U-series analysis. However, the attempt was not successful due to the failure in mass spectrometry run. Limited U-series data of whole-rock samples and mineral separates are listed in Table 5.4. Uranium and Th concentrations are variable, especially for mineral separates. Uranium ranges from 1.7 ppm to 5.6 ppm and Th from 13 ppm to 39 ppm in whole-rock samples. Three fresh whole-rock samples, all sampled above 200m, have similar Th/U ratios, averaging 7.7, which is much higher than the crustal average of 4.6 (Allegre et al., 1986) and the worldwide average of 5.1 for granites (Rogers and Adams, 1969). Gascoyne and Cramer (1987) also found high Th/U

Table 5.4   Uranium-series Disequilibrium Analyses of the Rocks And Minerals

Sam.#	A04	2 SIGMA	A48	2 SIGMA	A08	2 SIGMA	U(ppm)	2 SIGMA	Th(ppm)	2 SIGMA	Th/U
FRESH SAMPLE											
P1-WR					1.791	0.043	3.567	0.031	28.39	0.69	7.96
JSS1WR			0.872	0.019			5.448	0.121	39.12	0.42	7.18
JSS2WR			1.169	0.004			3.601	0.009	29.06	0.58	8.07
P3-PL	1.304	0.105	1.029	0.004	1.342	0.108	1.471	0.002	7.21	0.06	4.90
JSS19I			0.873	0.005			19.200	0.042	213.40	2.43	11.73
ALTERED SAMPLE											
HC01WR	1.031	0.015	1.330	0.006	1.372	0.021	5.615	0.025	24.31	0.42	4.33
HC02WR	1.169	0.021	1.058	0.010	1.237	0.025	4.380	0.039	25.45	0.10	5.81
HC19WR	1.107	0.024	0.952	0.004	1.055	0.023	2.620	0.006	19.94	0.13	7.61
301-1	1.298	0.022	0.996	0.004	1.293	0.021	1.771	0.004	13.78	0.10	7.78
301-2	1.911	0.020	0.993	0.004	1.898	0.020	2.734	0.010	12.82	0.94	4.69
301-3			0.927	0.006			1.670	0.010	18.19	0.36	10.89
302							2.081	0.002	23.01	0.22	11.06
303	1.320	0.046	1.194	0.004	1.577	0.055	2.365	0.007	25.74	0.57	10.88
304-2	1.266	0.047	1.041	0.004	1.317	0.049	1.959	0.006	17.92	0.37	9.15
305-1			0.971	0.005			3.595	0.016	25.74	0.20	7.16
HC01PL	0.911	0.014	1.387	0.004	1.263	0.020	2.329	0.002	4.71	0.03	2.02
HC19PL			0.942	0.002			1.139	0.001			
HC02BI	1.134	0.034	1.095	0.002	1.242	0.037	6.873	0.007	27.51	0.25	4.00
HC19BI	1.215	0.016	1.032	0.005	1.253	0.017	11.175	0.051	30.36	0.45	2.72

1. The A04, A48 and A08 are the activity ratios of Th-230/U-234,
   U-234/U-238 and Th-230/U-238 respectively.
2. The Th/U ratio is weight ratio.

ratios in near-surface samples. These high ratios imply significant U lost with respect to Th. The high (^{230}Th/^{234}U) and (^{230}Th/^{238}U) activity ratios suggest that this loss has occurred within the last 10^5 years. One sample JSS1 shows that ^{234}U was preferentially lost to ^{238}U. This ^{234}U loss is likely the result of the α-recoil effect and groundwater leaching in the near-surface environment. Biotite in this sample has an identical (^{234}U/^{238}U) activity ratio to the whole-rock, indicating either U isotopic equilibrium (not secular radioactive equilibrium) is reached within all the constituent mineral phases, or the biotite has controlled the U isotopic composition of the whole rock since biotite has high concentrations of both U and Th. More data from other mineral phases should resolve this problem.

There is only slightly ^{234}U enrichment in the plagioclase of fresh sample P3, but the ^{230}Th is enriched relative to both ^{234}U and ^{238}U. Similar phenomenon was observed by Gascoyne and Cramer (1987) and was interpreted as due to bulk U leaching without U isotope fractionation due to reaction with oxidizing groundwaters near the surface. Their poorer α-counting precision was unable to detect the slight ^{234}U enrichment with respect to ^{238}U.

Significant ^{234}U enrichment relative to ^{238}U was also

seen in JSS2, which was sampled a few meters away from JSS1. This ^{234}U enrichment could either be the result of ^{234}U migration (simple diffusion) from adjacent rocks which show ^{234}U loss (e.g., JSS1) or redeposition of ^{234}U from groundwater in the microfractures since all the water samples have the ($^{234}U/^{238}U$) activity ratios of larger than 2 (see chapter 6).

These data show that U-series disequilibrium is commonly observed in rocks and mineral phases in the near surface environment. Uranium migration has occurred in the last 300,000 years. Despite the ^{234}U enrichment observed in JSS2, high Th/U ratios and ^{230}Th enrichment suggest that U was lost either with or without preferential ^{234}U loss, within the last one million years. This U loss is more likely continuous in the near surface environment as suggested by the work of Gascoyne and Cramer (1987).

Compared to the fresh whole-rock samples, altered whole-rock samples show a wider variation in Th/U ratios, 4.3 to 11. ^{230}Th is found enriched relative to ^{234}U and ^{238}U in all samples except for the plagioclase HC01PL. Both ^{234}U enrichment and deficiency with respect to ^{238}U are observed by Gascoyne and Cramer (1987). However, ($^{234}U/^{238}U$) activity ratios are generally close to unity with the exception of two samples, HC01 and 3D3, having a

ratio equal or above 1.2. The plot of activity ratios versus Th/U ratios (Fig.5.6) suggests a positive correlation (though more data are needed) between the $(^{230}Th/^{234}U)$ activity ratio (with two exceptions, 3D1-2 and HC01WR) and the Th/U ratio, while $(^{234}U/^{238}U)$ ratio stays close to unity (with two exceptions 3D3 and HC01WR). This correlation indicates recent, possibly continuous, bulk U loss with little U isotopic fractionation. The average rate of U loss must be faster than the decay rate of the ^{230}Th otherwise this positive correlation would not be observed.

Preferential ^{234}U loss was observed in more altered samples, such as HC19 and 3D1-3, which also show highly anomalous D-Sr values. Samples, such as HC01 and 3D3, showing $(^{234}U/^{238}U)$ activity ratios above unity indicate gain of ^{234}U. Similar ^{234}U losses and gains were also observed by Gascoyne and Cramer (1987) and interpreted as the result of the local oxidizing/reducing groundwater front control as proposed by Osmond et al., (1983). The increase in Fe^{2+}/Fe^{3+} ratio close to the fractures observed by Gascoyne and Cramer, (1987), and Kamineni et al., (1986), and the high ^{234}U enrichment in groundwaters (chapter 6), suggest that the excess ^{234}U of some samples came from the groundwaters due to the immobility of U in the reducing environment.

Figure 5.6. Plot of the Th/U weight ratio-activity ratio of

the whole rock samples from URL. While the (^{234}U/^{238}U)

activity ratio (circles) scatters closely arrount one,

the (^{230}Th/^{234}U) activity ratio (triangles) increases

with the increasing Th/U ratio (with exception for 3D1-

2).   This relationship indicates the rapid bulk U loss

with little U isotope fractionation.

Activity Ratio vs Th/U Ratio

$\diamond \left({}^{230}Th/{}^{234}U \right)$
$\circ \left({}^{234}U/{}^{238}U \right)$
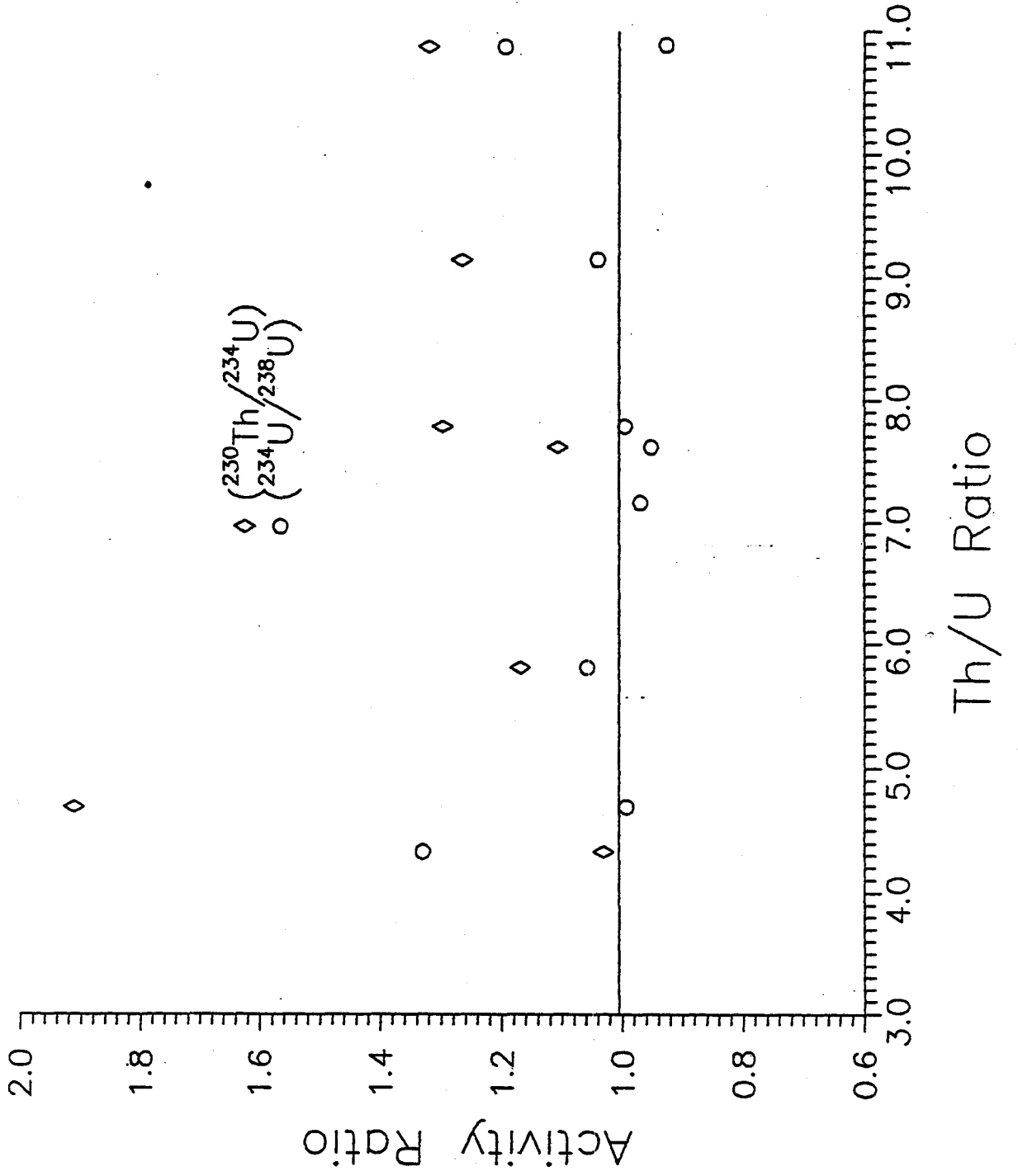
Uranium-series data of mineral phases from three samples show similar $(^{234}U/^{238}U)$ activity ratios among the constituent mineral phases. However two samples, HCO1 and HC19, show that plagioclase phase is further away from unity than its host rocks. This mineral phase is the most altered, and therefore, U migration is more visible in the vulnerable phase. The same conclusion has been drawn from the Sr isotopic study.

CHAPTER SIX

ISOTOPE GEOCHEMISTRY OF THE GROUNDWATERS

6.1 INTRODUCTION

Groundwaters occur in various types of crystalline rocks in the world. Brines with salinities of up to 550 g/L have been found in mines and drillholes in the Precambrian platform of the Canadian Shield and the U.S.S.R., up to the depth of 10 km below the surface. Study of groundwaters, especially those concentrated deep brines, has focussed on their origins and evolution. The occurrence and geochemistry of the groundwaters have been recently summarized by Fritz and Frape (1982), Frape et al., (1984), and Frape and Fritz (1987).

Based on the Total Dissolved Solids (TDS), groundwaters are divided into four groups (Table 6.1). The chemistry of the groundwaters varies with the depth at which the waters occur. TDS, density, and contents of Cl, Ca, and several other elements generally increase with the depth (Frape and Fritz, 1987). Fresh and brackish groundwaters are often found in active hydrological faults and joint systems in crystalline rocks above approximately 650 m below the surface, hence are called shallow waters (Frape et al., 1984). These faults and joints are normally highly

Table 6.1.   Chemical Classification of Groundwaters

	TDS (mg/L)
Fresh Water	<1,000
Brackish Water	1,000-10,000
Saline Water	10,000-100,000
Brines	>100,000

----

interconnected and therefore, considerable amount of fresh meteoric water is involved in the flow system. The chemistry of these groundwaters is variable and is often dominated by Na-Ca-HCO$_3$ or Ca-Na-HCO$_3$, with or without significant amounts of Mg and SO$_4$ depending on the chemistry of the local host rocks. The clear relationship between the waters and their host rocks indicates that the chemistry of the shallow groundwaters is controlled by a dissolution-dominant process of vulnerable silicate minerals.

In contrast, very saline waters and brines occur within major more or less isolated faults and shear zones at the depth below 650 m, hence they are called deep waters (Frape et al., 1984). They are characterized by uniform chemistry despite their variable occurrences. They have salinity up to 350 g/L and are dominated by Ca-Na-Cl and are, more or less, independent of the host rocks. Calcium, Na and Cl are found to increase with depth and eventually account for over 90% of the salinity. Bicarbonate is present in negligible amount, especially at depth.

The origin of these groundwaters, especially the deep saline waters and brines in crystalline rocks is still unclear. Results of the current geochemical studies lead to the conclusion that the origin of these groundwaters is very complicated. Possible precursors include meteoric

(including glacial) water, seawater or evaporative dissolution, hydrothermal water and sedimentary basin water. However, the water component and the saline component of these groundwaters may not have the same origin since their original chemical and isotope signatures are believed to have been significantly modified by various geological processes. Mixing between the deep and shallow groundwaters is widely recognized in all the locations in the Canadian shield.

6.2. ORIGIN OF THE WATER COMPONENT

Stable isotopic results have provided some clues to the origin of the groundwaters. Oxygen and hydrogen isotopes of the shallow groundwaters reflect local climatic regimes and plot on local Meteoric Water lines which are usually very close to the Global Meteoric Waterline (GMWL). Deviation below the GMWL is sometimes observed and is partly attributed to the involvement of the evaporated surface water (Fig. 6.1). High tritium concentration, normally more than 60 TU, is found in these shallow groundwaters (Frape et al., 1984; Frape and Fritz, 1987). The meteoric stable isotopic signature and high tritium concentration indicate that the shallow groundwaters are of local surface water origin. The isotopic shifts from the GMWL are likely due to some low-temperature interactions with local rocks in

Figure 6.1.   Stable isotope variations of groundwaters from
        four mines on the Canadian shield.   The local dilute
        groundwaters from each site are plotted on the Global
        Meteoric Water   Line (GMWL) while the deep saline
        groundwaters plotted above the GMWL.   Mixing trend
        between the local dilute waters and the more saline deep
        waters is observed at each site.   The extrapolated
        mixing lines from each mine site converge above the GMWL
        in the shaded area with $\delta^{18}O$ values between -10 and -7‰
        and δD between -20 and 0‰.   This convergence area is
        the locus of the highest salinities and is believed to
        represent the common source brine in the Canadian Shield
        (modified from Frape and Fritz, 1987).
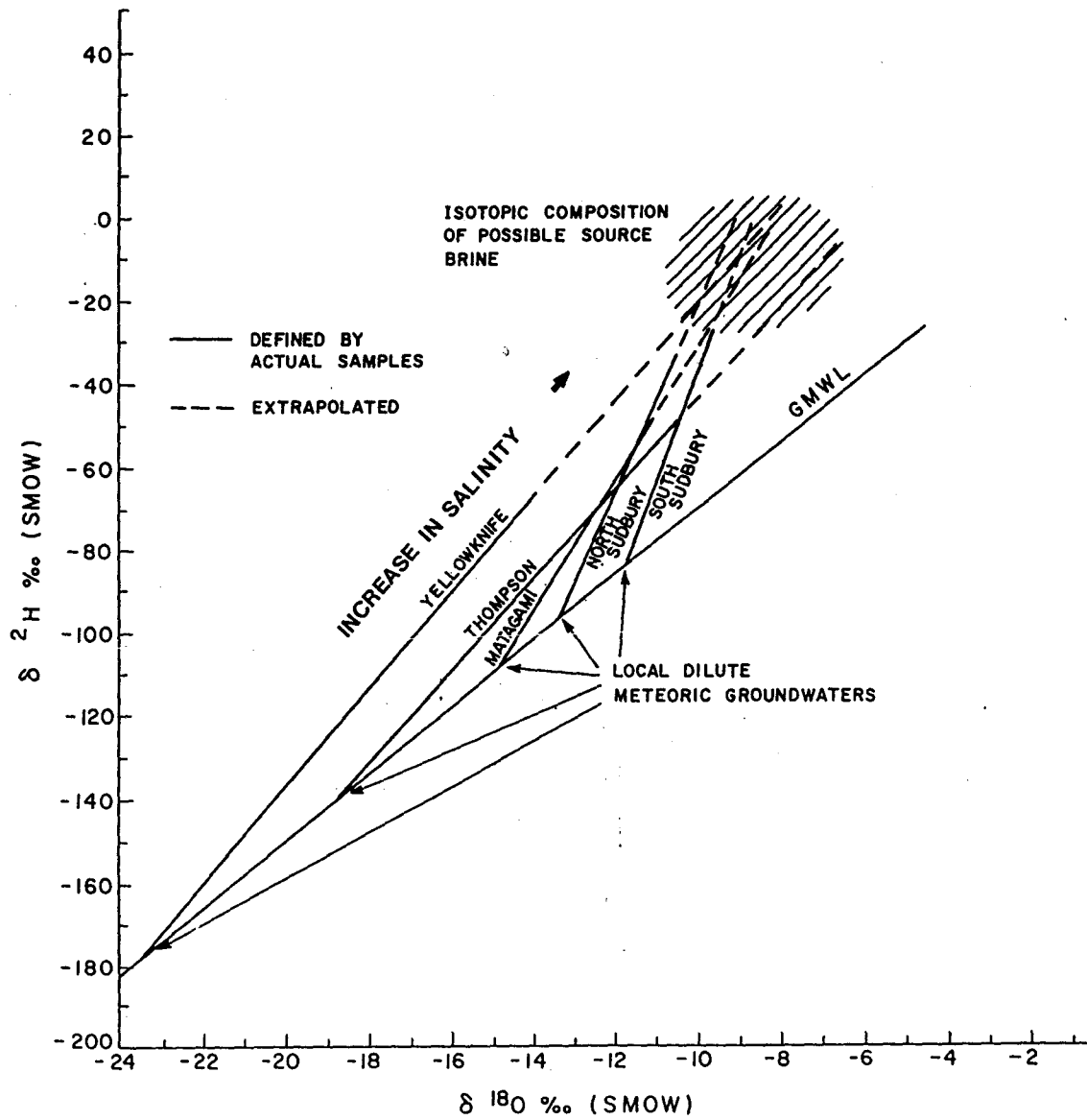
addition to evaporation.

In contrast, deep saline groundwaters and brines in crystalline rocks are enriched in deuterium and plotted above the GMWL (Fig.6.1). Deep groundwaters in various types of crystalline rocks from each of four different sites in the Canadian shield, Yellowknife, Thompson, Sudbury and Matagami, lay on a mixing line in a $\delta D - \delta^{18}O$ diagram between its local meteoric water and a more concentrated water with more enriched deuterium and ^{18}O (Fritz and Frape, 1982; Frape et al., 1984; Frape and Fritz, 1987). Increase in salinity is normally accompanied by decreases in tritium concentration. The most concentrated deep brines from these four sites have almost identical stable isotopic compositions. Extrapolated towards increasing salinities, the mixing lines from these four sites converge in an area with $\delta^{18}O$ values between −10 and −7‰, and δD between −20 and 0‰. This convergence area is the locus of the highest salinities and is believed to represent the possible common source brine in the Canadian shield, which is the end product of a long process of water/rock interaction in crystalline rocks.

However, the origin of the water component of such common source brine is still uncertain. The unusual isotopic composition is quite distinct from fluids from deep

sedimentary basins or hydrothermal systems, which are generally depleted, rather than enriched, in deuterium with respect to GMWL. Fritz and Frape (1982) attributed the deuterium enrichment to low-temperature water-rock interaction, specifically, the formation of clay minerals. The precursor or precursors of this common source brine are believed to have undergone intensive interaction with the rocks and do not preserve any of their original chemical and isotopic signatures. Therefore, the unique isotopic composition might reflect a state of equilibrium of low-temperature water-rock interaction in a closed system at uniform thermodynamic condition (Fritz and Frape, 1982).

6.3. MIXING OF THE GROUNDWATERS INDICATED BY THE CHEMISTRY

Study of the solute components is helpful in assessing the degree of water-rock interaction and identifying mixing processes and the specific sources in the host rocks of the solute components.

Different chemical characteristics of the shallow and deep groundwaters have been revealed by the accumulated data (Frape et al.,1984; Frape and Fritz, 1987). As indicated by the stable isotopes, mixing between shallow and deep groundwaters is widely recognized by the geochemical studies. Linear correlations between the anions and

cations, Cl, Ca, Na, Sr, and TDS are interpreted as mixing of different waters (Frape and Fritz, 1987). Strontium isotope studies on the groundwaters from Atikokan (Franklyn, 1988) also indicated mixing between deep and shallow waters.

6.4. GEOCHEMISTRY OF THE GROUNDWATERS FROM URL
6.4.1. CHEMISTRY OF THE GROUNDWATERS

Groundwaters from URL site were sampled from various depth interval of the drillholes. The locations of these drillholes are shown in Fig.6.2. Hydrological studies have shown that groundwaters are controlled by the three subhorizontal fracture zones (FZ) (Fig.5.2 and 6.3). All the water samples are analyzed for Sr concentrations and Sr isotopic ratios. Oxygen isotopic compositions and U activity ratios are determined for selected samples. Results are listed in Table 6.2 and summarized in Table 6.3.

Waters from each of the three fracture zones have distinct chemical composition (Gascoyne et al., 1987). Variations in chemical compositions is shown in Fig.6.3 and Table 6.3. The shallow groundwaters (IV) (Roman numbers refer to the types of groundwaters in Fig. 6.3), from FZ-3, are generally fresh Ca-HCO$_3$ waters with TDS less than 350 mg/L. Waters (III-3) from FZ-2, which is hydrologically connected to the surface by vertical fractures, are

Figure 6.2.   Map showing the locations of the boreholes from
that the groundwaters studied were sampled.

U.T.M. NORTH

● M-13

● M-10

● M-14

M-4A URL-10
M-4B

URL-6 ■ SHAFT   ■ URL-12

M-2A ●   ● M-8
M-2B

5571300

5570900

5570500

NORTHING U.T.M. (metres)

5570100

5569700

5569300

5568900

● M-7

■ URL-4

● M-6

■ URL-SERIES HOLES

● M-SERIES HOLES

294000   294400   294800   295200   295600   296000   296400
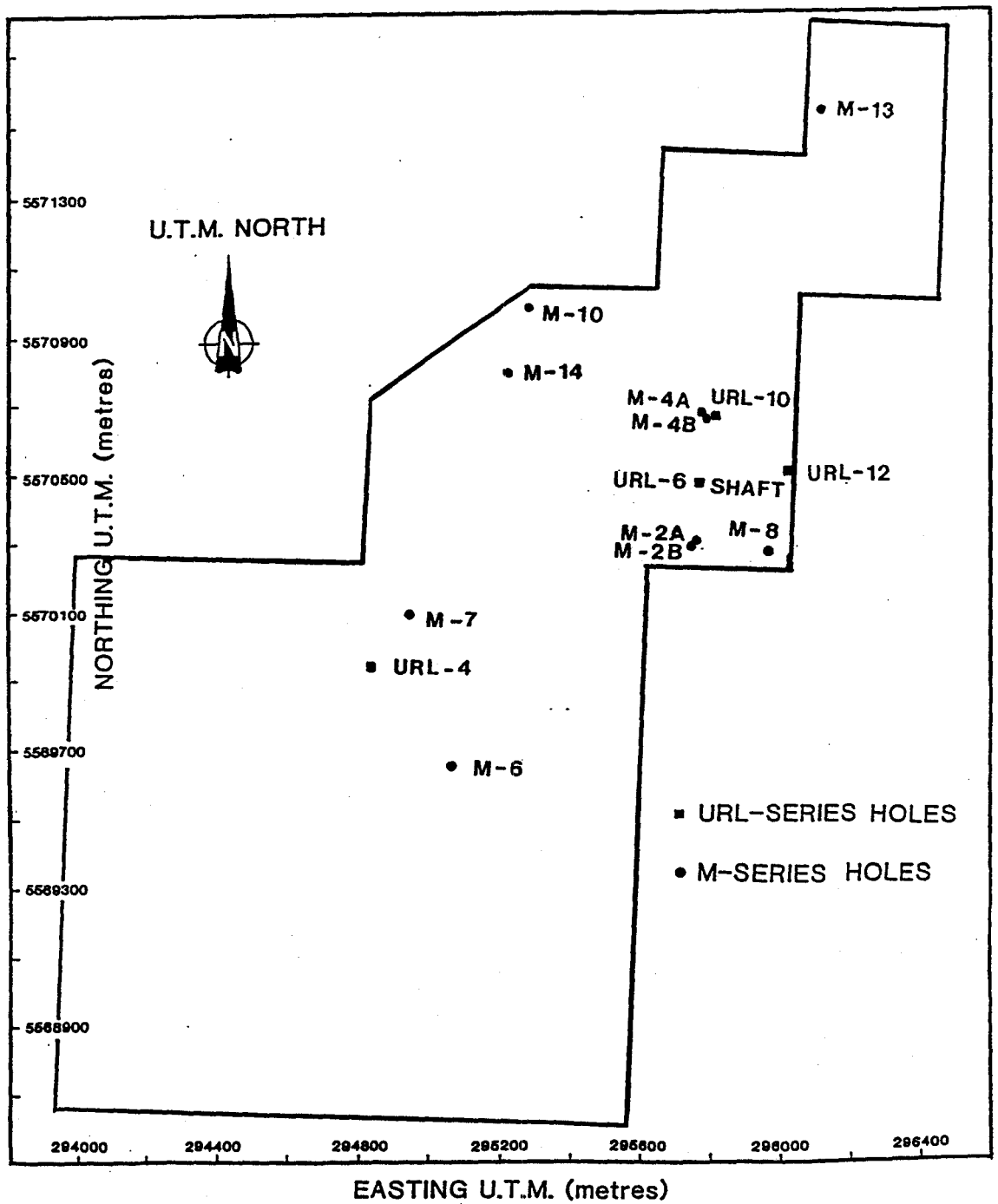
EASTING U.T.M. (metres)

Table 6.2. Isotopic Ratios and Sr Concentrations of the Groundwaters

SAMPLE	DEPTH (m)	MEAN DEPTH (m)	87/86Sr	2StdError (E-6)	O-18	Sr (ug/g)	A48	2 Sigma
FZ-3								
URL4-5-6	53-73	63	0.719339	12	-12.853	0.245	2.644	0.007
URL4-5-8	53-73	63	0.718963	14	-12.783	0.244		
URL4-5-10	53-73	63	0.718965	14	-13.326	0.248	2.707	0.006
URL10-3-2	54-121	88	0.714714	12	-13.684	0.232	2.839	0.010
H6-2-4		122	0.717611	11		0.223		
H6-2-5	81-163	122	0.717348	12	-13.148	0.202	5.617	0.012
FZ-2								
H2B-2-1	130-160	145	0.722530	13 11	-14.711	0.129	4.236	0.015
209-010-OC1	250	250	0.720737	11		0.528		
209-OC1-2	250	250	0.721098	11	-16.912	1.03	5.756	0.017
209-OC1-3	250	250	0.721075	12		1.04	6.072	0.010
209-OC1-4	250	250	0.721096	14	-17.013	1.04	5.750	0.015
URL6-SW9	255-275	265	0.722564	13	-16.035	0.216	5.605	0.028
206-007-HC7	253-282	268	0.721348	12		0.165		
201-010-HC7	253-282	268	0.721501	12	-16.519	0.182	7.730	0.017
URL10-6-5	270-302	286	0.720465	11	-15.386	0.454	4.402	0.012
URL10-6-6	270-302	286	0.720456	12	-15.472	0.442		
URL10-6-7	270-302	286	0.720475	11	-15.829	0.440	4.486	0.017
WN8-4	305-325	315	0.723861	11	-15.754	0.219	4.498	0.019
WN8-6	305-325	315	0.723940	11		0.268		
WN8-7	305-325	315	0.724030	8		0.301		
WN8-9	305-325	315	0.723791	23		0.289		
H13-2-4	226-443	335	0.720712	12	-19.755	2.25	3.723	0.016
H13-2-5	226-443	335	0.720646	14	-19.194	2.24		
H2A-3-2	270-400	335	0.720494	11	-12.999	0.172	6.736	0.020
H2A-3-4	351-400	375	0.720349	12	-13.053	0.159		
H4A-4-4	291-406	350	0.726070	13	-17.990	1.41		
H4A-4-6	291-406	350	0.726088	13	-18.059	1.42		
H8-3-4	340-380	360	0.724957	13		0.168		
H8-3-7	340-380	360	0.723907	17	-13.778	0.147	4.108	0.013
URL12-11-7	458-501.5	480	0.729610	13	-12.883	0.323	3.515	0.006
URL12-11-8	458-501.5	480	0.729167	13	-12.728	0.305		
URL12-11-13	458-501.5	480	0.728728	14	-12.766	0.282	3.611	0.010

Table 6.2. Isotopic Ratios and Sr Concentrations of the Groundwaters (continued)

| SAMPLE	DEPTH (m)	MEAN DEPTH (m)	87/86Sr	2StdError (E-6)	O-18	Sr (ug/g)	A48	2 Sigma
FZ-1								
M14-4-1	300-380	340	0.730556	14	-16.693	20.77		
M14-4-4	300-380	340	0.730476	13	-16.739	20.52	5.463	0.040
M7-4-4	351-400	375	0.736298	11		30.56	3.850	0.010
M7-4-6	351-400	375	0.736248	16		31.67		
M7-4-9	351-400	375	0.736320	13	-15.077	28.78		
M7-4-9	351-400	375	0.736375	14	-14.970	29.59	4.005	0.014
M7-4-9	351-400	375	0.736306	11		30.60		
M7-4-9	351-400	375	0.736264	13	-15.126	30.56	3.997	0.024
M7-4-11	351-400	375	0.736259	13	-15.037	30.79		
M7-SW28	385-398	392	0.735193	11	-13.299	0.761	2.651	0.01
M10-3-1	341-450	395	0.730126	13	-17.524	9.95	4.653	0.015
M10-3-2	341-450	395	0.730198	11	-17.472	11.13	4.240	0.013
M10-3-3	341-450	395	0.730205	11	-17.111	11.63		
URL12-7-8	637-699	668	0.737797	11	-13.929	7.18	2.847	0.011
URL12-7-10	637-699	668	0.737729	11	-14.477	8.47		
URL12-7-18	637-699	668	0.737670	10	-14.734	9.10	2.856	0.008
URL12-7-21	637-699	668	0.737767	14	-14.758	9.22		
WN11-19-15c			0.729155	11		22.98	3.665	0.036

1. The 87/86Sr is the Sr-87/Sr-86 isotopic ratio. O-18 is the delta oxygen-18 value in permil in respect to SMOW. A48 is the activity ratio of U-234/U-238.

Table 6.3. Representative Chemical and Isotopic Data of the Groundwaters

SAMPLE	DEPTH (m)	MEAN DEPTH (m)	Ca (mg/L)	Cl (mg/L)	HCO3 (mg/L)	SO4 (mg/L)	TDS (mg/L)	Sr (ug/g)	87/86Sr	O-18	A48	U (ng/g)
FZ-3												
URL4-5	53-73	63	32	1.6	208.0	0.0	295	0.245	0.71909	-12.99	2.681	31
URL10-3	54-121	88	35	1.2	170.3	12.5	274	0.232	0.71471	-13.68	2.839	75
M6-2	81-163	122	19.4	1.4	228.9	10.5	322	0.202	0.71748	-13.15	5.617	39
FZ-2												
M2B-1	130-160	145	39	5.4	204.0	10.0	309	0.129	0.72253	-14.71	4.236	37
209-010	250	250						0.528	0.72074			
209-oc1	250	250	75	374.4	113.0	248.0	1152	1.030	0.72109	-16.91	5.753	5
URL6-SW9	255-275	265	22	428.9	136.0	18.0	1111	0.216	0.72256	-16.04	5.605	23
206-HC7	253-282	268		427.9	155.5	112.4		0.178	0.72143	-16.52	7.730	17
URL10-6	270-302	286	35	163.5	163.0	106.0	654	0.445	0.72047	-15.56	4.444	19
WN-8	305-328	315	20	280.9	211.3	54.4	800	0.269	0.72391	-15.75	4.498	19
M2A-3	270-400	335	19	19.2	222.6	9.0	375	0.166	0.72042	-13.00	6.736	16
M13-2	226-443	335	185	1198.6	32.2	748.0	3000	2.250	0.72070	-19.50	3.723	7
M4A-4	291-406	350	121	641.0	74.0	354.0	1641	1.415	0.72608	-18.02		
M8-3	340-380	360	14	52.4	207.8	13.0	328	0.158	0.72442	-13.78	4.108	57
URL12-11	458-502	480	37	125.0	123.4	67.0	407	0.303	0.72917	-12.73	3.583	96
FZ-1												
M14-4	300-380	340	2600	5598.0	16.9	950.0	11030	20.650	0.73052	-16.71	5.463	1
M7-4	351-400	375	3700	8522.0	16.9	710.0	15390	30.356	0.73630	-15.06	4.001	2
M7-SW28	385-398	392						0.761	0.73519	-13.30	2.651	6
M10-3	341-450	395	1180	2909.0	33.3	690.0	6010	10.903	0.73018	-17.52	4.240	18
URL12-7	637-699	668	1040	2400.0	40.5	905.0	5032	8.492	0.73774	-14.56	2.852	13
WN11-19								22.980	0.72916		3.665	3

1. Ca, Cl, HCO3, and SO4 data are from AECL of Pinava.
2. Symbols are the same as Table 6.2.
3. Sr concentrations and ratios, A48 and oxygen isotope ratios
   are the means of several measurements.

Figure 6.3.   A schematic cross-section diagram showing the groundwater flow paths and geochemical patterns in the fracture zones indicated by the numbers in the circles. Roman numbers denote the types of groundwaters (modified from Davison, 1984).
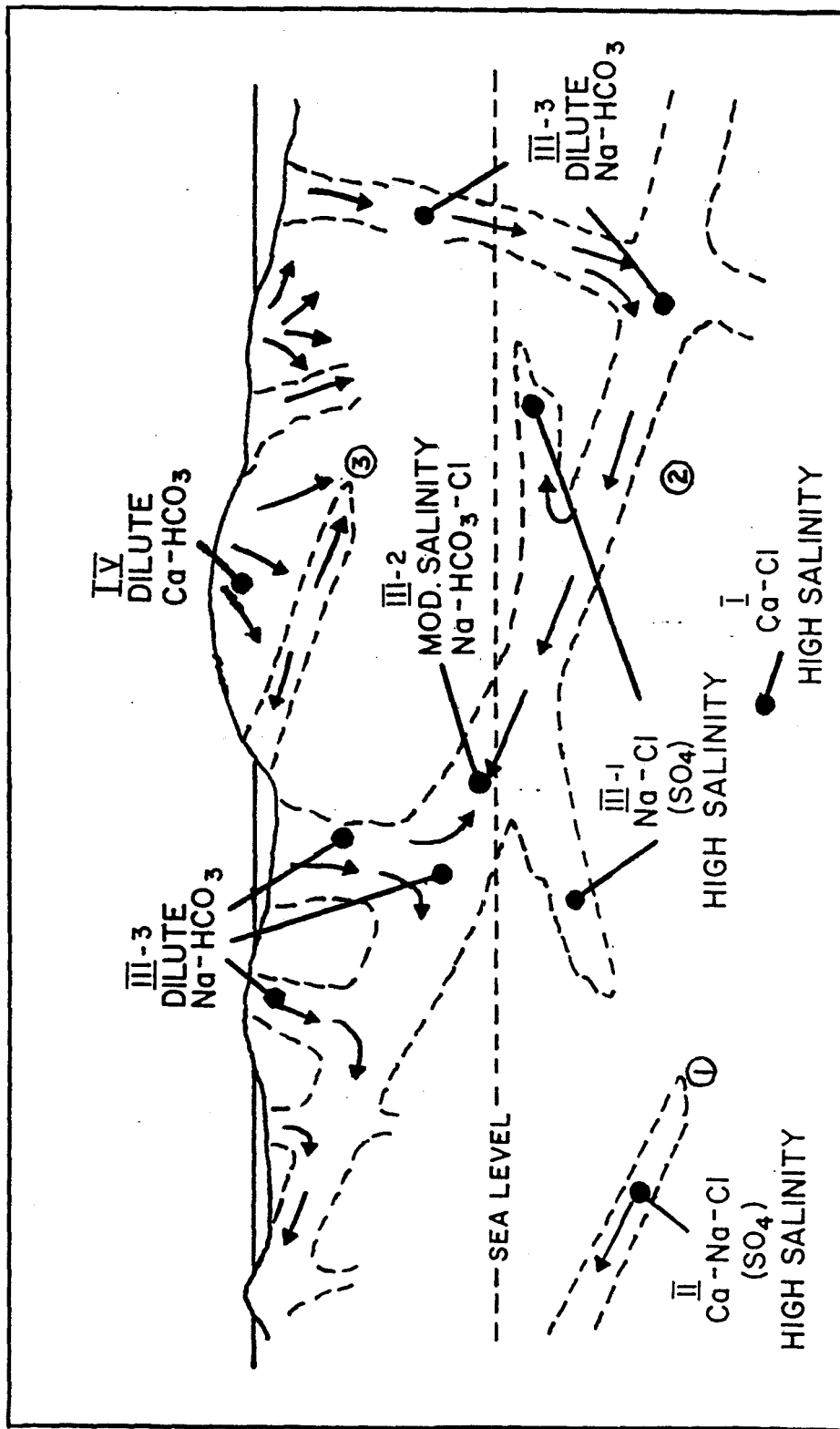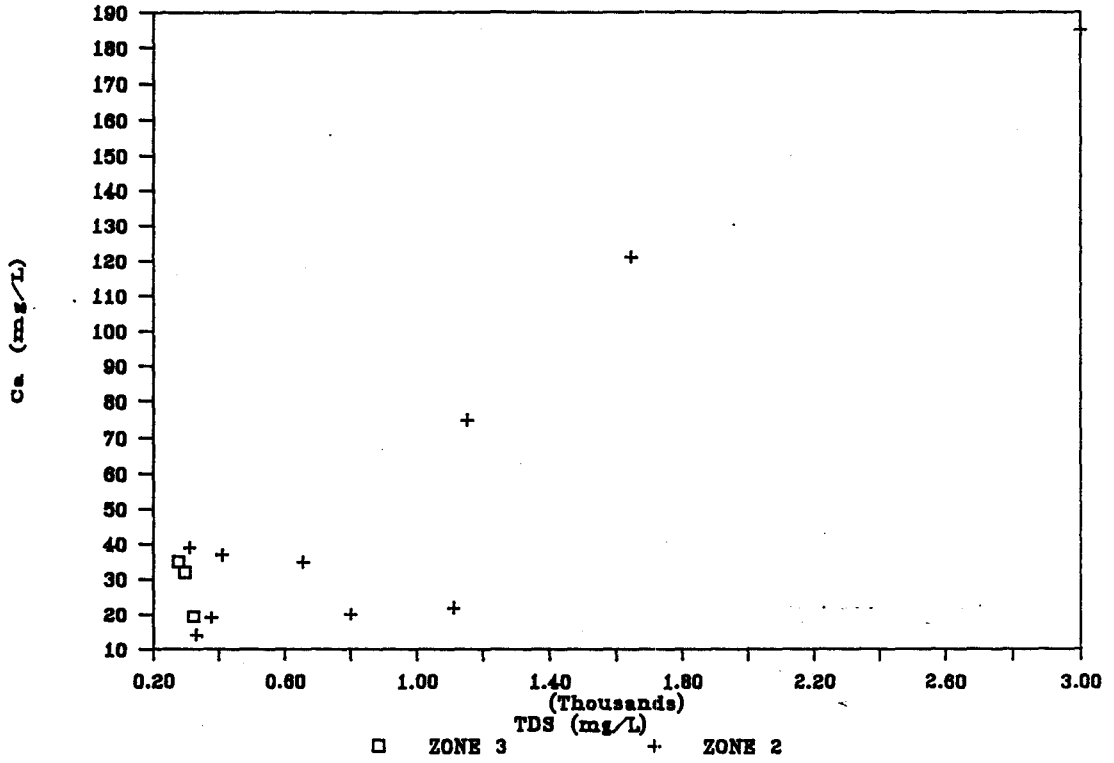
generally similar to those from FZ-3. In contrast, waters (III-1) from FZ-2 which is hydrologically relatively isolated and more saline with a TDS between 300 and 3000 mg/L. They are generally Na-Cl waters with significant amount of SO_4. With increasing depth, waters (II) from FZ-1 have very high salinities, above 5000 mg/L, and are Ca-Na-Cl dominant waters. Sulphate concentrations increase sharply relative to the dilute waters from FZ-2 and FZ-3. With further increasing depth, groundwaters (I) are simply Ca-Cl dominant with even high salinity. Evolution of the groundwater chemistry with depth towards Ca enrichment relative to Na in granite rocks is expected. Albitization of plagioclase and alteration of hornblende in contact with Na-rich groundwaters will occur and release significant amount of Ca accompanying the Na uptake as demonstrated by Franklyn (1988).

The relationships between Ca, Sr, HCO_3, SO_4 with Cl and TDS are found in shield groundwaters, indicating mixing between the waters (Fig.6.4). These correlations are stronger for the waters from FZ-1, which have higher salinities, than waters from FZ-2 and FZ-3. A change in the slope of these correlation lines is observed, especially in the cases of HCO_3 and SO_4 (Fig.6.4D and 6.4E). Waters from FZ-3 and FZ-2 lie on a correlation line with a larger scatter than the waters from FZ-3. This change in the

Figure 6.4.   TDS and element variation diagrams showing
    mixing of groundwaters from the three fracture zones. A
    change in the slopes of the mixing lines of groundwaters
    between FZ-3 and FZ-2, and FZ-2 and FZ-1 is observed,
    especially in D, E and F. Little mixing of groundwaters
    is seen between FZ-3 and FZ-1. A) Ca versus TDS, B) Ca
    versus Cl, C) Sr versus Cl, D) SO_4 versus Cl, E) HCO_3
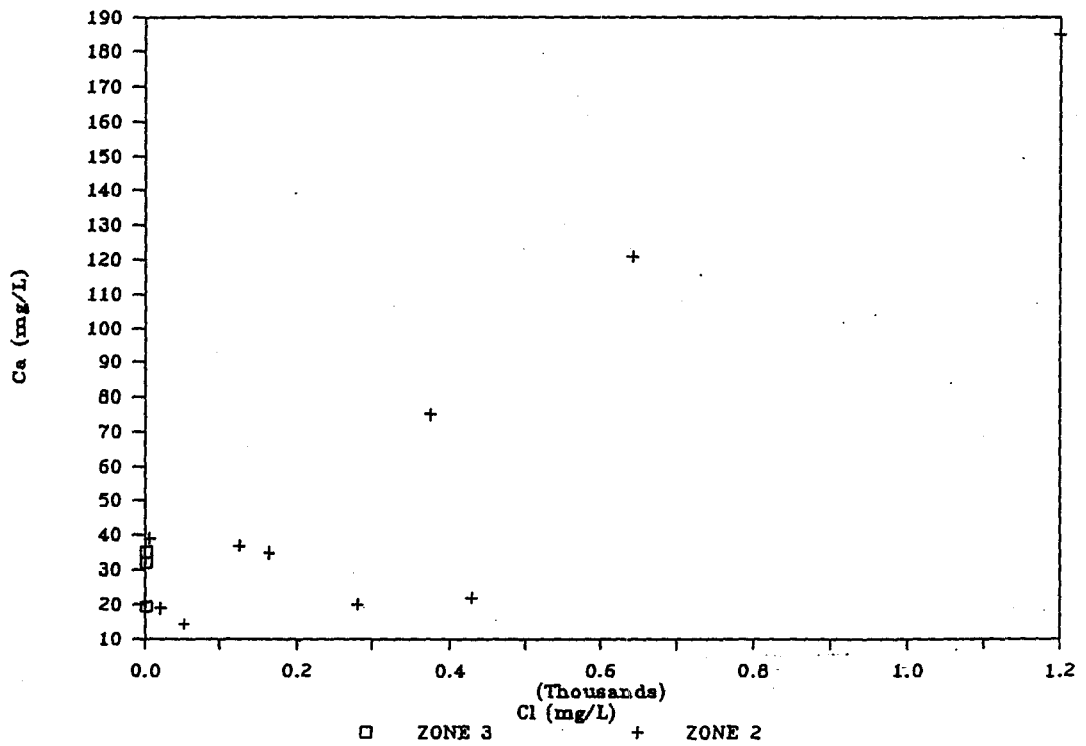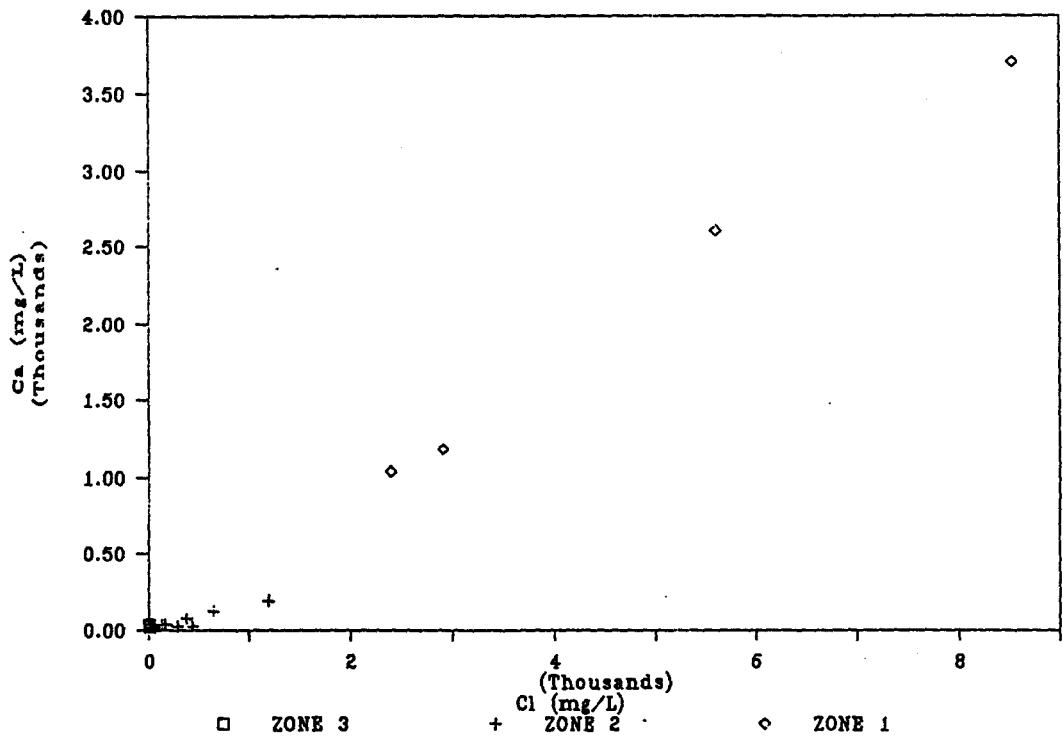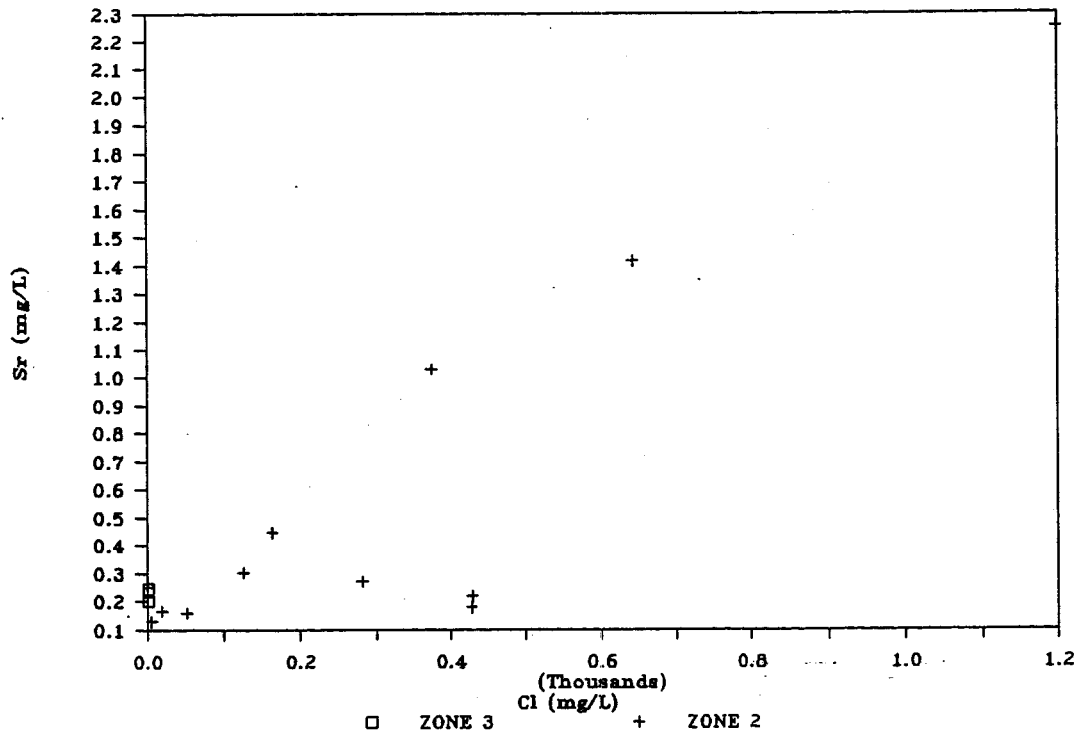   versus Cl, and F) HCO_3 versus Ca.

A

Ca VS TDS

Ca (mg/L) vs TDS (mg/L) (Thousands). ZONE 3 (□), ZONE 2 (+)

Ca VS TDS

Ca (mg/L) (Thousands) vs TDS (mg/L) (Thousands). ZONE 3 (□), ZONE 2 (+), ZONE 1 (◇)

B

Ca VS Cl

Ca (mg/L)

(Thousands)
Cl (mg/L)

□   ZONE 3   +   ZONE 2

Ca VS Cl

Ca (mg/L)
(Thousands)

(Thousands)
Cl (mg/L)

□   ZONE 3   +   ZONE 2   ◇   ZONE 1

C

Sr VS Cl

Sr (mg/L) vs Cl (mg/L) (Thousands)

□ ZONE 3   + ZONE 2

Sr VS Cl

Sr (mg/L) vs Cl (mg/L) (Thousands)

□ ZONE 3   + ZONE 2   ◇ ZONE 1
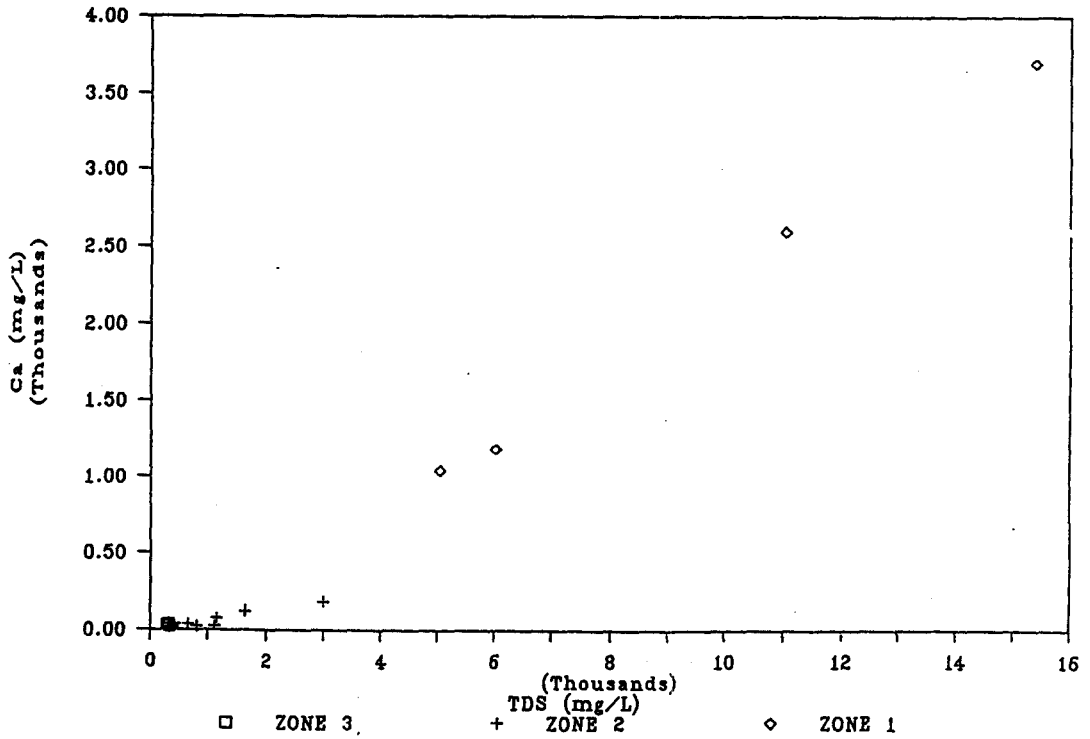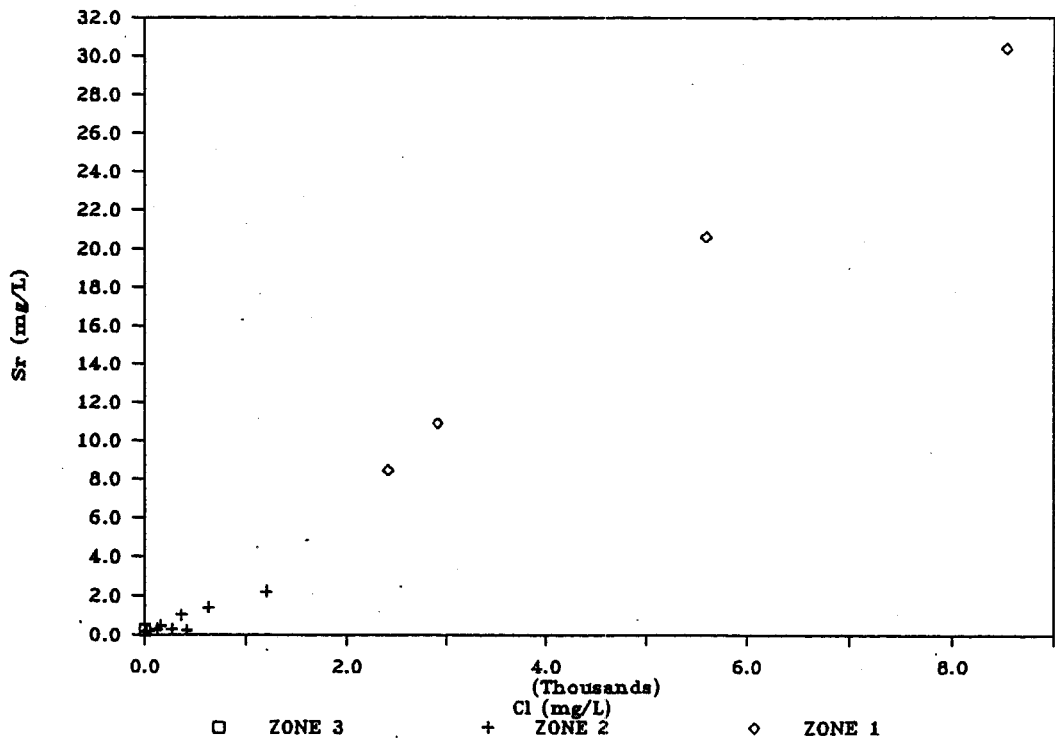
D

SO4 VS Cl

SO4 VS Cl

E

HCO3   VS   Cl

ZONE 3   +   ZONE 2

HCO3   VS   Cl

ZONE 3   +   ZONE 2   ◇   ZONE 1

F

HCO3 VS Ca

HCO3 (mg/L)

Ca (mg/L)

☐ ZONE 3   +   ZONE 2

HCO3 VS Ca

HCO3 (mg/L)

(Thousands)
Ca (mg/L)

☐ ZONE 3   +   ZONE 2   ◇   ZONE 1
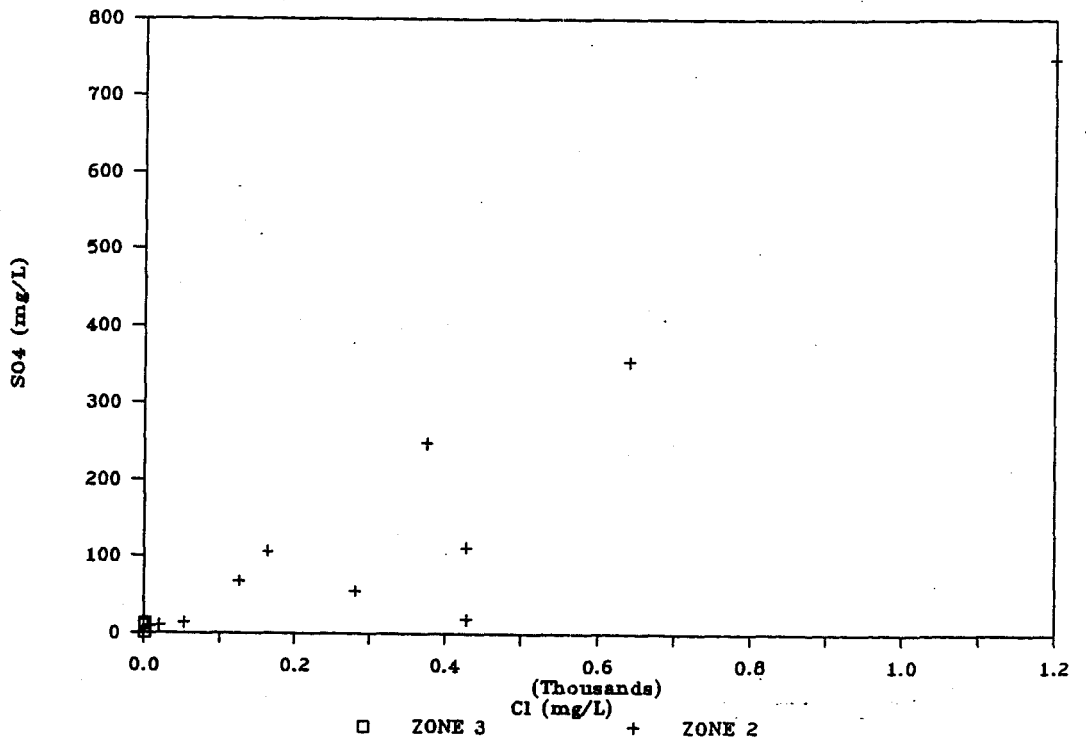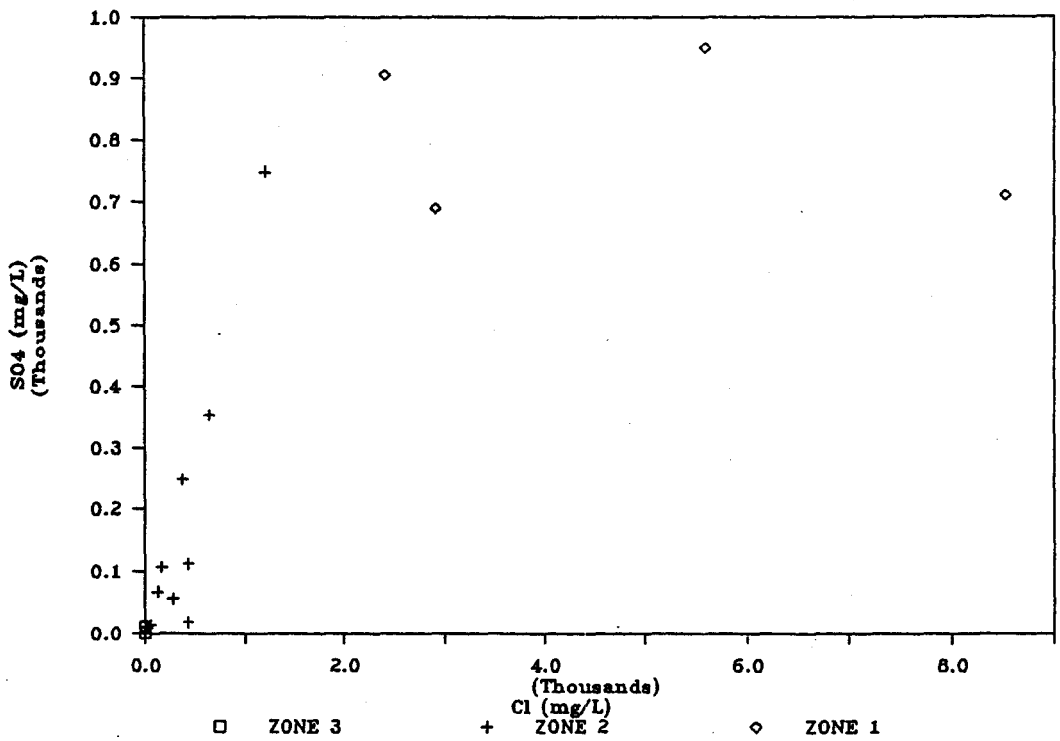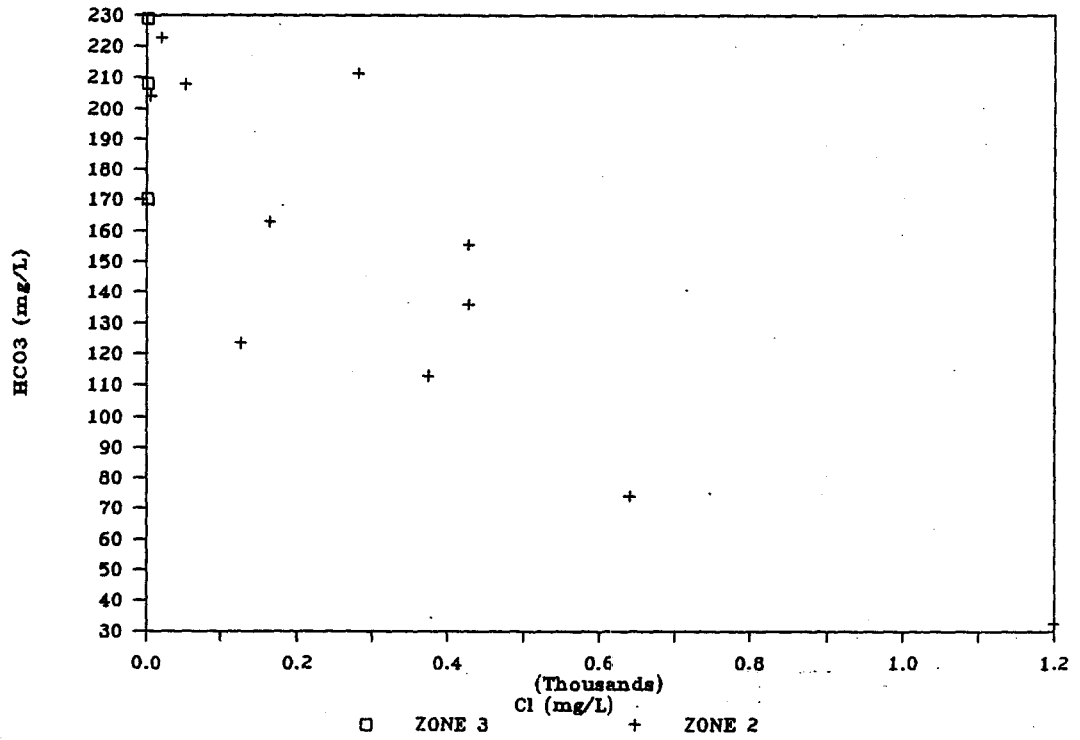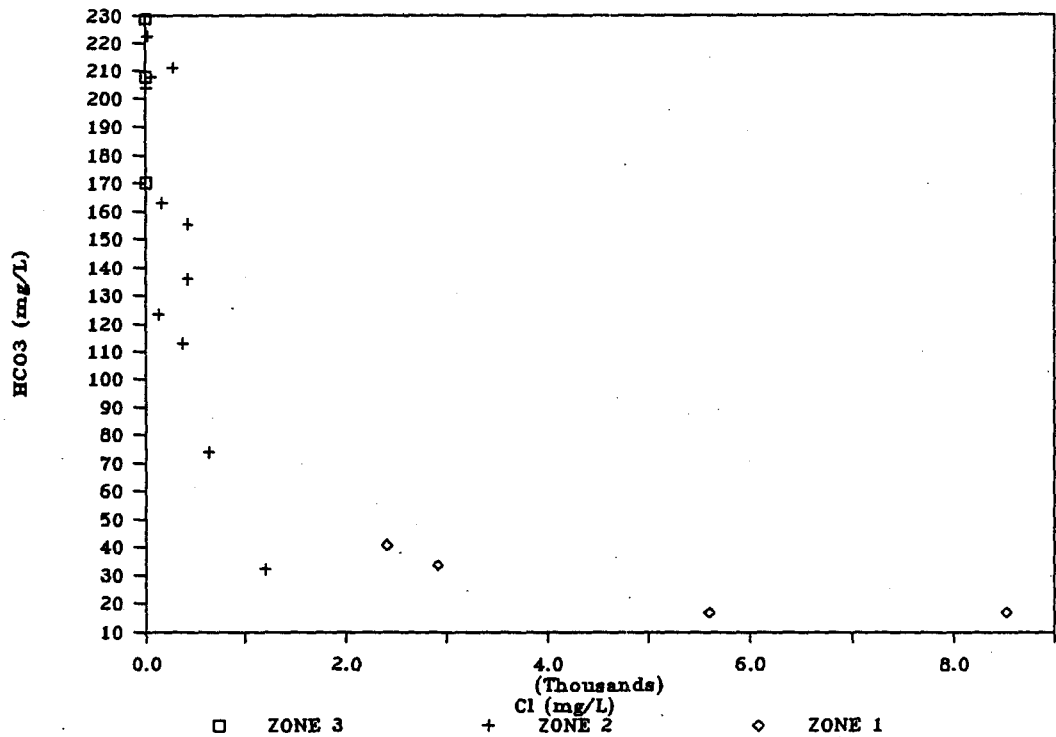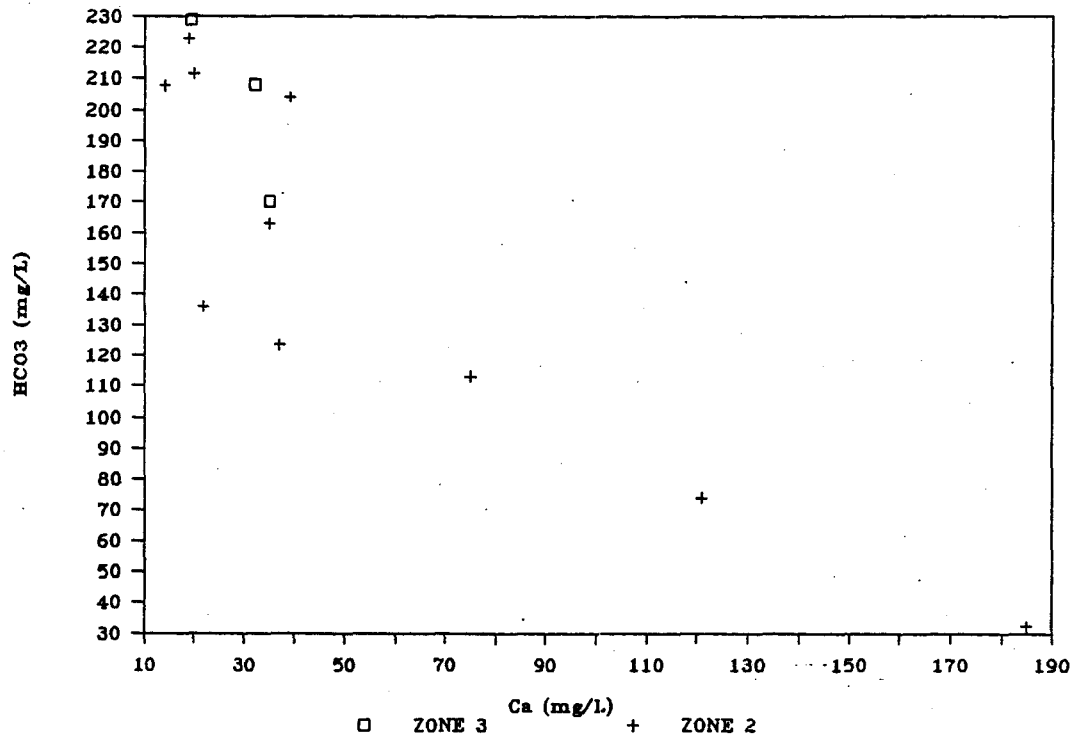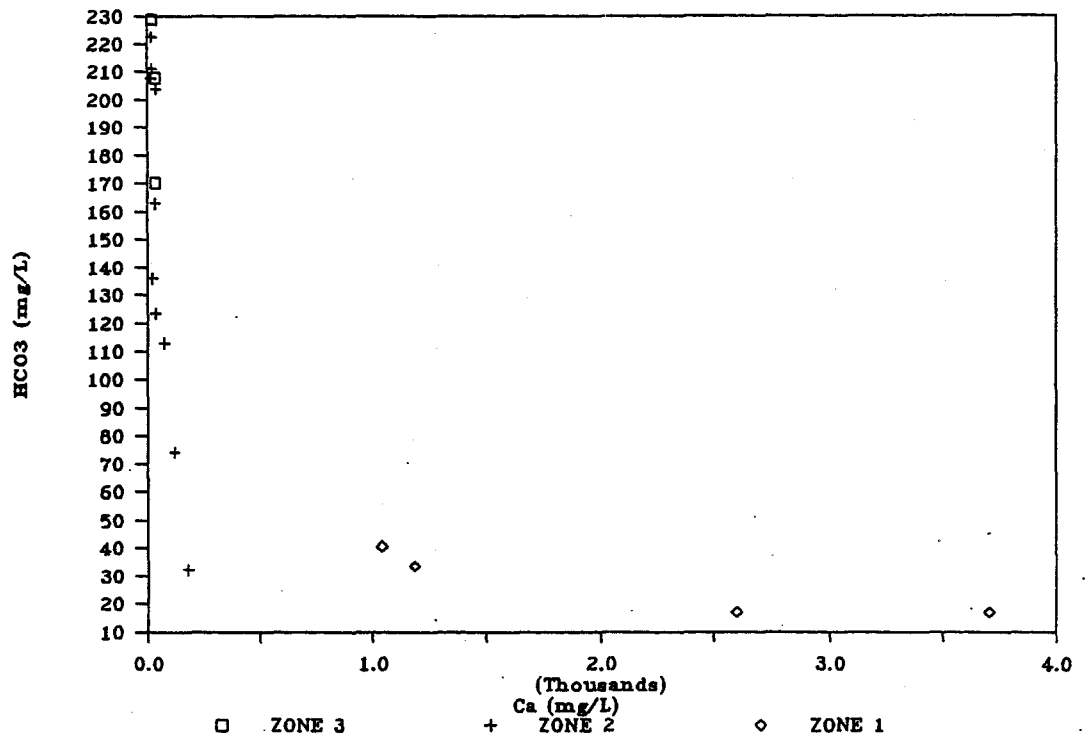
slope of the correlation lines indicates a change in the mixing patterns. Gascoyne et al., 1987, suggested that the relative scattering trend found in lower salinity waters between 0 and 300-400m depth represent an advective-dominant mixing between waters in hydrologically active regimes, while the tight trend found in higher salinity waters below 300m depth represent a diffusion-dominant mixing between shallower, less saline waters and deep, more saline waters or brines. Therefore the correlations between TDS, Ca, Sr, HCO_3 and SO_4 reflect mixing processes between waters from FZ-3 and FZ-2, and between waters from FZ-2 and FZ-1. Mixing of waters between FZ-1 and FZ-3 is not significant as seen on the above correlation diagrams. This conclusion is also supported by the higher permeability of the shallow rocks (Davison, 1984) and more abundant vertical fractures connecting FZ-2 and FZ-3 in the near surface zones (Fig.5.2 and Fig. 6.3).

6.4.2. OXYGEN ISOTOPES

Groundwaters from each of these three fracture zones show discrete oxygen isotopic signatures (Table 6.2 and 6.3). The $\delta^{18}O$ values of groundwaters from FZ-3 have a narrow range of -13 to - 14‰ and are similar to the local present-day precipitation and the surface waters that have a $\delta^{18}O$ value of -14‰ (Fritz, 1982). This indicates that the

shallow groundwaters are of the local meteoric water origin. The slight ^{18}O enrichment of the groundwaters from FZ-3 relative to the local surface waters is likely the result of the low-temperature water-rock interaction or infiltration of the surface water since the groundwaters in FZ-3 are, to certain degree, isolated from the surface waters.

In contrast, groundwaters from FZ-2 and FZ-1 have a wider variation in $\delta^{18}O$ values. The $\delta^{18}O$ of the waters of FZ-2 ranges from -13 to -20‰, while the waters of FZ-1 from -13 to -17‰. This wider $\delta^{18}O$ variation indicates that more than one water source exists at the URL site. Note that the isotopic shift is to the direction of lower $\delta^{18}O$ value which corresponds to a colder climate.

Stable isotope data of the groundwaters from Lac du Bonnet batholith in the Whiteshell area (WNRE) 20 km from the URL site (Fig.5.1) show similar characteristics (Fig.6.5) (Bottomley et al.,1984 and Gascoyne et al., 1987). All the waters from the WNRE plot on or close to the GMWL indicating the meteoric water origin. All the shallow fresh groundwaters (<50 m) have $\delta^{18}O$ value of -14.5 ± 0.5 ‰, which is the same as the local surface water. The $\delta^{18}O$ and δD values of the fresh groundwaters decrease with depth and reach about -17 and -125‰ respectively, at a depth of 315-322m. These deep fresh waters are old relative to the

Figure 6.5. Stable isotope variation diagram of the groundwaters from the WNRE area indicating the mixing between the shallow and deep fresh groundwaters and mixing between the deep fresh and the deep saline groundwaters (modified from Gascoyne et al., 1987).
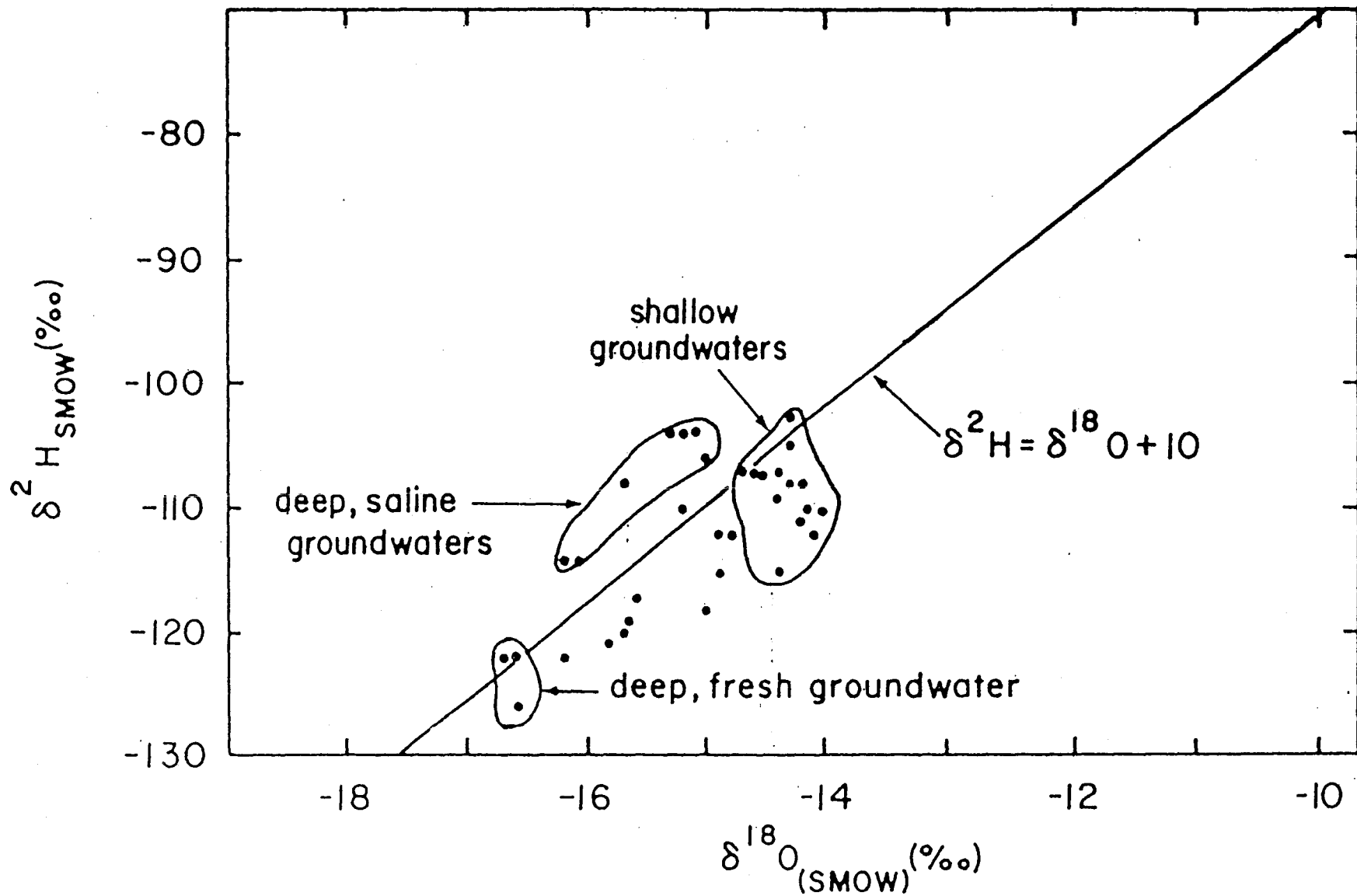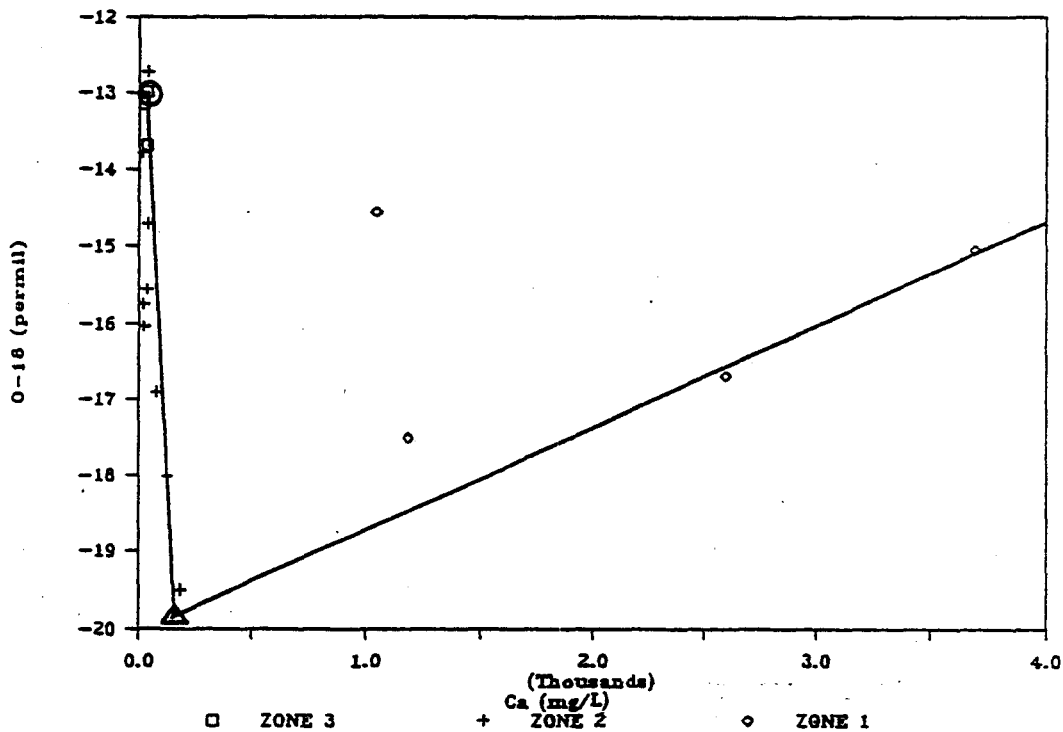
shallow fresh groundwaters because the deep waters do not contain tritium (Bottomley et al., 1984). The trend between the deep fresh waters and the shallow groundwaters in Fig.6.5 is likely a mixing line. The wide $\delta^{18}O$ range in the waters from FZ-2 is thus the result of mixing between the most ^{18}O depleted deep fresh water, -20‰ in the case of this study, and the surface water. The more saline waters from the WNRE area, in contrast, are enriched in deuterium and form a trend above the GMWL. The $\delta^{18}O$ and δD values generally increase with the salinity of the waters as seen from Table 2 and Table 3 of Bottomley et al.,(1984). In the case of WNRE, the trend of saline waters is likely a mixing line between the deep fresh waters, probably the glacial waters (see below) and the more saline waters.

The plots of $\delta^{18}O$ versus Ca, Sr, Cl and HCO_3 (Fig. 6.6) reveal a three-component mixing scenario as seen from the major cation and anion chemistry in 6.4.1. Because there are three end members involved, determining the three end members from the mixing lines is more difficult than in a two component mixing system. Fortunately mixing of waters between FZ-3 and FZ-2 and between FZ-2 and FZ-1 is clear while mixing between FZ-3 and FZ-1 is just visible. The mixing of waters from FZ-3 and FZ-2 revealed two end members: the local meteoric waters with $\delta^{18}O$ of around -13‰ and deep fresh groundwaters with $\delta^{18}O$ of around -20‰

Figure 6.6. Plots of $\delta^{18}O$ versus cation or anion concentrations of the groundwaters showing a three-component mixing. As shown in Fig.6.4, mixing of groundwaters between FZ-3 and FZ-2, and FZ-2 and FZ-1 is apparent while mixing between FZ-3 and FZ-1 is less so. Speculative mixing lines are drawn between the end members and the possible end members are indicated. The circle, triangle and the square stand for the shallow, the deep fresh and the saline end members. The $\delta^{18}O$ values of these three end-members are extrapolated to be: -13‰ for the shallow fresh groundwaters, -20‰ for the deep fresh groundwaters and -12.5‰ for the deep saline groundwaters. A) $\delta^{18}O$ versus Ca, B) $\delta^{18}O$ versus Sr, C) $\delta^{18}O$ versus Cl, and D) $\delta^{18}O$ versus HCO_3.
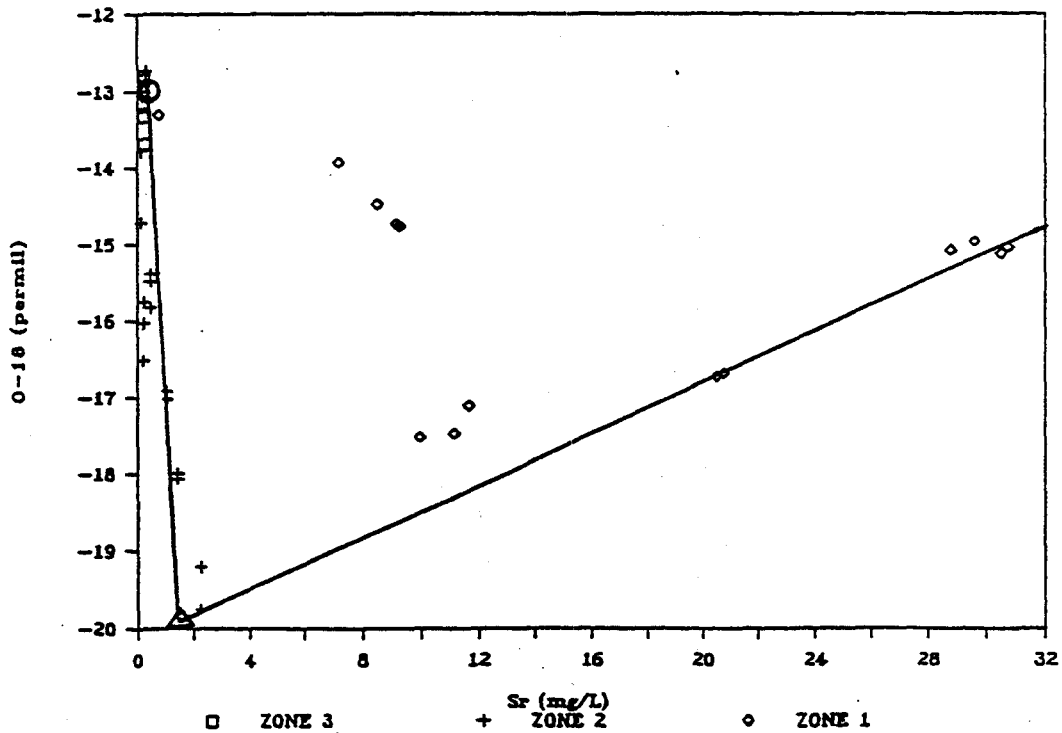
A

O-18 VS Ca

B

O-18 VS Sr

C
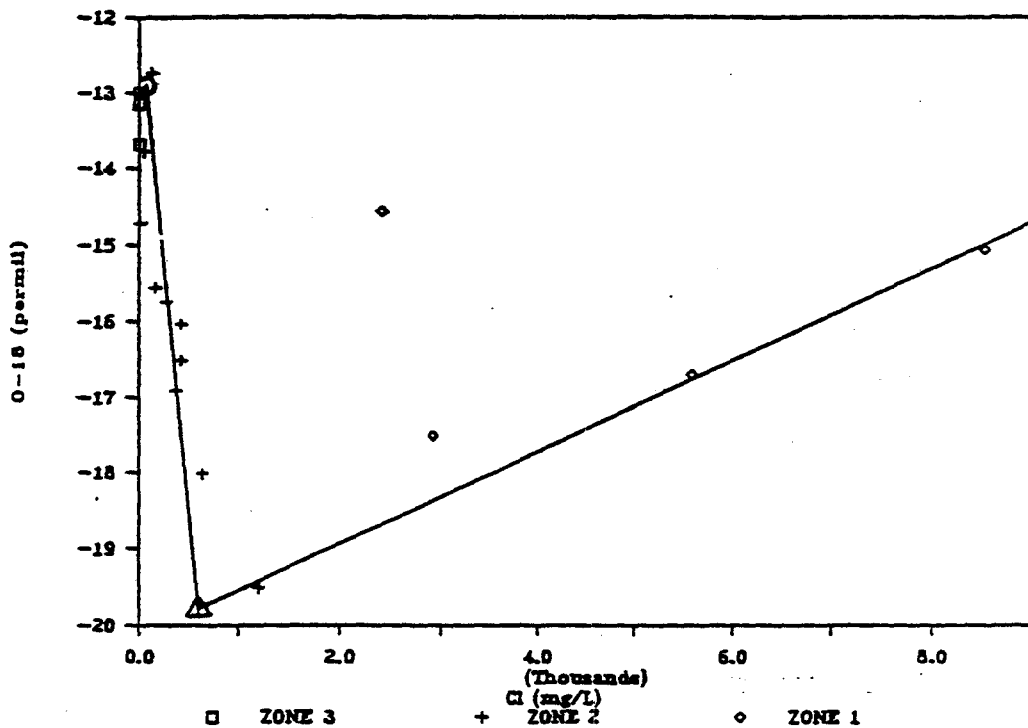
O-18 VS Cl

ZONE 3   +   ZONE 2   ◇   ZONE 1

D

O-18 VS HCO3

ZONE 3   +   ZONE 2   ◇   ZONE 1
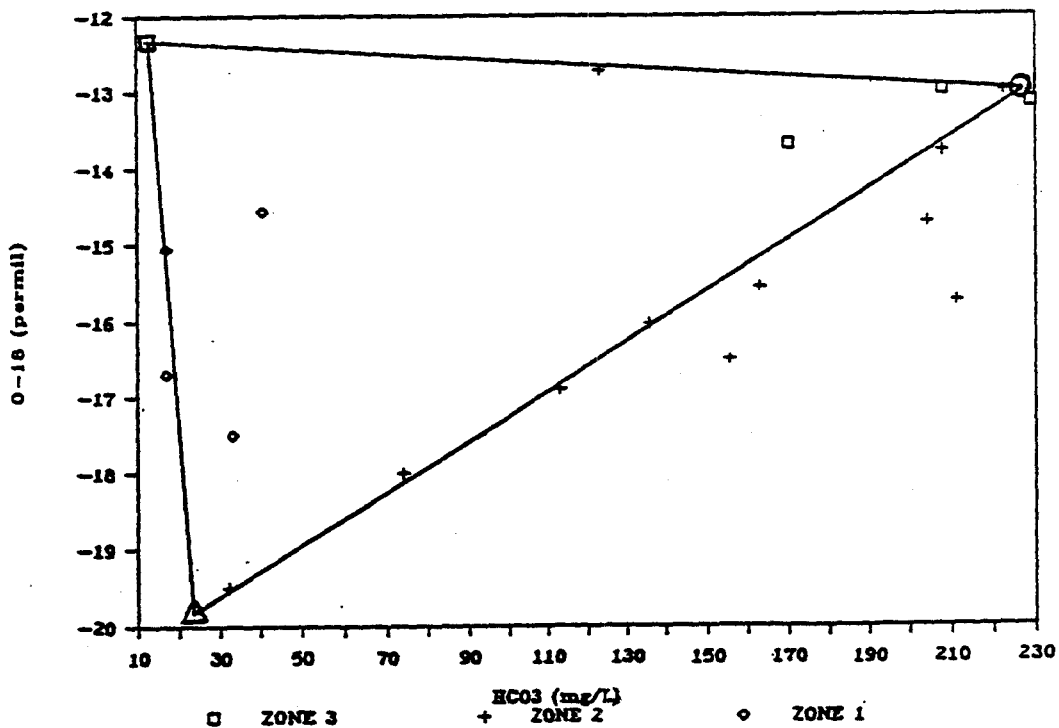
(Fig.6.6A, B, and C). The deep fresh waters observed here are even more depleted in ^{18}O than observed by Bottomley et al., (1984) (Fig.6.5). Such deep fresh waters are unlikely to be very old because of their low salinities. Their meteoric origin (Fig.6.5) and low $\delta^{18}O$ value (<-20‰) indicate that they are probably the local glacial melt waters of the last million years. Such glacial waters had $\delta^{18}O$ of about -24‰ (Frape, personal communication) and penetrated to depth in the batholith through fractures.

The more saline water end member is difficult to determine because of the lack of clear mixing with the shallow fresh waters and the limited number of data. Sample M7-4 with the highest TDS of 15400 mg/L has a $\delta^{18}O$ of -15‰. Generally the $\delta^{18}O$ values of the waters from FZ-1 increase with their salinities except for those obviously contaminated by the shallow fresh waters (URL12-7 and M7-SW28) indicated by the low TDS and Sr concentrations. Therefore higher $\delta^{18}O$ and TDS values are expected for the i3more saline end member. A $\delta^{18}O$ value of about -12.5‰ can likely be extrapolated from Fig.6.6D. If this extrapolation is corrected, then this extrapolated $\delta^{18}O$ value is very close to that found from the Canadian shield brines (Fig.6.1), supporting the idea of a common source brine for the groundwaters found in the Canadian shield.
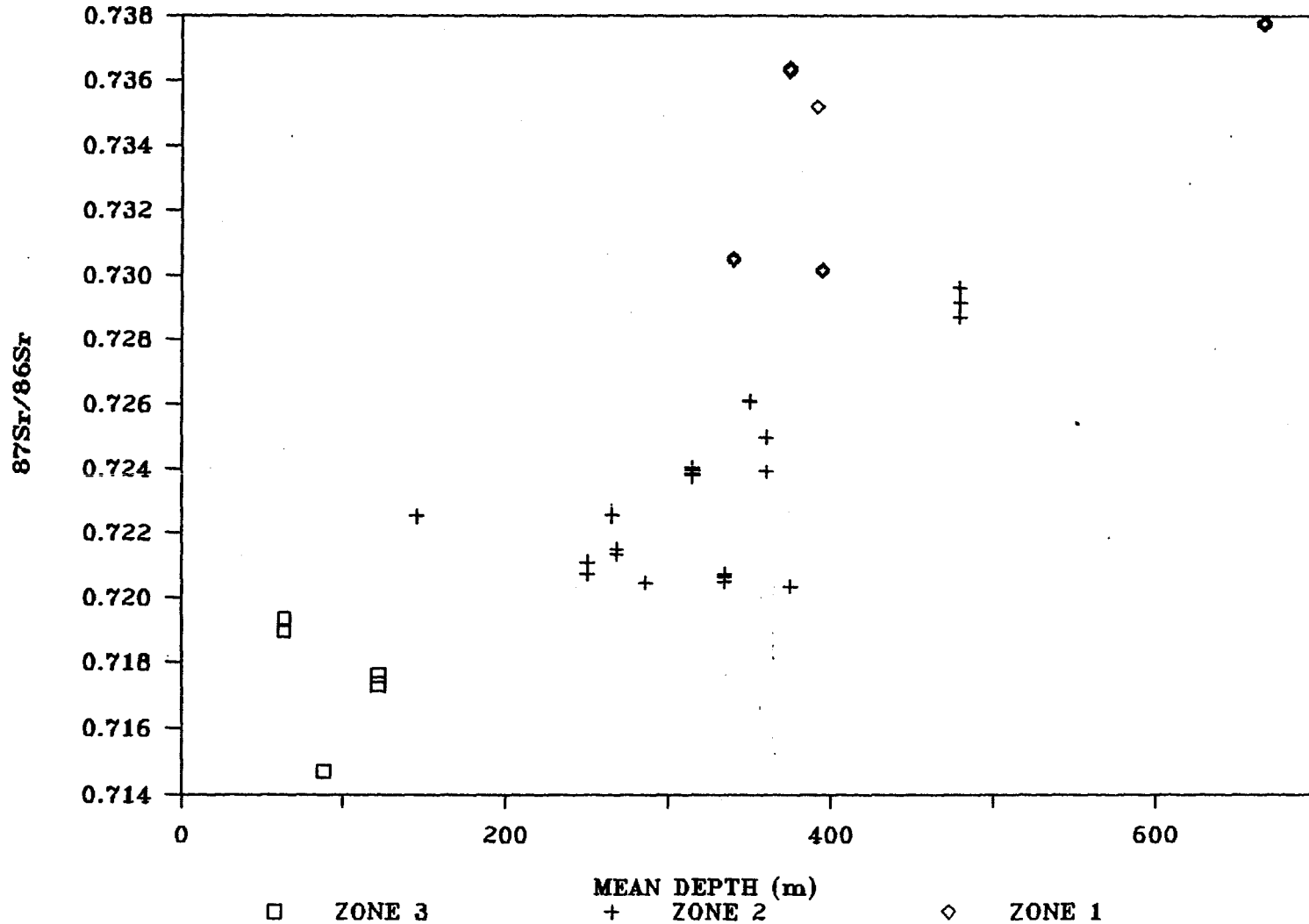
6.2.3. STRONTIUM ISOTOPES

Groundwaters from the three fractures have distinctive Sr isotopic ratios. The $^{87}Sr/^{86}Sr$ ratios of the waters increase generally with the depth (Fig.6.7). Waters from FZ-3 have ratios ranging from 0.715 to 0.719, waters from FZ-2 range from 0.720 to 0.729, while waters from FZ-1 vary between 0.730 to 0.738. The mixing scenario observed before can also be seen from the Sr isotopic ratios. Fig.6.8 shows the three component mixing system. The shallow fresh groundwater end member is most clear and plots tightly at the bottom-right corner of the diagram with a $^{87}Sr/^{86}Sr$ ratio of about 0.718 and a $\delta^{18}O$ value of about -13‰. The groundwaters from FZ-2 have $\delta^{18}O$ values ranging from -13 to -20‰ and most have virtually similar $^{87}Sr/^{86}Sr$ ratios of about 0.721. This wide variation in $\delta^{18}O$ is likely the result of mixing between the shallow groundwaters the $\delta^{18}O$ of -13‰ and deep fresh waters with $\delta^{18}O$ of -20‰ in this case. Therefore, the deep fresh end member is extrapolated to have a $^{87}Sr/^{86}Sr$ ratio of about 0.721 and a $\delta^{18}O$ value of about -20‰.

The more saline end member is more difficult to determine because of the weak trend between the saline and the shallow groundwaters. Waters with the highest $^{87}Sr/^{86}Sr$ ratio of 0.738 measured from FZ-1 are obviously not

Figure 6.7.   Diagram showing the variations of the $^{87}Sr/^{86}Sr$

ratios of the groundwaters with the mean depth.   The

$^{87}Sr/^{86}Sr$ increase   generally with mean depth and each

fracture zone has its distinct $^{87}Sr/^{86}Sr$ ratios.

87Sr/86Sr VS MEAN DEPTH

Scatter plot of $^{87}Sr/^{86}Sr$ (y-axis, ranging from 0.714 to 0.738) versus MEAN DEPTH (m) (x-axis, ranging from 0 to 600). Legend: □ ZONE 3, + ZONE 2, ◇ ZONE 1.

representative of the more saline end member as shown in Fig.6.8. However, a $^{87}Sr/^{86}Sr$ ratio of about 0.745 and a $\delta^{18}O$ value of about -12.5‰ for the more saline end member can likely be extrapolated from the interception of the mixing trends of FZ-1 with FZ-2 and FZ-3 (Fig. 6.8). This $\delta^{18}O$ value is identical to that obtained before.

Plots of $^{87}Sr/^{86}Sr$ ratio against Ca, 1/Sr, Cl and HCO_3 (only two are shown in Fig.6.9) do not show very clear mixing trends among the three end members discussed before. The shallow groundwaters plot out of the proposed possible mixing composition in Fig 6.9. This is not understood yet and likely reflects the effects of post-mixing processes such as uptake of Sr by secondary minerals.

6.2.4. URANIUM ACTIVITY RATIOS

Large variations in the U concentrations and $(^{234}U/^{238}U)$ activity ratios are observed for all the groundwaters (Table 6.2 and 6.3). Similar results were also obtained by Gascoyne and Cramer (1987).

The U concentrations increase generally with HCO_3 content (Fig.6.10) as observed in groundwaters by Osmond and Cowart, 1982 and Osmond et al., 1983. The shallow groundwaters from FZ-3 have U content above 30 ug/L, while

Figure 6.8. Plot of $^{87}Sr/^{86}Sr$ against $\delta^{18}O$ showing the three-component mixing of groundwaters. A $\delta^{18}O$ value of about -12.5 ‰ and a $^{87}Sr/^{86}Sr$ ratio around 0.745 for the deep saline waters can likely be extrapolated from the mixing trends of between FZ-1 and FZ-2, and FZ-1 and FZ-3.
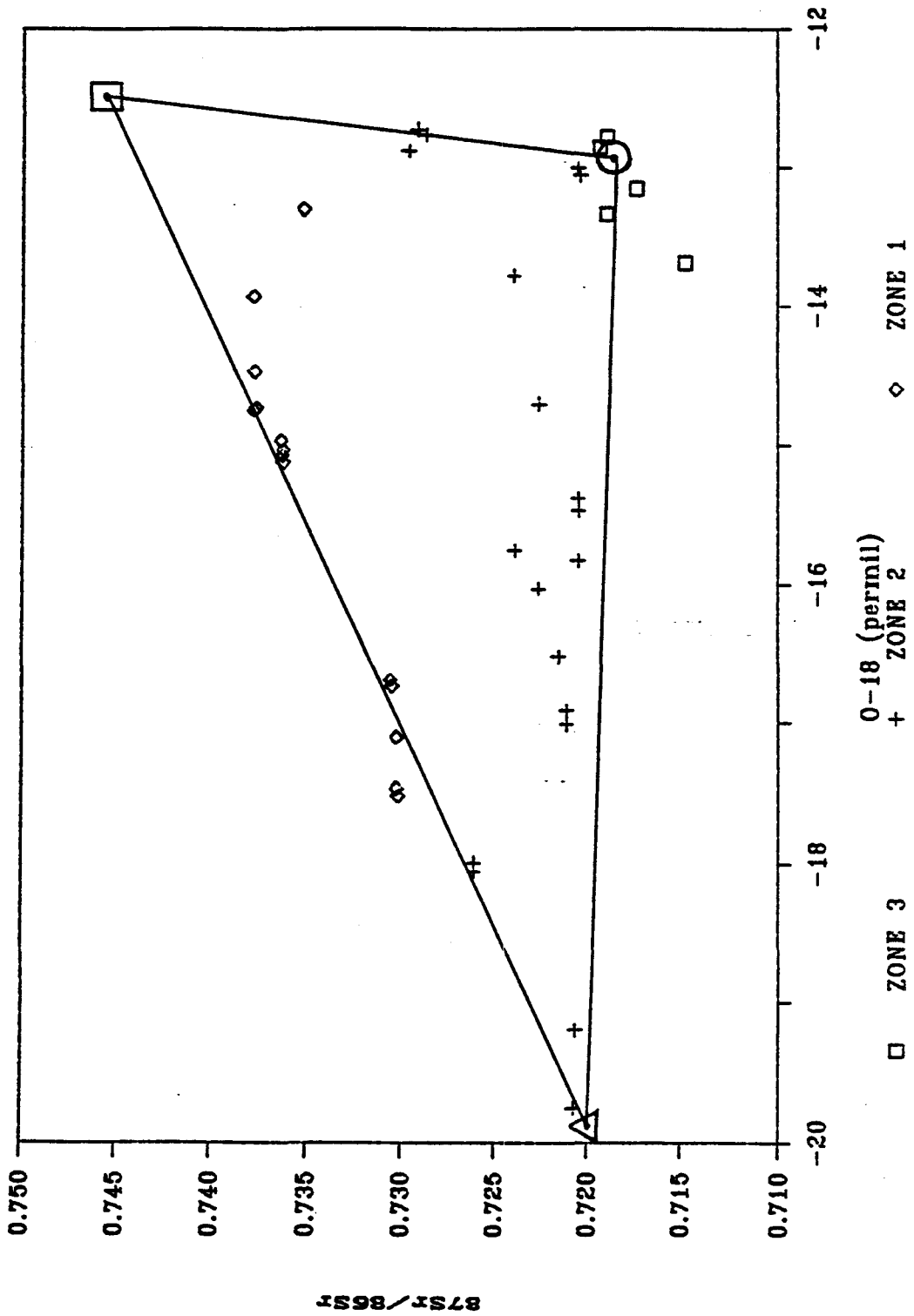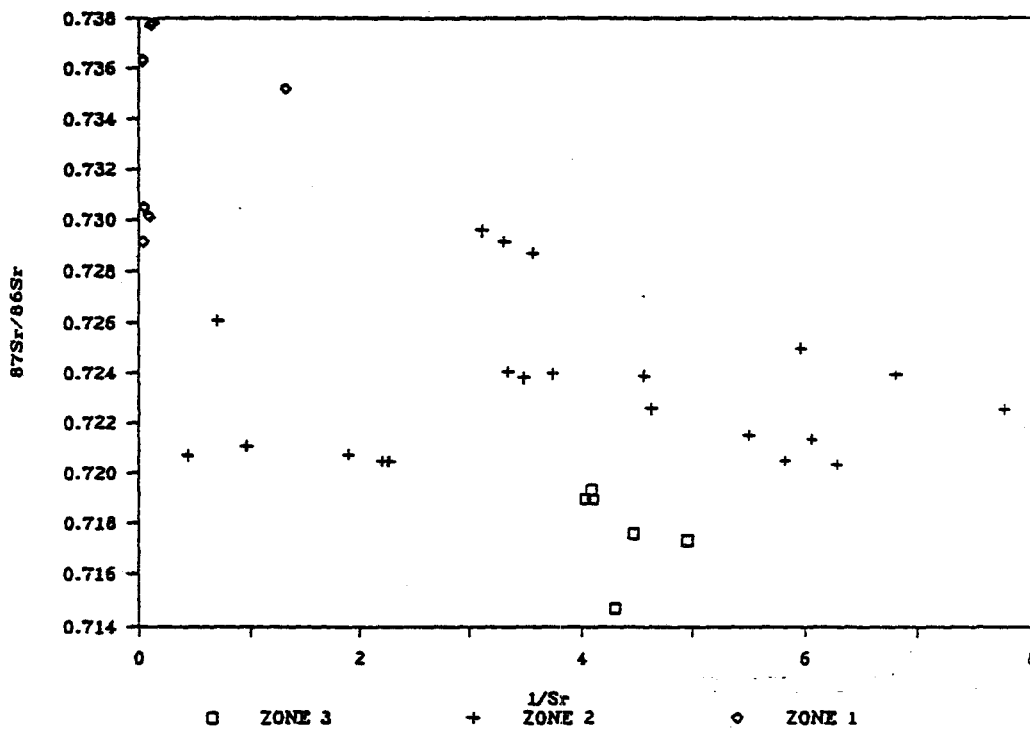
87Sr/86Sr VS O-18

87Sr/86Sr

O-18 (permil)

ZONE 1 ◇   ZONE 2 +   ZONE 3 □

Figure 6.9. Plots of $^{87}Sr/^{86}Sr$ ratio versus $1/Sr$ and HCO_3 do not show clearly the three component mixing as in Fig.6.8. In $^{87}Sr/^{86}Sr$ vs $1/Sr$ plot, the shallow groundwaters locate outside the proposed mixing area. The $^{87}Sr/^{86}Sr$ vs HCO_3 plot does not show any trends. This likely reflects the effects of post-mixing processes.

87Sr/86Sr VS 1/Sr

ZONE 3   ZONE 2   ZONE 1

87Sr/86Sr VS HCO3

ZONE 3   ZONE 2   ZONE 1
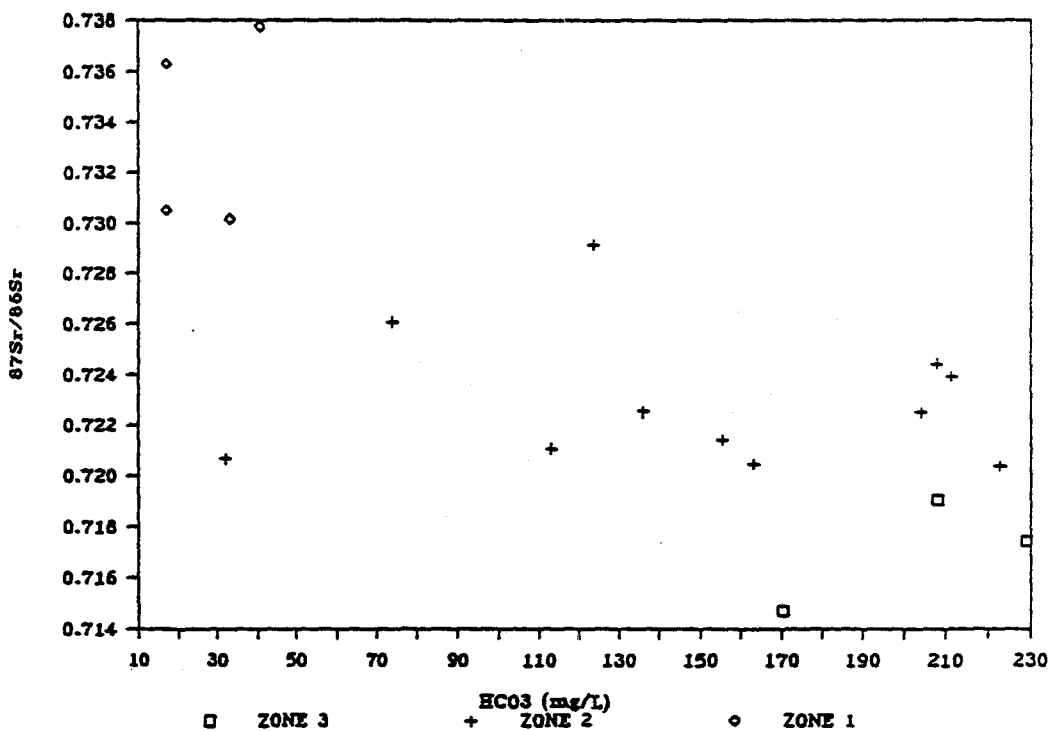
Figure 6.10.   Plot of U concentrations versus HCO_3. Waters

with low HCO_3 contents, from FZ-1 and some FZ-2 samples,

show generally low U contents and less variation.

Figure 6.11. Plot of $(^{234}U/^{238}U)$ activity ratios versus the

mean depth.   The shallow waters have generally low

$(^{234}U/^{238}U)$ ratio.   The waters from FZ-2 and FZ-3 show

large variations and their $(^{234}U/^{238}U)$ ratios are likely

controlled by local oxidation/reduction processe.

U VS HCO3
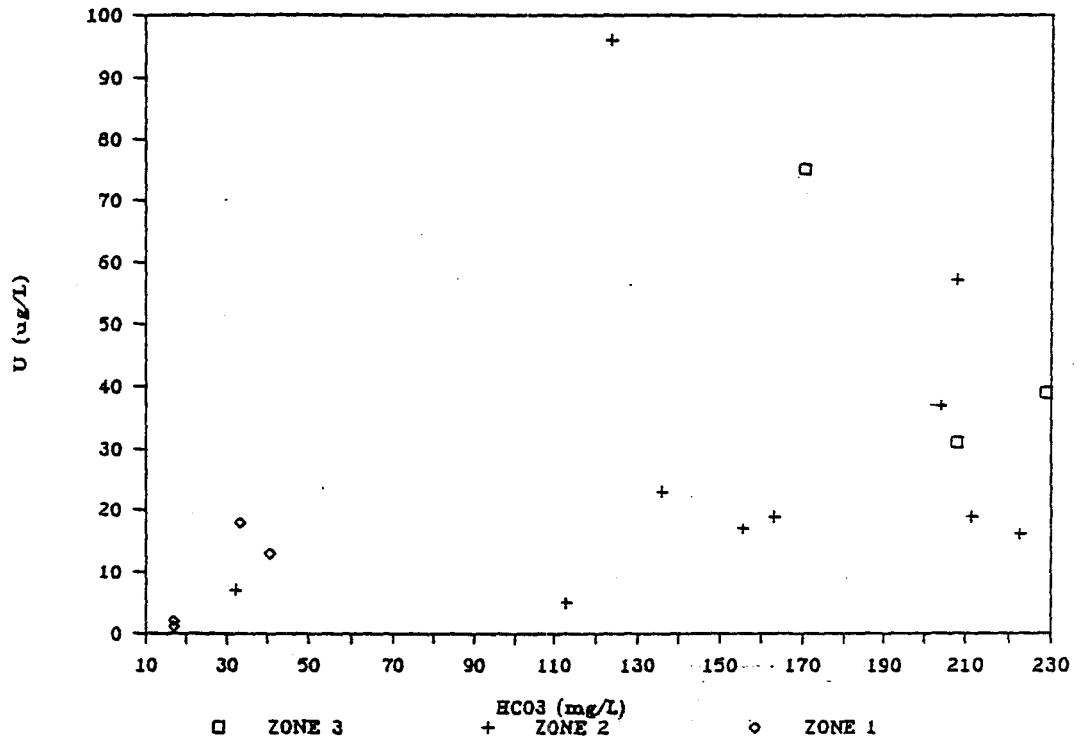
(234U/238U) VS MEAN DEPTH
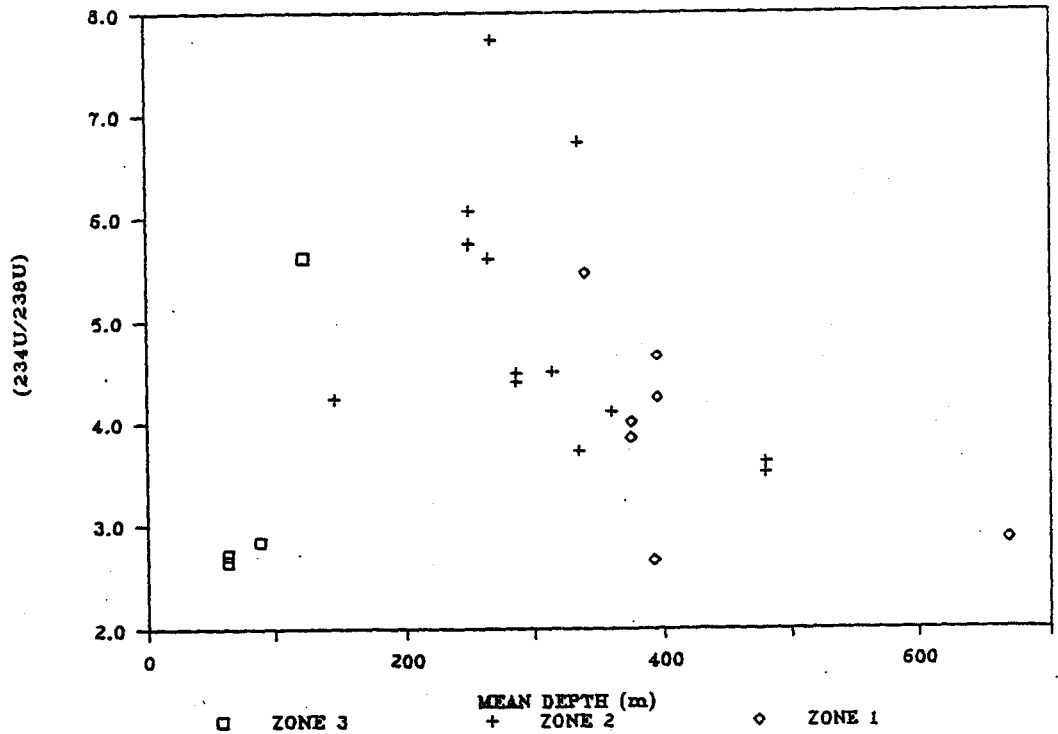
the deep saline waters from FZ-1 lower than 20 ug/L. The U concentration is also likely controlled by the Eh of the groundwaters due to the high mobility of the U in oxidizing environments (Cowart, 1980). The high U concentration in the shallow waters is simply the result of U loss from the near surface rocks as shown by the large ^{230}Th enrichment relative to U. The groundwaters from FZ-2 have large U variation, from 5 to 96 ug/L. This is believed to be controlled by the local oxidation/reduction condition as revealed by the enrichment and deficiency of ^{234}U observed on the altered rock samples from FZ-2.

^{234}U is highly enriched relative to ^{238}U and the (^{234}U/^{238}U) activity ratio varies from 2.6 to 7.7 (Fig.6.11). The shallow groundwaters from FZ-3 have generally low (^{234}U/^{238}U) ratios of about 2.7 (with one exception, M6-2). This is expected because of the high U contents in shallow groundwaters as demonstrated by Cowart, 1980, and Osmond et al., 1983. In contrast, the deep saline waters from FZ-1 have relative low U concentrations and more variable (^{234}U/^{238}U) ratios. Groundwaters from FZ-2 have the highest (^{234}U/^{238}U) ratios and the largest variation, from 3.5 to 7.7. This is most likely controlled by the local oxidation/reduction conditions. Uranium-series disequilibrium study of the altered rocks from FZ-2 (Gascoyne and Cramer, 1987 and in 5.2.2) has shown the local
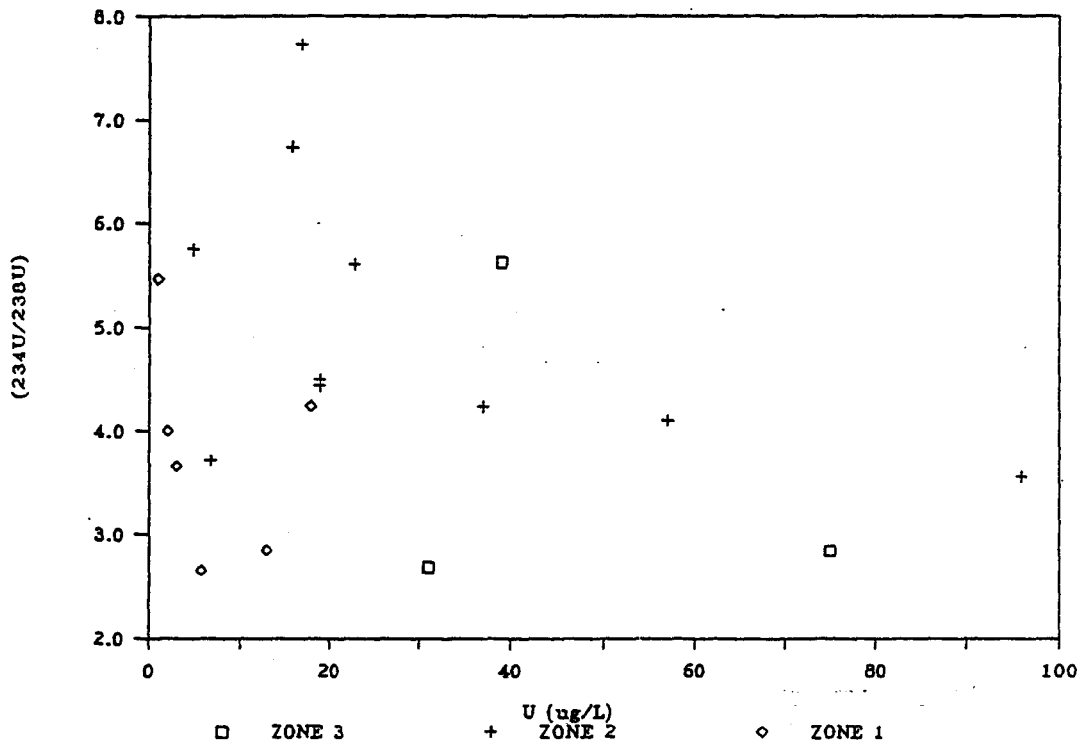
control on U loss or gain. Interaction of rocks with oxidizing groundwaters are believed to be responsible fo the U loss from the rocks and ^{234}U enrichment in the waters. Exchange of U in the rocks with reducing groundwaters is likely to introduce U isotope fractionation that favours ^{234}U remaining in the water phase due to its low chemical activity relative to ^{238}U in the waters (Osmond and Coward, 1982, Osmond et al., 1983 and Smellie et al., 1985). Therefore, interaction of rocks with reducing/oxidizing groundwaters will generate a wide range of (^{234}U/^{238}U) activity ratios as seen from the FZ-2 groundwaters.

The lack of clear correlations of (^{234}U/^{238}U) activity ratios with U, Sr, δ^{18}O and ^{87}Sr/^{86}Sr ratios (Fig.6.12) indicates the local and post-mixing control of the U in the groundwaters. This implies that the migration of U between rocks and waters is very fast relative to the rate of homogenization by the water by mixing processes.

Figure 6.12.   Plots of $(^{234}U/^{238}U)$ activity ratios versus U,

Sr, oxygen isotopes and $^{87}Sr/^{86}Sr$ ratios of the

groundwaters indicating the decoupling of $(^{234}U/^{238}U)$

ratio with other geochemical parameters. Mixing trends

shown in Fig. 6.8 cannot be observed. The scatter in

the plots indicates that the control on the $(^{234}U/^{238}U)$

ratio is differnt from those on other chemical species

like   Sr,   and   likely   reflects   the   local

oxidation/reduction processes of groundwaters.   A)

$(^{234}U/^{238}U)$ vs U, B) $(^{234}U/^{238}U)$ vs Sr,   C) $(^{234}U/^{238}U)$

vs $\delta^{18}O$ and D) $(^{234}U/^{238}U)$ vs $^{87}Sr/^{86}Sr$.

A

(234U/238U) VS U

B

(234U/238U) VS Sr

C

(234U/238U) VS O-18

O-18 (permil)

☐ ZONE 3   + ZONE 2   ◇ ZONE 1

D

(234U/238U) VS 87Sr/86Sr

87Sr/86Sr

☐ ZONE 3   + ZONE 2   ◇ ZONE 1
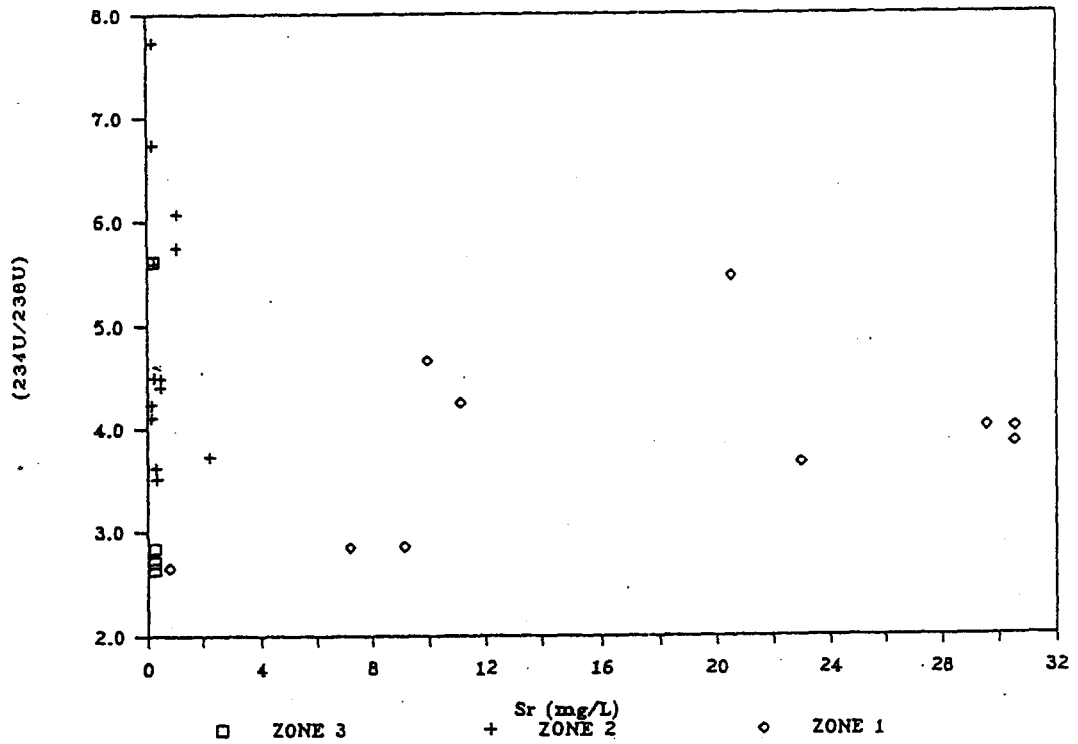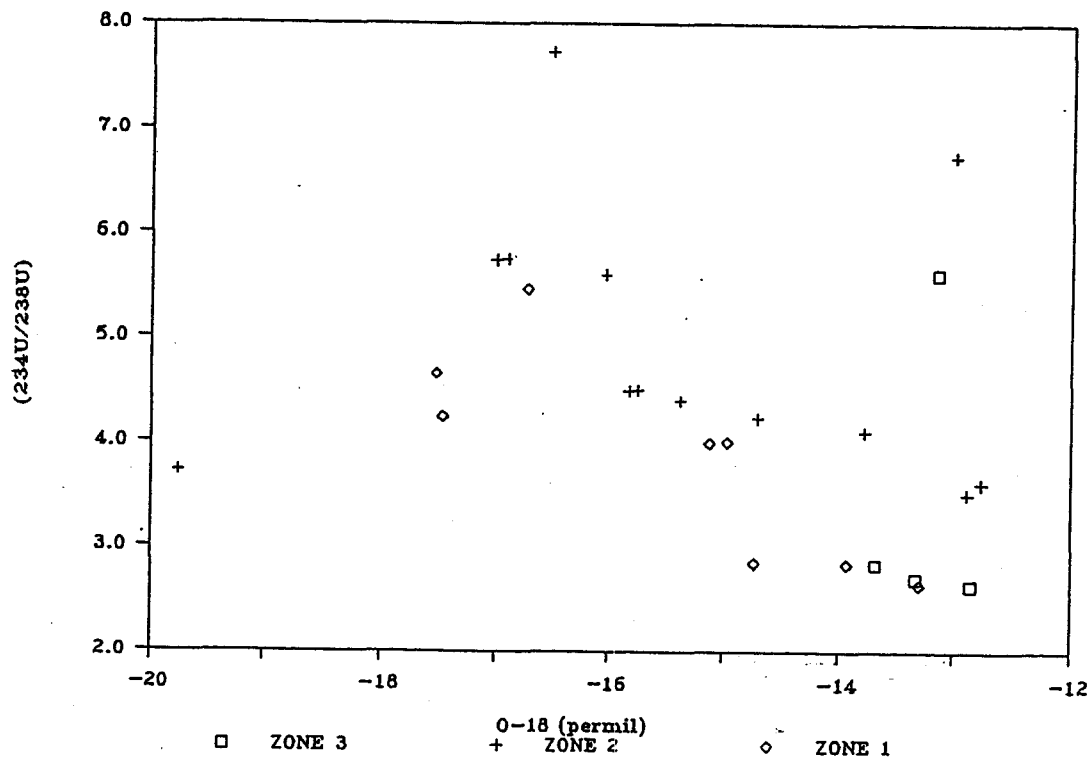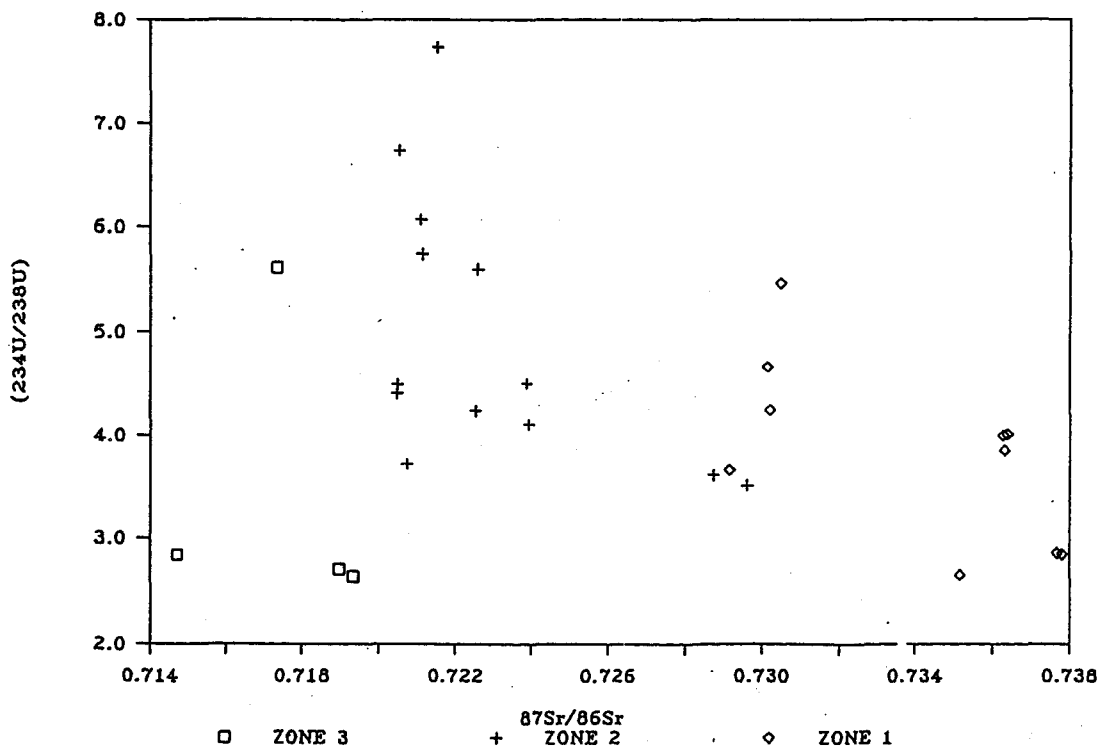
CHAPTER SEVEN

DISCUSSION: WATER-ROCK INTERACTION

7.1. THE ORIGIN OF THE SALINITY OF THE GROUNDWATERS

As previous discussed, isotopic and chemical studies of
the groundwaters in crystalline rocks have shown that mixing
of different water end-members is a rule rather than the
exception. The mixing between the local fresh meteoric
water and a deep, possibly common source, brine in the
locations of the Canadian shield is more obvious. These two
water end-members are widely accepted. However, controversy
still exists concerning the origins of the salinity of the
groundwaters, especially the deep brines with salinity up to
350 g/L, in addition to the origins of the water components.

The origins of the salinity of the deep groundwaters in
the crystalline rocks have been discussed by several
authors. The solute component of the groundwaters may be
primary, that is, of the same origin as the water component,
or secondary. Possible primary origins of the solute
include residual hydrothermal fluids, ancient seawaters
which has undergone subsequent concentration processes, and
invading sedimentary basin brines (Frape and Fritz, 1982;
Fritz and Frape, 1982). The secondary origins of saline
components are simply from the rocks during water/rock

168

interaction. These water/rock interaction processes include leaching of fluid inclusions (Nordstrom et al., 1985: Nordstrom and Olsson, 1987), dissolution of grain boundary salts (Grigsby et al., 1983), intense reaction with certain host rock or certain vulnerable mineral phases, such as mica, amphiboles and plagioclase (Fritz and Frape, 1982; Frape et al., 1984; McNutt et al., 1984; Edmunds et al., 1984; 1985; 1987; Smellie et al., 1986; Gascoyne et al., 1987; Kamineni, 1987; Franklyn, 1988).

Kelly (1986) and Guha (1987), based on the similarity of chemical and isotopic signatures between shield brines and the observed minewaters in two mine sites, argued for the emplacement of basin brines or modified Paleozoic seawater into the Canadian shield to explain the observed high salinity. However, the unique isotopic composition and chemical similarity of the deep brines from all the locations across the Canadian shield could not be accounted for. Attempts have been made to probe the origin of the groundwaters by using the chemically conservative elements, such as Br and Cl (Nordstrom et al., 1985; Edmunds et al., 1985 and 1987). Chemical studies of the groundwaters across the Canadian shield based on these conservative elements did not indicate seawater origin (Frape and Fritz, 1987). However, the involvement of sedimentary basin brines has been invoked by Gascoyne et al., (1987), in the WNRE/URL

site based on the Br/Cl ratios (Fig.7.1 and 7.2). Shield brines from Sudbury, Yellowknife and Thompson, and groundwaters from Atikokan, Chalk River and Stripa have Br/Cl molar ratios of about 0.003-0.006 and variable Ca/Mg and Na/Ca ratios depending on the chemistry of their host rocks, while groundwaters from WNRE/URL have a Br/Cl ratio ranging from less than 0.001 to 0.004. Plots of the Br/Cl ratio against Ca/Mg and Na/Ca ratios suggest mixing with the Western Canada Sedimentary Basin brines or Manitoba basin brines that have a Br/Cl ratio ranging from less than 0.001 to 0.003 (Fig.7.1 and 7.2).

It is generally agreed that the primary chemistry of the deep groundwaters is not preserved and hence, is not discernible even in the cases of the chemical conservative elements, such as Br and Cl. Bromine and Cl behave in conservative manner only after they are added to the waters.

Frape et al., (1984), Nordstrom (1985), Edmunds et al., 1985 and 1987, Gascoyne et al., 1987 argued that the high salinity is the product of the leaching of fluid inclusions or intense interaction with certain mineral phases such as micas and plagioclase. Strontium isotope study on both the host rocks and their associated groundwaters indicates Sr isotopic equilibrium of the waters with either host rocks or certain mineral phases such as plagioclase (McNutt et al.,

Figure 7.1.   Plot of Ca/Mg versus Br/Cl mole ratios showing

the mixing trend of the groundwaters at   the   URL site

with   the   Western   Canada   sedimentary   basin brines or

Manitoba   brines.   Groundwaters   found   in crystalline

rocks from other sites on the Canadian shield and Stripa

have relatively larger Br/Cl ratios which have a narrow

range compared with those in the URL/WN site (modified

from Gascoyne et al., 1987).

Figure showing Ca/Mg versus Br/Cl with data fields labeled: Manitoba brines, Western Canada Sedimentary Basin, Sudbury, Stripa, Yellow-knife, Thompson.

Legend:
- ● Yellowknife
- ○ Thompson ⎱ mines
- ◆ Sudbury
- ◇ ATK
- ▲ URL / WN
- ✻ seawater

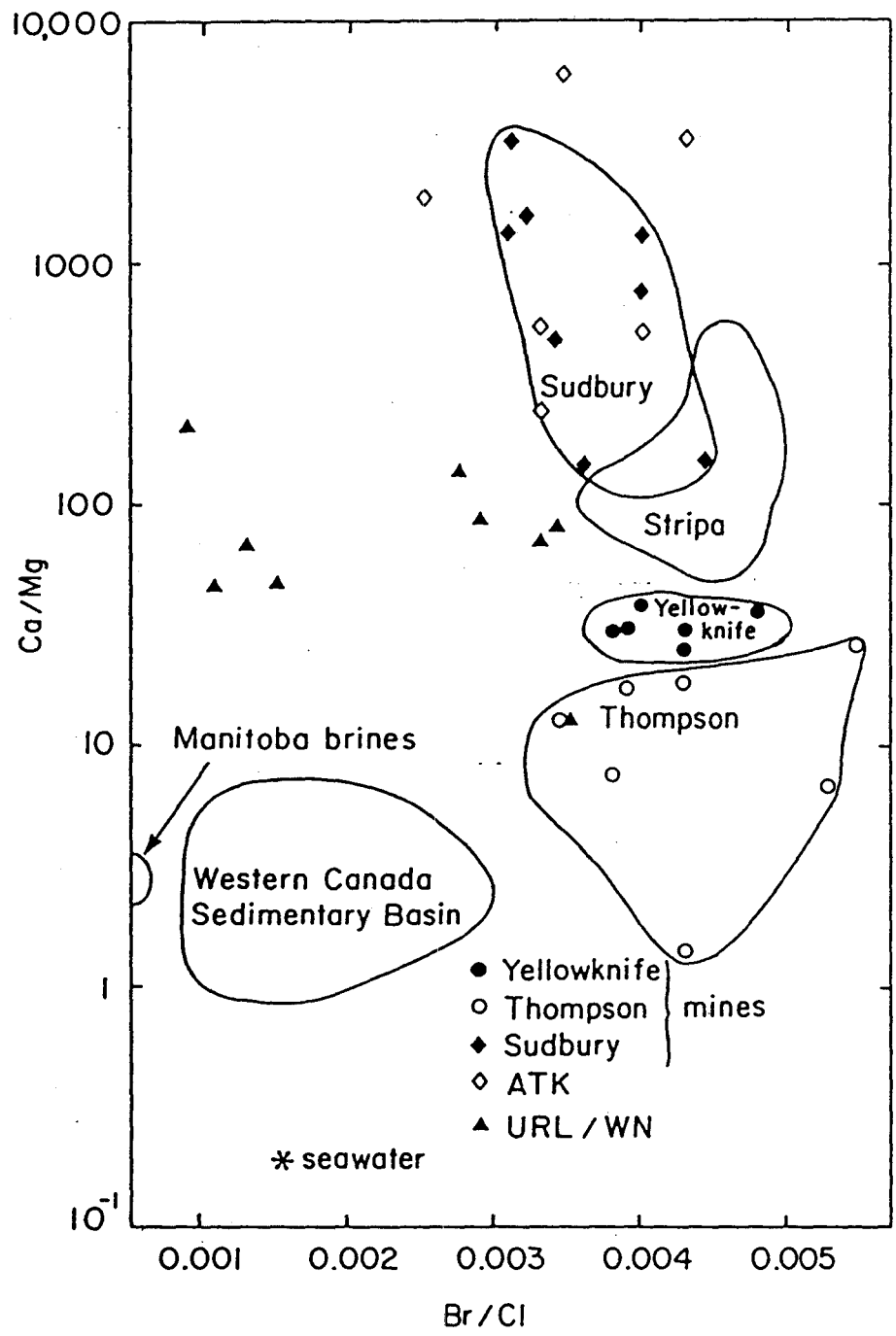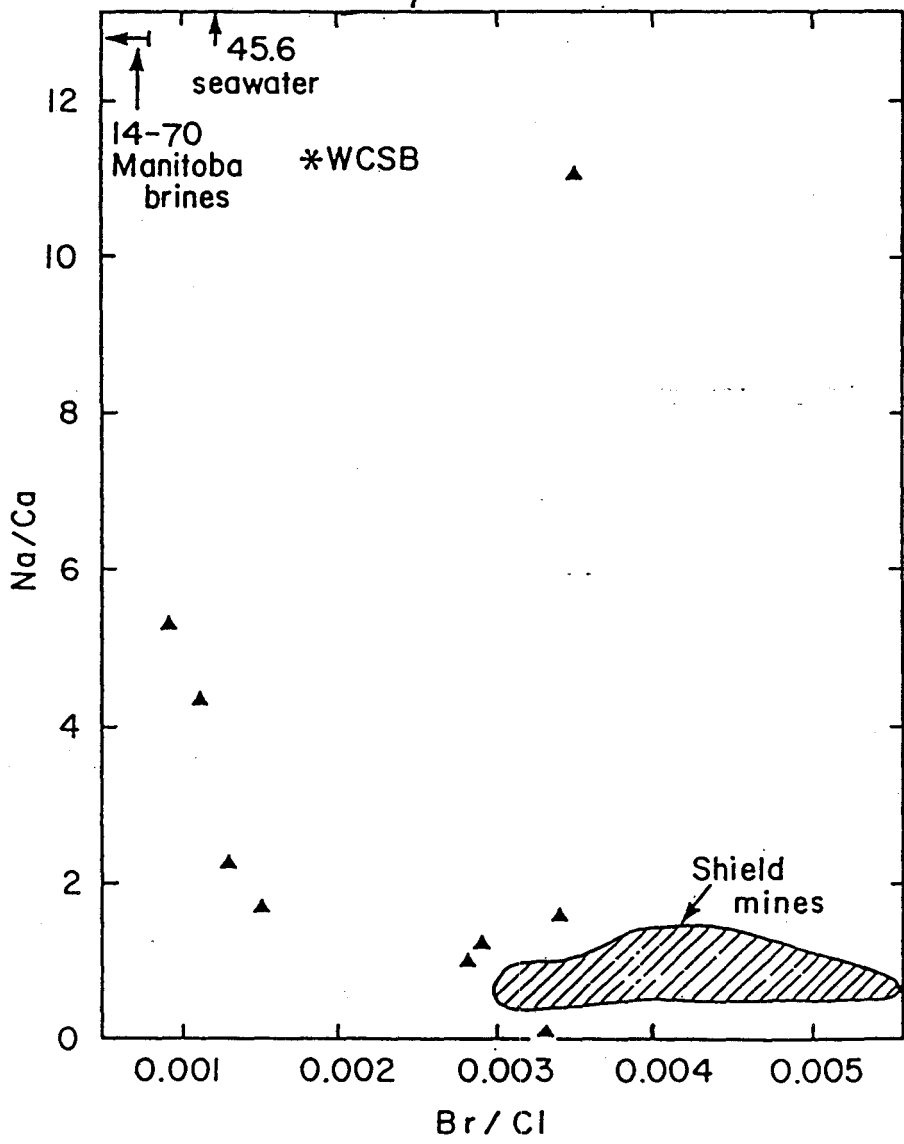Axes: Ca/Mg (vertical, 10⁻¹ to 10,000), Br/Cl (horizontal, 0.001 to 0.005)

Figure 7.2. Plot of Na/Ca versus Br/Cl mole ratios showing also the mixing of groundwaters at the URL/WN site with the Western Canada sedimentary brines or Manitoba basin brines. The Canadian shield brines plot at the buttom-right cornner of the diagram (modified from Gascoyne et al., 1987).

1984; McNutt, 1987; McNutt et al., 1987; Franklyn, 1988). The chemical and isotopic similarity of the common source brine is thus achieved by the maximum degree of low-temperature water-rock interaction and similar primary and secondary mineral controls.

7.2. EVIDENCE OF WATER-ROCK INTERACTION
7.2.1. CHEMISTRY

Different chemical characteristics for shallow (fresh and brackish) and deep (saline and brines) groundwaters have been revealed by the accumulated data (Frape et al.,1984, Frape and Fritz, 1987). The shallow groundwaters are variable in composition and are generally Ca-Na dominant. Mg is variable and is found to correspond to the chemistry of local host rocks. Based on the data of the groundwaters in three sites in the Canadian shield, Yellowknife, Thompson and Sudbury, Frape et. al., found that waters associated with granitic rocks, such as in Yellowknife, are dominated by Na and Ca, followed by Mg>K>Sr as the major cations, and HCO_3 as the major anion, followed by SO_4>Cl. Those waters found in mafic rocks, for instance, in Thompson, are dominated by Ca>Mg>Na as the major cations with much lesser amount of K and Sr. HCO_3 is still the major anion with Cl present in equal or greater concentration than SO_4. The comparisons of the Ca, Na and Mg mole ratios between the

groundwaters and their host rocks in each of the three sites show a clear similarity between waters and rocks. This similarity cannot be addressed in the URL site due to the limited data. This clear relationship between the rocks and their associated waters was long ago observed by Garrels (1967) and indicates that the chemistry of the shallow groundwaters is controlled by a dissolution-dominant process of vulnerable silicate minerals.

In contrast to the variable chemistry of the shallow groundwaters, the chemistry of deep groundwaters found in the Canadian shield is very uniform and independent of the host rocks. The Ca, Na and Cl are dominant and account for over 90% of the salinity. The lack of a clear similarity in chemistry between the waters and their host rocks suggest the chemistry of the deep groundwaters is unlikely related to the dissolution-dominant water-rock interaction. Their chemistry is not only controlled by the contribution of certain elements due to the dissolution of certain minerals of the host rocks, but also by their removal due to the formation of secondary minerals during a long sub-surface history. The most commonly found secondary minerals in fractures are calcite, gypsum, zeolites and clay minerals. The formation of these secondary minerals will inevitably change the stable isotope compositions of the waters, especially pronounced in a closed system. Therefore, the

chemical and isotopic similarity of the deep waters in Canadian shield is interpreted as the result of an "equilibrium state" between the dissolution of primary silicates and formation of secondary minerals.

7.2.2. STRONTIUM ISOTOPES

Strontium isotope study of both the groundwaters and the host rocks and minerals in Sudbury (McNutt et al., 1984, McNutt, 1987) and Atikokan (Franklyn, 1988) shows that the Sr in the groundwaters has isotopic signatures similar to either the host rocks or certain mineral phases, plagioclase in the case of Atikokan. This indicates that the Sr isotopic ratio of the waters is in "equilibrium" with either the whole-rock or certain mineral phases. The latter is most likely with the accumulated data and is in accord with the result of chemical kinetics of water-rock interactions. Based on the dissolution experiments at 25 ^{o}C and pH of 5, Lasaga (1984) calculated the mean lifetime of 1-mm crystals of different minerals (Table 7.1). There is a difference of more than five orders of magnitude in the lifetime. Quartz is the most resistant with a lifetime of 34 Ma and anorthite the least resistant with a lifetime of only 112 years, while K-feldspar and albite have lifetimes of 520,000 and 8,800 years, respectively. Therefore, plagioclase is the most vulnerable mineral and, with its

Table 7.1.   Mean Lifetime of a 1-mm Crystal

Mineral	Lifetime
Quartz	34 Ma
Muscovite	2.7 Ma
K-feldspar	520,000 years
Albite	80,000 years
Nepheline	211 years
Anorthite	112 years

1. Data from Lasaga, 1984.

large abundance in mafic and felsic igneous rocks, is expected to be the major control on the chemistry of the groundwater, especially for a short period of time in contact with groundwaters. This control can be easily shown by the $^{87}Sr/^{86}Sr$ ratios because of the high abundance, high Sr content and low $^{87}Sr/^{86}Sr$ ratios of plagioclase. With increase in ages of groundwaters, contribution of Sr from K-feldspar will increase and result in higher $^{87}Sr/^{86}Sr$ ratios in the waters. This is shown by the increase of $^{87}Sr/^{86}Sr$ ratio with depth at the URL (Fig.6.7).

When compared with the whole-rock and mineral phases of the host rock at URL, the groundwaters from FZ-3 have a $^{87}Sr/^{86}Sr$ ratio similar to the plagioclase of least altered rocks (Table 7.2). The $^{87}Sr/^{86}Sr$ ratios of the waters from FZ-2 correlate well with plagioclase of altered rocks from FZ-2. This clear relationship between the plagioclase and the groundwaters further supports the plagioclase's control on the chemistry of the groundwater as discussed above.

However, the plagioclase's control on the $^{87}Sr/^{86}Sr$ ratio of the groundwater is not a simple dissolution interaction. As discussed in chapter 5 (Table 5.3), plagioclase of altered samples has much lower Sr concentrations compared with that of least altered samples, indicating loss of Sr. On the other hand, the higher

Table 7.2. Comparison of Sr Ratios Between Groundwaters and the Host Rock

	WHOLE-ROCK	BIOTITE	K-FELDSPAR	PLAGIOCLASE	GROUNDWATER
FZ-3					
FRESH	0.751-0.783	1.807-3.012	0.809-0.825	0.710-0.715	0.715-0.719
FZ-2					
FRESH	0.771	3.34	0.866	0.712	0.720-0.729
ALTERED	0.764-0.819	6.928-12.14	0.847-0.868	0.721-0.734	

1.   The whole-rock and mineral data for FZ-3 are from samples P1,P2,JSS1 and JSS2.

2.   The data for the fresh sample of FZ-2 are from P3.

$^{87}Sr/^{86}Sr$ ratios of the plagioclase of the altered samples suggest the plagioclase has gained some radiogenic ^{87}Sr. Therefore, exchange of Sr isotopes must have occurred between the plagioclase and the associated groundwater. The altered plagioclase behaves like a buffer in the case of Sr isotopes in the groundwater. The plagioclase of least altered samples from FZ-2 does not show similar $^{87}Sr/^{86}Sr$ ratios as the associated groundwater, suggesting the dominant control of the altered samples on the chemistry of the groundwaters.

As previously pointed out, secondary minerals play an important role in controlling the chemical and isotopic composition of the waters. Comparison of the $^{87}Sr/^{86}Sr$ ratios and $\delta^{18}O$ between the fracture-filling calcite and associated groundwater is shown in Table 7.3. Analyses of four calcite samples from FZ-3 give the $^{87}Sr/^{86}Sr$ ratios similar to the associated present-day groundwater. Two calcite samples, URL10-6 and URL10-8, from FZ-2 show similar $^{87}Sr/^{86}Sr$ ratios as the associated groundwaters from FZ-2. This similarity of $^{87}Sr/^{86}Sr$ ratios between the calcites and their associated present-day groundwaters indicate an equilibrium state between these calcites and the waters. These calcites from the same fracture zone also have similar $\delta^{18}O$ and $\delta^{13}C$ values, indicating they formed recently under similar condition. However, the equilibrium of their $\delta^{18}O$

Table 7.3. Comparison of the Groundwaters and the Calcite from URL-10

| | CALCITE | | | | GROUNDWATERS | | |
	Depth(m)	87/86Sr	O-18	C-13	Depth(m)	87/86Sr	O-18
FZ-3							
URL10-1	69.5	0.71381	20.1	-9.8	54-121	0.7147	-13.7
URL10-2	71.1	0.71413	24.4	-5.7			
URL10-3	84.7	0.71533	24.3	-7.0			
URL10-4	89.9	0.71386	23.3	-7.8			
FZ-2							
URL10-5	277.5	0.71525	21.3	-10.3	270-302	0.7205	-15.6
URL10-6	279.6	0.71983	20.7	-10.6			
URL10-7	288.7	0.71272	18.9	-15.3			
URL10-8	302.1	0.72193	20.5	-11.1			

1. O-18 is the delta oxygen-18 value in permil in respect to SMOW. C-13 is the delta carbon-13 value in permil in respect to PDB.
2. The calcite data are from Jones (1988).
3. The groundwater data for FZ-3 and FZ-2 are URL10-3-2 and URL10-6 from Table 6.3 respectively.

and $\delta^{13}C$ with the groundwaters is not achieved as discussed by Jones (1988).

7.2.3. URANIUM-SERIES ISOTOPES

The water-rock interaction is also shown by the U-series isotopes both in the rocks and minerals and their associated groundwaters as discussed in chapter five and six. Groundwaters from all three fracture zones are highly enriched in ^{234}U, with $(^{234}U/^{238}U)$ activity ratio ranging from 2.6 to 7.7. The loss of U from the rocks is shown by the high chemical Th/U ratios as well as $(^{230}Th/^{234}U)$ activity ratios of whole-rock samples. Both ^{234}U depletion and enrichment in the rocks and minerals occurred, and no simple relationship exists between the $(^{234}U/^{238}U)$ activity ratio and the U concentration in the waters, suggesting a scenario of local U exchange between the rocks and the waters, likely due to oxidation/reduction of the groundwater. The lack of a correlation between degree of rock-water interaction as revealed by Sr isotopes and U-series is likely a result of different mineral control on Sr from those on U since U is more sensitive to the Eh of the environment. Limited data on mineral phases makes it unclear which particular mineral phases, such as biotite, control this U exchange. Certainly, this process occurs continuously in the last million years to the depth of the

pluton as already shown by the work on Eye-Dashwa lakes granite by Latham and Schwarcz (1987a, 1987b).

CHAPTER EIGHT

CONCLUSION

The U-series analytical technique using mass spectrometry developed in this study has shown the ability to analyze $^{234}U/^{238}U$ and $^{230}Th/^{234}U$ isotopic ratios to the precision of 1% (2σ) with 10^{-8} g of U and 10^{-11} g of ^{230}Th in carbonate samples. A two-stage, single-spike (^{236}U) method was taken to measure $^{234}U/^{238}U$ isotopic ratio with precise and accurate fractionation. A precision of better than 0.5% (2σ) in determining this ratio can be routinely achieved in geological samples such as carbonates, igneous rocks and groundwaters. The potential application of this method was attempted on dating using small speleothem samples (speleothem 76001) and the results of replicate analyses agree well with those of α-spectrometry. However, its application in measuring ^{230}Th in granitic rocks and minerals is not successful due to the large ^{232}Th tail in the mass spectrum. Better results are achievable if purer spike is used.

An ICP-MS isotope dilution method is developed for fast and precise determination of Sr concentrations in water sample. A precision of about 1% is obtained by careful consideration of the dead-time effect of the machine and the spike/sample ratio.

The isotopic study of both the groundwaters and their host rocks and minerals in the URL site of Pinawa, Manitoba, has revealed the processes of water mixing and water-rock interaction through the history of the Lac du Bonnet batholith. A three groundwater mixing system is identified by both the chemistry and the Sr and O isotopes. These three components are local shallow fresh groundwater, deep fresh groundwater (possibly glacial melt) and the deep saline groundwater. The Sr isotopes of both rocks and minerals show the loss of Sr on the whole-rock scale. The similarity of the Sr isotopic ratios between the groundwaters and altered plagioclase indicates that altered plagioclase is the major chemical and isotopic control of the groundwater. The U-series data of rocks and minerals indicate the common existence of disequilibrium in both fresh and altered rocks. The high $(^{230}Th/^{234}U)$ activity ratio (up to 1.9) and Th/U ratio suggest the loss of U in the last 350 ky. Comparison of the $(^{234}U/^{238}U)$ ratios between the rock and the groundwaters indicates that water-rock interaction has resulted in the migration of U on the whole-rock scale to the depth of at least 400 m in the last million years. This implies that disposal high-level radwaste in old plutons at shallow depth (<400m) is not recommended.

Future work on the mineral separates and fracture-filling minerals is desirable to study the kinetics of the water-rock interaction to assess the migration of elements, especially U. Stable isotope study on the groundwater samples, especially the deep waters are needed to clear the origin and evolution of the different water end-members.

REFERENCES

Airey, P.L., 1986, Radioniclide migration around uranium ore bodies in the Alligator rivers region of the Northern Territory of Austrilia -- Analogue of radioactive waste repositories -- A review. Chem. Geol., 55, 255-268.

Allegre, C.J. and Condomines, M., 1976, Fine chronology of volcanic processes using $^{238}U-^{230}Th$ systematics. Earth Planet. Sci. Lett., 28, 395-406.

Allegre, C.J. and Condomines, M., 1982, Basalt genesis and mantle structure studied through Th-isotopic geochemistry. Nature, 229, 21-24.

Allegre, C.J., Dupre, B. and Lewin, E., 1986, Thorium/Uranium ratio of the earth. Chem. Geol., 56, 219-227.

Anderson, R.F., Bacon, M.P. and Brewer, P.G., 1983, Removal of ^{230}Th and ^{231}Pa from the open ocean. Earth Planet. Sci. Lett., 62, 7-23.

Arden, J.W. and Gale, N.H., 1974, Separation of trace amounts of uranium and thorium and their determination by mass spectrometric isotope dilution. Anal. Chem., 46, 687-691.

Bacon, M.P. and Anderson, R.F., 1982, Distribution of thorium isotopes between dissolved and particulate forms in the deep sea. J. Geophys. Res., 87, 2045-2056.

Beakhouse, G.P., McNutt, R.H. and Krough, T.E., 1988, Comparative Rb-Sr and U-Pb zircon geochronology of late - to tectonic plutons in the Winnipeg river belt, northwestern Ontario, Canada. Chem. Geol. (Isotope Geosci. Section), 72, 337-351.

Bennett, J.T., Krishnaswami, S., Turekian, K.K., Melson, W.G. and Hopson, C.A., 1982, The uranium and thorium decay series nuclides in Mt. Helens effusives. Earth Planet. Sci. Lett., 60, 61-69.

Bottomley, D.J., Ross, J.D. and Clark, W.B., 1984, Helium andneon isotope geochemistry of some groundwaters from the Candadian Precambrian shield. Geochim. Cosmochim. Acta, 48, 1973-1985.

Broecker, W.S. and Peng, T-H., 1982, Tracers in the sea. Eldigio Press, New York.

Chen, J.H. and Wasserburg, G.J., 1981, A search for isotopic anomalies in uranium. Geophys. Res. Lett., 7, 275-278.

Chen, J.H., Edwards, R.L. and Wasserburg, G.J, 1986, ^{234}U, ^{238}U, and ^{232}Th in sea water. Earth Planet. Sci. Lett., 80, 241-151.

Condomines, M. and Allegre, C.J., 1980, Age and magma evolution of Strombilo volcano from $^{230}Th-^{238}U$ disequilibrium data. Nature, 288, 354-357.

Condomines, M., Benat, M. and Allegre, C.J., 1976, Evidence for contamination of recent Hawaiian lavas from $^{230}Th-^{238}U$ data. Earth Planet. Sci. Lett., 33, 122-125.

Condomines,M., Morand, P. and Allegre, C.J., 1981, $^{230}Th-^{238}U$ radioactive disequilibrium in tholeites form the FAMOUS zone (Mid Atlantic Ridge 36°50'N): Th and Sr isotopic geochemistry. Earth Planet. Sci. Lett., 55, 247-256.

Cowart, J.B., 1980, The relationship of uranium isotopes to oxidation/reduction in the Edwards carbonate aquifer of Texa. Earth Planet. Sci. Lett., 48, 277-283.

Daly, N.R., 1960, Scitillation type mass spectrometer detector. Rev. Scientific Instruments, 31, 264-267.

Davison, C.C., 1984, Hydrogeological characterization at the site of Canada's Underground Research Laboratory. In: Proceedings of International Groundwater Symposium on Groundwater Resources Utilization and Contaminant Hydrogeology, Vil. II, Montreal, Que., 310-335.

Dickin, A.P., McNutt, R.H. and McAndrew, J.I., 1988, Osmiun isotope analysis by inductively coupled plasma mass spectrometry, J. Anal. Atomic Spectrometry, 2,337-342.

Dietz, L.A., Pachucki, C.F. and Land, G.A., 1962, Internal standard technique for precise isotopic abundance measurements in thermal ionization mass spectrometry. Anal. Chem., 34, 709-710.

Donath, F.A., 1982, No technical barriers. Physics Today, Vol. 35, No. 12, 36-42

Edmunds, W.M., Andrews, J.N., Burgess, W.G., Kay, R.L.F. and Lee, D.J., 1984, The evolution of saline and thermal groundwaters in the Canmenellis granite. Mineral. Magazine, 48, 407-424.

Edmunds, W.M., Kay, R.L.F. and McCartney, R.A., 1985, Origin of saline groundwaters in the Canmenellis granite: natural processes and relation during hot dry rock reservoir circulation. Chem. Geol., 49, 287-301.

Edmunds, W.M., Kay, R.L.F., Miles, .L. and Cook, J.M., 1987, The origin of saline groundwaters in Canmenellis granite, Cornwall (U.K): further evidence from minor and trace elements. Geol. Assoc. Canada Special Paper 33, eds P. Fritz and S.K. Frape, 127-144.

Edwards, R.L., Chen, J.H. and Wasserburg, G.J., 1987a, $^{238}U-^{234}U-^{230}Th-^{232}Th$ systematics and precise measurement of time over past 500,000 years. Earth Planet. Sci. Lett., 81, 175-192.

Edwards, R.L., Chen, J.H., Ku, T.L. and Wasserburg, G.J., 1987b, Precise timing of the last interglacial period from mass spectrometric determination of Thorium-230 in corals. Science, 236, 1547-1553.

Edwards, R.L., Taylor, F.W. and Wasserburg, G.J., 1988, Dating earthquakes with high-precision thorium-230 ages of very young corals. Earth Planet. Sci. Lett., 90, 371-381.

Epstein, S. and Mayeda, T., 1953, Variations of O^{18} content of waters from natural sources. Geochim. Cosmochim. Acta, 4, 213-224.

Faris, J.P. and Buchanan, R.F., 1964, Anal. Chem., 36, 1157-1158.

Farquharson, R.D., 1975, Revised Rb-Sr age of the Lac du Bonnet quartz monzonite, southeastern Manitoba. Can. J. Earth Sci., 12, 115-118.

Franklyn, M.T., 1988, Sr isotope composition of the saline groundwaters in Eye-Dashwa Lakes pluton, Atikoken, Ontario. Unpub. M.Sc. thesis, Dept. of Geology, McMaster University, Hamilton, Canada.

Frape, S.K. and Fritz, P., 1987, Geochemical trends for groundwaters from the Canadian shield. Geol. Assoc. Canada Special Paper 33, eds P. Fritz and S.K. Frape, 19-38.

Frape, S.K., Fritz, P. and McNutt, R.H., 1984, Water-rock interactin and chemistry of groundwaters from Canadian shield. Geochim. Cosmochim. Acta, 48, 1617-1627.

Fritz, P., 1982, Environmental isotope hydogeology: tools to complement the classical techniques of physical hydrology and geochemistry. University of Waterloo internal manual.

Fritz, P. and Frape, S.K., 1982, Saline groundwaters in the Canadian shield - a first overview. Chem. Geol., 36, 179- 190.

Garbarino, J.R. and Taylor, H.E., 1987, Stable Isotope dilution analysis of hydrological samples by inductively coupled plasma mass spectrometry. Anal. Chem., 59, 1568-1575.

Gascoyne, M., 1977, Uranium series dating of speleothem: An investigation of technique, data processing and precision. Tech. Memo. 77-4, Dept. of Geology,

McMaster University, Hamilton, Canada.

Gascoyne, M. and Cramer, J.J., 1987, History of actinide and minor element mobility in an Archean granitic batholith in Manitoba, Canada. Appl. Geochem., 2, 37-54.

Gascoyne, M., Davison, C.C., Ross, J.D. and Pearson, R., 1987, Saline groundwaters and brines in plutons in the Canadian shield. Geol. Assoc. Canada Special Paper 33, eds. P. Fritz and S.K. Frape, 53-68.

Gascoyne, M. and Schwarcz, H.P., 1986, Radionuclide migration over recent geological time in a granitic pluton. Chem. Geol. (Isotope Geoscience Section), 59, 75-85.

Govindaraju, K., 1984, 1984 compilation of working values for 170 international reference samples of mainly silicate rocks and minerals. Geostandards Newsletter, 8 (special issue).

Gray, A.L., 1988, Inductively Coupled Plasma source Mass Spectrometry. In: Adams, F., Gijbels, R. and Van Grieken, R., Inoganic Mass Spectrometry, John Wiley & Sons, New York, pp.257-300.

Grigsby, C.O., Tester, J.W., Trujillo, P.E., Counce, D.A., Abbott, J., Holley, C.E. and Blatz, L.A., 1983, Rock-water interaction in hot dry geothermal system: field investigations of in situ geochemical behavior. J. Volcan. geotherm. Res., 15, 101-136.

Guha, J. aand Kanwar, R., 1987, Vug brines - fluid inclusions: a key to understanding of secondary gold enrichment processes and the evolution of the deep brines in the Canadian shield. Geol. Assoc. Canada Special Paper 33, eds P. Fritz and S.K. Frape, 95-102.

Harmon, R.S., 1975, Late Pleistocene paleotemperatures in North America as inferred from isotopic variations in speleothems. Unpub. Ph.D. thesis, Dept. of Geology, McMaster University, Hamilton, Canada.

Harmon, R.S., Ku, T.L., Mathews, R.K. and Smart, P.L., 1979, Limits of U-series analyses: Phase I results of the Uranium-series Intercomparison Project. Geol., 7, 405-409.

Houk, R.S. and Thompson, J.J., 1988, Inductively Coupled Plasma Mass Spectrometry. Mass Spectr. Reviews, 7, 425-461.

Huh, Chih-An and Beasly, T.M., 1987, Profiles of dissolved and particulate thorium isotopes in the water column of coastal Southern California. Earth Planet. Sci.Lett., 85, 1-10.

Inghram, M.G. and Chupka, W.A., 1953, Surface ionization source using multiple filaments. Rev. Scientific Instruments, 24, 518-520.

Ivanovich, M. and Harmon, R.S., eds., 1982, Uranium Series Disequilibrium: Application to Environmental Problems. Clarendon Press, Oxford.

Jannasch, H.W., Honeyman, B.D., Balistrieri, L.S. and Murray, J.W., 1988, Kinetics of trace element uptake by marine particles. Geochim. Cosmochim. Acta, 52, 567-577.

Jones, M.G., 1987, A study of the late-stage secondary mineralization at sites across the precambrian Canadian shield. Unpub. M.Sc. thesis, University of Waterloo.

Kamineni, D.C., 1986, Distribution of uranium, thorium and rare-earth elements in the Eye-Dashwa lakes pluton - a study of some analogue elements. Chemi. Geol., 55, 361-373.

Kamneni, D.C., 1987, Halogen-bearing minerals in plutonic rocks: a possible source of chlorine in saline groundwater in the Canadian shield. Geol. Assoc. Canada Special Paper 33, eds P. Fritz and S.K. Frape, 69-80.

Kamineni, D.C., Chung, C.F., Dugal, J.J.B., and Ejeeckham,

R.B., 1986, Distribution of uranium and thorium in core samples from the Underground Research Laboratory lease area, southeastern Manitoba, Canada. Chem. Geol., 54, 97-111.

Karlsson, F. and Wikberg, P., 1987, Some highlights on the isotope geochemistry studies within the Swedish research program on radioactive waste disposal. Appl. Geochem., 2, 25-31.

Kaufmann, A, and Broecker, W.S., 1965, Comparison of the ^{230}Th and ^{14}C ages for carbonate materials from Lakes Lahontan and Bonneville. J. Geophys. Res., 70, 4039-4054.

Kelly, W.C., Rye, R.O. and Livnat, A., 1986, Saline minewaters of Keweenaw Peninsula, northern Michigan: Their nature, origin and relation to similar deep waters in precambrian crystalline rocks of the Canadian shield. Amer. J. Sci., 286, 281-308.

Kerrich, R. and Kamineni, D.C., 1985, Oxygen and hydrogen isotope study of fracture related fluid flow in the Eye-Dashwa Lakes pluton, Atikokan, Northwestern Ontario. AECL, TR-361.

Knoll, G.F., 1979, Radiation detection and measurement. John Wiley, New York.

Krishnaswami, S., Turekian, K.K. and Bennett, J.T., 1984, The behavior of ^{232}Th and the ^{238}U decay chain nuclides during magma formation and volcanism. Geochim. Cosmochim. Acta, 48, 505-511.

Krogh, T.E., Harris, N..W. and Davis, G.L., 1976, Archean rocks from the eastern Lac Seul region of the English River gneiss belt, northwestern Ontario, Part 2: geochronology. Can. J. Earth Sci., 13, 1212-1215.

Ku, T.L., 1976, The Uranium-series mrthods of age determinatin. Ann. Rev. Earth Planet. Sci., 4, 347-380.

Lasaga, A.C., 1984, Chemical kinetics of water-rock interactions. J. Geophys. Res., 89B, 4009-4025.

Latham, A.G. and Schwarcz, H.P., 1987a, On the possibility of determining rates of removal of uranium from crystalline igneous rocks using U-series disequilibria--1: a U-leach model, and its applicability to whole-rock data. Appl. Geochem., 2, 55-65.

Latham, A.G. and Schwarcz, H.P., 1987b, On the possibility of determining rates of removal of uranium from crystalline igneous rocks using U-series disequilibria--2: applicability of a U-leach model to mineral separates. Appl. Geochem., 2, 67-71.

Longerich, H.P., Fryer, B.J. and Strong, D.F., 1987, Determination of lead isotope ratios by inductively coupled plasma-mass spectrometry (ICP-MS). Spectrochimi. Acta, 42B, 39-48.

Marcantonio, F., 1989, Isotopic study of plutonic and metamorphic rocks. Unpub. M.Sc. thesis, Dept. of Geology, McMaster University, Hamilton, Canada.

McCrank, G.F.D., 1985, Results of a geological survey of the Lac du Bonnet Batholith, Manitoba. Atomic Energy of Canada Limited Rep., AECL-7816, 63pp.

McLaren, J.W., Beauchemin, D. and Berman, S.S., 1987, Application of isotope dilution inductively coupled plasma mass spectrometry to the analysis of marine sediments. Anal. Chem., 59, 610-613.

McNutt, R.H., 1987, $^{87}Sr/^{86}Sr$ ratios as indicators for rock-water interactions: application to brines formed in Precambrian age rocks from Canada. Geol. Assoc. Canada Special Paper 33, eds P. Fritz and S.K. Frape, 81-88.

McNutt, R.H., Frape, S.K. and Fritz, P., 1984, Strontium isotopic composition of some brines from the precambrian shield of Canada. Isotope Geoscience, 2, 205-215.

McNutt, R.H., Gascoyne, M. and Kamineni, D.C., 1986, Sr-87/Sr-86 values in grounwaters of East Bull Lake pluton, Superior Province, Ontario, Canada. Appl. Geochem., 2, 93-102.

Nesbitt, H.W., 1979, Mobility and fractionation of rare earth elements during weathering of a granodiorite. Nature, 279, 206-210.

Newman, S., Finkel, R.C. and MacDougall, J.D., 1984, Comparison of ^{230}Th-^{238}U disequilibrium systematics in lavas from three hot spot regions: Hawaii, Prince Edward, and Samoa. Gochim. Cosmochim. Acta, 48,315-324.

Newman, S., MacDougall, J.D. and Finkel, R.C., 1986, Petrogenesis and ^{230}Th-^{238}U disequilibrium at Mt. Shasta, California, and in the Cascades. Contrib. Mineral. Petrol., 93, 195-206.

Nordstrom, D.K., Andrews, J., Carlson, L., Fontes, J.C., Fritz, P., Moser, H. and Olssen, T., 1985, Hydrogeological and hydrogeochemical investigations in boreholes - final report of the phase I geochemical investigations of the Stripa groundwaters: SKB Stripa project. Swedish Nuclear Fuel and Waste Management Company, Report 85-06, 250 p.

Nordstrom, D.K. and Olssen, T., 1987, fluid inclusions as a source of dissolved salts in deep granitic groundwaters. Geol. Assoc. Canada Special Paper 33, eds P. Fritz and S.K. Frape, 111-120.

Nozaki, Y., Horibe, Y. and Tsubota, H., 1981, The water column distribution of thorium isotopes in the Western North Pacific. Earth Planet. Sci. Lett., 54, 203-216.

Nozaki, Y., Yang, H-S. and Yamada, M., 1987, Scavenging of thorium in the ocean. J. Geophys. Res., 92, 772-778.

Osmond, J.K. and Cowart, J.B., 1982, Groundwater, In: M.Ivanovich and R.S. Harmon (Editors), Uranium series disequilibrium -applications to environmentaal problems. Oxford Science Publications, Oxford, 202-245.

Osmond, J.K., Cowart, J.B. and Ivanovich, M., 1983, Uranium isotopic disequilibrium in groundwater as an indicator of anomalies. Int. J. App. Radiat. Isot., 34, 283-308.

Oversby, V.M. and Gast, P.W., 1968, Lead isotope compositions and uranium decay series disequilibrium in recent volcanic rocks. Earth Planet. Sci. Lett., 5, 199-206.

P.de Bievre, 1978, Accurate isotope ratio mass spectrometry: some problems and possibilities. Adv. Mass Spectrom., 7A, 395-447.

Penner, A.P. and Clark, G.S., 1971, Rb-Sr determinations from the Bird River area, southeastern Manitoba. In: A.C. Turnock (Editor), Geoscience Studies in Manitoba. Geol. Assoc. Can., Spec. Pap., 9, 105-109.

Pohl, R.O., 1982, Will it stay out?. Physics Today, Vol. 35, No.12, 37-45.

Ragers, J.J.W. and Adams, J.A.S., 1969, Uranium. In Handbook of Geochemistry, ed. K.H.Wedepohl, Springer, Berlin.

Rec, J.R., Myers, W.G. and White, F.A., 1974, Deffusion controlled, thermal ionization source for mass spectrometric analysis of trace metals. Anal. Chem., 46, 1243-1247.

Riddle, C., Vander Voet, A. and Doherty, W., 1988, Rock analysis using inductively coupled plasma mass spectrometry: A review. Geostandards Newsletter, 12, 203-234.

Rokop, D.J., Perrin, R.E., Knobeloch, G.W., Armijo, V.M. and Shields, W.R., 1982, Thermal ionization mass spectrometry of uranium with electrodeposition as loading technique. Anal. Chem., 54, 957-960.

Russ, G.P. and Bazan, J.M., 1987, Isotopic ratio

measurements with an inductively coupled plasma mass spectrometer. Spectrochimi. Acta, 42B, 49-62.

Russell, W.A., Papanastassiou, D.A. and Tombrello, T.A., 1978, Ca isotope fractionation on the earth and other solar system materials. Geochim. Cosmochim. Acta, 42, 1075-1090.

Schwarcz, H.P. and Gascoyne, M., 1984, Uranium-series dating of Quaternary deposits, In: Mahaney, W.C. (Editor), Quarternary Dating Methods. Elsevier, Amsterdam, pp. 33-51.

Schwarcz, H.P., Gascoyne, M. and Ford, D.C., 1982, Uranium-series disequilibrium studies of granitic rocks. Chem. Geol., 36, 87-102.

Shimield, G.B. and Price, N.B., 1988, The scavenging of U, ^{230}Th, and ^{231}Pa during pulsed hydrothermal activity at 20°S, East Pacific Rise. Geochim. Cosmochim. Acta, 52, 669- 678.

Smellie, J.A.T., MacKenzie, A.B. and Scoot, R.D., 1986, An analogue validation study of natural radionuclid migration in crystalline rocks using uranium-series disequilibrium studies. Chem. Geol., 55, 233-254.

Stuckless, J.S., 1986, Applications of U-Th-Pb isotope systematics to the problems of radioactive waste disposal. Chem. Geol., 55, 215-226.

Ting, B.T.G. and Janghorbani, M., 1987, Application of ICP-MS to accurate isotopic analysis for human metabolic studies. Spectrochimi. Acta, 42B, 21-27.

Vandergraaf, T.T., 1987, The role of isotope geochemistry studies in Canadian Nuclear Fuel Waste Management Program. Appl. Geochem., 2, 5-9.

Wasserburg, G.J., Jacobsen, S.B., DePaolo, D.J., McCulloch, M.T. and Wen, T., 1981, Precise determination of Sm/Nd ratios, Sm and Nd isotopic abundances in standard solutions. Geochim. Cosmochim. Acta, 45, 2311-2323.

APPENDIX 2.1

ROCK SAMPLE DESCRIPTION

SAMPLE	DEPTH (m)	DESCRIPTION
P-1	0-200	Pink granite from the shaft with K-fld (40%), Plg (20%), Qtz (35%) and Biot (5%). Slight alteration of Plg to sericite and Biot to chloride.
P-2	0	Pink granite from the surface with K-fld (50%), Plg (15%), Qtz (30%) and Biot (5%). Similar to P-1 but slightly more altered.
P-3	>200	Grey granite from the shaft with K-fld (25%), Plg (45%), Qtz (20%) and Biot (10%).Slight alteration of Plg to sericite and Biot to chloride and some hematite stain on Plg.
JSS1	62	Grey granite from a horizontal core in the shaft with K-fld (30%), Plg (45%), Qtz (15%) and Biot (10%). Similar to P-3 in alteration.
JSS2	60	Grey granite from a horizontal core in the shaft. Very similar to JSS1.
HCO	275.7-276	Pink granite from a core with K-fld (30%), Plg (30%), Qtz (30%) and Biot (10%). Severe alteration of Plg to sericite and Biot to chlorite. Concentrated hematite stain on Plg. It was sub sampled as the lower part, HCO1 (275.9-276m), and the upper part, HCO2 (275.7-275.9m). HCO2 is more altered than HCO1.
HC19	272.1-272.4	Pink granite with K-fld (40%), Plg (20%), Qtz (35%) and Biot (5%). Complete alteration of Plg and K-fld to sericite and Biot to chloride. Concentrated hematite stain in Plg,K-fld and some Biot.
3D1	FZ-2	Granite from the shaft with pink and deep grey bands and was sub-

SAMPLE	DEPTH (m)	DESCRIPTION
		sampled. 3D1-1 is the transition part of the pink and grey bands. 3D1-2 is the grey part with K-fld (20%), Plg (40%),Qtz (20%) and Biot (20%). Severe alteration of Plg to sericite and Biot to chloride. Some hematite stain on Plg. 3D1-3 is the pink part with K-fld (35%), Plg (25%), Qtz (35%) and Biot (5%). Similar alteration to 3D1-2.
3D2	FZ-2	Pink granite from the shaft with K-fld (35%), Plg (35%),Qtz (25%) and Biot (5%). Severe alteration of Plg to sericite and Biot to chloride. Some hematite stain on Plg.
3D3	FZ-2	Pink granite from the shaft with K-fld (35%), Plg (35%),Qtz (25%) and Biot (5%). Severe alteration of all Plg and some K-fld to sericite and Biot to chloride. Heavy hematite stain on Plg.
3D4	FZ-2	Granite from the shaft with pink and deep grey bands and was sub-sampled. 3D4-1 is the pink part with K-fld (50%), Plg (25%), Qtz (20%) and Biot (5%). Severe alteration of Plg and to sericite and Biot to chloride. Some hematite stain on Plg. 3D4-2 is the grey part with K-fld (40%), Plg (20%), Qtz (15%) and Biot (15%). Similar ateration to 3D4-1.
3D5	FZ-2	Granite from the shaft with pink and deep grey bands and was sub-sampled. It is very similar to 3D4 in alteration. 3D5-1 is the pink part with K-fld (35%), Plg (35%), Qtz (25%) and Biot (5%). 3D5-2 is the grey part with K-fld (20%), Plg (40%), Qtz (25%) and Biot (15%).

```
5 CLS : PRINT "U/Th DISEQUILIBRIA CALCULATION"
8 REM:          XXXXXXXXXXXXXXXXXXXXXXXXXXXXXXXXXXXXXX
10 REM:         X  Wangxing Li,                      X
12 REM:         X  DEPT.OF GEOLOGY, McMASTER UNIVERSITY X
14 REM:         X  MAY, 1988                          X
16 REM:         XXXXXXXXXXXXXXXXXXXXXXXXXXXXXXXXXXXXXX
20 LPRINT "       U/Th CALCULATION"
30 LPRINT
40 REM: CONSTANTS XXXXXXXXXXXXXXXXXXXXXXXXXX
45 DU234 = 2.835E-06
50 DU238 = 1.55125E-10
55 DTH230 = 9.195E-06
60 DTH232 = 4.9475E-11
65 USP = 4.471: Eusp = .0036
70 THSP = 4.8466: Ethsp = .0143
75 ASPU = 236.0501
80 ASPTH = 230.7328
85 ASMU = 238.028
90 ASMTH = 232.0382
95 RSP86 = .002242: Esp86 = .00001
100 RSP09 = .009054: Esp09 = .000058
105 RSP29 = 1.3114: Esp29 = .0023
110 RSP96 = .47993: Esp96 = .00147
115 FSPU6 = .997689
120 FSPU8 = .002237
125 FSPTH9 = .431583
130 FSPTH0 = .003907
135 FSPTH2 = .56451
140 FSMU8 = .9927456
145 FSMTH2 = 1
155 REM: VARIABLE INITIALIZATION XXXXXXXXXXXXXXXXXX
165 TH = 0: TEL = 0: TEU = 0
170 A04 = 0: Ea04 = 0
175 A08 = 0: Ea08 = 0
180 A48 = 0: Ea48 = 0
185 A28 = 0: Ea28 = 0
187 Ainit48 = 0: EAinit48 = 0
190 R58 = 0: Er58 = 0
195 R56 = 0: Er56 = 0
200 TR56 = 0
205 R68 = 0: Er68 = 0
210 R86 = 0: Er86 = 0
215 R46 = 0: Er46 = 0
220 R09 = 0: Er09 = 0
225 R02 = 0: ErC2 = 0
230 R92 = 0: Er92 = 0
235 R48 = 0: Er48 = 0
240 R04 = 0: Er04 = 0
245 R08 = 0: Er08 = 0
250 R28 = 0: Er28 = 0
255 RSMK86 = 0: Esmk86 = 0
```

```
260 RSMK09 = 0: Esmk09 = 0
265 RSMK29 = 0: Esmk29 = 0
270 USM = 0: Busm = 0
275 THSM = 0: Ethsm = 0
280 FRACTU1 = 1: FRACTU2 = 1
285 FRACT92 = .99351: FRACT02 = .99568: FRACT09 = 1.00218
290 LPRINT : LPRINT
300 REM: DATA INPUT ::::::::::::::::::::::::
305 INPUT "ENTER SAMPLE NAME"; AAA$
310 INPUT "ENTER SAMPLE WT. (g)"; WSM
315 INPUT "ENTER SPIKE WT (g)"; WSP
320 INPUT "ENTER MEASURED U234/U236 RATIO AND STD DEVIATION"; R46, Er46
325 INPUT "ENTER MEASURED U236/U238 RATIO AND STD DEVIATION"; R68, Er68
330 INPUT "ENTER MEASURED Th230/Th229 RATIO AND STD DEVIATION"; R09, Er09
335 INPUT "ENTER MEASURED Th229/Th232 RATIO AND STD DEVIATION"; R92, Er92
340 INPUT "ENTER MEASURED Th230/Th232 RATIO AND STD DEVIATION"; R02, Er02
345 INPUT "ARE ALL DATA FRACTIONATION CORRECTED? (Y OR N)"; ANS1$
350 IF ANS1$ = "" THEN 345
355 IF ANS1$ = "Y" OR ANS1$ = "y" THEN GOTO 375
360 IF ANS1$ = "N" OR ANS1$ = "n" THEN GOTO 365
365 INPUT "ENTER MEASURED U235/U238 RATIO AND STD DEVIATION"; R58, Er58
370 INPUT "ENTER MEASURED U235/U236 RATIO AND STD DEVIATION"; R56, Er56
375 INPUT "DO YOU WANT ANY CHANGES OF THE INPUTS? (Y OR N)"; ANS2$
380 IF ANS2$ = "" THEN 375
385 IF ANS2$ = "Y" OR ANS2$ = "y" THEN GOTO 305
390 IF ANS2$ = "N" OR ANS2$ = "n" THEN GOTO 392
392 IF ANS1$ = "Y" OR ANS1$ = "y" THEN GOTO 455
395 INPUT "IS U236/U238 RATIO FRACTIONATION CORRECTED? (Y OR N)"; ANS3$
400 IF ANS3$ = "" THEN 395
405 IF ANS3$ = "Y" OR ANS3$ = "y" THEN 430
410 IF ANS3$ = "N" OR ANS3$ = "n" THEN 415
415 REM: FRACTIONATION CORRECTION ::::::::::::::::::::::
420 IF R58 <> 0 THEN FRACTU1 = (.0072526# / R58) ^ (1 / 3)
425 R68 = R68 * (FRACTU1) ^ 2
430 IF R68 = 0 OR R56 = 0 THEN 440
435 TR56 = .0072526# / R68: FRACTU2 = TR56 / R56
440 R46 = R46 * (FRACTU2) ^ 2
445 R09 = R09 * FRACT09
450 R92 = R92 * FRACT92: R02 = R02 * FRACT02
452 REM: RATIO CALCULATION ::::::::::::::::::::::
455 IF R68 = 0 THEN 470
460 R86 = 1 / R68: Er86 = R86 * Er68 / R68
465 RSMK86 = (R86 - RSP86): Esmk86 = (Er86 ^ 2 + Esp86 ^ 2) ^ .5
470 IF R09 = 0 AND R02 = 0 THEN 495
475 IF R09 <> 0 THEN 490
480 R09 = R02 / R92
485 Er09 = R09 * ((Er02 / R02) ^ 2 + (Er92 / R92) ^ 2) ^ .5
490 RSMK09 = (R09 - RSP09): Esmk09 = (Er09 ^ 2 + Esp09 ^ 2) ^ .5
495 IF R46 = 0 THEN 525
500 R46 = R46 / RSMK86
505 Er46 = R46 * ((Er46 / R46) ^ 2 + (Esmk86 / RSMK86) ^ 2) ^ .5
510 IF RSMK09 = 0 THEN 565
```

```
515 R04 = RSHK09 / R46 x RSP96
520 Er04 = R04 x ((Esmk09 / RSHK09) ^ 2 + (Er46 / R46) ^ 2 + (Esp96 / RSP96) ^ 2) ^ .5
525 IF RSHK86 = 0 THEN 545
530 R08 = RSHK09 x RSP96 / RSHK86
535 IF RSHK09 = 0 THEN 545
540 Er08 = R08 x ((Esmk09 / RSHK09) ^ 2 + (Esp96 / RSP96) ^ 2 + (Esmk86 / RSHK86) ^ 2) ^ .5
545 A04 = 3.2424 x R04
550 IF A04 <> 0 THEN Ea04 = A04 x Er04 / R04
555 A08 = 59274.8 x R08
560 IF A08 <> 0 THEN Ea08 = A08 x Er08 / R08
565 A48 = 18275.6 x R48
570 IF A48 <> 0 THEN Ea48 = A48 x Er48 / R48
575 IF R68 = 0 THEN 590
580 USH = ASHU / ASPU x WSP x USP x (PSPU6 - R68 x FSP8) / (WSH x PSHU8 x R68 x 1000)
585 IF R68 <> 0 THEN Eusm = USH x ((Er68 / R68) ^ 2 + (Eusp / USP) ^ 2) ^ .5
590 IF R92 = 0 THEN 635
595 RSHK29 = 1 / R92 - RSP29: Esmk29 = ((Er92 / R92 ^ 2) ^ 2 + Esp29 ^ 2) ^ .5
600 IF RSHK86 = 0 THEN 620
605 R28 = RSHK29 x RSP96 / RSHK86
610 Er28 = R28 x ((Esmk29 / RSHK29) ^ 2 + (Esp96 / RSP96) ^ 2 + (Esmk86 / RSHK86) ^ 2) ^ .5
615 A28 = R28 x DTH232 / DU238: Ea28 = A28 x Er28 / R28
620 THSH = ASHTH / ASPTH x WSP x THSP x (PSPTH9 - R92 x PSPTH2) / (WSH x PSHTH2 x R92 x 1000)
625 IF R92 <> 0 THEN Ethsm = THSH x ((Er92 / R92) ^ 2 + (Ethsp / THSP) ^ 2) ^ .5
630 GOSUB 830
635 LPRINT "        SAMPLE NAME="; AAA$
640 LPRINT "        SAMPLE WT ="; WSH
645 LPRINT "        SPIKE WT ="; WSP
650 LPRINT "        R46="; R46, "+/-"; Er46
655 LPRINT "        R68="; R68, "+/-"; Er68
660 LPRINT "        R09="; R09, "+/-"; Er09
665 LPRINT "        R92="; R92, "+/-"; Er92
670 LPRINT "        R02="; R02, "+/-"; Er02
675 LPRINT
680 LPRINT "        RSHK86="; RSHK86, "+/-"; Esmk86
685 LPRINT "        RSHK09="; RSHK09, "+/-"; Esmk09
690 LPRINT "        RSHK29="; RSHK29, "+/-"; Esmk29
695 LPRINT
700 LPRINT "        R04="; R04, "+/-"; Er04
705 LPRINT "        R48="; R48, "+/-"; Er48
710 LPRINT "        R08="; R08, "+/-"; Er08
715 LPRINT "        R28="; R28, "+/-"; Er28
720 LPRINT
725 LPRINT "        Th230/U234="; A04, "+/-"; Ea04
730 LPRINT "        U234/U238="; A48, "+/-"; Ea48
735 LPRINT "        Th230/U238="; A08, "+/-"; Ea08
740 LPRINT "        Th232/U238="; A28, "+/-"; Ea28
745 IF A04 > 1 THEN 775
750 LPRINT "        (U234/U238)init="; Ainit48, "+/-"; EAinit48
755 LPRINT "                    -"; TEL
```

```
760 LPRINT "        Th230 AGE ="; TH
765 LPRINT "                          +"; TEU
770 GOTO 785
775 LPRINT
780 LPRINT "        Th230 AGE > 400,000 YEARS"
785 LPRINT
790 LPRINT "        U="; USM, "+/-"; Eusm; "ppm"
795 LPRINT "        Th="; THSM, "+/-"; Ethsm; "ppm"
800 PRINT
805 INPUT "DO YOU WISH TO DO ANOTHER? (Y OR N)"; ANS4$
810 IF ANS4$ = "" THEN 805
815 IF ANS4$ = "Y" OR ANS4$ = "y" THEN GOTO 155
820 IF ANS4$ = "N" OR ANS4$ = "n" THEN GOTO 825
825 END
828 REM: AGE CALCULATION ::::::::::::::::::
830 TH230AGE:
835 Ainit48 = 0: EAinit48 = 0
840 TH = 0: THIGH = 0: TLOW = 0
845 TEL = 0: TEU = 0
850 IF A48 = 0 OR A04 = 0 THEN 1000
855 IF A04 > 1 OR A04 < .1 THEN 1000
860 FOR I = 1 TO 3
865 TL = 1: TU = 600000
870 T = (TL + TU) / 2
875 A84 = 1 / A48: Er84 = A84 * Er48 / A48
880 Ainit04 = 1.7 * A28 * A84
885 K1 = DTH230 - DU234: K2 = DTH230 / K1
890 IF I = 1 THEN LE1 = A04
895 IF I = 2 THEN LE1 = A04 - Ea04
900 IF I = 3 THEN LE1 = A04 + Ea04
905 IF LE1 < .05 OR LE1 > .99 THEN 965
910 T = (TL + TU) / 2
915 LE2 = Ainit04 * EXP(-DTH230 * T)
920 RE1 = A84 * (1 - EXP(-DTH230 * T))
925 RE2 = (1 - A84) * K2 * (1 - EXP(-K1 * T))
930 LE = LE1 + LE2: RE = RE1 + RE2
935 IF LE > RE THEN TL = T
940 IF LE < RE THEN TU = T
945 IF ABS(LE / RE - 1) > .0005 THEN 910
950 IF I = 1 THEN TH = T
955 IF I = 2 THEN TLOW = T
960 IF I = 3 THEN THIGH = T
965 NEXT
970 Ainit48 = 1 + (A48 - 1) * EXP(DU234 * TH)
975 HAinit48 = 1 + (A48 + Ea48 - 1) * EXP(DU234 * THIGH)
980 LAinit48 = 1 + (A48 - Ea48 - 1) * EXP(DU234 * TLOW)
985 EAinit48 = (HAinit48 - LAinit48) / 2
990 TEL = TH - TLOW
995 TEU = THIGH - TH
1000 RETURN
```